Novel Insights into the Functions of CCR2 in Tumor Cell Metastasis and Lymphotoxin in Liver Cancer Development

Dissertation

zur

Erlangung der naturwissenschaftlichen Doktorwürde
(Dr. sc. nat.)

vorgelegt der

Mathematisch-naturwissenschaftlichen Fakultät

der

Universität Zürich

von

Monika Julia Wolf

aus

Deutschland

Promotionskomitee

Prof. Dr. Adriano Aguzzi (Vorsitz)

Prof. Dr. Mathias Heikenwälder (Leitung)

Prof. Dr. Anne Müller

Prof. Dr. Christian Münz

Zürich, 2011

TABLE OF CONTENTS

1 ABBREVIATIONS

ALT	alanine transaminase
APC	antigen presenting cell
ASH	alcoholic steato-hepatitis
AST	aspartate transaminase
BSA	bovine serum albumin
BM	bone marrow
CaP	prostate cancer
CRaP	castration-resistant prostate cancer
CCL2/MCP-1	CC chemokine 2/ monocyte chemoattractant protein 1
CCR2	CC chemokine receptor 2
cDNA	copy DNA
CFP	cyan fluorescent protein
CH	cholestasis
CIR	end stage liver cirrhosis due to alcoholic liver disease
dpi	days post injection
DNA	deoxyribonucleic acid
DT	diphtheria toxin
EC	endothelial cell
ERK	extracellular signal regulated kinase
FACS	fluorescence activated cell sorter
FCS	fetal calf serum
FDC	follicular dendritic cell
FNH	focal nodular hyperplasia
FSC	fibrosarcoma
GFP	green fluorescent protein
GP73/GOLPH2	golgi protein 73
GRK	G-protein coupled receptor kinase
HBV	hepatitis B virus
HBsAg	hepatitis B virus surface antigen
HCC	hepatocellular carcinoma
HCV	hepatitis C virus
H&E	hematoxylin-eosin staining
HGF	hepatic growth factor
HMEC	human dermal microvascular endothelial cells
hr	hour
HRP	horse-radish peroxidase
HUVEC	human umbilical vein endothelial cells

HVEM	herpes virus entry mediator
IFN	interferon
IκB	inhibitor of κB
IKK	IκBα kinase complex
IL	interleukin
i.p.	intraperitoneal
i.v.	intravenous
JAK2	Janus kinase 2
JNK	c-Jun N-terminal kinase
kDa	kilo Dalton
LPS	lipopolysaccharide
LT	lymphotoxin
LTα	lymphotoxin alpha
LTβ	lymphotoxin beta
LTβR	lymphotoxin beta receptor
MAPK	mitogen-activated protein kinase
mdr2	multidrug resistance gene 2
min	minute
mRNA	messenger ribonucleic acid
NFκB	nuclear factor kappa B
NIK	NFκB inducing kinase
NK cells	natural killer cells
NPC	non-parenchymal cells
NPC	nasopharyngal carcinoma (exclusively in chapter 6.5.3)
NVH	non-viral hepatitis
OLD	other liver diseases
PBC	primary bilary cirrhosis/ autoimmune cholangitis
PBS	phosphate-buffered saline
PBST	phosphate-buffered saline (with) Tween-20
PCR	polymerase chain reaction
p.i.	post injection
PI3K	phosphoinositol 3 kinase
PLC	phospholipase C
qPCR	quantitative PCR (real-time PCR)
Rag1	recombination activating gene 1
RIN	RNA integrity index
RNA	ribonucleic acid
ROS	reactive oxygen species
RT	reverse transcriptase

SDS-PAGE	sodium dodecyl sulphate polyacrylamide gel electrophoresis
siRNA	silencing RNA
ST	steatosis
STAT	signal transducers and activator of transcription
TAK1	TGFβ activated kinase
TAM	tumor associated macrophages
TBS	tris-buffered saline
TGF	transforming growth factor
TLR	toll like receptor
TNFα	tumor necrosis factor alpha
TNFR	tumor necrosis factor receptor
TNFSF	TNF super family

2 SUMMARY

It is conveyed that Hippocrates was most likely the first person to use the term “cancer” as he had observed similarities to the legs of crustacean when he treated a patient with an abscess within breast tissue. Cancer is one of the leading causes of death worldwide and accounted for 7.6 million deaths in 2008. This indicates that approximately 13% of all deaths were due to cancer. The incidence of cancer is rising worldwide and estimations expect over 11 million deaths from cancer in 2030. Most deaths from cancer occur in low- and middle-income countries, but also in industrialized countries a rising cancer incidence is found [1].

The term cancer comprises a lot of different diseases summarizing tumors that can arise in almost any organ – however, depending on the type of tissue affected survival rates can vary drastically. Most patients die due to tumors within lungs (1.4 million deaths/ year) followed by stomach (740,000 deaths), liver (700,000 deaths), colon (610,000 deaths) and breast (460,000 deaths) [1]. However, primary tumors rarely are the main cause of death (10% of patients), in most cases metastases lead to the majority of deaths in cancer-affected individuals (90% of patients) [2].

Despite a lot of effort in research in the past, we are only beginning to understand the cellular and molecular mechanisms that lead to the transformation of normal cells into malignant ones.

In my thesis I am focusing on two different projects – both dealing with the role of inflammatory mediators (cytokines and chemokines) in cancer development and metastasis – however in different experimental models and settings.

CCR2 in Tumor Cell Extravasation and Lung Metastasis

Metastasis is a multistage process comprising tumor cell dissemination, survival in the circulation, extravasation and ultimately colonization of distant organs [3, 4]. Increased expression of the chemokine CCL2 correlates with poor prognosis and increased tumor burden in metastatic breast, prostate and colon cancer [5-9]. Recent results suggest that tumor cell-derived CCL2 attracts Ly6C^{hi} monocytes to facilitate tumor metastasis [5]. However, the exact mechanisms how CCL2 expression by tumor cells can enable the independent steps of metastasis upon the attraction of inflammatory monocytes remain elusive. Furthermore, the role of the corresponding chemokine receptor CCR2, which is found to be expressed on various cell types, is only poorly characterized in metastasis.

Together with Alexandra Hoos, I could show in a model of experimental metastasis how tumor cell-derived CCL2 activates the endothelium through activation of its receptor CCR2 and thereby inducing vascular permeability sufficient for driving tumor cell extravasation. In the absence of CCR2 (in *Ccr2*$^{-/-}$ mice), we could observe attenuation of metastasis with ablated

vascular permeability and decreased interaction of tumor and myeloid cells, indicating an involvement of CCR2 signaling in metastasis.

In order to identify the role of CCR2 expression in the hematopoietic and stromal compartment, I performed reciprocal bone marrow reconstitutions experiments which suggested a critical role of endothelial CCR2 expression as mice expressing CCR2 only in the hematopoietic compartment had significantly fewer tumors within their lungs compared to mice with stromal expression of CCR2. With a genetic approach, using mice that express CCR2 exclusively on endothelial cells (Tie2CCR2/*Ccr2*$^{-/-}$ mice), metastasis could be restored confirming an essential role of endothelial CCR2 expression for tumor cell extravasation. Additionally, using mice with specific depletion of myeloid-derived CCR2 (*LysMCreCcr2*$^{loxP/loxP}$ mice) we could show that lack of CCR2 expression on monocytes did reduce but could not prevent metastasis, further corroborating the involvement of CCR2 expression on both compartments.

In a simplified approach focusing on the step of tumor cell extravasation using primary pulmonary endothelial cells we could confirm the essential role of CCR2 expression on endothelial cells for tumor cell transmigration but also show the importance of monocytes again.

By using the above mentioned *in vitro* model we elucidated that tumor cell extravasation was induced by activation of JAK2-Stat5 and p38MAPK pathways, which turned out to be integrated through CCR2. Stat3, Rac1 or PI3K activation did not turn out to play an important role in CCL2-driven tumor cell extravasation.

Our study identifies two yet undescribed molecular pathways in CCL2 driven tumor cell extravasation that go beyond the role of immune cell attraction by tumor cell-derived chemokines opening new targets for treating CCL2-dependent metastases.

Lymphotoxin's Role in Inflammation-Induced Carcinogenesis

Hepatitis B and C viruses (HBV and HCV) cause chronic hepatitis and hepatocellular carcinoma (HCC) by poorly understood mechanisms. Worldwide, approximately 500 million people are chronically infected with HBV or HCV, leading to a rising incidence of HCC [10]. Involvement of cytokines in chronic hepatitis and HCC was described in the past but no causal link found.

Together with Johannes Haybäck, I could show that cytokines lymphotoxin (LT) α and β and their receptor LTβR are up-regulated in HBV- or HCV-induced hepatitis and HCC. However, other non-viral induced forms of hepatitis seemed to depend on TNF rather than on LTβR-signaling with strong up-regulation of TNFα. Interestingly, up-regulation of LT$\alpha\beta$ was not only seen on immune cells, but also on hepatocytes of HCV and HBV-infected patients. Furthermore, I could show that HCV replication can be triggered by stimulation of LTβR signaling in a non-infectious and an infectious setting *in vitro* and that silencing of LTβR

decreases HCV replication, suggesting a positive feedback loop between LTβR signaling and HCV replication identifying a potential target for therapeutical interventions.

We characterized a mouse model with liver-specific LTαβ over-expression (*tg*1223 mice) and found liver inflammation and HCC linking hepatic LT over-expression to hepatitis and HCC.

Detailed analysis of this mouse model on *mRNA* and protein level revealed alternative expression of various genes at time points at which the liver still lacked any histopathology. At later time points *tg*1223 mice develop chronic hepatitis, modest liver damage and liver cancer. Various tumor markers such as gp73, glutamine synthetase and alpha-fetoprotein were expressed in the HCC of *tg*1223 mice and besides sustained oval cell proliferation was found.

By intercrossing these mice with $Ikk\beta^{\Delta hep}$ mice (mice lacking classical NFκB signaling in hepatocytes) and $Rag1^{-/-}$ mice (mice lacking B- and T-cells), we could show the importance of inflammation and of NFκB signaling in hepatitis-induced HCC development in this mouse model. Intercrossing *tg*1223 mice with $Tnfr1^{-/-}$ mice showed that TNF signaling is not important in this context. By applying LTβR-Ig – an inhibitor of LTβR signaling – we could completely suppress HCC formation and moreover reduced the incidence of hepatitis in LTαβ-transgenic mice.

In this study, we were able to show that sustained LT signaling in mice can be injurious, causing chronic hepatitis and HCC. Enhanced hepatic LTβR signaling might be of potential clinical relevance because LTβR and its ligands are drastically increased in human HBV- and HCV-induced hepatitis and HCC, compared with normal livers or nonviral, benign liver diseases.

3 ZUSAMMENFASSUNG

Überlieferungen zufolge war Hippokrates mit großer Wahrscheinlichkeit der Erste, der den Begriff „Krebs“ verwendet hat, da ihm, als er einen Abszess innerhalb des Brustraumes behandeltet, Ähnlichkeiten zu den Beinen von Krustentieren auffielen. Heute gelten Krebserkrankungen als eine der meistverbreiteten Todesursachen und als Auslöser für 7,6 Millionen Todesfälle im Jahr 2008 (13% aller Todesfälle waren auf Krebserkrankungen zurückzuführen). Die Krebshäufigkeit steigt weltweit an und Prognosen zufolge werden 2030 über 11 Millionen Todesfälle aufgrund von Krebserkrankungen zu erwarten sein. Die meisten Todesfälle, die auf Krebserkrankungen zurückzuführen sind, wurden in Entwicklungs- und Schwellenländern verzeichnet, jedoch steigt die Zahl auch in den Industrienationen stetig an [1].

Der Begriff Krebs umfasst viele verschiedene Krankheitsbilder die alle die Bildung eines Tumors gemeinsam haben, der sich in fast jedem Organ formen kann. Die Überlebenschancen variieren jedoch in Abhängigkeit von dem befallenen Gewebe beträchtlich. Die meisten Patienten sterben aufgrund von Tumoren in der Lunge (1,4 Millionen Todesfälle), gefolgt von Magen- (740000 Todesfälle), Leber- (700000 Todesfälle), Kolon- (610000) und Brustkarzinomen (460000 Todesfälle) [1]. Der Primärtumor ist nur für eine Minderheit der Todesfälle verantwortlich (10% der Patienten), die Mehrheit der Patienten stirbt an Metastasen (90% der Patienten) [4].

Trotz zunehmender Forschungsaktivität auf dem Gebiet der Krebserkrankungen stehen wir erst am Anfang die zellulären und molekularen Mechanismen zu verstehen, die zur Umwandlung normaler Zellen in maligne Zellen führen können.

In meiner Doktorarbeit beschreibe ich zwei Projekte, die sich mit der Rolle von Entzündungsmediatoren (Zytokine und Chemokine) in der Krebsentstehung und Metastasierung befassen.

CCR2 in Tumorzellextravasierung und Metastasierung in der Lunge

Die Metastasierung ist ein vielstufiger Prozess der Tumorzellstreuung, Überleben im Blutkreislauf, Extravasierung und schließlich die Besiedlung entfernter Organe umfasst [3, 4]. Erhöhte Expression des Chemokins CCL2 wurde im Zusammenhang mit einer schlechten Prognose und erhöhtem Tumorwachstum in metastasierendem Brust- Prostata- und Kolonkarzinom beschrieben [5-9]. Vor kurzem publizierte Forschungsarbeiten legen nahe, dass das von der Tumorzelle produziertes CCL2 Ly6C^{hi} Monozyten anlockt und somit die Metastasierung begünstigen kann [5].

Die genauen Mechanismen, wie CCL2-Produktion von Tumorzellen die verschiedenen Schritte der Metastasierung durch Anlocken von entzündungsfördernden Monozyten begünstigen kann, sind weiterhin unbekannt. Außerdem ist die Rolle des zugehörigen Chemokinrezeptors CCR2, der auf einer Vielzahl unterschiedlicher Zelltypen zu finden ist, im Zusammenhang mit Metastasierung nur wenig beschrieben.

Gemeinsam mit Alexandra Hoos konnte ich in einem experimentellen Metastasierungsmodell zeigen, wie CCL2, das von Tumorzellen produziert wird, das Endothel über CCR2 aktiviert und Permeabilität der Blutgefässe hervorruft, die ausreicht um Extravasierung von Tumorzellen auszulösen. In Abwesenheit von CCR2 (in *Ccr2*$^{-/-}$ Mäusen) beobachteten wir eine Verminderung der Metastasierung mit abgeschwächter Permeabilität der Blutgefäße und weniger Interaktion zwischen Tumorzellen und Monozyten, was auf eine Beteiligung der CCR2 Expression in der Metastasierung schließen lässt.

Um die Rolle der CCR2 Expression auf hämatopoetischen und stromalen Zellen zu untersuchen, habe ich Experimente mit Knochenmarksrekonstitutionen durchgeführt, die der endothelialen CCR2 Expression einen wesentlichen Anteil an der Metastasierung zuschreiben. Mäuse, die CCR2 nur auf hämatopoetischen Zellen exprimieren, hatten wesentlich weniger Metastasen in der Lunge als Mäuse, die nur auf stromalen Zellen CCR2 exprimierten. In einem Versuch mit Mäusen, die CCR2 spezifisch auf Endothelzellen exprimieren (Tie2CCR2/*Ccr2*$^{-/-}$ Mäuse), wurde die Metastasierung zum Teil wiederhergestellt, was auf eine wesentliche Rolle der endothelialen CCR2 Expression bei der Tumorzellextravasierung schließen lässt. In zusätzlichen Experimenten mit Mäusen, denen CCR2 auf Zellen myeloischen Ursprungs fehlt (*LysMCreCcr2*$^{loxP/loxP}$ Mäuse), konnten wir eine verminderte Metastasierung beobachten, was die wesentliche Rolle der CCR2 Expression in hämatopoetischen und stromalen Zellen weiter untermauert.

Mit einem vereinfachten Versuchsaufbau, der der Tumorzellextravasierung gleichen soll, konnten wir unter Verwendung primärer Endothelzellen die wesentliche Rolle der endothelialen CCR2 Expression für Tumorzelltransmigration bestätigen und erneut die Wichtigkeit von Monozyten zeigen.

Mit Hilfe des zuvor erwähnten *in vitro* Modells konnten wir nachweisen, dass die Tumorzell-extravasierung durch Aktivierung von JAK2-Stat5 und p38MAPK Signaltransduktionswegen induziert wird. Stat3-, Rac1- oder PI3K-Aktivierung hingegen spielt bei der CCL2-vermittelten Tumorzellextravasierung keine Rolle.

Unsere Studie identifiziert zwei bisher nicht beschriebene Signaltransduktionswege in der CCL2-vermittelten Tumorzellextravasierung, was über die Funktion der Chemokine Immunzellen anzulocken hinaus geht und damit neue therapeutische Angriffsziele gegen CCL2-abhängige Metastasierung bilden.

Die Funktion von Lymphotoxin in entzündungsinduzierter Krebsentstehung

Hepatitis B und C Viren (HBV und HCV) verursachen chronische Leberentzündung (Hepatitis) und hepatozelluläres Karzinom (HCC) durch bisher unverstandene Mechanismen. Weltweit sind ca. 500 Millionen Menschen chronisch mit HBV oder HCV infiziert, was zu einer steigenden Inzidenz von HCC führt [10]. Eine Beteiligung von Zytokinen an der chronischen Leberentzündung

und der Entstehung von HCC wurde bereits beschrieben, aber bisher konnte kein ursächlicher Zusammenhang gefunden werden.

Gemeinsam mit Johannes Haybäck konnte ich zeigen, dass die Zytokine Lymphotoxin (LT) α und β und ihr Rezeptor (LTβR) in HBV- und HCV-induzierter Hepatitis und HCC hochreguliert sind. Hochregulierung von LT$\alpha\beta$ wurde nicht nur auf Immunzellen beobachtet, sondern auch auf Hepatozyten in HBV- oder HCV-infizierten Patienten.

Zusätzlich konnte ich mit einem nicht-infektiösen und einem infektiösen Versuchsaufbau zeigen, dass die Replikation von HCV durch Aktivierung des LTβR Signaltransduktionsweges verstärkt werden kann und das Abschalten der Signaltransduktion durch LTβR die Replikation von HCV vermindert. Diese Daten legen nahe, dass eine positive Rückkopplung zwischen der Signaltransduktion durch LTβR und der HCV Replikation besteht, was ein neues Ziel für einen therapeutischen Ansatz bedeuten kann.

Wir haben ein Mausmodell charakterisiert, in dem LT$\alpha\beta$ spezifisch in der Leber überexprimiert wird (*tg*1223 Mäuse) und beobachteten die Entstehung von Hepatitis und HCC in diesen Mäusen. Diese Ergebnisse deuten auf einen ursächlichen Zusammenhang zwischen LT Überexpression und der Entstehung von Hepatitis und HCC hin.

Die detaillierte Analyse dieses Mausmodells auf RNA und Proteinniveau ergab, dass verschiedenste Gene bereits an Zeitpunkten, an denen noch keine histopathologische Veränderung der Leber erkennbar war, verändert waren.

Zu späteren Zeitpunkten entwickelten die *tg*1223 Mäuse chronische Hepatitis, Leberschaden und schliesslich HCC. Die Tumore von *tg*1223 Mäusen waren positiv für verschiedene Tumormarker wie gp73, Glutaminsynthetase und Alpha-Fetoprotein. Außerdem beobachteten wir anhaltende Proliferation von Ovalzellen. Durch Rückkreuzung dieser Mäuse mit $Ikk\beta^{\Delta hep}$ Mäusen (keine klassische NFκB Signaltransduktion in Hepatozyten vorhanden) und mit $Rag1^{-/-}$ Mäusen (keine Ausbildung von B- und T-Zellen) konnte die Entstehung von chronischer Hepatitis und HCC verhindert werden. Rückkreuzung von *tg*1223 Mäusen mit $Tnfr1^{-/-}$ Mäusen zeigte, dass die Signaltransduktion über TNF in diesem Zusammenhang keine wichtige Rolle spielt. Durch die Anwendung von LTβR-Ig - einem Inhibitor der Signaltransduktion über LTβR – konnten wir die Entstehung von HCC vollständig unterdrücken und außerdem die Hepatitisinzidenz in den LT$\alpha\beta$-transgenen Mäusen verringern.

Mit dieser Studie können wir zeigen, dass anhaltende Signaltransduktion über LTβR schädlich sein kann und zur Entstehung von chronischer Hepatitis und HCC beiträgt. Verstärkte Signaltransduktion über LTβR kann von klinischer Relevanz sein, da LTβR und seine Liganden in HBV und HCV-induzierter Hepatitis und HCC im Patienten verstärkt vorliegen, verglichen mit normalen Lebern und nicht-viraler, gutartiger Lebererkrankung.

4 DEFINITIONS

Cytokines & chemokines

Cytokines are small signaling proteins that regulate immune-mediated signaling through interactions with specific receptors mainly for intracellular communication. This term comprises a large group of immuno-modulating substances, which can be produced by almost every cell type and can be found in either secreted or membrane bound forms. Chemokines are a small family of cytokines, which are usually secreted. They are able to induce chemotaxis, so their name is an abbreviation of “chemotactic cytokines”.

Endothelial cells

A cell type at the interior surface of the blood vessel forming a thin layer between the circulating blood in the lumen and the vessel wall.

Extravasation

One of the rate limiting steps in the metastatic process: The time frame in the dissemination phase of a malignant tumor when tumor cells leave the endothelial vasculature and enter the surrounding tissue and consequently colonize new organs.

Inflammation

A complex biological response of the immune system and vascular tissue to potentially dangerous stimuli like damaged cells, pathogens or other irritants. It means “to set on fire” and is characterized by its basic symptoms such as heat, swelling and redness. Inflammation is a mechanism of the innate immunity, a protective attempt to remove the stimuli and to initiate healing and is therefore non-specific. Inflammation can be either acute or chronic – the acute inflammation is the initial response to the stimuli and in general short and self-limiting. If the inflammatory state is prolonged, it is called chronic inflammation and sustained infiltration of immune cells can lead to tissue destruction and loss of proper function.

Monocytes

A bone marrow-derived cell type of myeloid origin with a relatively short half-life. Monocytes are non-dividing cells. In mice, bone marrow-resident and circulating blood monocytes are defined by their expression of CD115, F4/80, CD11b and CX_3CR1. Two subsets of blood monocytes have been described according to their expression of Ly6C and CX_3CR1 being $Ly6C^{hi}CX_3CR1^{lo}CCR2^{+}$ and $Ly6C^{lo}CX_3CR1^{hi}CCR2^{-}$ blood monocyte subsets. Upon infection, $Ly6C^{hi}$ monocytes migrate from the bone marrow to the peripheral circulation in a CCR2-dependent fashion. Challenged mice therefore often have increased numbers of circulating $Ly6C^{hi}$ monocytes [11].

5 CCR2 IN TUMOR CELL EXTRAVASATION AND LUNG METASTASIS

'Introduction' (in parts), 'Material and Methods', 'Results' and parts of the 'Discussion' are taken from the following manuscript (in preparation):

"Endothelial CCR2 signaling induced by colon carcinoma cells licenses extravasation via the JAK2-Stat5 and p38MAPK pathway"

Monika Julia Wolf[1]*, Alexandra Hoos[2]*, Judith Bauer[3], Steffen Böttcher[4], Markus Knust[5], Achim Weber[6], Nicole Simonavicius[3], Holger Moch[6], Markus Manz[4], Michael Stürzl[7], Roland Croner[7], Manfred Kopf[8], Adriano Aguzzi[1], Manolis Pasparakis[9], Marco Prinz[5], Lubor Borsig[2]*, Mathias Heikenwalder[1,3]*

1 Institute of Neuropathology, University Hospital Zurich, Switzerland

2 Institute of Physiology, University of Zurich, Switzerland

3 Institute of Virology, Technische Universität München/Helmholtz Zentrum München, Munich, Germany

4 Division of Hematology, University Hospital Zurich, Switzerland

5 Department of Neuropathology, University of Freiburg, Germany

6 Insitute of Surgical Pathology, University Hospital Zurich, Switzerland

7 Division of Molecular and Experimental Surgery, University Hospital Erlangen, Germany

8 Institute for Integrative Biology, ETH Zurich, Switzerland

9 Institute of Genetics, Centre for Molecular Medicine (CMMC), University of Cologne, Germany

* These authors contributed equally to this work

5.1 Introduction

5.1.1 Chemokines and the CCL2-CCR2 axis

Chemokines are chemotactic cytokines, being small proteins with a molecular weight of approximately 8-14 kDa. To date, 4 different groups of chemokines are known – the CC, CXC, C and CX_3C families [12], which all differ in the position of the two highly conserved cysteine residues at their N-terminus. Monocytes and T-cells are primarily targeted by CC chemokines, whereas neutrophils are targeted by members of the CXC family [13]. In general, two main functions of chemokines are described – mediation of inflammation and maintenance of homeostasis – both act via similar mechanisms, namely controlling leukocyte migration into and within the tissue [14]. However, the outcome strongly depends on the involved chemokines and is some cases beneficial for and in other cases detrimental to the organism. In the last few years, chemokines have caught the attention of researchers as they were shown to be involved in the pathogenesis of several diseases, such as autoimmune diseases, infectious diseases (e.g. HIV, HCV) and cancer (e.g. in metastasis) [15]. In 1983, CCL2 was the first human CC chemokine to be discovered [16], which is now the most prominent member of the monocyte chemoattractant protein subfamily within the CC chemokines. Five members of this subfamily are known: MCP-1 (CCL2), MCP-2 (CCL8), MCP-3 (CCL7); MCP-4 (CCL13) and MCP-5 (CCL12) [13, 17]. All of them serve as ligands for CC chemokine receptor 2 (CCR2), a G-protein coupled receptor. Binding of one of these ligands to the receptor induces conformational changes which lead to its dimerization [18]. As a consequence, Janus kinase 2 (JAK2) association and activation (phosphorylation) are triggered, necessary for effective G protein coupling to CCR2 [19]. Besides, the JAK/Stat pathway becomes activated. Signal transduction through GRK and arrestins lead to desensitization and internalization. Effector pathways downstream of CCR2 are JAK2, PI3K (phosphoinositol 3-kinase; p85/p110 and C2α), phospholipase C (PLC) and mitogen-activated protein kinase (MAPK) via ERK1, ERK2 and p38, as well as the stress-activated kinase JNK1 being involved in up-regulation of adhesion molecules and chemotaxis [20-24]. Figure 1 summarizes all signaling pathways downstream of CCR2.

Several cell types were shown to produce CCL2, including endothelial, epithelial and smooth muscle cells as well as microglia, fibroblasts, astrocytes and monocytes [13]. Moreover, CCL2 signaling was shown to lead to firm arrest of rolling monocytes on endothelial cells expressing E-selectin [25] and monocyte arrest and transmigration on inflamed endothelium [26]. Various kinds of tumor cells were shown to produce CCL2 [27]. Several studies showed that CCL2 expression levels correlate with tumor aggressiveness in various types of cancer such as prostate [28-30] or breast cancer [31-34]. However, up to date, it is not known, which cell types are the main producers of CCL2 within the tumor microenvironment [27] and what exact role CCR2 activation plays in tumor cell extravastion and growth.

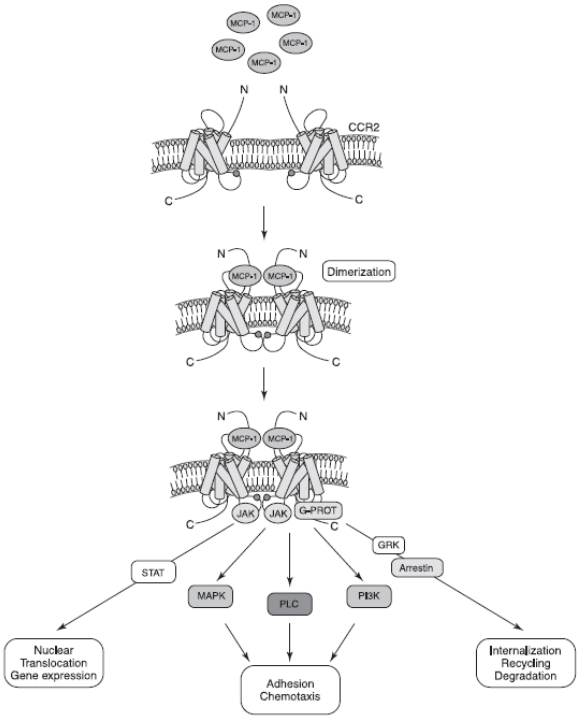

Figure 1: Schematic representation of signaling pathways activated through CCR2 [35]. Binding of the ligand induces dimerization of CCR2 and enables activation of the G-coupled protein receptor. JAK2 becomes activated and one of the several downstream effector pathways, such as Stat, MAPK, PLC or PI3K signaling will be triggered. CCR2 signaling can be terminated via GRK and arrestin.

In 1997, three research groups reported the generation of mice lacking CCR2 [36-38]. In all three cases, mice appeared to have a normal phenotype; however, upon challenge with pro-inflammatory stimuli, defects due to the lack of CCR2 became obvious: Kuziel *et al.,* reported severe reduction in leukocyte firm adhesion to microvascular endothelium and monocyte extravasation in *Ccr2*$^{-/-}$ mice. After thioglycollate injection they could observe that resolution of inflammatory responses can be independent of macrophage influx and the CCR2-mediated activation of peritoneal macrophages, meaning that CCR2 is essential for macrophage trafficking *in vivo* [38]. Boring *et al.,* could show that *Ccr2*$^{-/-}$ mice have an impaired monocyte migration and a reduced type 1 (T_H1) cytokine response by confirming the results from Kuziel *et al.,* and showing that the size of granulomas is reduced in these mice as well as interferon γ (IFNγ) production in draining lymph nodes. Therefore, they concluded that *Ccr2*$^{-/-}$ mice have a delayed type hypersensitivity response and production of T_H1 type cytokines [36]. Last but not least, Kurihara *et al*., reported defects in macrophage recruitment and host defense in *Ccr2*$^{-/-}$ mice by showing that these mice could not recruit macrophages in an experimental peritoneal inflammation model and that they were unable to clear infection (*Listeria monocytogenes*) [37].

In 1998, Lu *et al.,* reported the generation of mice lacking CCL2 expression. Similar to *Ccr2*$^{-/-}$ mice, *Ccl2*$^{-/-}$ mice showed abnormalities in monocyte recruitment and cytokine expression as tested by thioglycollate administration. Also in these mice, the accumulation of macrophages at the site of inflammation was altered and after induction of granulomas the expression of interleukin 4 (IL4), IL5 and IFNγ was reduced. However, in comparison to C57BL/6 mice, *Ccl2*$^{-/-}$ mice did not show any differences in the capacity to clear infections (with *Mycobacterium tuberculosis*) [39].

Due to intense research with *Ccr2*$^{-/-}$ mice in the past years, it was finally discovered in 2006 that CCR2 is indispensable for the emigration of Ly6C^{hi} monocytes from bone marrow (BM) and therefore *Ccr2*$^{-/-}$ mice have strongly reduced numbers of circulating Ly6C^{hi} monocytes. However, CCR2 is not needed for the trafficking of monocytes from the circulation into tissue. Furthermore, *Ccr2*$^{-/-}$ mice show an increased accumulation of activated monocytes in BM upon infection (with *Listeria monocytogenes*) suggesting that CCR2 signaling within BM is solely needed for the release of Ly6C^{hi} monocytes into the blood [40].

5.1.2 Tumor cell metastasis into the lung

Tumors can be found in various tissues and are classified as benign or malignant tumors. Benign tumors only grow locally and do not invade adjacent tissue. Malignant tumors however can invade surrounding tissues and form secondary tumors throughout the body [41]. Those secondary tumors are termed metastases – a word derived from ancient Greek meaning "displacement" and describing the spread of tumor cells from the primary tumor to various sites within the body.

The metastatic process is a multi-stage process with fatal outcome as it is the leading cause of cancer-related death in humans. Approximately 90% of all cancer-related deaths are due to metastatic spread to vital organs, whereas only about 10% of all deaths are conditioned by primary tumors [2]. Therefore, understanding the mechanisms driving metastasis is required for potential therapeutic intervention. Yet, metastasis is a highly inefficient process due to the complexity of the different steps involved. This might explain why only a small fraction of the large numbers of cells disseminating from the primary tumor finally result in the growth of metastases [42]. But at which sites of the body can metastatic tumor growth be observed? The location of the metastatic sites varies among different primary tumors. Stephen Paget proposed already more than 120 years ago that disseminated cancer cells (which he called "seeds") would only colonize organs where a specific microenvironment ("soil") is present that would be compatible to their growth [43]. Recently, studies suggested that a gene expression pattern in the primary tumor mediates metastasis [44] and that tumor cells can influence distal organs by inducing changes in the microenvironment prior to colonization [45]. However, the exact mechanisms how the metastasis-supporting niche is created are only bit by bit revealed and it is very likely that many different processes work together.

Figure 2 represents the metastatic cascade including all steps that tumor cells have to undergo in order to form metastasis at various sites of the body.

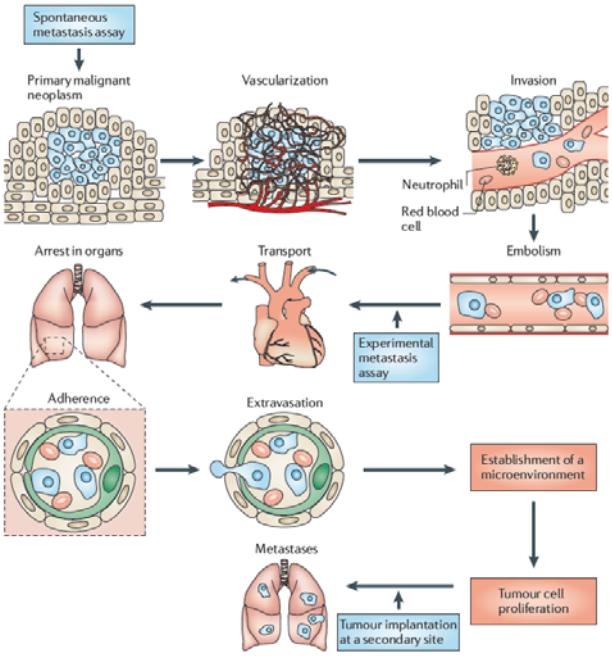

Figure 2: The metastatic cascade. Six distinct steps essential to tumor growth at distal sites in the body (e.g. in the lung) are depicted [46]. Vascularization of the primary tumor, invasion into and transport via blood vessels, arrest in organs (adherence), extravasation into the parenchyma of various organs and ultimately colonization and subsequent growth are considered as main steps which lead to the growth of metastases at distant sites in the body.

In a process called angiogenesis new blood vessels start to grow within the tumor, thereby assuring its supply with nutrients via the blood stream. When a certain size/mass is reached, single tumor cells can leave the primary tumor by invading either these newly formed blood vessels or the lymphatic system. If these cells manage to survive in the circulation where they can encounter different forms of stress, they are transported via the blood or the lymph flow to distant sites, where they may be captured in organs and adhere at the wall of the vessel. In the subsequent step, which is called extravasation and is considered to be one of the rate-limiting steps of the metastatic process [44], tumor cells can leave the vessel and move into the surrounding tissue. Thus, if a suitable microenvironment is formed tumor cells start to proliferate and colonize organs resulting in metastases in various sites of the body [3, 4, 41].

The lung is an organ commonly affected in patients with metastatic disease, partly because the whole cardiac blood flow circulates through the lung-capillary network [44]. Tumor cells can easily be captured and adhere to cell walls in the capillaries of the lung which are small vessels with many branchings. Many different types of primary tumors form metastases in the lungs, including breast cancer, gastrointestinal tumors, melanoma, sarcoma and kidney cancer [44].

Figure 2 also summarizes the different mouse models available for studying metastasis (blue boxes). Depending on the tumor of interest, various tumor cell lines can be used and injections or implantations are made at different sites of the body. Many of them are used for studying metastatic disease in the lung. For spontaneous metastasis assays, tumor cells are implanted (e.g. in peripheral sites), a primary tumor is established and metastatic spread to distant sites can be followed. In experimental metastasis assays, no primary tumor is found, tumor cells are

intravenously injected (directly into the blood stream) and extravasation and subsequent tumor growth can be studied. Furthermore, tumor implantation at secondary sites allows study of metastatic growth [46].

5.1.3 The microenvironment and the immune system in metastasis

Tumor cell extravasation and outgrowth are considered to be the limiting steps in metastasis [44]. The tumor cell microenvironment has been recognized to significantly influence both, tumor growth and metastatic dissemination [45]. A variety of stromal cell types were found within tumors, including endothelial cells, pericytes and fibroblasts which have been associated with cancer progression [45, 47]. However, BM-derived cells, including macrophages, mast cells, neutrophils, myeloid cell-derived suppressor cells and mesenchymal stem cells were also shown to contribute to tumor promotion [45]. Tumor-associated macrophages are the major population detected at primary tumor sites while myeloid-derived and/or inflammatory monocytic cells make up the major part of stromal cells in metastatic lesions [48, 49]. Myeloid-derived monocytes and macrophages were shown to facilitate tumor cell extravasation and metastatic outgrowth [48, 49]. Host-derived as well as tumor cell-derived cytokines and chemokines actively shape the tumor microenvironment by recruitment of leukocytes and activation of pro-inflammatory mediators [50]. In a screen for tumor promoting cytokine release by myeloid cells, conditioned medium from highly metastatic vs. non-metastatic cancer cell lines was used and it could be shown that highly metastatic cancer cell lines induce the expression of tumor promoting cytokines (such as tumor necrosis factor α (TNFα) and IL6) in BM-derived macrophages via toll-like receptor (TLR) 2 and TLR6 [51]. With this study it became obvious how tumor cells can manipulate the host immune system to induce a microenvironment beneficial for metastatic growth. Moreover, chemokines and chemokine receptors were found to be involved in metastasis and also represent direct targets of oncogene activation [52, 53].

The sources of chemokine expression were postulated to be endothelial cells, infiltrating leukocytes and tumor cells themselves, both, at primary tumors and metastatic sites [50, 54, 55]. Indeed, local activation of the endothelium by metastasizing tumor cells is associated with enhanced production of the chemokine CCL5. This led to enhanced recruitment of monocytes during the initial phase of metastasis, while inhibition of this CCL5-dependent monocyte recruitment strongly attenuated metastasis [56].

Recently, another inflammatory chemokine, CCL2, has been identified as the major factor affecting breast cancer metastasis to the lung [5].

Elevated levels of CCL2 and CCL5 have been detected at primary as well as metastatic sites in various cancers including breast, colon, prostate and cervix and correlated with poor prognosis

due to metastatic progression [6, 8, 9, 57]. Monocytes recruited to tumors through the CCL2-CCR2 chemokine axis polarized to an alternatively activated M2-phenotype of macrophages that contributes to immune-suppression, enhanced tumor cell survival and angiogenesis [57-59]. CCL2 has been shown to induce angiogenic activation of endothelial cells along with an inflammatory response [60] and CCL2-mediated recruitment of inflammatory monocytes promoted metastasis [5]. Accordingly, treatment of mice carrying tumors with CCL2-neutralizing antibody significantly increased survival due to inhibition of metastasis [5, 60]. Other studies using CCL2-neutralizing antibody report retarded tumor growth due to decreased macrophage infiltration and decreased microvascular density [61] as well as reduction of metastatic tumor burden in mouse models of metastatic prostate cancer [59, 62]. Although, elevated CCL2 expression is clearly linked to metastasis through the recruitment of monocytes and macrophages, the exact mechanisms how CCL2 signaling facilitates tumor cell extravasation at the endothelial barrier and subsequent metastatic colonization remain elusive.

5.2 Scientific aims

Increased expression of CCL2 was shown to correlate with poor prognosis and increased tumor burden in metastatic breast, prostate and colon cancer. Recent results suggest that tumor cell-derived CCL2 attracts Ly6C^{hi} monocytes which were shown to facilitate metastasis. However, the exact mechanisms how CCL2 expression by tumor cells can enable metastasis remain elusive.

The goal of this project was to assess whether tumor cell-derived CCL2 has additional functions apart from the attraction of immune cells in metastasis and to investigate whether also other CCR2 expressing cells (e.g. radio-resistant cells) contribute to the CCL2-driven induction of tumor cell metastasis.

5.3 Material and methods

5.3.1 Mice

Animals were maintained under specific pathogen-free conditions and experiments approved and conform to the guidelines of the Swiss Animal Protection Law, Veterinary Office, Canton Zurich. C57BL/6 and *Ccl2*$^{-/-}$ mice were purchased from The Jackson Laboratory, *Ccr2*$^{-/-}$ mice [36] were either purchased from The Jackson Laboratory or obtained from Marco Prinz [38]; Tie2CCR2/*Ccr2*$^{-/-}$ [63] were also received from Marco Prinz; *LysMCreCCR2*$^{loxP/loxP}$ mice were received from Manolis Pasparakis and BacCCR2CFP [64] from Eric Pamer were bred in house.

5.3.2 Bone marrow reconstitutions

C57BL/6 and *Ccr2*$^{-/-}$ mice were used to generate BM chimeras. Recipient animals were irradiated with 900 rad in one dose and reconstituted by i.v. injection of purified BM cells (isolated from femur and tibia). Reconstitution efficiency was assessed by flow cytometry for CCR2^{+}Ly6C^{hi} cells in the blood 6-7 weeks after reconstitution and before injection of tumor cells.

5.3.3 Cell lines

Mouse colon carcinoma cell line MC-38 stably expressing GFP (MC38-GFP) [65], naive MC-38 and mouse melanoma cell line B16-BL6 [66, 67] were grown in DMEM supplemented with 10% FCS. Lewis lung carcinoma cells (3LL) were grown in RPMI supplemented with 10% FCS [54]. MC-38GFP with low level expression of CCL2 (MC-38GFP^{CCL2kd}) was generated by viral transduction with shRNA lentivirus construct (Sigma NM_002982). Tumor cells were seeded on 24-well plates ($3x10^4$) until 50% confluence and incubated with lentivirus for 16 hrs. Cells were passaged after 48 hrs and plated into 6 well plates in the presence of puromycin (10µg/ml). Three days later, cells were split again and the knock-down efficiency was determined by quantitative PCR and immuno-blotting. Lentivirus containing a scrambled shRNA construct was used for preparation of control cells (MC-38GFP^{scr}).

5.3.4 Experimental metastasis model

Mice were i.v. injected with syngeneic MC38-GFP^{+} cells ($3x10^5$) and metastasis was evaluated after 28 days. Metastatic foci were counted, macroscopic pictures of lungs were taken and tumor load was quantified by green fluorescent protein (GFP) measurement in lung homogenates [65]. For experiments using 3LL and B16-BL6 cell lines, $1.5x10^5$ cells were i.v. injected and the number of tumor foci was quantified on day 12 or day 14 days p.i. respectively.

5.3.5 Histology, immunohistochemistry and electron microscopy

Paraffin sections (2µm) of lungs were stained with Hematoxylin/Eosin or various antibodies. Paraformaldehyde (4%) fixed and paraffin embedded lung tissue was incubated in Ventana buffer and staining was performed on a NEXES immunohistochemistry robot (Ventana instruments, Switzerland) using an IVIEW DAB Detection Kit (Ventana) or on a Bond MAX (Leica). Antibodies against murine $B220^+$ B-cells (Pharmingen; 1:400), F4/80 (Serotec, 1:50) for macrophages, $CD3^+$ T-cells (clone SP7, Neomarkers; 1:300) were kindly provided by R. Zinkernagel [68]. Anti-GFP (Fitzgerald Industries International, clone 20R-GR011; 1:1000) antibody was used as tumor marker to visualize MC-38GFP. Ki67 (NeoMarkers Code RM-9106-S; 1:200) stained proliferating tumor cells and lymphocytes. Image acquisition was performed on an Olympus SZX12, equipped with a JVC digital camera (KY-F70; 3CCD) using Analysis software.

For electron microscopy, sections from epon-embedded, glutaraldehyde-fixed lungs were cut and stained with toluidine blue. The tissue was then trimmed and ultrathin cross sections of the lung were cut and treated with uranyl acetate and lead citrate as described previously [69]. Electron micrographs were analyzed for cell composition and localization using the analySIS Docu System (Soft Imaging System GmbH, Germany).

5.3.6 Endothelial cell stainings

Cryosections (5µm) were thawed and fixed in 4% paraformaldehyde for 20 mins at room temperature. Slides were incubated with 5µg/ml anti-CD31 antibody (MEC 13.3; BD Biosciences) followed by 2µg/ml Alexa594-conjugated anti-rat IgG (Molecular Probes). Nuclei were counterstained with Hoechst. Images were captured on an Olympus BX53 microscope fitted with an Olympus DP72 camera and processed with cellSens Dimension 1.4.1 software.

5.3.7 Flow cytometry analysis

Blood and lung cell samples were prepared at 4°C in buffer solution (PBS containing 2% FCS and 2mM EDTA) and stained against Ly6C, F4/80 (both eBioscience), CD45, CD19, CD4, CD8, Ly6G, NK1.1 (all BD Biosciences) and/or CCR2 [70].

For flow cytometry analysis of mononuclear cells in lung tissue, mice were perfused with PBS and lungs were removed, minced and subsequently digested under shaking conditions for 1 hr at 37°C in 2mg/ml Collagenase D (Roche). Cells were separated using 40µm cell strainers. For the analysis of blood samples, erythrocytes were lysed with BD FACS lysing solution and cell suspensions were analyzed on a FACS Calibur and FACS Canto II (BD Biosciences). Data were acquired using Cell Quest software version 6.0 (FACS Calibur) and FACS Diva software

v6.1.3 (FACS Canto II) analyzed using Flow Jo (v7.6 for FACS Calibur data and v8.8.4 for FACS Canto II data). For the analysis of spleen and BM samples, spleens were minced and BM was isolated from tibia and femur and cells were stained as described above.

5.3.8 RNA isolation and real time PCR

RNA isolation: Total RNA from flash-frozen PBS-perfused lungs, colon from C57BL/6 mice and cell pellets was isolated using RNeasy Mini Kit (Qiagen). The quantity and quality of the RNA was determined spectroscopically using a nanodrop (Thermo Scientific). Purified RNA was reversely transcribed into cDNA using Quantitect Reverse Transcription Kit (Qiagen) according to the manufacturer's protocol.

Real-time PCR: For *mRNA* expression analysis real-time PCR was performed using Fast Start SYBR Green Master Rox (Roche). Primers were custom made by Microsynth. Real-time PCR was performed on an ABI PRISM 7900 HT Fast Real-Time PCR System (AB). Data were generated and analyzed using SDS 2.4 and RQ manager 1.2 software.

mRNA expression levels were normalized to the housekeeping gene *Gapdh*. For RT-PCR, *β-actin* served as a housekeeping gene and samples were run on a 2% agarose gel and images were acquired using red gel imaging system from Alpha Innotech with Pronto software.

For human samples, *GAPDH* and *β-ACTIN* served as housekeeping genes and *CCL2* expression levels were determined using the following primers: CCL2-FWD: 5'-GAA GCT CGC ACT CTC GCC TCC-3' and CCL2-REV: 5'-TGA GCG AGC CCT TGG GGA ATG A-3'

5.3.9 Isolation of pulmonary endothelial cells

Pulmonary endothelial cells were isolated using a positive immuno-magnetic selection as described previously [71]. Briefly, perfused lungs were removed, minced and digested in 0.1% collagenase A (Roche). A single-cell suspension was generated by passing the digested lungs through 100μm and 40μm cell strainers (BD Falcon). Cells were incubated with FITC labeled anti-CD31 antibody (Invitrogen) for 30 mins. Anti-rat IgG beads (Miltenyi Biotec) were added to the cells and incubated for 15 mins, followed by magnetic separation. The purity of isolated endothelial cells was determined by flow cytometry and isolated endothelial cells were cultured in gelatin-coated 6-well plates in medium containing endothelial cell growth supplement (BD Biosciences).

5.3.10 Tumor cell survival

Cryosections (8μm) of lungs were prepared at different time points after i.v. injection of MC-38GFP cells as described previously [72]. Lung sections were stained with DAPI and the number of surviving GFP^+ tumor cells was counted per view field at 40x magnification.

5.3.11 Tumor cell extravasation assay

Mice were i.v. injected with MC-38GFP cells and after 24 hrs lungs were perfused with PBS followed by perfusion with 100μg tomato lectin conjugated with Texas red (Vector Laboratories). After 10 min, lungs were again perfused with PBS, fixed and frozen as described previously [72]. Frozen lung sections (8μm) were stained with DAPI. Three-dimensional images were captured with a SP5 confocal microscope (Leica) of total 5μm in a z-section and were further analyzed with Imaris software (Bitplane). The contact area of tumor cells with the tomato lectin-stained vasculature was determined.

5.3.12 Vascular permeability assay

Permeability of the lung microvasculature was determined by the Evans blue dye extravasation technique [73]. Briefly, mice were injected with tumor cells as described above. After 24 hrs, 2mg of Evans blue were i.v. injected followed by euthanasia 30 min later. In experiments using inhibitors of various signaling pathways [AG490 and SB202190 (Sigma), NSC23766 (Calbiochem), S3I-310 and Stat5 inhibitor (Santa Cruz)], inhibitors were i.p. injected 1 hr before tumor cell injection and 5 hrs post-tumor cell injection at concentrations of 10-25mg/kg. Lungs were perfused with PBS, dissected, photographed and homogenized. Evans blue was extracted by incubation with formamide at 60°C for 18 hrs. The Evans blue concentration in the lung homogenates was measured spectrophotometrically (absorbance at 620 nm).

5.3.13 Analysis of leukocyte-tumor cell association

Cryosections (8μm) prepared from lungs of mice i.v. injected with MC-38GFP cells, were stained with following antibodies: CD11b (BD Biosciences) for myeloid cells, Ly6G (BD Biosciences) for neutrophils, F4/80 (AbD Serotec) for macrophages/monocytes, biotinylated Ly6C (BD Biosciences) for inflammatory monocytes. Alexa568-conjugated anti-rat antibody or Streptavidin-Alexa568 (Invitrogen) was used for the visualization of signals with a fluorescence microscope (Zeiss). Nuclei were stained with DAPI. Tumor cells were counted and the percentage of tumor cells associated with leukocytes was determined.

5.3.14 Adoptive transfer

Monocytes derived from C57BL/6 mice were prepared by conditional derivation of primary BM progenitors as described previously [74]. Differentiated monocytes were characterized by expression of F4/80, CD11b and Ly6C staining (L. Borsig, unpublished data)

In vitro-differentiated monocytes were labeled with PKH26-Red Fluorescent Cell Linker (Sigma), and $2x10^5$ labeled cells were infused i.v. 6 hrs post tumor cell injection (MC38GFP). After 15 hrs

mice were terminated, lungs were perfused with PBS and frozen as previously described [72]. Frozen lung sections (8μm) were stained with DAPI. The extent of tumor cell association with macrophages was visualized with a SP5 confocal microscope (Leica) and quantified.

5.3.15 Cytokine protein array

For cytokine expression pattern of cell lines, Proteome Profiler arrays (mouse cytokine array panel A; R&D Systems) were used according to the manufacturer's protocol. In brief, flash frozen cell pellets were lysed in buffer containing 20mM Tris HCl pH 8.0, 137mM NaCl, 2mM EDTA and 1% NP40. Protein concentration was determined using BCA protein assay reagent (Thermo Scientific) and 50μg protein was used for each protein array. Membranes were developed using SuperSignal West Pico Chemiluminescent Substrate (Thermo Scientific) on Min-R 2000 films (Kodak) and quantified using Aida software (Raytest).

5.3.16 Isolation of bone marrow monocytes

Long bones from 6-8 week old mice were flushed with PBS containing 2% FCS and 2.5mM EDTA. Red blood cells were lysed using ammonium chloride solution. BM-nucleated cells were pre-enriched by magnetic activated cell sorting (MACS) using biotinylated M-CSFR antibody (clone AFS98, Biolegend) and streptavidin-conjugated magnetic beads (Miltenyi Biotec). Following staining with Gr-1 (Ly6G) monoclonal antibody conjugated to phycoerythrin and streptavidin-allophycocyanin (eBioscience), BM monocytes were sorted as M-CSFR^{+}Gr-1^{int} cells using a FACSAria III cell sorter (BD Biosciences).

5.3.17 Transendothelial migration assay

Primary lung microvascular endothelial cells ($3x10^4$) were seeded on gelatin-coated 24-well transwell inserts (8μm pores; BD) and allowed to grow to confluence for 2 days. Tumor cells ($2x10^4$) were seeded into transwell inserts with or without monocytes ($1x10^5$) in 5% FCS/RPMI in the upper chamber and 10% FCS/RPMI in the lower chamber. After 16 hrs of co-culture, the upper side of the insert was scraped off and the insert was fixed in 3% paraformaldehyde. The transwell membrane was removed and mounted on a slide. Tumor cells on the lower side of the membrane as well as in the lower wells were analyzed with a fluorescence microscope (Zeiss).
For inhibitor studies AG490 (8μM final concentration), NSC23766 (20μM), SB202190 (10μM), S3I-201 (50μM), Wortmannin (1μM) and Stat5 inhibitor (100μM) were added to the culture media in the upper and the lower chamber of the 24-well plates. All experiments were performed in duplicates and repeated several times.

5.3.18 Western blot analysis

Lung homogenates (10%) were prepared in RIPA buffer (50mM Tris; 1%NP40; 0.25% Deoxycholic acid sodium salt; 150mM NaCl; 1mM EGTA) containing Halt Protease and Phosphatase Inhibitor Cocktail (Thermo Scientific) and quantified with a BCA protein assay kit (Thermo Scientific) according to the manufacturer's manual. 50μg protein were denatured in Laemmli buffer containing 5% β-mercaptoethanol and separated by gel electrophoresis on a 8% or 11% Tris-glycine SDS-PAGE with Tris-glycine running buffer and blotted with a semi-dry blotting system (Trans-Blot SD cell, Biorad) onto a nitrocellulose membrane (Protran BA 85 pore size 0.45μm; Whatman). After blotting the membrane was blocked in 5% BSA-TBST for 2 hrs at RT. Primary antibodies pJak2, Jak2, phospho-p38, p38, pStat5 and Stat5 (all Cell Signaling, 1:1000 dilution) were incubated at 4°C over night under shaking conditions. Incubation with the secondary antibody (HRP-anti rabbit IgG, 1:5000; Promega) was performed under shaking conditions for 1 hr. Detection was achieved with Supersignal West, chemiluminescent substrate (Pierce) using Stella 3200 imaging sytem (Raytech). To assure equal loading, the membranes were re-probed with anti-GAPDH antibody (Chemicon) and detected as described above.

5.3.19 *In vivo* cell depletion

For depletion of $CCR2^{+}Ly6C^{hi}$ cells, 20μg MC21 antibody [70] was i.v. injected into C57BL/6 mice 24 hrs prior to MC-38GFP injection and every 24 hrs for the first 3 dpi of MC-38GFP tumor cells. On the day of tumor cell injection blood was checked for the presence of $CD11b^{+}Ly6C^{hi}$ monocytes. For depletion experiments using diphtheria toxin (DT; Calbiochem), 10ng DT per g bodyweight were i.p. injected every 24 hrs for the first 4 days post tumor cell injection and one day prior. Inhibitor treatments: JAK2 inhibitor (AG490) and p38 inhibitor (SB202190) were injected every 24 hrs at 15mg/kg or 12mg/kg bodyweight for the first 3 days post tumor cell injection as well as 6 hrs prior to tumor cell injection.

5.3.20 Resection of human colon tumor tissue

Patients with colon carcinomas stage UICC I (n=10), II (n=10), III (n=10) and IV (n=9) were selected from the Erlangen Registry for Colorectal Carcinomas (ERCRC). The regulations of the local ethics committee of the clinical center Erlangen were obeyed.

Tumors with a distance of at least 16cm proximal the anal verge measured with a rigid endoscope were classified as colon carcinomas. Cases arising from a history of inflammatory bowel disease or hereditary syndromes (e.g. familial adenomatous polyposis) were not included. Uninvolved colon tissues (n=4) at least 10cm distant from the tumor site were harvested as controls. The patients underwent colon resection with a standardized regional

lymph node dissection. This technique and standard oncological colon resections performed in our institution are described elsewhere [75]. Adjuvant or palliative treatment was carried out following the current German guidelines for colorectal carcinomas [76].

5.3.21 RNA isolation from human colon tumor tissue

RNA was isolated using a fully automated extraction method from FFPE tissue (Tissue Preparation System with VERSANT Tissue Preparation Reagents, Siemens Healthcare Diagnostics, Tarrytown, NY) has been described previously [77]. In brief, 5μm paraffin sections were directly subjected to automated total nucleic acid extraction. Samples were heat-lysed in 150μL FFPE buffer at 80ºC for 30 mins with shaking. After cooling, enzymatic lysis was carried out at 65ºC for 30 mins with proteinase K. Any residual tissue debris was removed by nonspecific binding to silica-coated iron-oxide beads and subsequent magnetic separation. Deparaffinized and clarified lysates were transferred to new tubes and nucleic acids were bound to fresh silica-coated beads under chaotrophic conditions. Beads were washed 3 times and total nucleic acids were eluted with 100μL of elution buffer at 70ºC followed by an automated DNase I digestion.

5.3.22 Statistical analysis

Statistical analysis was performed with the GraphPad Prism software (version 4.0). All data are presented as mean ± SEM and were analyzed by ANOVA with the post-hoc Bonferroni multiple comparison test, unless specified differently. Analysis of two samples was performed with Student *t* test.

5.4 Results

5.4.1 CCR2 promotes metastasis of syngeneic colon carcinoma cells

We first investigated whether tumor cell extravasation and growth depend on CCR2 and are therefore altered in lungs of *Ccr2*$^{-/-}$ compared to C57BL/6 mice. Twenty-eight days post injection (dpi) of syngeneic GFP^{+} colon carcinoma cells (MC-38GFP), lungs of C57BL/6 mice were displaced with tumor foci. In contrast, significantly less or no tumors could be detected in lungs of *Ccr2*$^{-/-}$ mice on macroscopic level. Development of tumors in lungs of mice depended on CCR2 expression levels of the recipient host. *Ccr2*$^{+/-}$ mice showed a CCR2 expression level within lung tissue that is on average 30% of the expression level found in lungs of C57BL/6 mice and displayed significantly less lung tumors than C57BL/6 ($p<0.001$) but significantly more than *Ccr2*$^{-/-}$ mice ($p<0.5$). This was confirmed by quantification of relative GFP fluorescence in lung homogenates of C57BL/6, *Ccr2*$^{+/-}$ and *Ccr2*$^{-/-}$ mice (Figure 3).

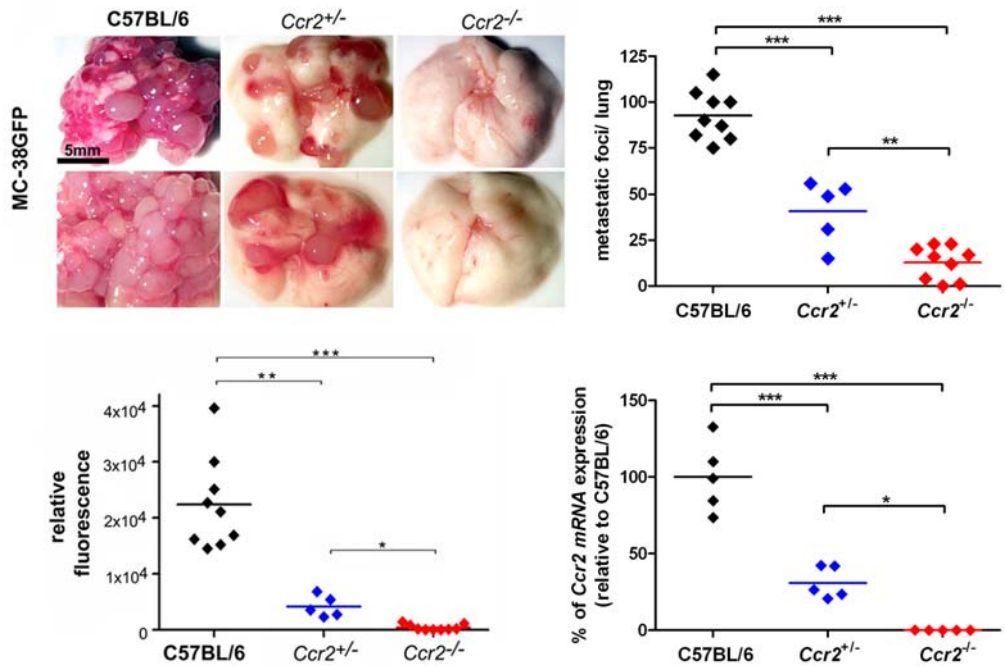

Figure 3: *Ccr2*$^{-/-}$ mice show altered tumor growth upon injection with MC-38GFP cells. Macroscopy of lungs of C57BL/6, *Ccr2*$^{+/-}$ and *Ccr2*$^{-/-}$ mice 28 dpi with MC-38GFP (upper left panel). Quantification of macroscopically visible tumor foci in lungs of all genotypes (left: C57BL/6, n=9; middle: Ccr2$^{+/-}$, n=5; right: Ccr2$^{-/-}$, n=9; upper right panel). Quantification of tumor load by measurement of relative GFP fluorescence in lung homogenates of all three genotypes at 28 dpi (lower left panel). Relative *mRNA* expression of CCR2 in C57BL/6 (n=5), Ccr2$^{+/-}$ (n=5) and Ccr2$^{-/-}$ (n=5) mice normalized to C57BL/6 levels (lower right panel). Statistical significance: ***=$p<0.001$; **=$p<0.01$; *=$p<0.05$.

Immunohistochemical analysis on paraffin-sections prepared from lungs derived from C57BL/6 and *Ccr2*$^{-/-}$ mice 28 dpi with MC-38GFP cells revealed no obvious differences in the relative composition of Ki67^{+}, CD3^{+}, F4/80^{+} and B220^{+} cells within the tumors (Figure 4).

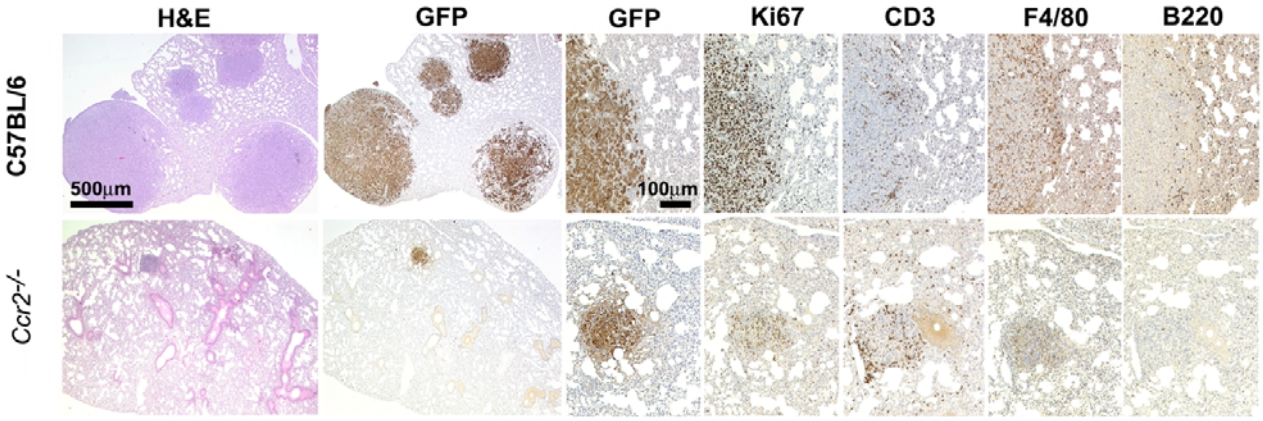

Figure 4: Histological analysis of colon carcinoma (MC-38GFP$^+$) tumors in C57BL/6 and *Ccr2*$^{-/-}$ lungs. Low and high magnifications (scale bars) are indicated. H&E: Hematoxylin-Eosin, Ki67 stains for proliferating cells, CD3 stains for T-cells, F4/80 for monocytes and macrophages, B220 for B-cells.

Next, I studied the immune cell composition in lungs of C57BL/6 and *Ccr2*$^{-/-}$ mice in order to find out whether potential differences could underlie the afore mentioned phenotype. I investigated the presence and composition of cells of hematopoietic origin in lung tissue derived from naïve C57BL/6 or *Ccr2*$^{-/-}$ mice using flow cytometry analysis. As expected, lungs of C57BL/6 or *Ccr2*$^{-/-}$ mice did not reveal significant differences in the numbers of CD4$^+$ or CD8$^+$ T-cells, CD19$^+$ B-cells, CD45$^+$NK1.1$^+$ NK cells and F4/80$^+$ macrophages (Figure 5).

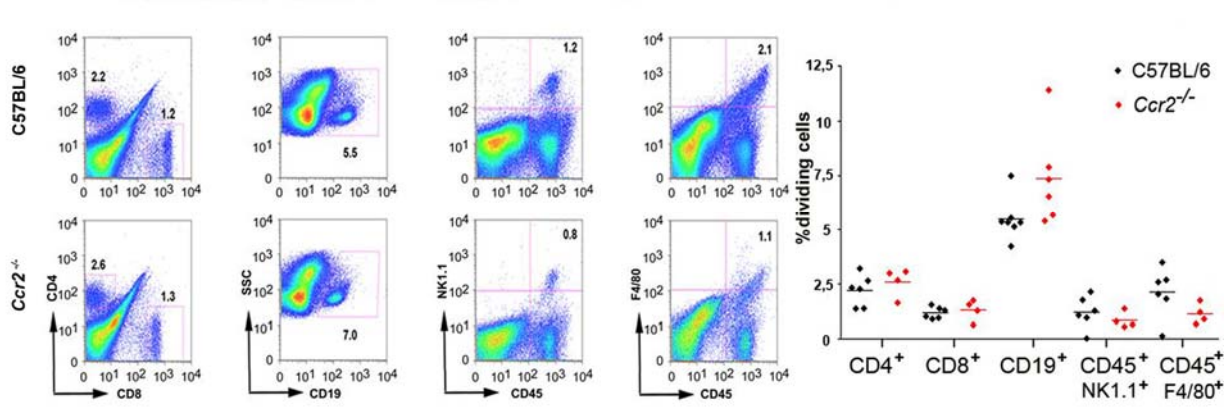

Figure 5: Flow cytometry analysis of various immune cell types in naïve lungs of C57BL/6 and *Ccr2*$^{-/-}$ mice. No significant differences were found in the numbers of CD4$^+$ and CD8$^+$ T-cells, CD19$^+$ B-cells, NK1.1$^+$ NK cells or F4/80$^+$ macrophages in *Ccr2*$^{-/-}$ (lower row) when compared to C57BL/6 (upper row) lungs. Representative FACS plots (left) and quantification of results (right panel) are shown. Each symbol represents one individual mouse (n=4-7).

For studying the presence of monocytic cells in lung tissue of C57BL/6 or *Ccr2*$^{-/-}$ mice in detail, I used the following gating strategy (Figure 6). This allowed determination of the numbers of Ly6C^{hi} cells and Ly6G$^+$ cells as percentage of CD11b$^+$ cells by flow cytometry in lung tissue and peripheral blood.

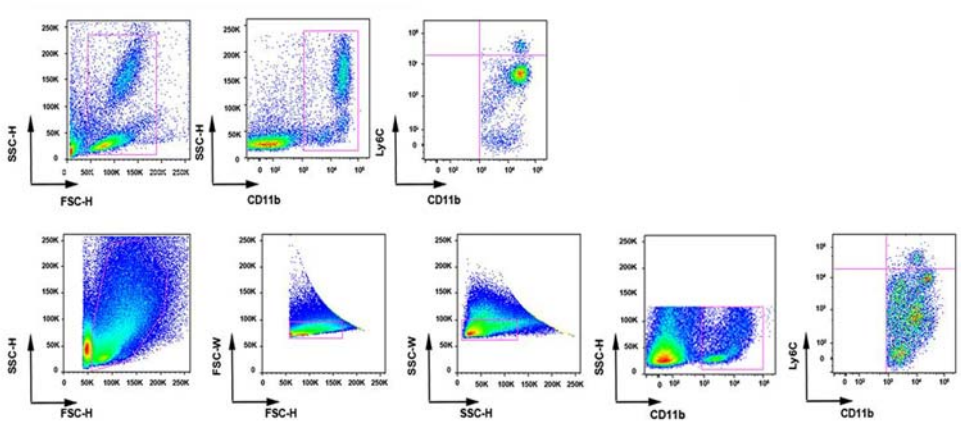

Figure 6: Gating strategy used for the flow cytometric analysis of CD11b^{+}Ly6C^{hi} cells in peripheral blood (upper panel) and lung tissue (lower panel). Cells of interest were located in the live cell gate and were characterized by the expression of CD11b and Ly6C and were negative for Ly6G.

As indicated in the literature, the presence of monocytic cells is altered in blood of *Ccr2*$^{-/-}$ mice compared to C57BL/6 mice. Therefore I investigated, whether this reduction is also present in lung tissue. *Ccr2*$^{-/-}$ mice display a significant reduction of CD11b^{+}Ly6C^{hi}Ly6G^{-} monocytes in lungs (further denoted as Ly6C^{hi}) [78] ($p<0.001$) and a significant, relative increase of CD11b^{+}Ly6G^{+} cells ($p<0.01$; Figure 7).

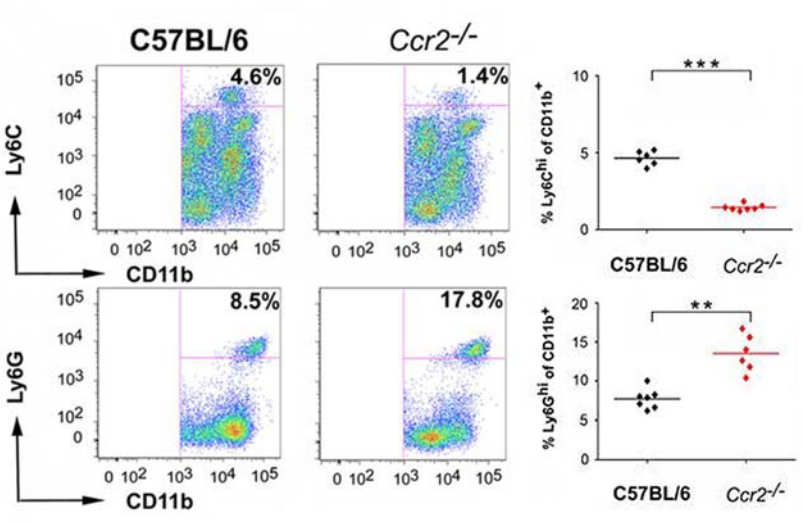

Figure 7: Flow cytometric analysis of monocyte subsets in naïve lungs of C57BL/6 and *Ccr2*$^{-/-}$ mice. A significant reduction of CD11b^{+}Ly6C^{hi} monocytes and relative significant increase of CD11b^{+}LyG^{+} cells was found in *Ccr2*$^{-/-}$ lungs when compared to C57BL/6. Representative FACS plots and quantification of results are shown. Each symbol represents one individual mouse (n=5-6). Statistical significance: ***=$p<0.001$; **=$p<0.01$.

Next, I analyzed CCR2 expression on hematopoietic cells within the lung using BacCCR2CFP reporter mice, in which cells with an activated CCR2 promoter are CFP^{+} [64]. Flow cytometric analysis of lung tissue-derived leukocytes and peripheral blood leukocytes revealed that most of the CD11b^{+}Ly6C^{hi} monocytes were CFP positive. In contrast, CD11b^{+}Ly6G^{+} cells were CFP negative ($p<0.001$). Besides, lymphocytes, such as CD19^{+} B-cells, CD4^{+} and CD8^{+} T-cells lacked detectable CFP expression in peripheral blood and lung tissue (Figure 8).

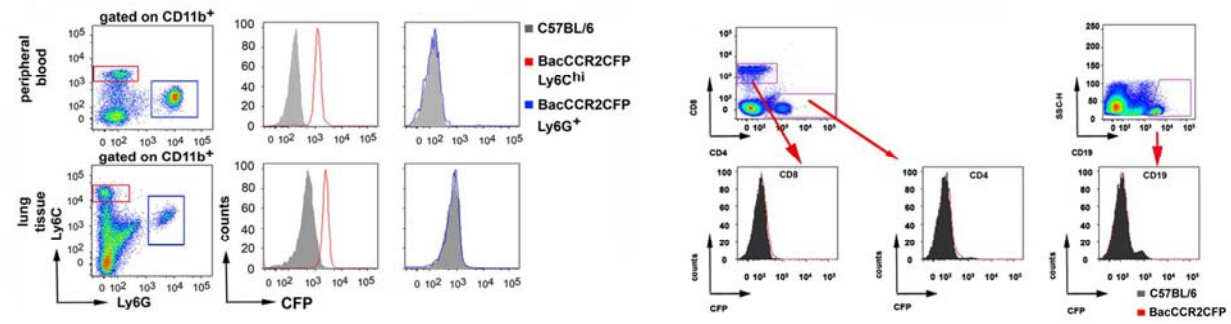

Figure 8: Flow cytometric analysis of CFP/CCR2 expressing cells in peripheral blood and lung tissue of BacCCR2CFP transgenic mice. Ly6C$^+$ cells (red) express CFP/CCR2 in peripheral blood and lung whereas Ly6G$^+$ cells (blue) were negative for CFP as shown with representative FACS plots and histograms (left panel). Neither CD8$^+$ or CD4$^+$ T-cells nor CD19$^+$ B-cells express CFP in these mice (right panel). Histograms do not reveal any difference in CFP expression between BacCCR2CFP mice (red line) and C57BL/6 (gray, filled) mice.

I then investigated whether non-hematopoietic cells express CCR2 in the lungs of mice. From the literature, it was obvious that human endothelial cell lines express CCR2 [60], however, there were no reports showing that CCR2 is expressed on murine endothelial cells in the lung. Therefore immunofluorescence staining for CD31 was carried out on frozen sections of lung tissue derived from BacCCR2CFP mice and confocal microscopy revealed that CD31$^+$ lung endothelial cells are CFP$^+$ (Figure 9).

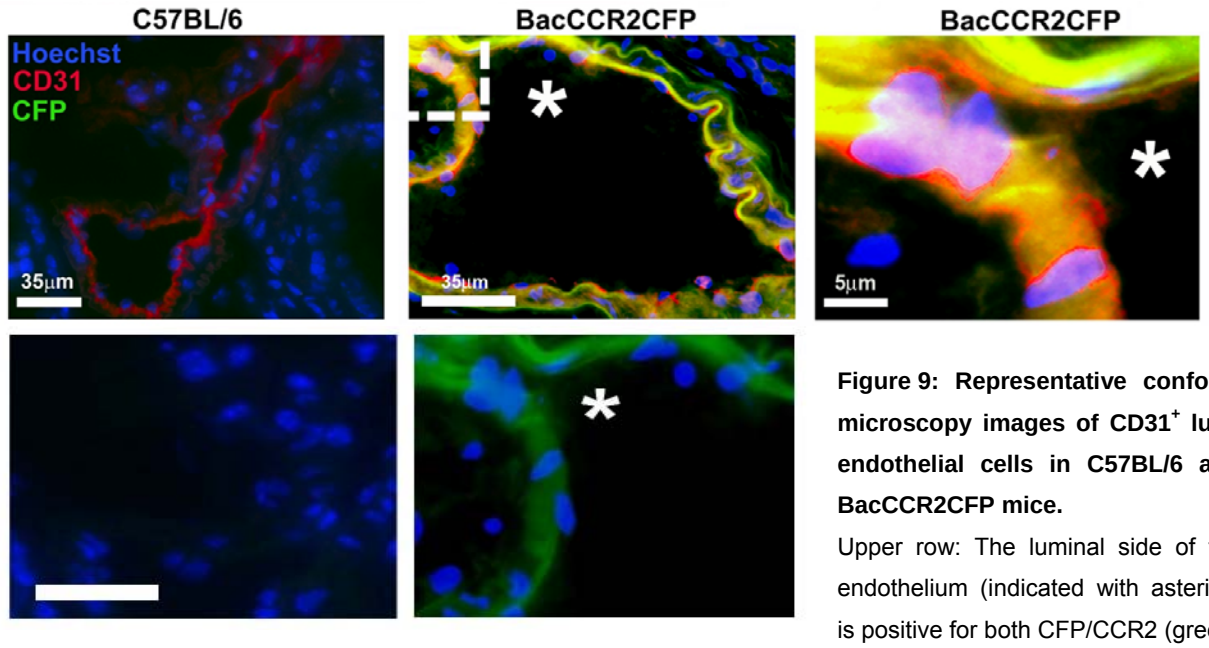

Figure 9: Representative confocal microscopy images of CD31$^+$ lung endothelial cells in C57BL/6 and BacCCR2CFP mice.
Upper row: The luminal side of the endothelium (indicated with asterisk) is positive for both CFP/CCR2 (green) and CD31/Pecam (red), whereas the basolateral side is only positive for CFP/CCR2. Nuclei are stained in blue (Hoechst). Size of scale bars is indicated. Lower row: Staining for CFP shows specific staining in BacCCR2CFP (right) but no signal in C57BL/6 mice (left).

To confirm these data, I analyzed *mRNA* expression levels of *Ccr2* in isolated primary pulmonary endothelial cells of C57BL/6 and *Ccr2*$^{-/-}$ mice and could show that indeed CCR2 expression is found in CD31-sorted endothelial cells from lungs of C57BL/6 mice (Figure 10).

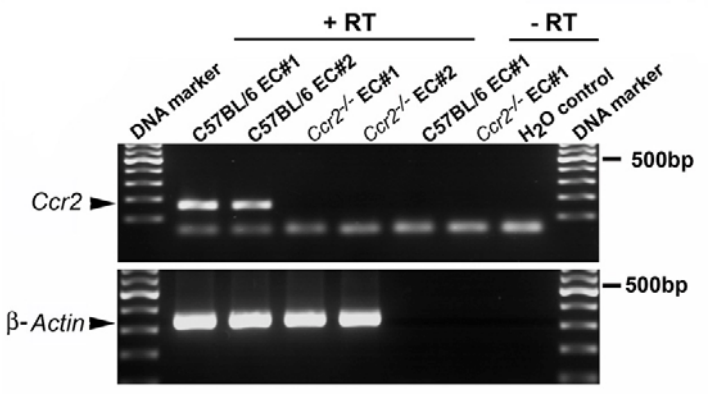

Figure 10: RT-PCR for *Ccr2* expression in CD31-sorted primary endothelial cells isolated from lungs of C57BL/6 and *Ccr2*$^{-/-}$ mice. Two representative samples of each genotype are shown (+ RT), including controls without reverse transcriptase treatment (- RT). β-actin served as control. One DNA marker band is indicated (bp = base pairs).

The purity of the CD31-sorted endothelial cells was verified with flow cytometry for the presence of CD31-FITC signal (Figure 11), resulting in a purity of around 85-97% for the different lung preparations.

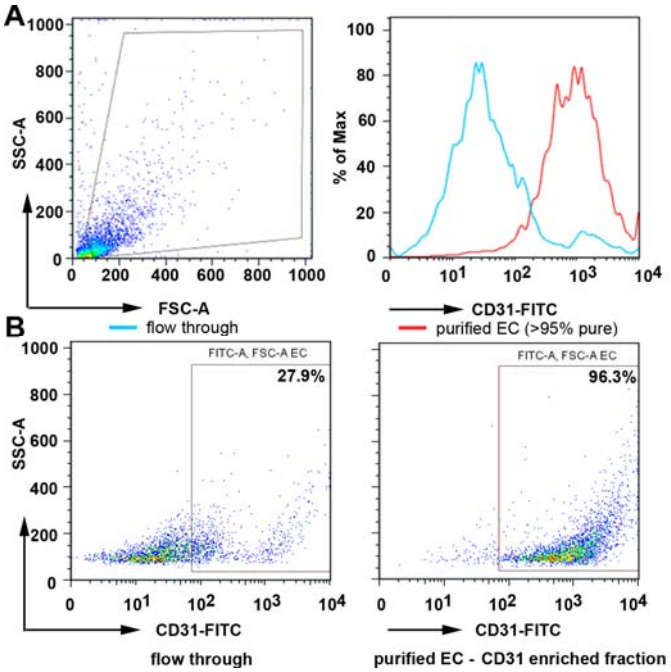

Figure 11: Flow cytometric analysis to control for the purity of CD31-sorted pulmonary endothelial cells from C57BL/6 or *Ccr2*$^{-/-}$ mice. (A) Sideward scatter (SSC) and forward scatter (FSC) of a representative flow cytometry analysis for cells analyzed from a lung preparation (left). Histogram-analysis of the sorted CD31^{+} fraction (red line) derived from a representative lung preparation as well as the flow through (blue line) for CD31 expression (right). (B) Representative dot blot analyses for the presence of CD31-FITC^{+} cells in flow through (middle) and CD31-sorted fractions (right). Percent of CD31-expressing cells are indicated.

Altered numbers of colon carcinoma cells in lungs of *Ccr2*$^{-/-}$ mice could explain the observed inability of MC-38GFP cells to form tumors in lungs. However, no difference in the amount and distribution of MC-38GFP cells in the lung vasculatur were found in either genotype as early as 30 min post injection (Figure 12). At later time points (24 and 72 hrs), numbers of MC-38GFP cells decreased in both genotypes, although slightly more pronounced in *Ccr2*$^{-/-}$ mice.

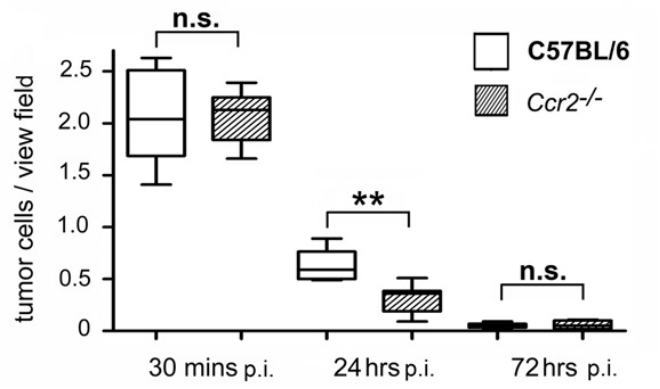

Figure 12: Time course analysis of tumor cell survival in lung tissue. Numbers of tumor cells/ view field were analyzed on sections of C57BL/6 and *Ccr2*$^{-/-}$ lungs 30 min, 24 hrs and 72 hrs post injection (n=3). Statistical significance: **=p<0.01; n.s. = not significant.

5.4.2 CCR2 controls endothelial permeability and tumor cell extravasation

An alternative explanation for the observed alteration in tumor growth in lungs of *Ccr2*$^{-/-}$ mice could be a decreased capacity of MC-38GFP cells to extravaste into parenchyma of *Ccr2*$^{-/-}$ lungs. Confocal microscopy revealed that MC-38GFP cells remained attached to tomato lectin-stained endothelia of blood vessels in *Ccr2*$^{-/-}$ mice at 24 hrs p.i. In contrast, in lungs of C57BL/6 mice MC-38GFP cells had minimal contact with endothelia at 24 hrs p.i. indicating that tumor cells had already extravasated into lung parenchyma at that time point, thus having lost their interaction with the endothelium. Three-dimensional reconstruction of cell-cell contact between tumor and endothelial cells demonstrated a significantly increased interaction of MC-38GFP cells with endothelia in lungs of *Ccr2*$^{-/-}$ mice compared to C57BL/6 lungs (p<0.001; Figure 13).

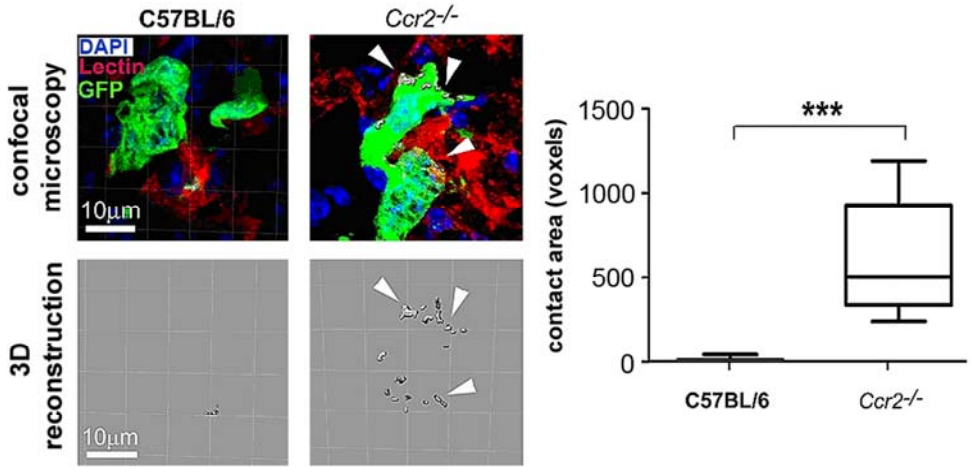

Figure 13: CCR2 deficiency reduces tumor cell extravasation. Confocal microscopy of MC-38GFP cells (green) and endothelial cells (red; lectin^{+}) in C57BL/6 and *Ccr2*$^{-/-}$ lungs 24 hrs post-challenge with MC-38GFP cells (left panel; upper row). Size of scale bar is indicated. Three-dimensional reconstruction of the interaction of both cell types (left panel; lower row). Quantification of the 3D contact area in voxels performed in lungs of both genotypes (n=3) is shown as percentiles (right panel). Asterisks indicate statistical significance: ***=p<0.001.

This indicated an inability of tumor cells to extravasate in *Ccr2*$^{-/-}$ mice. The reduced capability of MC-38GFP cells to extravasate into *Ccr2*$^{-/-}$ lung parenchyma could be due to decreased permeability of the lung endothelium as tested by Evans blue accumulation. With this technique it is possible to test the integrity of the blood vasculature as blue staining of tissue is only found when blood vessels become permeable. Naïve lungs of either genotype were impermeable for Evans blue, resulting in white or only weakly stained lung tissue, indicating full vascular integrity. However, 24 hrs upon challenge with MC-38GFP cells, C57BL/6 mice displayed strong Evans blue accumulation, resulting in blue-colored lung tissue. In contrast, lungs of *Ccr2*$^{-/-}$ mice remained white, indicative of vascular impermeability. Spectrophotometric quantification of accumulated Evans blue in lung homogenates of both genotypes confirmed these macroscopic data ($p<0.001$; Figure 14).

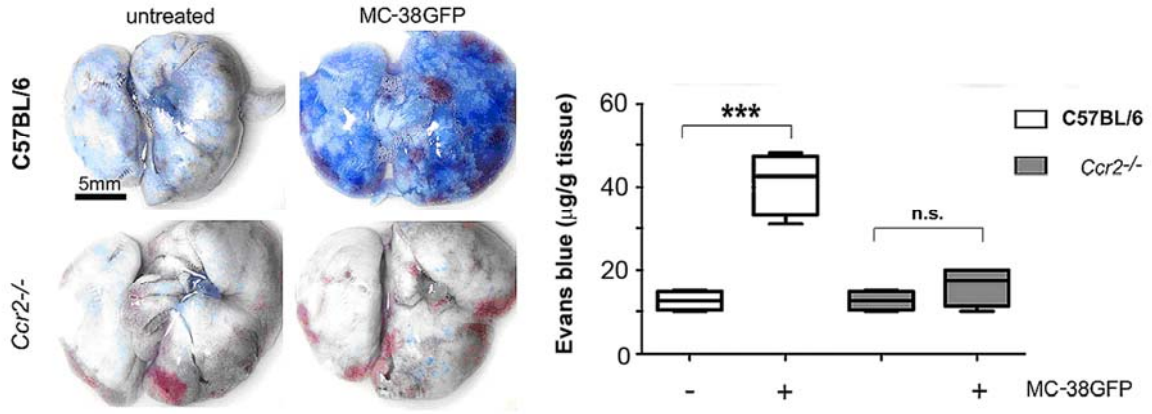

Figure 14: CCR2 deficiency reduces vascular permeability upon tumor cell injection. Macroscopy of Evans blue leakage in lungs of naïve C57BL/6 and *Ccr2*$^{-/-}$ mice (upper row) and in lungs at 24 hrs p.i. with MC-38GFP cells (lower row). Size of scale bar is indicated. Spectrophotometric quantification of Evans blue leakage (extracted from lung tissue) shows a significant increase in C57BL/6 mice 24 hrs post MC-38 challenge but not in *Ccr2*$^{-/-}$ mice (n=3, each; ***=$p<0.001$).

Interestingly, the increase in permeability of endothelial cells of lung vessels is transient as revealed by time course analysis of Evans blue leakage (Figure 15). The strongest accumulation of Evans blue in the lung tissue of C57BL/6 mice was found between 12 and 24 hrs p.i. with MC-38, indicating that indeed the very early phase of tumor cell seeding determines successful tumor cell extravasation and subsequent growth. After 7 days, the lung became completely impermeable again, meaning that the permeability of the endothelial cell layer is only transient and no continuous impairment of the vessel function and structure is caused by the extravasation process.

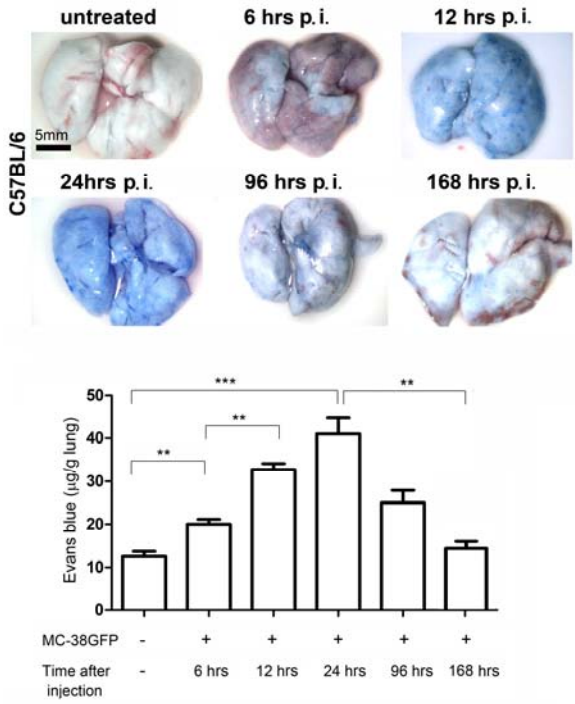

Figure 15: Induction of vessel permeability in lungs upon tumor cell challenge is transient. Macroscopy of lungs derived from C57BL/6 mice to study kinetics of Evans blue accumulation after MC-38GFP injection. Various time points between 6 hrs and 7 days p.i. with MC-38GFP are shown (upper panel). Quantification of Evans blue accumulation within lungs of C57BL/6 mice at 6 hrs, 12 hrs, 24 hrs, 96 hrs and 168 hrs p.i. with MC-38GFP, showing that the induction of lung permeability is transient, with the strongest accumulation between 12 and 24 hrs p.i. with tumor cells (lower panel). Statistical significance: ***=p<0.001; **=p<0.01; (n=3).

Thus, besides a strong reduction in numbers of Ly6C^{hi} cells and lack of endothelial CCR2 expression, a reduced capacity of tumor cell extravasation and decreased permeability of lung endothelium was observed in lungs of *Ccr2*$^{-/-}$ mice upon tumor cell challenge.

Next, I tested the hypothesis whether the reduced capacity of MC-38GFP cells to extravasate is linked to reduced recruitment of leukocytes [5, 79]. Flow cytometry analysis of lungs derived from C57BL/6 mice injected with MC-38GFP cells revealed a specific recruitment of CD11b^{+}Ly6C^{hi} cells that was entirely absent in *Ccr2*$^{-/-}$ mice. The increased presence of Ly6C^{hi} cells in lung tissue upon challenge with MC-38GFP cells persisted for approximately 12-24 hrs p.i. (Figure 16). No significant increase of other immune cells (e.g. CD4^{+}, CD8^{+}, CD11c^{+}, NK1.1^{+}) was found in lungs of both genotypes upon challenge with MC-38GFP cells (data not shown).

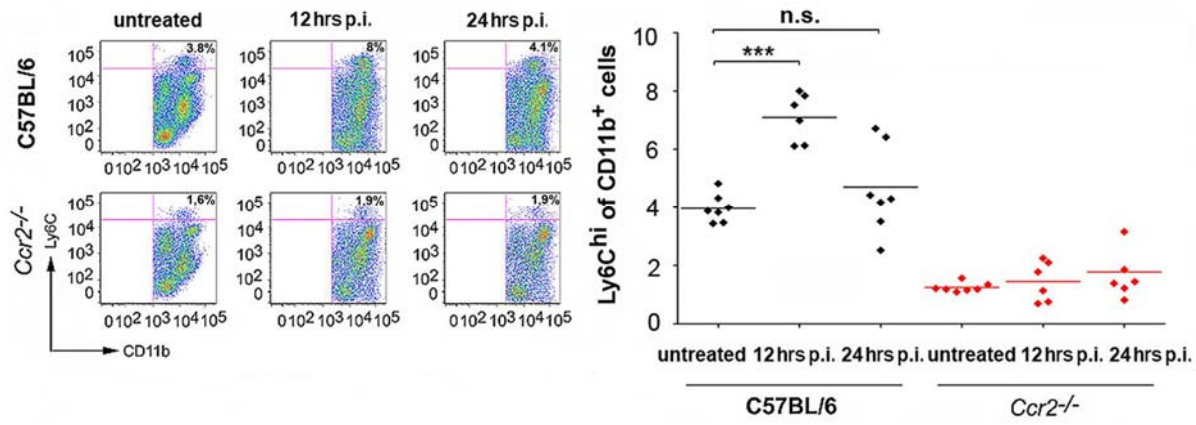

Figure 16: Analysis of the influx of Ly6C^{hi} cells into lung tissue upon tumor cell challenge of C57BL/6 and *Ccr2*$^{-/-}$ mice over time. Representative flow cytometry analyses of each time point are shown for both genotypes (left panel). Ly6C^{hi} cells are quantified and presented in the right panel. Each symbol depicts an individual mouse (n=6-7). Asterisks indicate statistical significance: ***=p<0.001.

Next, we investigated whether infiltrating myeloid cell populations are recruited to MC-38GFP cells in lungs of both genotypes at sites of vascular arrest. Tumor cells in *Ccr2*$^{-/-}$ lungs were associated significantly less degree with F4/80^{+}, Ly6C^{+} and CD11b^{+} cells when compared to C57BL/6. In contrast, endogenous Ly6G^{+} cells appeared to associate significantly stronger with MC-38GFP cells in *Ccr2*$^{-/-}$ lungs when compared to C57BL/6 mice ($p<0.001$; Figure 17).

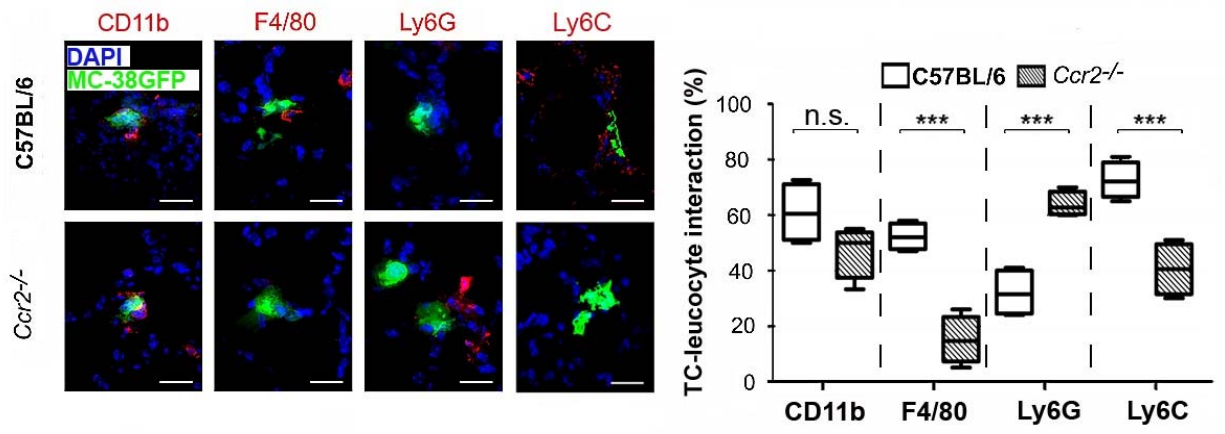

Figure 17: Confocal and quantitative analysis of tumor cell interaction with endogenous myeloid cells of C57BL/6 and *Ccr2*$^{-/-}$ lungs challenged with MC-38GFP cells. Representative images of the interaction of various myeloid cells (CD11b: left; F4/80: second from left; Ly6G: second from right, Ly6C; right; all red) with MC-38GFP cells (green) in C57BL/6 and *Ccr2*$^{-/-}$ mice 24 hrs post-injection (left panel). Quantification of the myeloid - tumor cell interaction in lungs of in C57BL/6 and *Ccr2*$^{-/-}$ mice; percentiles are indicated (right panel). Asterisks indicate statistical significance: ***=$p<0.001$. Scale bar: 20μm; (n=3, each).

To test whether MC-38GFP tumor cells injected into *Ccr2*$^{-/-}$ mice have still the ability to efficiently recruit myeloid cells, we adoptively transfered myeloid cells 6 hrs post tumor cell injection. MC-38GFP cells specifically recruited adoptively transferred myeloid cells in *Ccr2*$^{-/-}$ but not in C57BL/6 lungs ($p<0.001$; Figure 18) since MC-38GFP cells were already bound by endogenous myeloid cells (e.g. CD11b^{+}, F4/80^{+} or Ly6C^{+}) in C57BL/6 lungs. These results indicated that the capability of tumor cells to bind myeloid cells in *Ccr2*$^{-/-}$ lungs is not altered, however, the cellular environment within tumor cell challenged *Ccr2*$^{-/-}$ lung is different.

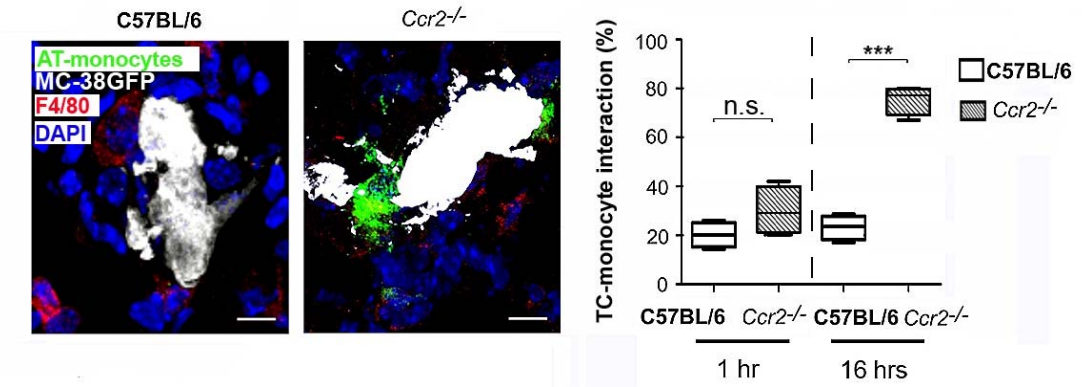

Figure 18: Tumor cells in lungs of *Ccr2*$^{-/-}$ mice are capable of interacting with myeloid cells. Confocal analysis and representative images of the interaction of adoptively transferred, PKH26-labeled monocytes (green) with MC38-GFP cells (white) and endogenous F4/80^{+} macrophages (red) in C57BL/6 and *Ccr2*$^{-/-}$ mice 16 hrs post injection (left panel). Scale bar: 10μm. Quantification of myeloid - tumor cell interaction in lungs of in C57BL/6 and *Ccr2*$^{-/-}$ mice; percentiles are indicated (right panel). Asterisks indicate statistical significance: ***=p<0.001 (n=3, each).

Therefore, a plausible explanation for the strongly decreased extravasation of MC-38GFP cells in *Ccr2*$^{-/-}$ lungs is the lack of vascular permeability together with a reduction in interacting Ly6C^{hi} inflammatory cells [5].

5.4.3 Depletion of CD11b^{+}Ly6C^{hi} cells does not reduce lung metastasis

As a next step, I tested whether depletion of Ly6C^{hi} inflammatory cells would alter tumor cell extravasation and subsequent lung metastasis. Therefore, MC21 antibody (a CCR2 depleting antibody) [70] was injected for 5 days, starting one day prior to tumor cell injection. On the day of tumor cell injection, the presence of CD11b^{+}Ly6C^{hi} cells was tested by flow cytometry (Figure 19), indicating that numbers of CD11b^{+}Ly6C^{hi} cells were significantly reduced compared to C57BL/6 mice injected with ratIgG. Still, the reduction was only to a level comparable to *Ccr2*$^{+/-}$ mice.

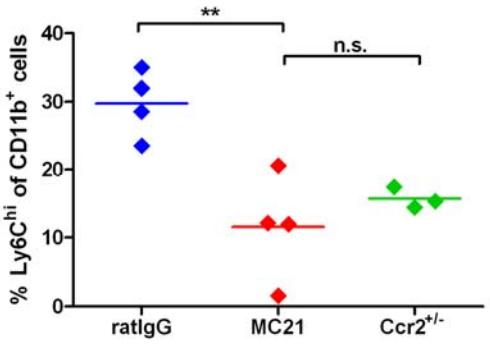

Figure 19: Depletion of Ly6C^{hi} cells using MC21 antibody led to monocyte levels comparable to *Ccr2*$^{+/-}$ mice. Quantification of flow cytometry analysis of CD11b^{+}Ly6C^{hi} cells in blood of C57BL/6 mice injected with ratIgG control or MC21 antibody as well as *Ccr2*$^{+/-}$ mice. Statistical significance: **=p<0.01; n.s. = not significant (n=3-4).

After 28 days, lungs were analyzed for tumor load and measurement of GFP fluorescence revealed no difference between untreated C57BL/6 mice and C57BL/6 mice treated with MC21 or ratIgG control antibody (Figure 20).

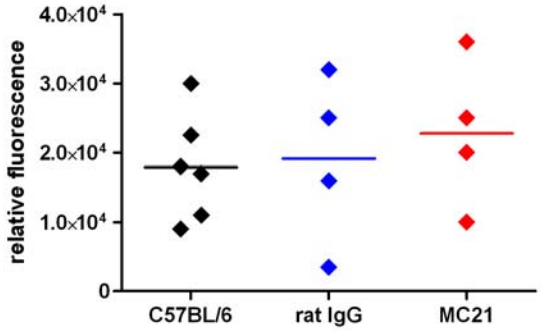

Figure 20: Lung metastasis is unaltered upon depletion of CCR2^{+}Ly6C^{hi} monocytes. Quantification of relative fluorescence in lungs of untreated C57BL/6, control antibody injected (ratIgG) and CCR2-depleting antibody (MC21) mice at 28 dpi (n=4-5).

These results indicate that even in situations with significantly reduced numbers of Ly6C^{hi} monocytes within the circulation, metastatic growth of MC-38GFP tumors is not altered. This also suggests that an approximately 50% reduction of inflammatory monocytes does not suffice to induce a biological effect in our seeding model.

To further study the role of Ly6C^{hi} monocytes in metastatic growth of lung tumors, I used BacCCR2DTCFP mice, in which all CCR2 expressing cells can be depleted upon injection of diphtheria toxin (DT). I established a protocol, which allowed me to efficiently deplete CCR2^{+}Ly6C^{hi} monocytes for the first 4 days after tumor cell injection as tested by flow cytometry analysis for the presence of CD11b^{+}Ly6C^{hi} cells in blood of DT-injected mice each 24 hrs. Figure 21 shows the experimental set-up used in the BacCCR2DTCFP model system as well as the efficient depletion of CD11b^{+}Ly6C^{hi} cells in the peripheral blood of these mice.

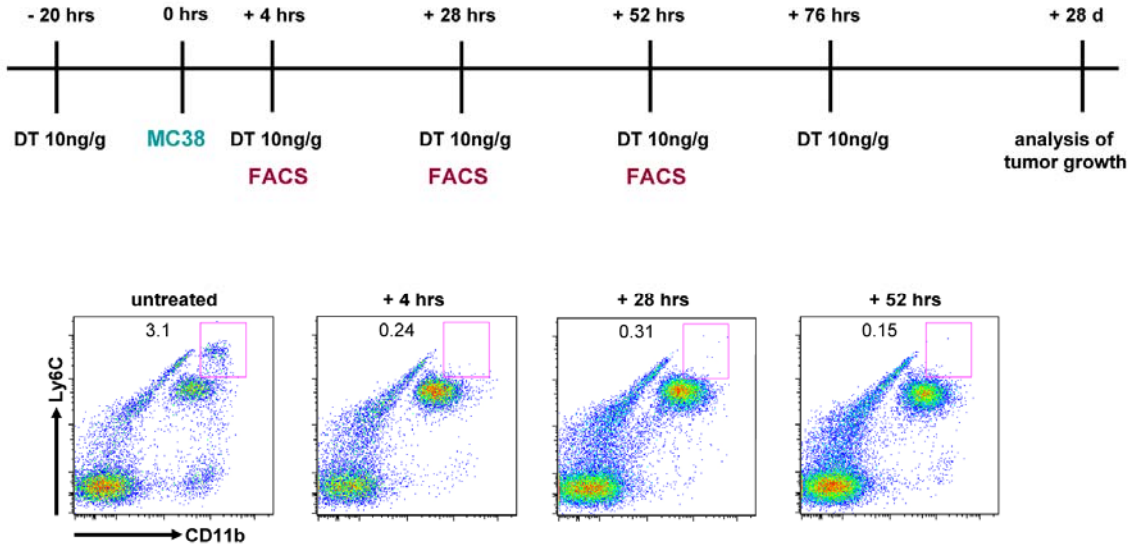

Figure 21: Efficient depletion of CFP^{+}Ly6C^{hi} cells in BacCCR2DTCFP mice upon DT injection. Injection of DT every 24 hrs allowed conditional depletion of Ly6C^{hi} cells for at least the first 52 hrs after tumor cell injection. The time line represents the treatment protocol (upper panel) and the representative FACS plots for the presence of CD11b^{+}Ly6C^{hi} cells in blood confirm efficient depletion of this cell type (lower panel).

Mice were injected with MC-38GFP and after 28 days lungs were analyzed for tumor load. Quantification of metastatic foci within the lungs revealed no reduction in tumor burden in DT-treated BacCCR2DTCFP mice. In contrary, an increase in tumor burden was found, which might be due to the fact that CCR2 is expressed on endothelial cells and DT treatment might have increased vessel permeability leading to an increased extravasation of tumor cells and subsequent metastasis (Figure 22).

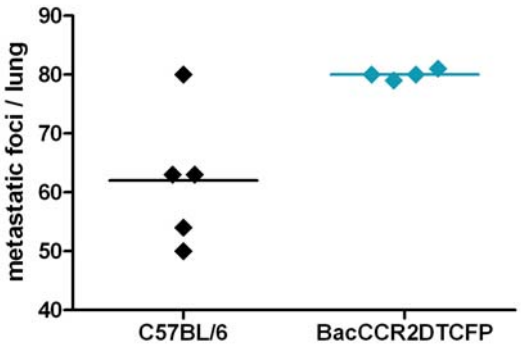

Figure 22: Depletion of CFP/CCR2^{+} cells in BacCCR2DTCFP mice leads to enhanced tumor growth. Quantification of metastatic foci in lungs of C57BL/6 (n=5) and BacCCR2DTCFP (n=4) mice 28 dpi with MC-38GFP cells.

These results suggest that depletion of Ly6C^{hi} monocytes does not suffice to attenuate metastasis.

5.4.4 CCR2 on radio-resistant cells contributes to efficient tumor metastasis

Next, we tested whether reconstitution of *Ccr2*$^{-/-}$ mice with CCR2^{+} BM cells could restore the ability of MC-38GFP cells to extravasate and metastasize in lungs. Therefore, I performed reciprocal BM reconstitution of C57BL/6→*Ccr2*$^{-/-}$ and *Ccr2*$^{-/-}$→C57BL/6 mice as well as control groups (C57BL/6→C57BL/6 and *Ccr2*$^{-/-}$→*Ccr2*$^{-/-}$ mice) and analyzed blood 6-8 weeks after reconstitution for the presence of CCR2^{+}Ly6C^{hi} monocytes by flow cytometry. Successfully reconstituted mice (efficiency >90%) were administered MC-38GFP cells and analyzed for tumor growth in lungs 28 dpi. As expected C57BL/6→C57BL/6 mice displayed robust lung metasasis, whereas *Ccr2*$^{-/-}$→*Ccr2*$^{-/-}$ mice lacked or had strongly reduced tumor metastases in lungs. However, CCR2 expression on radio-resistant cells (*Ccr2*$^{-/-}$→C57BL/6 mice) resulted in more lung tumors when compared to mice devoid of CCR2 expression in the stromal compartment (C57BL/6→*Ccr2*$^{-/-}$ mice; $p<0.05$; Figure 23).

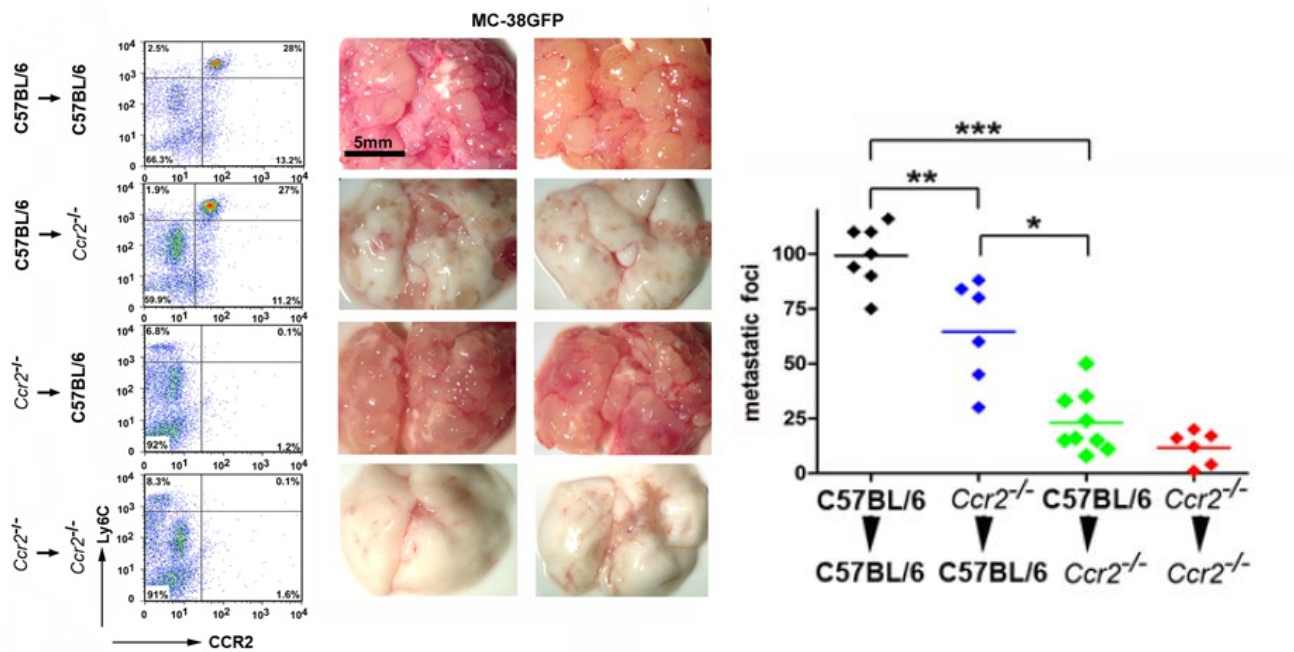

Figure 23: CCR2 expression in the stromal and the hematopoietic compartment is crucial for tumor cell extravasation and tumor growth. Representative FACS plots of peripheral blood from C57BL/6→C57BL/6 (n=8), C57BL/6→*Ccr2*$^{-/-}$ (n=7), *Ccr2*$^{-/-}$→C57BL/6 (n=9) and *Ccr2*$^{-/-}$→*Ccr2*$^{-/-}$ chimeric mice (n=5) for the presence of CCR2^{+}Ly6C^{hi} monocytes (left row). Macroscopy of lungs 28 dpi with MC-38GFP cells. Size of scale bar is indicated (middle and right row). Quantification of metastatic foci in lungs of C57BL/6→C57BL/6 (black; n=8), *Ccr2*$^{-/-}$→C57BL/6 (blue; n=6); C57BL/6→*Ccr2*$^{-/-}$ (green; n=9) and *Ccr2*$^{-/-}$→*Ccr2*$^{-/-}$ (red; n=6) mice. Statistical significance: ***=p<0.001; **=p<0.01; *=p<0.05 (right panel).

These data indicate that hematopoietic – but even more important – stromal expression of CCR2 is involved in efficient tumor cell extravasation of MC-38GFP cells in lung tissue.

To delineate the role of stromal CCR2 expression in metastasis in more detail, we next assessed whether CCR2 expression specifically on endothelial cells under the Tie2 promoter in *Ccr2*$^{-/-}$ mice (denoted as Tie2CCR2/*Ccr2*$^{-/-}$ mice [63, 80]) would enable tumor cell extravasation and formation of metastasis. First, I analyzed Tie2CCR2/*Ccr2*$^{-/-}$ mice by flow cytometry extensively for CCR2 expression on hematopoietic and stromal cells as well as for the presence of Ly6C^{hi} cells. The obtained data clearly show that Tie2CCR2/*Ccr2*$^{-/-}$ mice lack Ly6C^{hi} monocytes in peripheral blood and lung tissue similar to *Ccr2*$^{-/-}$ mice (Figure 24).

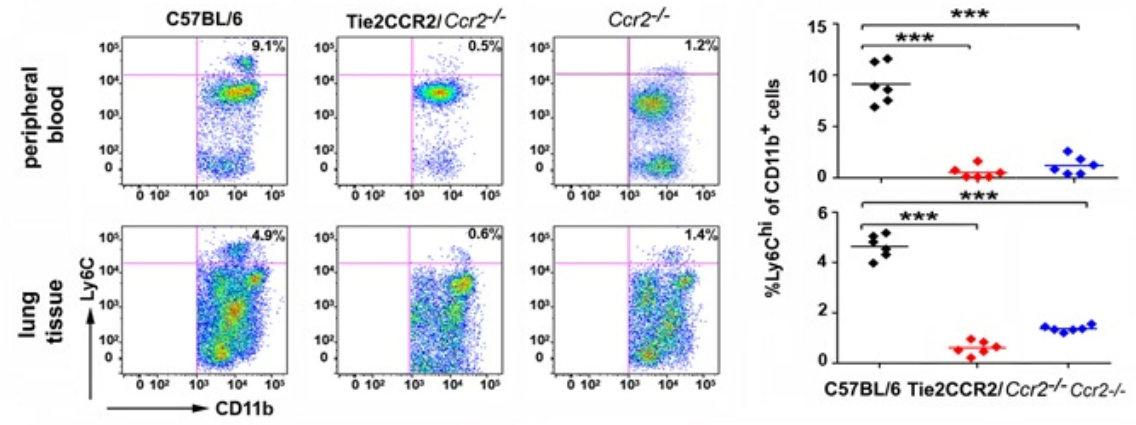

Figure 24: Tie2CCR2/Ccr2-/- mice lack Ly6C^{hi} monocytes in peripheral blood and lung tissue. Representative FACS plots for CD11b^{+}Ly6C^{hi} monocytes in blood (upper row) and lungs (lower row) of naïve C57BL/6, Tie2CCR2/*Ccr2*$^{-/-}$ and *Ccr2*$^{-/-}$ mice (left panel). Quantification of Ly6C^{hi} cells is presented in the right panel. Each symbol depicts an individual mouse (n=6 for each genotype). Asterisks indicate statistical significance: ***=p<0.001.

Further, Tie2CCR2/*Ccr2*$^{-/-}$ mice are devoid of CCR2 expression on CD11b^{+}, CD19^{+} or CD3^{+} cells in peripheral blood, spleen or BM, indistinguishable from *Ccr2*$^{-/-}$ mice (Figure 25).

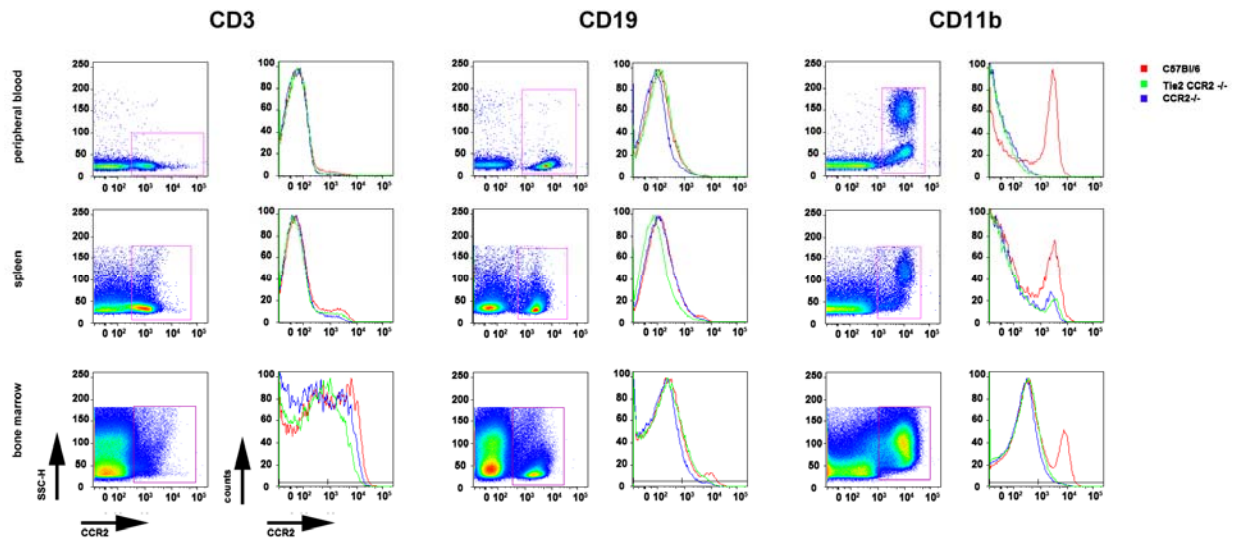

Figure 25: Characterization of mice with endothelium specific over-expression of CCR2. Representative FACS plots for the expression of CCR2 on $CD3^+$ T-cells, $CD19^+$ B-cells and $CD11b^+$ monocytes in the blood (upper row), spleen (middle row) and bone marrow (lower row) of C57BL/6 (red), Tie2CCR2/*Ccr2*$^{-/-}$ (green) and *Ccr2*$^{-/-}$ mice (blue). Histograms reveal no difference in the CCR2 expression pattern between Tie2CCR2/*Ccr2*$^{-/-}$ and *Ccr2*$^{-/-}$ mice (lower panel).

In addition, I analyzed expression levels of *Ccr2 mRNA* in whole lung tissue and primary endothelial cells of Tie2CCR2/*Ccr2*$^{-/-}$ mice. Overall, *Ccr2 mRNA* expression levels in lungs of Tie2CCR2/*Ccr2*$^{-/-}$ mice were reduced by more than 50% when compared to C57BL/6 mice, most likely due to the lack of infiltrating $CCR2^+Ly6C^{hi}$ monocytes. However, transcriptional analysis of *Ccr2* expression in purified lung endothelial confirmed that Tie2CCR2/*Ccr2*$^{-/-}$ mice express *Ccr2* in pulmonary endothelial cells (Figure 26).

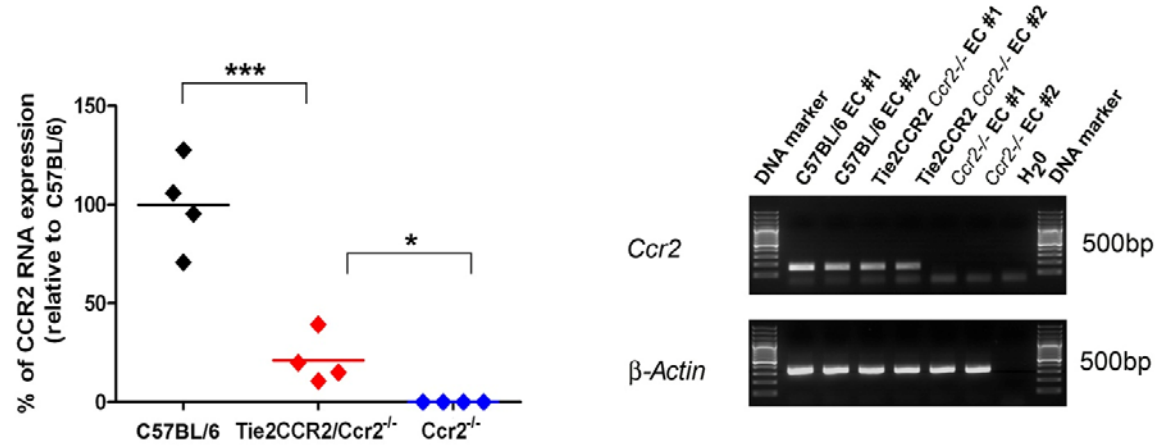

Figure 26: Characterization of endothelium specific over-expression of CCR2 in Tie2CCR2/*Ccr2*$^{-/-}$ mice. Real-time PCR for the expression of *Ccr2 mRNA* in lung tissue derived of C57BL/6, Tie2CCR2/*Ccr2*$^{-/-}$ and *Ccr2*$^{-/-}$ mice. Each symbol represents an individual mouse (n=4, for each genotype); values are normalized to the average of *Ccr2 mRNA* expression in C57BL/6 lungs and shown in percentage of the average C57BL/6 expression level. Statistical significance: ***=p<0.001; *=p<0.05 (left panel). RT-PCR for the expression of *Ccr2* in CD31-sorted endothelial cells

isolated from lungs of C57BL/6, Tie2CCR2/*Ccr2*$^{-/-}$ and *Ccr2*$^{-/-}$ mice. All samples are shown in duplicates, *β-actin* served as control (right panel).

Upon injection of Tie2CCR2/*Ccr2*$^{-/-}$ mice with MC-38GFP cells, tumor cell extravasation and tumor growth was restored approximately to a 50% level of C57BL/6 mice. The macroscopic finding was further confirmed by quantification of GFP fluorescence in lungs of C57BL/6, Tie2CCR2/*Ccr2*$^{-/-}$ and *Ccr2*$^{-/-}$ mice as well as by immunohistochemical analysis (Figure 27).

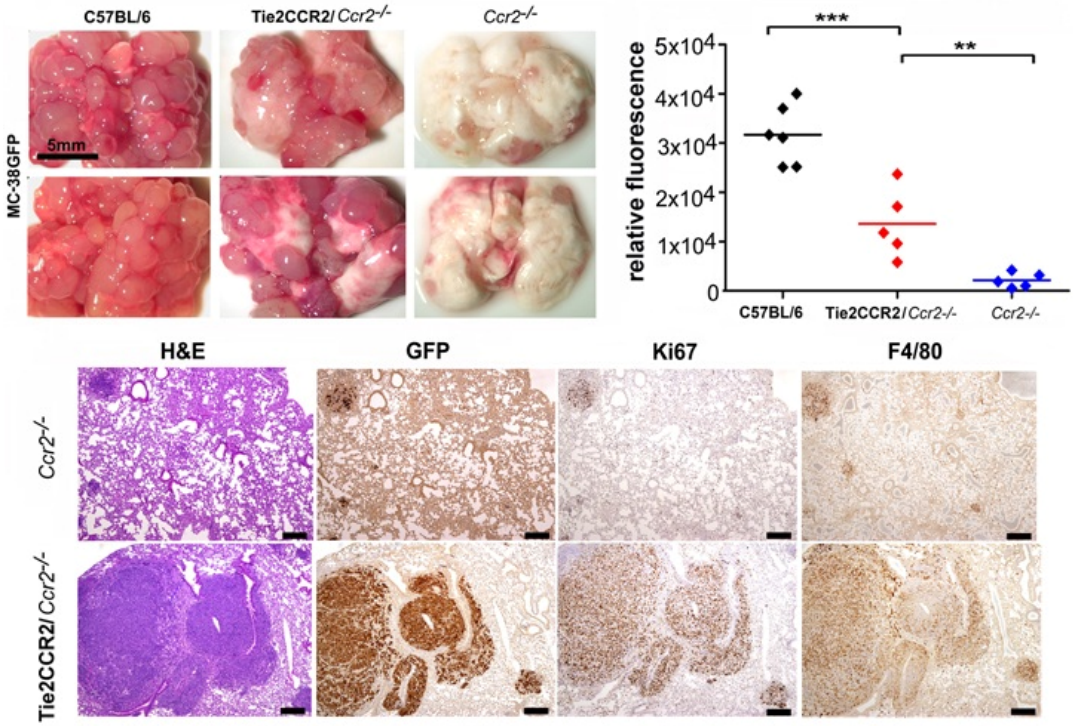

Figure 27: Endothelial expression of CCR2 facilitates lung metastasis. Macroscopy of lungs of C57BL/6, Tie2CCR2/*Ccr2*$^{-/-}$ and *Ccr2*$^{-/-}$ mice 28 dpi with MC-38GFP cells. Size of scale bar is indicated (upper left panel). Quantification of GFP fluorescence in lung homogenates of C57BL/6 (n=5), Tie2CCR2/*Ccr2*$^{-/-}$ (n=5) and *Ccr2*$^{-/-}$ (n=5) mice. Asterisks indicate statistical significance: ***=p<0.001; **=p<0.01 (upper right). Histological analysis of colon carcinoma (MC-38GFP) tumors in lung sections of *Ccr2*$^{-/-}$ and Tie2CCR2/*Ccr2*$^{-/-}$ mice 28 dpi. H&E: Hematoxylin-Eosin, GFP for tumor cells, Ki67 stains for proliferating cells, F4/80 for monocytes and macrophages. Size of scale bar: 50μm (lower panel).

Hence, expression of CCR2 on endothelial cells was sufficient to partially restore tumor cell extravasation and metastasis.

5.4.5 CCR2 expression by myeloid cells is dispensable for tumor cell extravasation and metastasis

Over-expression of CCR2 on endothelial cells was sufficient to partially restore tumor cell extravasation and metastasis. To assess the role of CCR2 expression on myeloid cells during metastasis, we bred *Ccr2*$^{loxP/loxP}$ mice with LysMCre [81] mice, resulting in a mouse potentially devoid of CCR2 expression on myeloid cells. Flow cytometry analysis of peripheral blood revealed similar amounts of Ly6C^{hi} cells in *LysMCreCcr2*$^{loxP/loxP}$ and C57BL/6 mice, however depletion of CCR2 expression was found to be 90-95% efficient on Ly6C^{hi} monocytes in *LysMCreCcr2*$^{loxP/loxP}$ mice (Figure 28) indicating that the LysMCre promoter is active on circulating monocytes [82, 83].

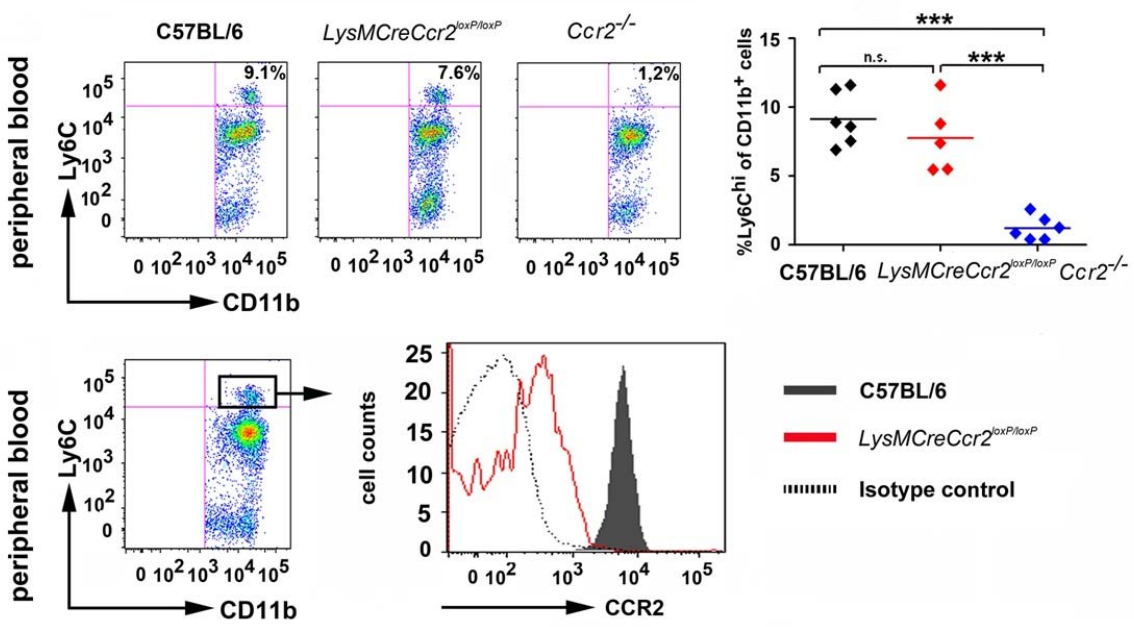

Figure 28: Characterization of mice lacking CCR2 expression specifically on myeloid cells. Upper panel: representative FACS plots for CD11b^{+}Ly6C^{hi} cells in peripheral blood of C57BL/6, *LysMCreCcr2*$^{loxP/loxP}$ and *Ccr2*$^{-/-}$ mice (left panel). Quantification of Ly6C^{hi} cells is presented in the right panel. Each symbol depicts an individual mouse (n=5-7). Asterisks indicate statistical significance: ***=p<0.001; n.s. = not significant. Lower panel: representative FACS plot for CCR2 expression on Ly6C^{hi} cells in blood of C57BL/6 and *LysMCreCcr2*$^{loxP/loxP}$ mice. The histogram depicts CCR2 expression on Ly6C^{hi} cells of C57BL/6 (gray, filled) and *LysMCreCcr2*$^{loxP/loxP}$ mice (red line). The isotype control is shown as dashed line.

I next challenged *LysMCreCcr2*$^{loxP/loxP}$ mice with MC-38GFP cells and analyzed the lungs for the presence of Ly6C^{hi} monocytes 12 hrs p.i. Interestingly, *LysMCreCcr2*$^{loxP/loxP}$ mice did not display a specific recruitment of Ly6C^{hi} monocytes at 12 hrs p.i. or at later time points, indicating that lack or reduction of CCR2 on Ly6C^{hi} monocytes leads to a shortened retention in tumor cell-challenged lungs (Figure 29).

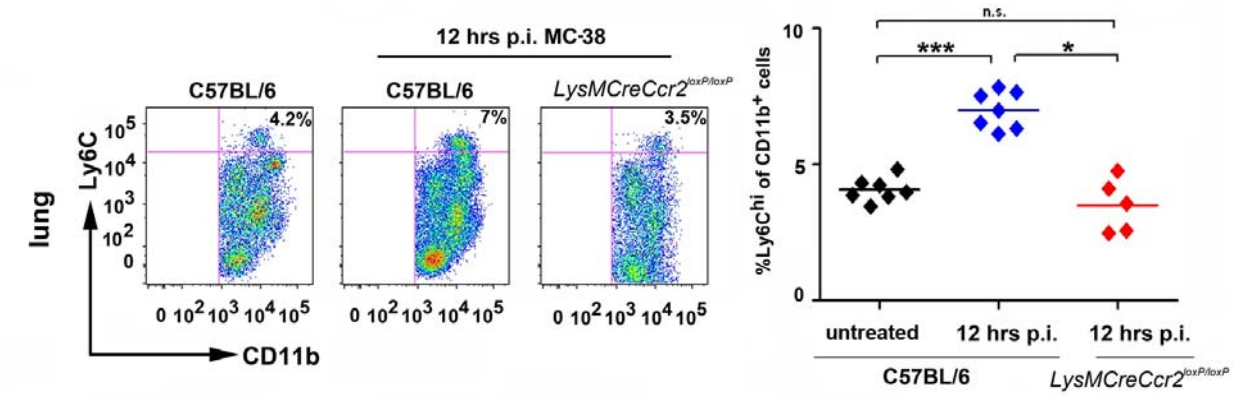

Figure 29: Lack of CCR2 on Ly6C^{hi} cells abrogates influx of Ly6C^{hi} cells upon tumor cell injection. Representative FACS plots for the presence of CD11b^{+}Ly6C^{hi} cells in the lung of naïve C57BL/6, C57BL/6 and LysMCre*Ccr2*$^{loxP/loxP}$ mice 12 hrs p.i. with MC-38GFP (left panel). Quantification of Ly6C^{hi} cells in the right panel. Each symbol depicts an individual mouse (n=5-7). Asterisks indicate statistical significance: ***=p<0.001; *=p<0.05; n.s. = not significant.

To gain insight into the role of myeloid cell derived CCR2 expression in tumor cell growth, *LysMCreCcr2*$^{loxP/loxP}$, *Ccr2*$^{-/-}$ and C57BL/6 mice were injected with MC-38GFP. A significantly reduced amount of tumor nodules was found in lungs of *LysMCreCcr2*$^{loxP/loxP}$ mice, when compared to C57BL/6 mice (p<0.05). This was confirmed by quantification of GFP fluorescence in lung homogenates and by immunohistochemistry on lung tissue (Figure 30).

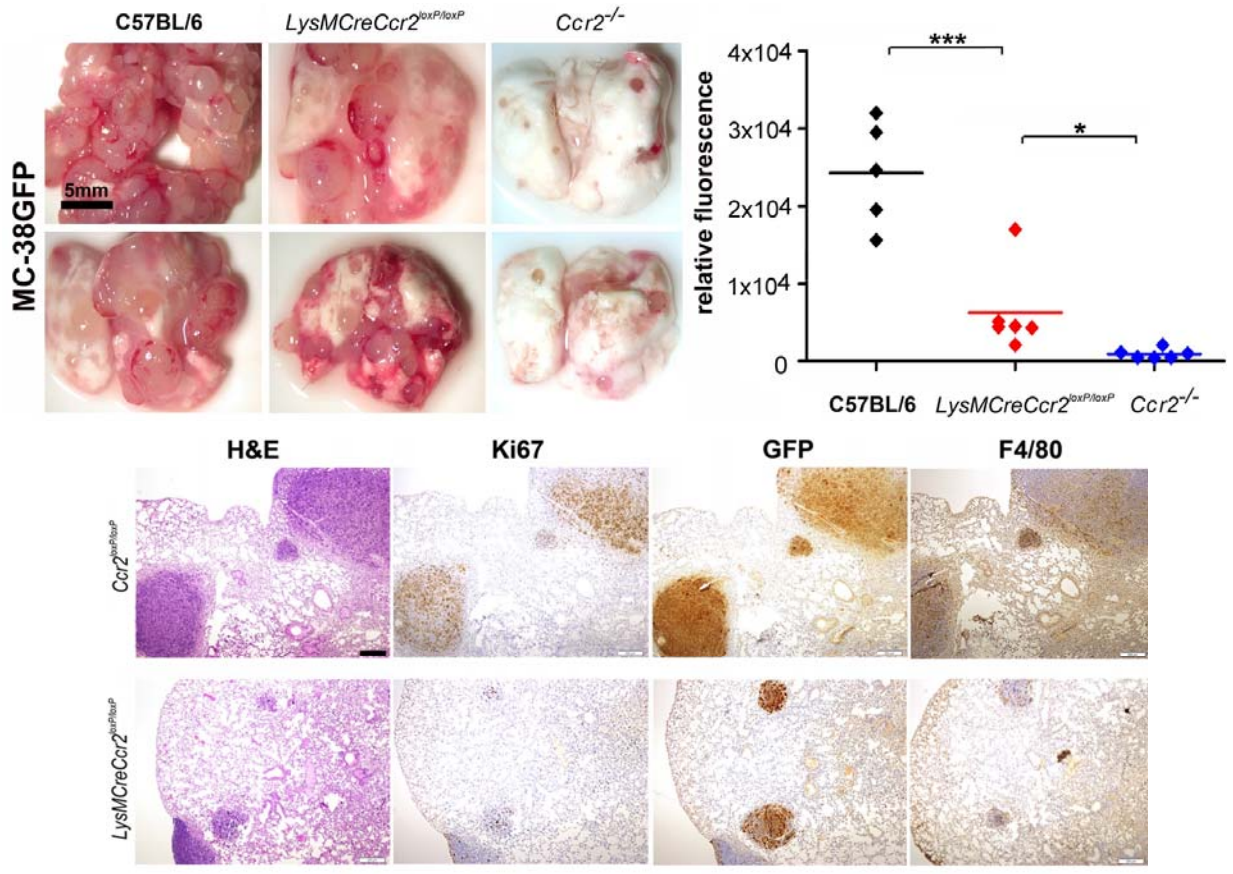

Figure 30: Lack of CCR2 on Ly6C^{hi} cells leads to reduced tumor growth in *LysMCreCcr2$^{loxP/loxP}$* mice. Macroscopy of lungs of C57BL/6, *LysMCreCcr2$^{loxP/loxP}$* and *Ccr2$^{-/-}$* mice 28 dpi with MC-38GFP cells. Size of scale bar is indicated (left upper panel). Quantification of GFP fluorescence in lung homogenates of C57BL/6 (n=5), *LysMCreCcr2$^{loxP/loxP}$* (n=6) and *Ccr2$^{-/-}$* (n=6) mice. Each symbol depicts an individual mouse. Asterisks indicate statistical significance: ***=p<0.001; *=p<0.05 (right upper panel). Histological analysis of colon carcinoma tumors (MC-38GFP) in *Ccr2$^{loxP/loxP}$* (upper row, lower panel) and *LysMCreCcr2$^{loxP/loxP}$* (lower row, lower panel) lungs 28 dpi H&E: Hematoxylin-Eosin, Ki67 stains for proliferating cells, GFP for tumor cells, F4/80 for monocytes and macrophages. Scale bar: 200µm.

Similar to our data obtained from reconstitution experiments as well as from Tie2CCR2/*Ccr2$^{-/-}$* mice, these results demonstrate that CCR2 expression on the stromal compartment suffices for tumor cell extravasation and metastasis of MC-38GFP cells. However, CCR2 expression on Inflammatory monocytes facilitates metastasis.

5.4.6 Tumor cell-derived CCL2 expression controls myeloid cell recruitment

To test whether CCR2-dependent lung metastasis of MC-38GFP colon carcinoma cells could be also observed with different tumor cells, we injected C57BL/6 and *Ccr2$^{-/-}$* mice with Lewis lung carcinoma cells (3LL). Similar to MC-38GFP cells, attenuation of metastasis was observed in *Ccr2$^{-/-}$* lungs when compared to C57BL/6 lungs as demonstrated by quantification of tumor nodules in lungs (p<0.05; Figure 31).

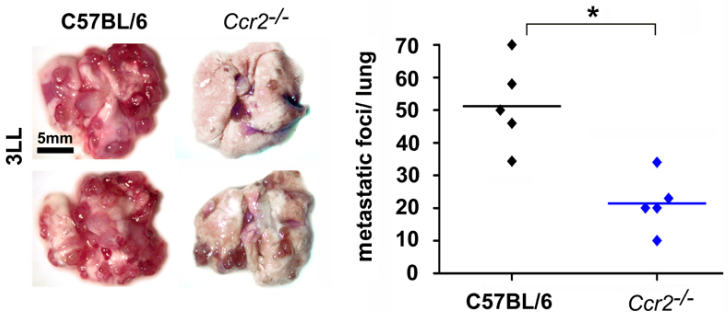

Figure 31: Tumor cell-derived CCL2 dependent mechanisms of tumor cell extravasation. Macroscopy of C57BL/6 and *Ccr2$^{-/-}$* lungs at 12 dpi with Lewis lung carcinoma cells (3LL) (left panel, size of scale bar is indicated) and quantification of tumor nodules (right panel; n=5). Asterisks indicate statistical significance: *=p<0.05.

Next, we investigated the metastatic behaviour of B16-BL6 melanoma cells. Of note, B16-BL6 melanoma cells showed lung metastases both in C57BL/6 and *Ccr2$^{-/-}$* mice to a similar extent, indicating that these melanoma cells extravasate independently from CCR2 (Figure 32).

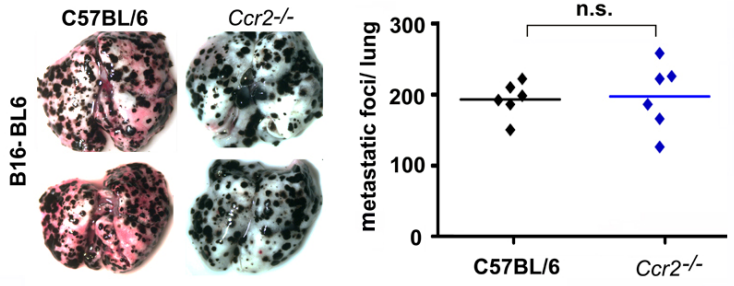

Figure 32: Tumor cell-derived CCL2 independent mechanisms of metastasis. Macroscopy of C57BL/6 and *Ccr2$^{-/-}$* lungs at 14 dpi with melanoma cells (B16-BL6) and quantification of tumor numbers (right). Each symbol depicts one individual mouse (n=6).

Tumor cell intrinsic mechanisms are likely to contribute to the observed CCR2 dependent differences in respect to extravasation and tumor metastasis. I first analyzed chemokine and chemokine receptor *mRNA* expression levels in lungs of C57BL/6 and *Ccr2*$^{-/-}$ mice injected with MC-38GFP cells. A strong increase in transcription levels of *Ccl2*, *Ccl7*, *Ccl12*, *Cxcl1* and *Cxcl10* was detected already at 4 hrs post tumor cell injection in lungs of C57BL/6 mice. Transcriptional changes of these genes persisted at 8 and 12 hrs p.i. however decreased over time. A similar pattern in the expression levels of chemokines upon injection of MC-38GFP was found in *Ccr2*$^{-/-}$ lungs (Figure 33, upper panels). This suggested that the majority of the induced chemokine expression in lung is unlikely to dependent on host derived CCR2. Alternatively, tumor cells could directly contribute to chemokine expression, altering the cellular composition and the activation status of cells in MC-38 challenged lungs. Besides, *mRNA* expression levels of most chemokine receptors were not altered in lungs of C57BL/6 and *Ccr2*$^{-/-}$ mice upon tumor cell injection (Figure 33, lower panels).

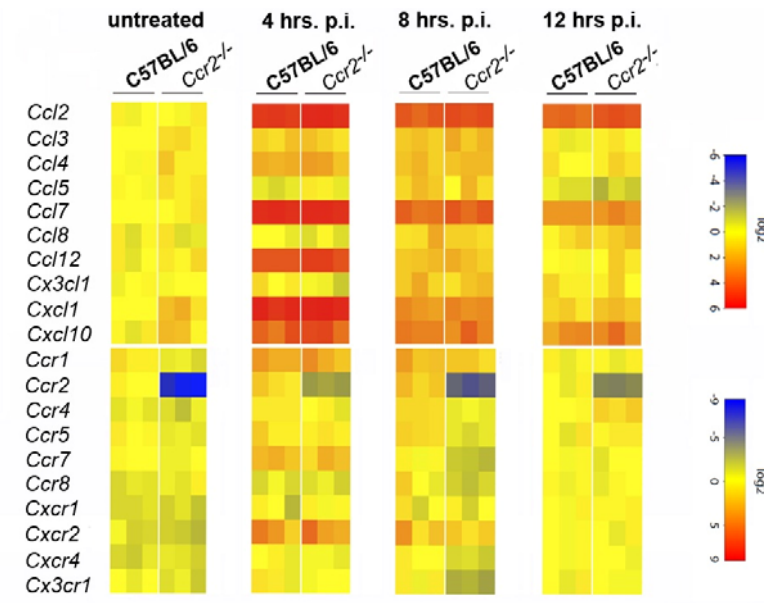

Figure 33: Real time PCR analysis for the expression of selected chemokines (upper panel) and chemokine receptors (lower panel) in lungs of C57BL/6 and *Ccr2*$^{-/-}$ mice. Untreated, 4 hrs p.i., 8 hrs p.i. and 12 hrs p.i. with MC-38GFP is shown from left to right. Data are presented in a log2 scale (red: up-regulated; blue: down-regulated). Columns indicate individual mice; rows represent particular genes. Each data point reflects the median expression of a particular gene resulting from three to four technical replicates, normalized to the mean expression value of the respective gene in C57BL/6 lungs.

Therefore, the majority of the induced chemokine expression found in lung tissue was probably CCR2 independent. We hypothesized that the observed expression pattern might derive from tumor cells themselves. Consequently, I analyzed chemokine *mRNA* expression in MC-38GFP in comparison to colon tissue. Indeed, *Ccl2*, *Ccl7* but also *Cxcl1* and *Cxcl10* were strongly expressed by MC-38GFP tumor cells (Figure 34, left panel).

Next, I investigated whether expression of CCR2 ligands (e.g. *Ccl2* and *Ccl7*) correlated with the inability of MC-38 and 3LL cells to extravasate and to form tumor nodules in *Ccr2*$^{-/-}$ mice. Similar to MC-38GFP cells, 3LL cells express high levels of *Ccl2* and *Ccl7* on *mRNA* level whereas B16-BL10 melanoma cells – which extravasated and formed tumors in lungs

independent of CCR2 – lacked or expressed extremely low *Ccl2* and *Ccl7 mRNA* levels (Figure 34, right panel).

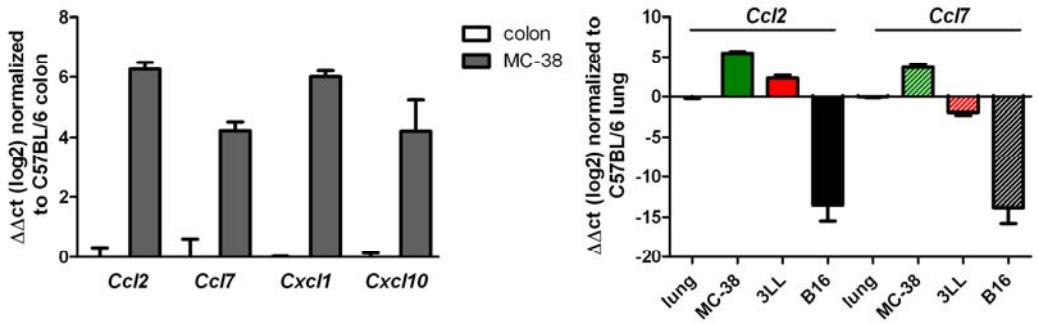

Figure 34: *mRNA* expression levels of selected chemokines in tumor cell lines. Real time PCR analysis for the expression of *Ccl2*, *Ccl7*, *Cxcl1* and *Cxcl10 mRNA* in MC-38GFP cells compared to colon tissue derived from C57BL/6 mice (left panel). Quantitative *mRNA* analysis for the expression of *Ccl2* and *Ccl7* in MC-38, 3LL and B16-BL6 compared to *mRNA* isolated from lungs of C57BL/6 mice (right panel). Data are presented as ΔΔct values on a log2 scale. Each bar reflects the median expression of a particular gene resulting from three to four biological samples with three to four technical replicates.

These results were also confirmed on protein level – MC-38 expressed high levels of CCL2 (left), 3LL medium levels (middle) and B16-BL6 melanoma cells did not show any CCL2 protein expression. Interestingly, B16-BL6 cells in general expressed only minimal amounts of cytokines and chemokines when compared to the other cell lines investigated (Figure 35).

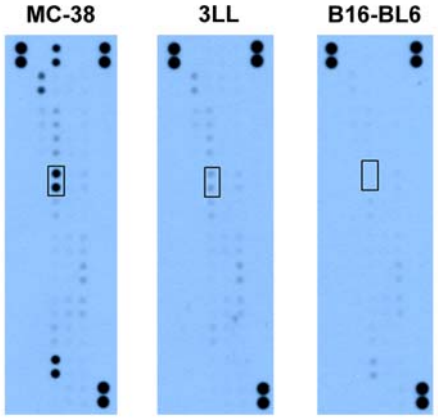

Figure 35: Cytokine and chemokine expression pattern in MC-38, 3LL and B16-BL6 cells. MC-38 cells (left blot) highly express a variety of cytokines and chemokines, whereas B16-BL6 in general only express low levels of these proteins. The box represents CCL2 expression, which was highly expressed in MC-38 cells, medium levels were found in 3LL cells (middle) and almost no CCL2 expression was found in B16-BL6 cells. Proteins dots in the upper right and left as well as lower right corners of each blot serve as positive controls for loading. Lower left corner serves as negative control.

Thus, we next investigated whether tumor cell-derived CCL2 is essential for the capacity of colon tumor cells to extravasate. Therefore, endogenous CCL2 was silenced in MC-38GFP cells (further denoted as MC-38GFP^{CCL2kd}) by lentiviral transduction and the silencing efficiency was around 75-90% on *mRNA* and 60-85% on protein level leaving the expression pattern of other investigated chemokines and cytokines unaltered (Figure 36). Cells stably transfected with scrambled RNA were prepared as control (further denoted as MC-38GFP^{scr}).

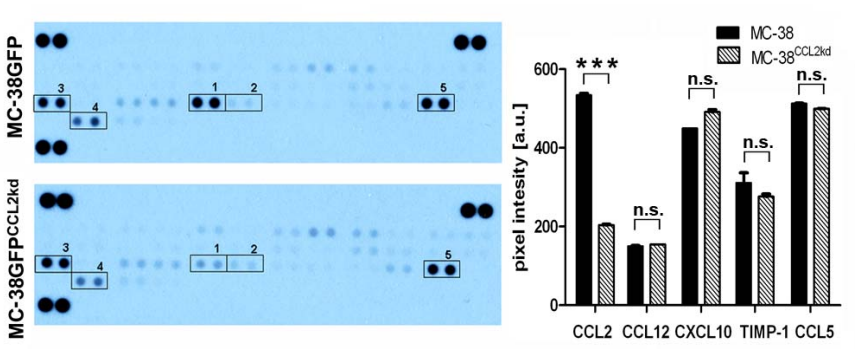

Figure 36: Efficient silencing of CCL2 in MC-38GFP^{CCL2kd} cells. Expression profile of chemokines and cytokines in MC-38GFP and MC-38GFP^{CCL2kd} cells. Only the protein level of CCL2 (1) is reduced, other expression levels (2: CCL12; 3: CXCL10; 4: TIMP-1; 5: CCL5) remain unaffected. Protein dots in the upper right and left corners serve as positive controls for loading (left). Quantification of pixel density (shown in arbitrary units [a.u.] of the before described chemokines; right). Statistical significance: ***=p<0.001; n.s. = not significant.

First, I examined the capability of MC-38GFP^{CCL2kd} cells to recruit monocytes. Therefore, C57BL/6 mice were injected MC-38GFP or MC-38GFP^{CCL2kd} cells and investigated by flow cytometry analysis for the capacity to recruit Ly6C^{hi} monocytes 4 and 12 hrs p.i. Similar amounts of Ly6C^{hi} cells were detected in lungs of C57BL/6 mice 4 hrs p.i. with MC-38GFP^{CCL2kd} or MC-38GFP cells, indicating that primary recruitment of inflammatory Ly6C^{hi} monocytes is rather systemic and most likely independent of tumor cell-derived CCL2 expression. However, 12 hrs p.i. Ly6C^{hi} cells were no longer efficiently retained in C57BL/6 lungs injected with MC-38GFP^{CCL2kd} tumor cells when compared to mice injected with MC-38GFP cells (Figure 37).

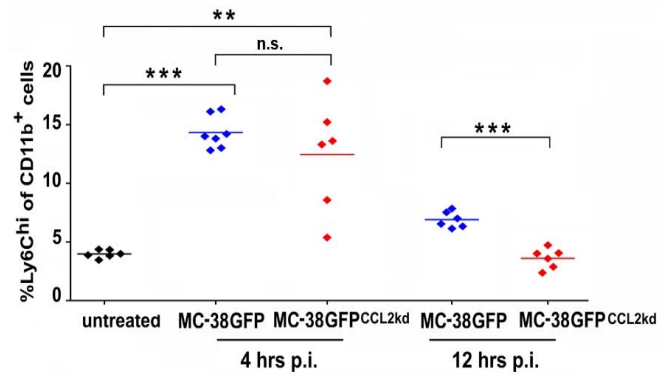

Figure 37: CCL2 expression levels of tumor cells determine retention of CD11b^{+}Ly6C^{hi} cells in the lungs after tumor cell challenge. Quantification of naïve C57BL/6 mice and 4 and 12 hrs post challenge with MC-38GFP (blue) and MC-38GFP^{CCL2kd} (red) cells. Each symbol depicts an individual mouse (n=6-7). Asterisks indicate statistical significance: ***=p<0.001; **=p<0.01; n.s. = not significant.

Therefore, the CCL2-CCR2 signaling axis controls the specific recruitment of Ly6C^{hi} cells upon tumor cell challenge. We next studied tumor cell extravasation and metastasis in lungs of C57BL/6 mice upon injection of MC-38GFP^{CCL2kd}, MC-38GFP or MC-38GFP^{scr} cells. C57BL/6 mice injected with MC-38GFP^{CCL2kd} cells displayed minimal or no lung metastasis, whereas MC-38GFP or MC-38GFP^{scr} cells induced strong tumor burden within lungs. These macroscopic findings were confirmed by quantification of GFP fluorescence of lungs of the respective groups ($p<0.001$; Figure 38).

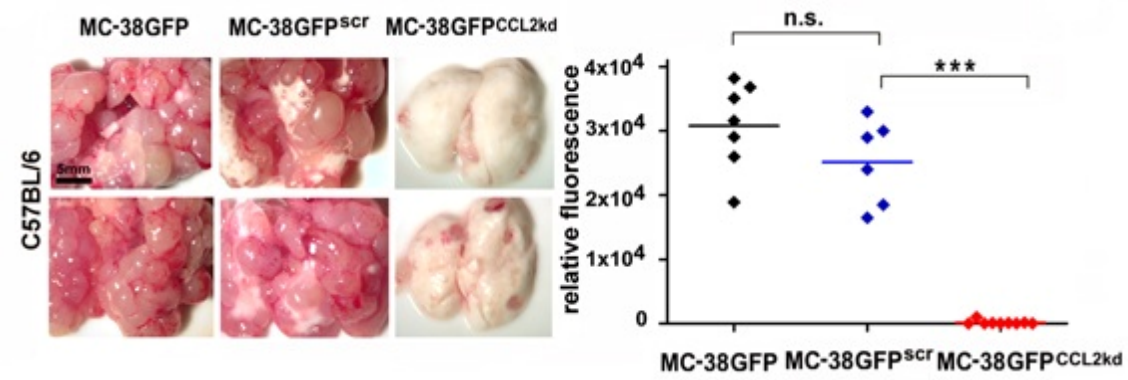

Figure 38: Loss of CCL2 expression in tumor cells leads to reduced tumor growth in the lungs of C57BL/6 mice. Macroscopy of lungs derived from C57BL/6 mice challenged with MC-38GFP (left), MC-38GFP^{scr} (middle) and MC-38GFP^{CCL2kd} (right) cells at 28 dpi. Size of scale bar is indicated. Quantification of GFP-fluorescence at 28 dpi in lung homogenates from C57BL/6 mice challenged with MC-38GFP (n=7), MC-38GFP^{scr} (n=6) and MC-38GFP^{CCL2kd} (n=9) cells. Each symbol represents an individual mouse (n=6-9). Asterisks indicate statistical significance: ***=p<0.001.

Interestingly, the extent of reduction in tumor growth observed in MC-38GFP^{CCL2kd}-injected C57BL/6 mice was similar to MC-38GFP-injected *Ccr2*$^{-/-}$ mice, indicating that CCL2-CCR2 interaction is important for efficient extravasation and metastasis of colon carcinoma cells.

To further assess the crucial role of tumor cell-derived CCL2 in metastasis, C57BL/6 mice were challenged with 3LL cells with reduced CCL2 expression (further denoted as 3LL^{CCL2kd}).

A strong decrease in lung metastasis was observed on macroscopic level in lungs of C57BL/6 mice challenged with 3LL^{CCL2kd} cells when compared to injection with 3LL cells. This was also confirmed by quantification of tumor foci (p<0.01; Figure 39).

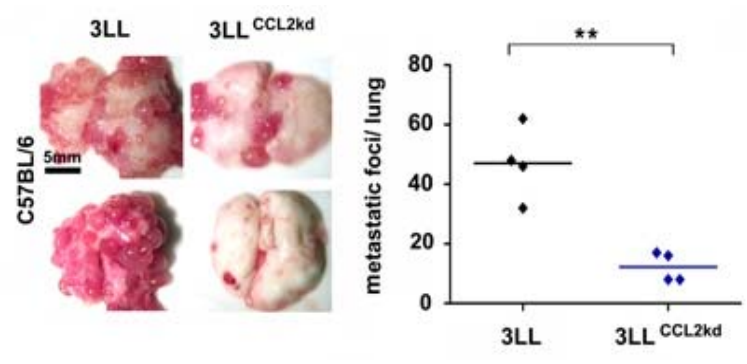

Figure 39: Loss of CCL2 expression on tumor cells leads to reduced tumor growth in the lungs of C57BL/6 mice. Macroscopy of lungs from C57BL/6 mice challenged with 3LL (left) and 3LL^{CCL2kd} (right) cells at 12 dpi. Size of scale bar is indicated. Quantification of tumor nodules of C57BL/6 mice injected with 3LL (n=4) and 3LL^{CCL2kd} (n=4) cells at 12 dpi. Statistical significance: **=p<0.01.

We next addressed whether tumor cell-derived CCL2 expression is crucial for efficient recruitment and association with myeloid cells in lungs of C57BL/6 mice. Reduced expression of CCL2 on MC-38GFP cells (MC-38GFP^{CCL2kd}) significantly diminished the capacity to interact CD11b^{+}, F4/80^{+} or Ly6C^{+} cells (p<0.001). Instead, MC-38GFP^{CCL2kd} tumor cells showed significantly enhanced interaction with Ly6G^{+} cells (p<0.001; Figure 40) that was similar to

observations with MC-38GFP cells injected *Ccr2*$^{-/-}$ mice. Interestingly, MC-38GFP^{CCL2kd} tumor cells failed to recruit adoptively transferred myeloid cells, when compared to MC-38GFP cells (Figure 40). The failure of MC-38GFP^{CCL2kd} to recruit myeloid cells, independent of the mouse genotype (*Ccr2*$^{-/-}$ or C57BL/6), supports the conclusion that CCL2 expression on tumor cells is a physical denominator for efficient myeloid cell – tumor cell interaction.

This indicates that recognition of tumor cells by monocytes is strongly decreased if CCL2 expression is missing or reduced on MC-38GFP cells.

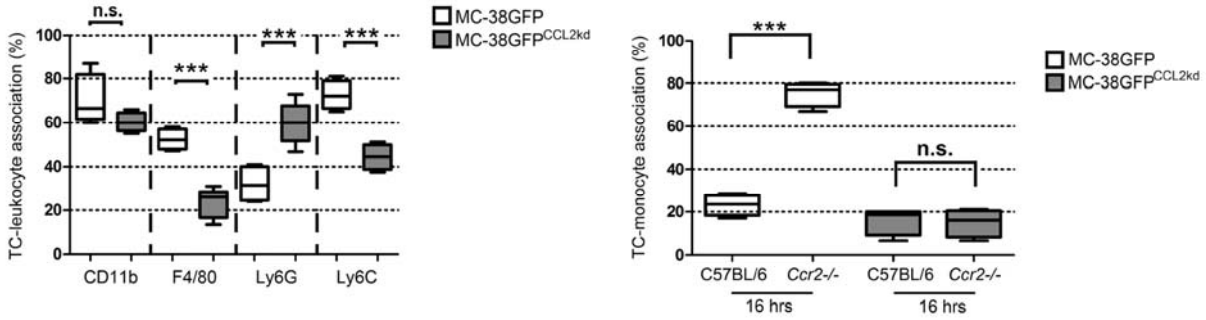

Figure 40: Tumor cell-derived CCL2 is important for interaction with myeloid cells. Quantitative analysis of confocal microscopy of tumor cell interaction with endogenous myeloid cells in C57BL/6 lungs challenged with MC-38GFP (white percentiles) and MC-38GFP^{CCL2kd} (gray percentiles) cells. Myeloid cell - tumor cell interaction in lungs of in C57BL/6 mice (from left to right: myeloid cells positive for CD11b, F4/80, Ly6G or Ly6C are quantified) 24 hrs post tumor cell challenge. Asterisks indicate statistical significance: ***=p<0.001; n.s. = not significant. Quantification of interaction of tumor cells (MC-38GFP: white percentiles, MC-38GFP^{CCL2kd}: gray percentiles) with adoptively transferred, PKH26-labeled monocytes in lungs of C57BL/6 and *Ccr2*$^{-/-}$ mice 16 hrs p.i. of tumor cells. Asterisks indicate statistical significance: ***=p<0.001; n.s. = not significant.

5.4.7 Interaction of CCR2^{+} endothelial cells and tumor cell-derived CCL2 determines lung permeability

To determine whether endothelial CCR2 expression was sufficient to induce vascular permeability, we injected Tie2CCR2/*Ccr2*$^{-/-}$ mice with MC-38GFP cells. Elevated levels of Evans blue in Tie2CCR2/*Ccr2*$^{-/-}$ lungs strongly indicate that endothelial CCR2 activation is sufficient to induce lung vascular permeability. As host-derived CCL2 has been implicated in metastasis [5], we injected *Ccl2*$^{-/-}$ mice with MC-38GFP cells. Interestingly, upon injection of tumor cells, increased lung vascular permeability has been detected both by macroscopical analysis and quantification of Evans blue in lung tissue. In line, MC-38GFP^{CCL2kd} cells failed to induce vascular permeability in C57BL/6 lungs (Figure 41).

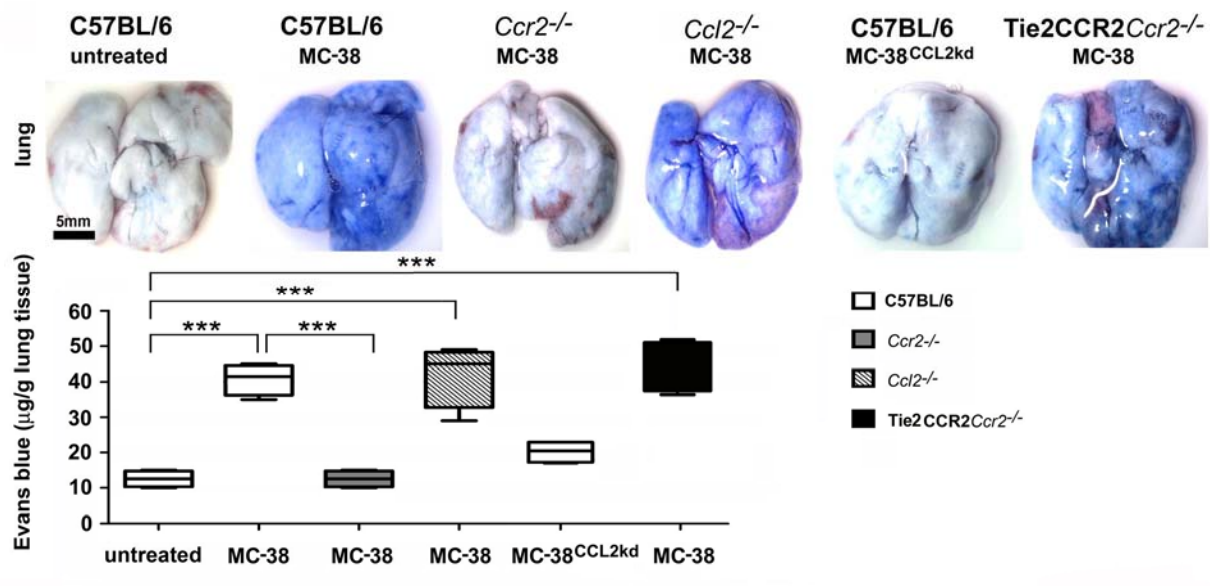

Figure 41: Permeability of lung tissue upon tumor cell injection depends on tumor cell-derived CCL2 and endothelial CCR2. Macroscopy of lungs with Evans blue accumulation derived from untreated C57BL/6 mice (very left) or C57BL/6 (left), *Ccr2*$^{-/-}$ (second from left) and *Ccl2*$^{-/-}$ mice (second from right) 24 hrs post-challenge with MC-38GFP and C57BL/6 mice 24hrs post-challenge with MC-38GFP^{CCL2kd} cells (right). Size of scale bar is indicated. Spectrophotometric quantification of Evans blue (extracted from lung tissue) from C57BL/6 mice (white), *Ccr2*$^{-/-}$ mice (gray), *Ccl2*$^{-/-}$ mice (hatched) 24 hrs post challenge with MC-38GFP and MC-38GFP^{CCL2kd} cells. Statistical significance is indicated: ***=p<0.001.

These results strongly suggest that tumor cell-derived CCL2 as well as endothelial CCR2 expression are sufficient for induction of lung vascular permeability and that CCL2 production from the host tissue can be neglected in this context.

To investigate whether the local microenvironment (e.g. CCL2 expression; monocytes; stromal cells) could rescue the incapability of CCL2-deficient tumor cells (MC-38GFP^{CCL2kd}) to extravasate and metastasize, we co-injected equal amounts of MC-38 and MC-38GFP^{CCL2kd} cells into C57BL/6 mice. Similar numbers of metastases were observed in lungs of C57BL/6 mice injected with MC-38 versus MC-38GFP^{CCL2kd}/MC-38 mixed cells 28 dpi (p=0.6).
As observed before, injection with MC-38GFP^{CCL2kd} cells led to significantly reduced numbers of metastases. Of note, in lungs of mice injected with equal amount of MC-38GFP^{CCL2kd} and MC-38 cells, histological analyses revealed more GFP^{-} than GFP^{+} tumors (p<0.001; Figure 42). Only few GFP^{+} metastases were found, suggesting that tumors have mainly originated from CCL2-expressing MC-38 cells.

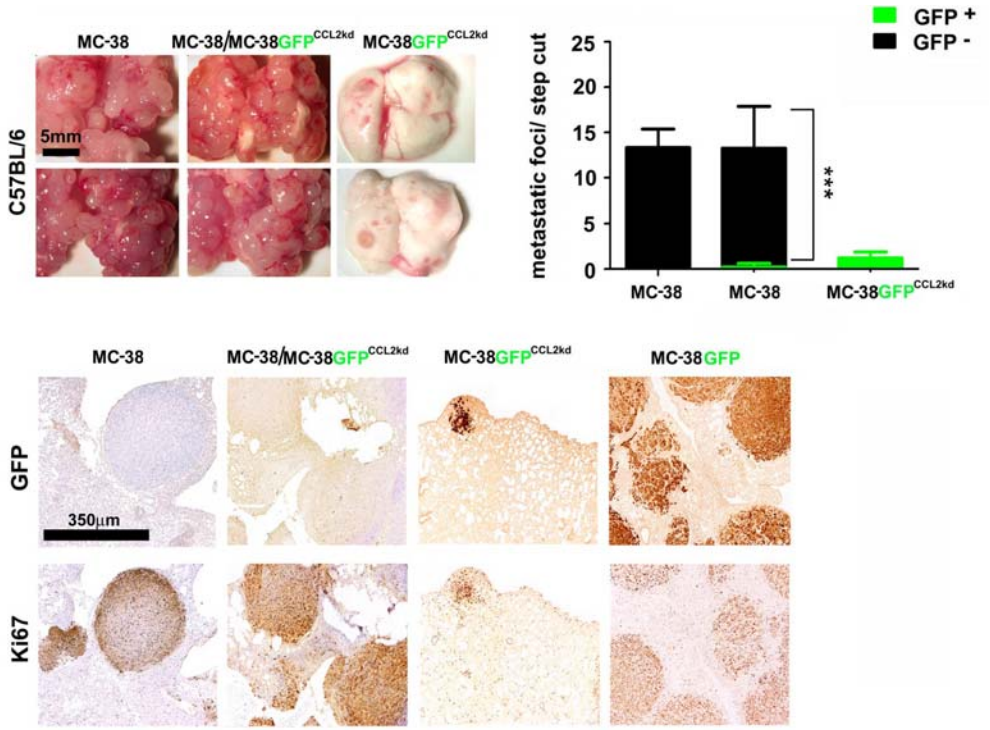

Figure 42: An identical microenvironment does not lead to lung metastasis in tumor cells devoid of CCL2 expression. Macroscopy of lungs derived from C57BL/6 mice at 28 dpi upon injection of MC-38 (left, n=3) MC-38 and MC-38GFP^{CCL2kd} (1:1 ratio; middle, n=5) and MC-38GFP^{CCL2kd} cells (right, n=3). Quantification of tumor nodules on step cuts through lungs (black bars represent MC-38 cells, green bars MC-38GFP^{CCL2kd} cells). Statistical significance: ***=p<0.001 (right panel). Representative images of step cuts used for the quantification of tumor nodules. GFP and Ki67 staining served as markers for tumor cells. Size of scale bar is indicated.

This indicates that the inability of MC-38GFP^{CCL2kd} cells to establish lung metastases cannot be restored by a local microenvironment, where CCL2, inflammatory monocytes and lung permeability were generally increased. The fact that only CCL2 expressing tumor cells can extravasate efficiently and form lung tumors, suggests that cell-cell interaction mediated by the CCL2-CCR2 axis is essential for efficient tumor cell extravasation and subsequent metastasis.

We next examined lungs of C57BL/6 and *Ccr2*$^{-/-}$ mice 12 hrs p.i. with MC-38 tumor cells at ultrastructural level. In general, injection of MC-38 cells induced broad changes in C57BL/6 lung tissue including increased thickness of airway epithelial cells in the bronchi and thickened smooth muscle cells. Tumor cells were found inside the alveoli (Figure 43, left panel) and rarely in the vessels. Alveoli in C57BL/6 mice appeared shrunken and contained numerous alveolar macrophages and type I, II pneumocytes. Moreover, we observed an intimate interaction between MC-38 tumor cells and endothelium in C57BL/6 mice, with tumor cell protrusions spanning through the apical side of the endothelium resembling ongoing tumor cell transmigration (Figure 43, middle panel, inset). In contrast, *Ccr2*$^{-/-}$ lung endothelium appeared to

be grossly unaffected by the injection of MC-38 tumor cells with no visible indication for endothelial attachment (Figure 43, right panel, inset).

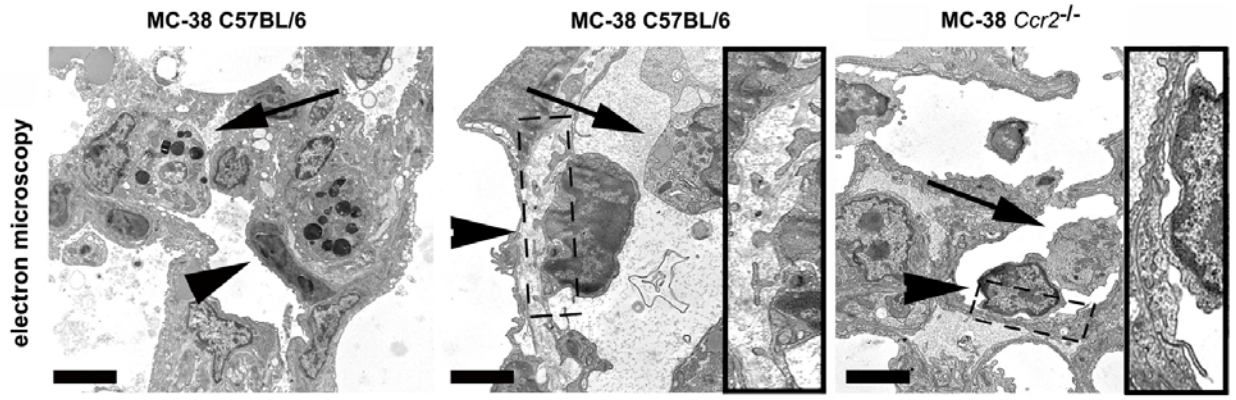

Figure 43: Electron microscopical images of lungs of C57BL/6 (left and middle) and *Ccr2*$^{-/-}$ mice (right) 12 hrs p.i. with MC-38GFP cells. Left panel: arrowhead points towards a tumor cell in the alveolar space in close contact to a type II pneumocyte (arrow). Middle panel: arrowhead shows an attached and transmigrating tumor cell localized within the vessel. The arrow indicates a monocyte within the vessel. The insert shows the interaction between the tumor cell and the vessel wall at higher magnification. Right panel: No visible transmigration of tumor cells. Arrowhead shows a tumor cell, arrow indicates a monocyte within the vessel. Size of scale bar: 5μm.

5.4.8 Endothelial CCR2 signaling controls tumor cell extravasation through the JAK2-Stat5 and p38MAPK pathways

Our data suggest that tumor cell extravasation depends on the CCR2-mediated increase in endothelial permeability induced through tumor cell-derived CCL2. In addition, recruitment of Ly6C^{hi} monocytes through CCR2 significantly contributes to metastasis. To delineate the exact mechanism of this signaling cascade we examined the efficiency of tumor cell transmigration on endothelial cells derived either from C57BL/6 or *Ccr2*$^{-/-}$ mice, in presence or absence of monocytes *in vitro*. MC-38GFP cells incubated on C57BL/6 endothelial cells for 16 hrs transmigrated only minimally towards an FCS gradient. In contrast, co-cultivation of MC-38GFP cells with BM-derived monocytes induced efficient transmigration of MC-38GFP cells through C57BL/6 endothelial cells ($p<0.001$; Figure 44). We next asked whether endothelial cells isolated from *Ccr2*$^{-/-}$ mice would impair tumor cell transmigration. Similarly to CCR2^{+} endothelial cells, MC-38GFP cells alone were unable to transmigrate through the CCR2-deficient endothelial monolayer. However, co-cultivation with monocytes failed to induce significant transmigration of MC-38GFP tumor cells through the CCR2-deficient endothelial monolayer, although monocytes were able to interact with the tumor cells through the CCL2-CCR2 axis ($p=0.6$; Figure 44).

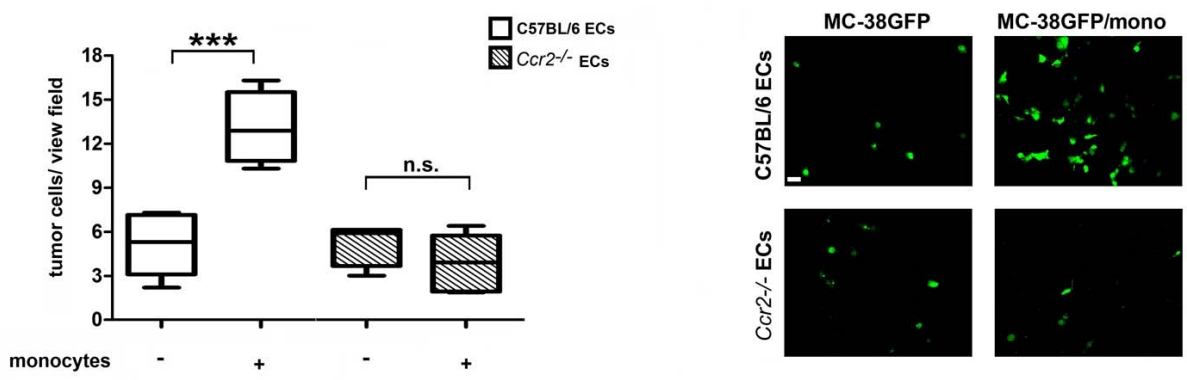

Figure 44: Transmigration of MC-38GFP cells through endothelial cells is facilitated by monocytes. BM-derived monocytes were co-cultured with MC-38GFP cells on a monolayer of endothelial cells derived either from C57BL/6 or *Ccr2*$^{-/-}$ mice for 16 hrs. Transmigrated GFP^{+} tumor cells in the lower chamber were counted. Statistical significance is indicated: ***=p<0.001; n.s. = not significant. Representative images of transmigrated tumor cells for each co-culture are presented in the right panel. Scale bar: 10µm.

Monocytes were observed to efficiently transmigrate through the *Ccr2*$^{-/-}$ endothelial monolayer – similar to experiments with a C57BL/6 monolayer (data not shown), indicating that the CCR2-deficient endothelium per se allows cell transmigration. Taken together, our *in vitro* and *in vivo* experiments provide evidence for the specific role of endothelial CCR2 signaling to facilitate tumor cell transmigration without affecting monocyte transmigration.

To examine whether transmigration of tumor cells is dependent on tumor cell-derived CCL2, we tested the capability of MC-38GFP^{CCL2kd} cells to transmigrate through CCR2^{+} endothelial cells. In contrast to MC-38GFP, MC-38GFP^{CCL2kd} cells could not efficiently transmigrate through the monolayer of C57BL/6 endothelium in the presence of monocytes (p<0.001; Figure 45).

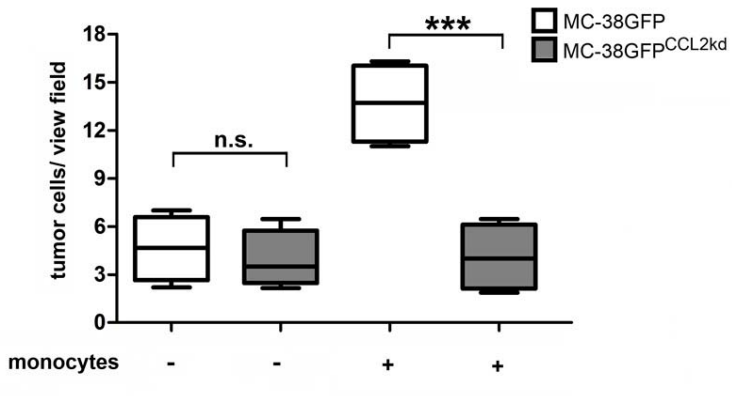

Figure 45: Transmigration of tumor cells is dependent on tumor cell-derived CCL2 expression. MC-38GFP cells were compared with MC-38GFP^{CCL2kd} cells for their efficiency to migrate through C57BL/6 endothelial cells in the presence or absence of monocytes. Statistical significance: ***=p<0.001.

We next set out to identify the signaling mechanism(s), induced by CCR2 activation on endothelial cells, responsible for tumor cell extravasation. The CCR2 receptor has been identified to integrate CCL2 activation via the Janus kinase 2 (JAK2) [19], thereby activating downstream targets such as Stat1, Stat3 and Stat5, p38MAPK and the PI3K pathway [35, 84].

We first tested whether inhibition of JAK2 phosphorylation with AG490 can block tumor cell transmigration. Inhibition of JAK2 phosphorylation indeed blocked tumor cell transmigration, demonstrating the requirement of CCR2-JAK2 signaling cascade ($p<0.001$). We next tested inhibitors of Stat3 or Stat5 phosphorylation for its efficacy to block tumor cells transmigration. Inhibition of Stat3 (S3I-201) failed to significantly affect tumor cell migration ($p=0.8$), while inhibition of Stat5 significantly blocked tumor cell transmigration of MC-38GFP cells compared to untreated controls ($p<0.001$). This finding suggested the CCR2-JAK2-Stat5 axis as important for tumor cell transmigration. Whereas inhibition of the PI3K pathway (Wortmannin) did not alter efficacy of tumor cell extravasation, inhibition of p38 (SB202190) significantly blocked tumor cell extravasation ($p<0.001$). Therefore, the CCR2-JAK2-Stat5 and the p38MAPK pathways appeared to efficiently block *in vitro* transmigration of MC-38GFP cells through the C57BL/6 endothelium. We next addressed, whether tumor cells would transmigrate through endothelial junctions or transinvade endothelial cells, which was shown to depend on Rac/Rho GTPases [85]. However, inhibition of Rac1 (with NSC23766) failed to block tumor cell transmigration, indicating that tumor cell transmigration occurs via junctions in the endothelial barrier (Figure 46).

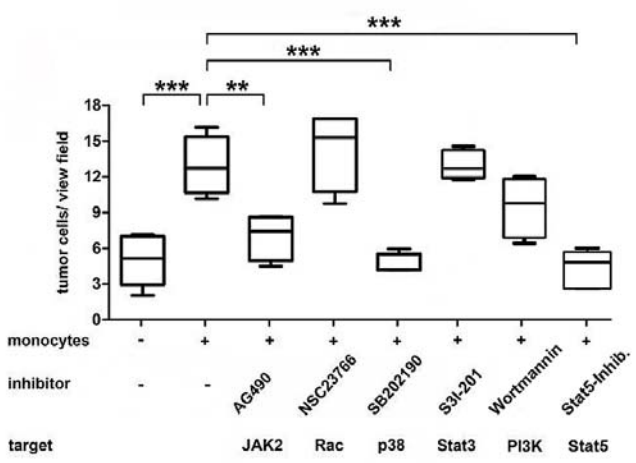

Figure 46: CCL2-CCR2 mediated permeabilization of the endothelium is driven by JAK2-Stat5 and p38MAPK activation. Transmigration of tumor cells through an endothelial monolayer is dependent on JAK2-Stat5 and p38MAPK pathway. Inhibitors of JAK2 (AG490), Rac1 (NSC23766), Stat3 (S3I-201), p38MAPK (SB201290), PI3K (Wortmannin) and Stat5 pathway were added to the co-culture of MC-38GFP cells with monocytes. Transmigrated tumor cells were counted in the lower chamber. Statistical significance: ***=$p<0.001$; **=$p<0.01$.

To provide further evidence for the involvement of CCR2-JAK2 axis in tumor cell extravasation, I analyzed JAK2 phosphorylation in lung homogenates of tumor cell-challenged C57BL/6 and *Ccr2*$^{-/-}$ mice. Indeed, increased JAK2 phosphorylation was observed at 8 and 12 hrs p.i. in lungs of C57BL/6 mice, whereas JAK2 protein levels remained unaltered. AG490 strongly reduced JAK2 phosphorylation, while keeping JAK2 protein levels comparable to controls. Since p38MAPK is thought to be downstream of JAK2, inhibition of p38 phosphorylation with SB202190 did not affect JAK2 phosphorylation. Importantly, no or minor phosphorylation of JAK2 has been detected in *Ccr2*$^{-/-}$ mice after tumor injection proving that CCR2 expression in lungs is crucial to integrate and activate this signaling cascade. Similarly, p38MAPK phosphorylation and Stat5 activation are induced upon tumor challenge in C57BL/6 lungs

(between 8 to 12 hrs p.i.) and were minimal or missing in lungs of *Ccr2*$^{-/-}$ mice. Taken together, these data strongly indicate that both the JAK2-Stat5 and the p38MAPK pathways are linked to tumor cell transmigration (Figure 47).

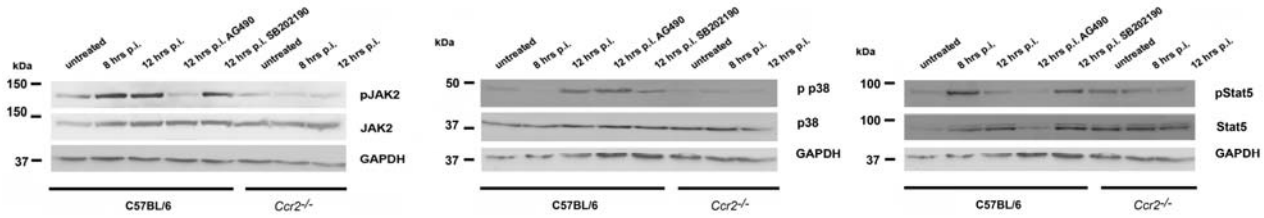

Figure 47: JAK2, p38 and Stat5 become activated in lungs of C57BL/6 but not in lungs of *Ccr2*$^{-/-}$ mice upon challenge with MC-38 tumor cells. Immuno-blot analysis of lung samples derived from C57BL/6 mice (untreated, 8 hrs p.i. and 12 hrs p.i.), C57BL/6 mice treated with AG490 (JAK2 inhibitor) or SB202190 (p38 inhibitor) and *Ccr2*$^{-/-}$ mice (untreated, 8 hrs p.i. and 12 hrs p.i.). Left panel from top to bottom: pJAK2, JAK2, GAPDH are shown, middle panel from top to bottom: phospho-p38, p38 and GAPDH are shown, right panel from top to bottom: pStat5, Stat5 and GAPDH are shown.

Next, I investigated whether the observed effects of the CCR2-JAK2-Stat5 or p38MAPK pathway activation in C57BL/6 mice upon tumor cell injection are triggered exclusively in endothelial cells, in monocytes or in both cell types. I therefore challenged Tie2CCR2/*Ccr2*$^{-/-}$ mice (which lack Ly6C^{hi} monocytes but express CCR2 on the endothelium) with MC-38GFP cells in order to see whether endothelial activation of CCR2 would suffices to induce Stat5 and p38MAPK phosphorylation. Phosphorylation of JAK2, Stat5 as well as p38MAPK was observed in lungs of Tie2CCR2/*Ccr2*$^{-/-}$ mice 8 and 12 hrs p.i. with tumor cells to a similar degree as in C57BL/6 mice. Therefore, JAK2 and p38MAPK phosphorylation in endothelial cells occur in the absence of Ly6C^{hi} monocytes, indicating that this activation is due to CCR2 expression on endothelial cells (Figure 48).

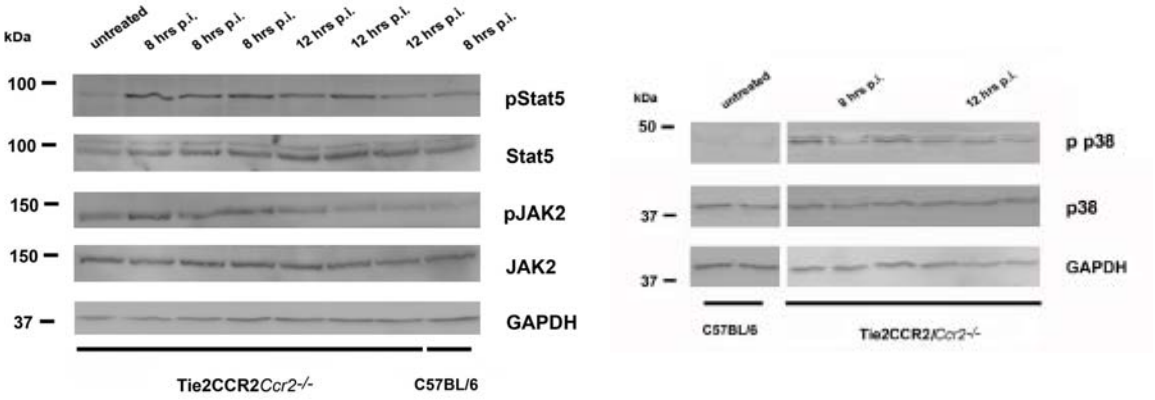

Figure 48: JAK2-Stat5 becomes phosphorylated in Tie2CCR2/*Ccr2*$^{-/-}$ mice upon tumor cell challenge. Immuno-blot analysis of lung samples derived from Tie2CCR2C57BL/6 mice (untreated, 8 hrs p.i. and 12 hrs p.i.) and C57BL/6 mice (8 hrs p.i.). From top to bottom: pStat5, Stat5, pJAK2, JAK2, GAPDH are shown.

We next aimed at investigating the effect of JAK2, p38MAPK, Stat5, Stat3 and Rac1 inhibition *in vivo*. First we analyzed whether MC-38GFP cells increase vascular permeability in presence of JAK2 inhibition. Lungs of C57BL/6 mice injected with MC-38GFP cells and concomitant treatment with JAK2 inhibitors were analyzed for Evans blue accumulation. As previously shown injection of MC-38GFP significantly induced vascular permeability, resulting in blue-colored lung tissue. In contrast, JAK2 inhibition prevented endothelial permeability. Treatment of mice with Rac1 (NSC23766) and Stat3 (S3I-201) inhibitors failed to block endothelial permeability, while treatment with inhibitors of Stat5 and p38MAPK (SB202190) blocked or strongly reduced the vascular permeability induced by MC-38GFP cells. These data were confirmed by spectrophotometrical quantification of Evans blue in lung homogenates (Figure 49). Taken together, these data suggest that inhibition of Stat5 and p38MAPK signaling pathways block tumor cell-triggered induction of vascular permeability *in vivo*.

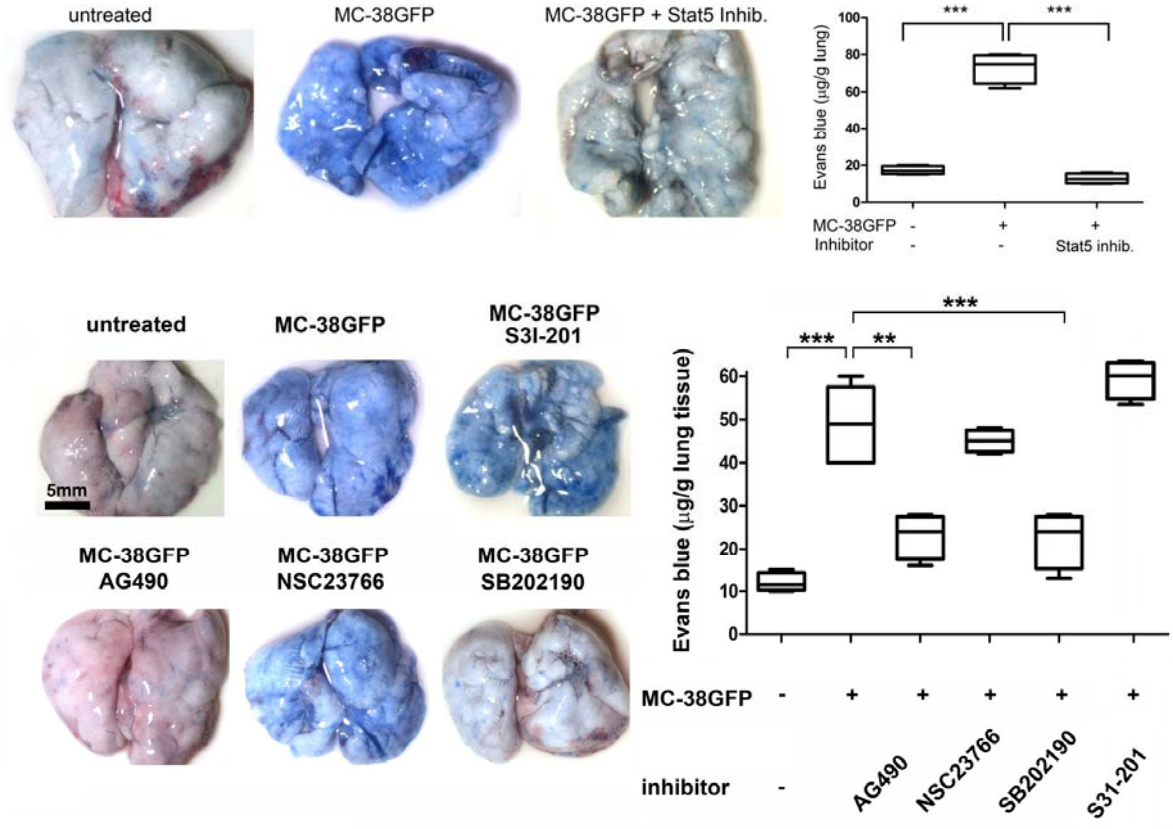

Figure 49: Inhibition of JAK2-Stat5 and p38MAPK signaling reduces vascular permeability upon tumor cell challenge. Vascular permeability of lungs was tested in presence or absence of inhibitors for Stat5 (upper panel) Stat3 (S3I-201), pJAK2 (AG490), Rac (NSC23766), and p38MAPK (SB202190) (lower panel) at 16 hrs after intravenous challenge with MC-38GFP cells. Evans blue extracted from lung tissue was quantified spectrophotometrically (n=4, each). Statistical significance: ***=p<0.001; **=p<0.01.

Having observed that endothelial CCR2 expression is essential for tumor cell extravasation, I investigated whether lack of CCR2 signaling *in vivo* would result in the deregulation of particular

target genes downstream of Stat5 and p38MAPK being tightly associated with the interaction and vascular integrity of endothelial cells. For this reason, I analyzed *E-selectin*, *Vcam*, *Icam*, *Vegfa*, *Vegfb, Occludin*, *Claudin5* and *VE-Cadherin* expression on *mRNA* levels in lung tissue of C57BL/6 and *Ccr2*$^{-/-}$ mice 8 hrs p.i. with MC-38GFP. Indeed, I could find a significantly decreased induction of *E-selectin* and *Icam* expression ($p<0.05$) in lungs of *Ccr2*$^{-/-}$ mice upon tumor cell injection when compared to C57BL/6 mice (Figure 50). These data suggest the pro-inflammatory endothelial response associated with metastasis [86] was reduced in *Ccr2*$^{-/-}$ mice.

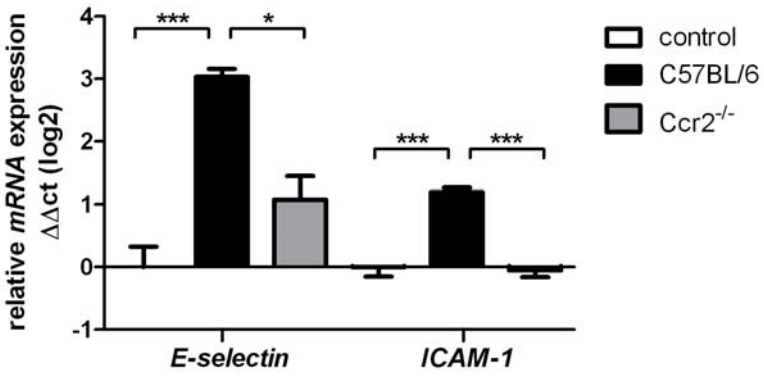

Figure 50: The inflammatory response of endothelial cells is altered in lungs of *Ccr2*$^{-/-}$ mice. Real-time PCR analysis for *E-selectin* and *ICAM-1* expression in lungs of C57BL/6 (black) and *Ccr2*$^{-/-}$ (gray) mice 8 hrs p.i. with MC-38GFP. Each bar reflects the median expression resulting from three to four technical replicates, normalized to the mean expression value of the respective gene in C57BL/6 lungs (control). Data are presented in a log2 scale; (n=3). Statistical significance: ***=$p<0.001$; *=$p<0.05$.

Finally, to test whether targeting phosphorylation of JAK2 and p38MAPK pathways would affect lung metastasis, we treated MC-38GFP-injected mice with AG490 and SB202190 during the first 3 dpi. Indeed both, blocking of JAK2 and p38MAPK signaling pathways, led to a significant decrease in tumor burden in lungs of C57BL/6 mice, as confirmed by quantification of metastatic foci in lungs of JAK2 and p38 inhibitor treated mice 26 dpi ($p<0.05$). These findings strongly indicate that these two pathways resemble valid therapeutic targets for blocking CCL2-mediated tumor cell extravasation and metastasis (Figure 51).

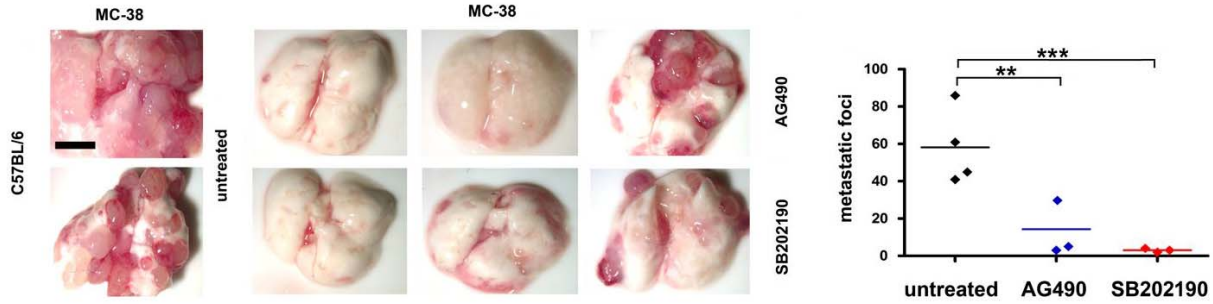

Figure 51: Inhibition of JAK2-Stat5 and p38MAPK signaling leads to reduced lung metastasis. Macroscopy of C57BL/6 lungs at 26 dpi with MC-38GFP cells of untreated control mice or mice treated with AG 490 or SB202190. Size of scale bar: 5mm (left panels). Quantification of metastatic foci in lungs of untreated C57BL/6 (n=4), AG490- or SB202190-treated mice (n=3, each). Asterisks indicate statistical significance: ***=$p<0.001$; **=$p<0.01$.

5.4.9 CCL2 expression correlates with metastatic potential in human colon cancer tissue

Elevated CCL2 expression correlates with metastasis and poor prognosis in various cancer types, including breast, prostate and colon cancer [6, 87, 88]. I therefore analyzed *CCL2* expression in human primary non-metastasized colon tumors (UICC stages I and II) and in colon tumors that metastasized into the lymph nodes (UICC stage III) or into distant organs (UICC stage IV). RNA from these tissues was obtained from Prof. Michael Stürzl from the University Hospital Erlangen. *CCL2* transcripts were more abundant in primary colon tumors of stages I, II and III when compared to healthy colon samples. However *CCL2* expression was particularly high in colon tumors stage IV that have developed metastases in distant organs indicating that upregulation of *CCL2* correlates with metastatic potential (Figure 52).

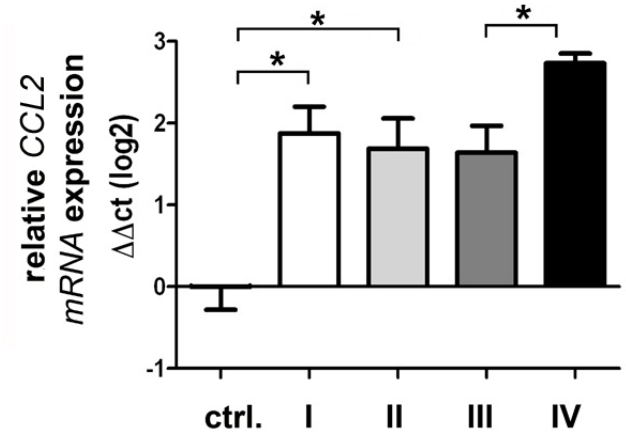

Figure 52: Transcriptional analysis of *CCL2* levels in tissue obtained from colon-cancer patients. *mRNA* expression levels in healthy control tissues (ctrl.; n=4), in tumor samples classified as stage I (white bar; n=10), stage II (light gray bar; n=10) both being non-metastatic; stage III: metastastic in lymph nodes (gray bar; n=10), stage IV: metastatic in distant organs (black bar; n=9) colon carcinomas were studied. Data are presented in a log2 scale. Each bar reflects the median expression of a gene resulting from three to four technical replicates, normalized to the mean expression value of *CCL2* in control samples. Statistical significance: * = $P<0.05$.

If tumor cell-derived CCL2 expression is also involved in facilitating extravasation of metastatic colon carcinoma cells in the human situation remains to be determined. It seems to be feasible to test this in an *in vitro* model systems using human endothelia and tumor cell lines, however, to determine in patients whether CCL2 mediates extravasation for at least some types of tumors will be very challenging.

5.5 Discussion

5.5.1 Tumor cell-derived CCL2 induces vascular permeability and extravasation

This study uncovered a novel role for chemokine receptors in regulating tumor cell extravasation. We could show that activation of the chemokine receptor CCR2 on endothelial cells by tumor cell-derived CCL2 is crucial for enabling efficient tumor cell extravasation and metastatic colonization of the lung. Using MC-38 colon carcinoma and 3LL lung carcinoma cells in an experimental metastasis mouse model in chimeric, transgenic and knock-out mice we could define the role of tumor cell-derived CCL2 in inducing lung vascular permeability and facilitating extravasation into the surrounding parenchyma, recruitment of Ly6C^{hi} monocytes and thereby metastasis.

Upon injection of MC-38 cells, C57BL/6 mice displayed strong metastatic growth within the lungs upon tumor cell challenge, whereas metastases were significantly reduced or almost absent in the lungs of *Ccr2*$^{-/-}$ mice. Tumor cell-derived CCL2 controlled this extravasation process not only by attracting Ly6C^{hi} monocytes but also – and even more important – by direct signaling via the CCL2-CCR2 axis between tumor cells and endothelial cells as tested with tumor cells devoid of CCL2 expression.

During the multistep process of metastasis chemokine-chemokine receptor interactions have been described to have pro- or anti-tumorigenic effects [5, 42, 89]. So far, the understanding of the involvement of chemokine receptors in metastasis was that cancer cells were shown to express chemokine receptors (e.g. CXCR4, CCR7, CCR9 and CCR10) [90-93] and therefore the tropism of cancer cell metastases was explained by chemokine production in the future host tissue. CXCL12, the ligand for CXCR4 was found to be expressed at high levels in the lung, liver and lymph nodes – organs that are frequently sites of metastases. In addition, CCL21 the ligand of CCR7 is expressed in lymph nodes [91, 94]. However, there have been no reports so far in the literature that chemokine receptors are capable of deciding about the fate of tumor cells by allowing tumor cell extravasation and induction of vessel permeability.

In line, the description of CCR2 expression in metastasis was mainly restricted to its expression on tumor cells, which was assessed in several studies. In prostate to bone metastasis, knock-down of CCR2 on prostate cancer cells led to reduced invasion [95] and expression levels of CCR2 in prostate tumors correlated with aggressiveness and progression [96]. Furthermore, it was shown that human multiple myeloma cells express CCR2, which facilitates the bone marrow homing of these tumor cells [97].

The importance of CCR2 expression on endothelial cells (HUVECs and HMECs) was only described in the context that CCL2 is important for angiogenesis [60]. Besides, several reports addressed the role of CCR2 expression on monocytes in tumor progression and metastasis. CCR2 expression on myeloid suppressor cells, which are thought to contribute to the immune

evasion of tumor cells, was shown to be essential for efficient migration of these cells to tumor sites and for tumor growth [98].

It was shown that over-expression of CCL2 in metastatic tumor cell lines increased metastasis of breast cancer cells to the lung and to the bone [95]. In line, elevated CCL2 levels in lungs have been linked to malignancy and increased metastasis in various types of cancer [6, 7, 9, 87]. Furthermore increased infiltration with tumor associated macrophages was reported. By using macrophages and bone marrow cells isolated from *Ccr2*$^{-/-}$ mice it could be clarified that CCR2 expression in these stromal cells is essential for tumor-derived CCL2 to recruit macrophages and to promote osteoclastogenesis – the first step to bone metastasis [96]. Another study focused on the tumor growth and tumor infiltrating cells comparing C57BL/6 and *Ccr2*$^{-/-}$ mice. Interestingly, no alterations in tumor growth were observed (in a model with subcutaneous injections of tumor cells), however, tumors in *Ccr2*$^{-/-}$ mice seemed to be more necrotic and their cellular composition was altered, with more tumor infiltrating neutrophils (CD11b^{+}Gr1^{+} cells) and less macrophages (CD11b^{+}Ly6C^{hi}) [99]. However, the differences in the cellular composition of tumors in C57BL/6 and *Ccr2*$^{-/-}$ mice are not surprising considering that *Ccr2*$^{-/-}$ mice lack CD11b^{+}Ly6C^{hi} cells. In line with these data we could show increased interaction of MC-38GFP tumor cells with CD11b^{+}Gr1^{+} (in our case Ly6G) cells in lungs of *Ccr2*$^{-/-}$ mice in the early phase of tumor seeding.

A recent publication showed that CCR2^{+}Gr1^{+} inflammatory monocytes are preferentially found in pulmonary metastases of breast tumors and not within the primary tumors [5]. These cells facilitate metastasis via the CCL2-CCR2 axis and subsequent attraction of growth-promoting metastasis-associated macrophages. Depletion of tumor-derived CCL2 could attenuate metastatic seeding [5] – however with poor efficiency and leaving the question unanswered which cell type is responsible for the CCL2 production. The weak rescue in metastasis could be explained by the fact that treatment with neutralizing antibodies always leads to residual presence of the ligand, which might suffice to allow growth of some metastatic cells. Especially when our data are taken into account, it becomes obvious that tumor cell-derived CCL2 is important in the induction of vessel permeability and extravasation and knock-down or depletion of CCL2 must be very efficient to avoid these steps. Moreover, we could also show that depletion of CCR2^{+}Ly6C^{hi} cells with MC21 (a CCR2-depleting antibody) does not suffice to attenuate metastasis – most likely due to the unaltered presence of tumor cell-derived CCL2 as well as stromal CCR2 expression. Also in the approach chosen by Qian *et al*., the expression of CCR2 on the endothelium is unaltered and therefore it is not astonishing that metastatic spread at relatively high levels is still found in this model.

We identified that increase in vascular permeability in the lung, tumor cell extravasation and recruitment of Ly6C^{hi} monocytes are initiated by CCL2-expressing tumor cells at the sites of vascular arrest. Furthermore, initial seeding of tumor cells to the lungs appeared to be

independent of CCL2 expression, indicating that tumor cell-derived CCL2 is critical for the subsequent steps of metastasis. Increase in lung vascular permeability has also been recently identified as a prerequisite for lung metastasis of Lewis lung carcinoma [100]. Challenging of C57BL/6 mice with MC-38GFP cells significantly increased lung vascular permeability as tested by Evans blue accumulation, while no alteration in *Ccr2*$^{-/-}$ mice was observed.

To test the contribution of host (microenvironmental)-derived CCL2 on tumor cell extravasation we examined *Ccl2*$^{-/-}$ mice. Increased vascular permeability was detected both in *Ccl2*$^{-/-}$ and C57BL/6 mice suggesting that the contribution of host-derived CCL2 seems to be less likely. Our data rather demonstrated that tumor cell-derived CCL2 is sufficient for the induction of vascular permeability. This was further confirmed by the observation that silencing of CCL2 expression in two different syngeneic tumor cell lines (MC-38GFP or 3LL) resulted in inability to induce lung vascular permeability, and as a consequence could not form metastasis. Tumor cell-derived CCL2 is essential for this retention of monocytes within the lungs as MC-38GFP^{CCL2kd} cells failed to retain Ly6C^{hi} cells and to interact with CD11b^{+}, F4/80^{+} or Ly6C^{+} cells within lungs of C57BL/6 mice.

5.5.2 CCR2 – a chemokine receptor involved in controlling tumor cell extravasation and metastatic growth

Which cellular compartment integrates CCL2 signaling through CCR2 and thereby facilitates tumor cell extravasation and metastasis?

From the literature, it is obvious that human endothelial cell lines express CCR2 [60] however, there were no reports showing that CCR2 is expressed on murine endothelial cells in the lung. I could confirm expression of CCR2 on endothelial cells both on histological and *mRNA* expression level in C57BL/6 mice, suggesting that CCR2 expression on endothelial cell might play an important role – besides Ly6C^{hi} monocytes – in tumor cell extravasation and metastasis leading to the decreased metastatic tumor load in the lungs of *Ccr2*$^{-/-}$ mice. Therefore we examined mice expressing CCR2 exclusively on endothelial cells (Tie2CCR2/*Ccr2*$^{-/-}$ mice) – which resemble C57BL/6 mice depleted of Ly6C^{hi} monocytes. In these mice the expression levels of *Ccr2 mRNA* are comparable to the levels found in pulmonary endothelial cells of C57BL/6 mice. Upon challenge with MC-38GFP cells, reduced but still marked metastatic tumor growth in the lungs of Tie2CCR2/*Ccr2*$^{-/-}$ mice was observed – emphasizing the importance of stromal CCR2 expression and that CCR2^{+}Ly6C^{hi} monocytes are important in facilitating some but not all steps of metastasis. Testing the induction of lung permeability in Tie2CCR2/*Ccr2*$^{-/-}$ mice upon tumor cell challenge using Evans blue further revealed that the induction of lung permeability is dependent on the expression of CCR2 on endothelial cells.

In line, ultrastructural analyses of lungs derived from C57BL/6 and *Ccr2*$^{-/-}$ mice challenged with tumor cells further confirmed these data. Tumor cells failed to closely interact with endothelial cells in lungs of *Ccr2*$^{-/-}$ mice 12 hrs p.i. with MC-38 cells, which is necessary for allowing activation of the endothelium and subsequent transmigration and observed in lungs of C57BL/6 mice at this time point.

Next, we analyzed the contribution of CCR2^{+} monocytes as CCL2-dependent recruitment of monocytes to metastatic sites has been shown to contribute to tumor cell metastasis and to facilitate colonization in lung and bone [5, 62, 96]. In line, I have observed significant recruitment of Ly6C^{hi} monocytes in lungs of C57BL/6 mice but not in *Ccr2*$^{-/-}$ mice correlating with metastasis. Efficient depletion of CCR2 from inflammatory monocytes in *LysMCreCcr2*$^{loxP/loxP}$ mice without altering the numbers of Ly6C^{hi} monocytes in blood and in lung tissue led to reduced numbers of metastases. In the early phase after tumor cell seeding a reduced recruitment of inflammatory monocytes was found within the lungs of *LysMCreCcr2*$^{loxP/loxP}$ mice compared to C57BL/6 mice confirming the data that interaction of CCR2^{+} monocytes and tumor cells expressing CCL2 are needed in this step. However, we cannot exclude that in these experiments the presence of any other myeloid cell type is assisting to facilitate tumor cell extravasation as a recent study showed that Ly6G^{+}Ly6C^{+} granulocytes facilitates metastasis [101].

Yet, the amount of metastases in *LysMCreCcr2*$^{loxP/loxP}$ mice as well as in C57BL/6 mice reconstituted with BM from *Ccr2*$^{-/-}$ mice was considerably higher than in *Ccr2*$^{-/-}$ mice, indicating a role of stromal CCR2 in metastasis. *Ccr2*$^{-/-}$ mice reconstituted with C57BL/6 BM showed minimal lung metastasis of MC-38GFP cells, comparable to *Ccr2*$^{-/-}$ mice. Taken together, these data indicate that endothelial CCR2 expression is sufficient for induction of vascular permeability and thereby metastasis. Moreover, these data indicate that inflammatory monocytes appear to be necessary but not sufficient for metastasis.

To our knowledge, we show for the first time that endothelial CCR2 signaling facilitates and licenses metastasis through promoting tumor cell-extravasation. But what is the exact function of endothelial CCR2? We hypothesized that CCR2 on endothelial cells could resemble a “key-lock” signal for opening the vasculature and enabling extravasation of CCL2^{+} tumor cells into the lung parenchyma. Indeed, we found that expression of CCR2 on endothelial cells is linked to the induction of vascular permeability. This “key-lock” relation was solely dependent on CCL2 expression by tumor cells since MC-38^{CCL2kd} cells failed to induce vascular permeability and metastasis in C57BL/6 mice. Of note, proximate interaction of CCL2 expressing colon carcinoma cells with the CCR2^{+} endothelium but not just a local CCL2 gradient is needed for efficient tumor cell-extravsation and subsequent metastasis, as MC-38GFP^{CCL2kd}/MC-38 co-injection only induced efficient metastasis of MC-38 but not of MC-38GFP^{CCL2kd} cells.

5.5.3 JAK2-Stat5 and p38MAPK pathways facilitate tumor cell extravasation and metastasis downstream of CCR2 expressed on endothelial cells

We established an *in vitro* tumor cell transmigration assay with primary pulmonary endothelial cells isolated from C57BL/6 and *Ccr2*$^{-/-}$ mice to delineate the molecular mechanisms of CCR2 dependent tumor cell extravasation. Efficient tumor cell transmigration in the presence of monocytes was only observed through a CCR2^{+} endothelial monolayer while no increase in tumor cell transmigration was detected through a CCR2^{-} endothelial monolayer, confirming the crucial role of CCR2 expression on endothelial cells. Interestingly, monocyte transmigration through endothelial cells was not affected by CCR2 expression, indicating that CCR2^{-} endothelium per se allows cell transmigration. Moreover, in this approach tumor cells devoid of CCL2 expression failed to transmigrate – indicating that tumor cell-derived CCL2 is not only needed for retention and interaction with monocytes but as well for the transmigration through the endothelial barrier. These results highlight that the ability of monocytes to cross endothelial barriers does not affect the capacity of tumor cells to migrate and that CCR2 expression on endothelial cells specifically enables transmigration of CCL2^{+} tumor cells underlining our *in vivo* results that endothelial-derived CCR2 signaling is a major contributor to efficient tumor cell extravasation.

CCR2 deficiency of endothelial cells did not allow tumor cell transmigration, indicating that this chemokine receptor most likely triggers a signaling which leads to opening of the endothelial cell layer and therefore allows passage of tumor cells.

Several signaling pathways where shown to participate in endothelial cell activation for diapedesis of leukocytes during inflammation [102, 103] and some of them are pathways downstream of CCR2 (e.g. Stat3; PI3K) [35, 104]. Therefore, we used the transmigration assay to test which downstream pathways could be involved in efficient tumor cell transmigration. Inhibition of JAK2 as well as Stat5 and p38MAPK led to efficient blockage of tumor cell transmigration indicating that these pathways might be involved in extravasation of colon carcinoma cells from blood vessels within the lung. Inhibition of PI3K, Rac or Stat3 pathway however did not affect endothelial transmigration.

Testing these inhibitors *in vivo*, we could reproduce these findings as inhibition of either JAK2, Stat5 or p38MAPK pathways almost completely reduced vascular permeability upon tumor cell challenge. Previously, the p38MAPK pathway has been identified in endothelial cells to be activated by transmigrating tumor cells [105]. Our data provide evidence about the upstream activation of p38MAPK pathway that is triggered by CCR2 and integrated through JAK2 leading to priming of endothelia. Western blot analysis of JAK2, Stat5 and p38 phosphorylation in homogenates prepared from lungs of C57BL/6 mice challenged with MC-38 cells revealed that these two pathways act independently of each other, since inhibition of p38 phosphorylation did

not block Stat5 or JAK2 phosphorylation. In contrast, JAK2 inhibition blocked Stat5 but not p38 phosphorylation. It was therefore plausible that the two identified signaling pathways originated from two different cell types and that the significant effects of the two inhibitors stem from a timely organized cascade. By challenging Tie2CCR2/*Ccr2*$^{-/-}$ mice with MC-38GFP cells and subsequently analysing lung tissue for Stat5, JAK2 and p38MAPK phosphorylation, I could rule out that both pathways are triggered by CCR2 expressed on endothelial cells as JAK2, Stat5 and p38MAPK were activated 8 and 12 hrs after tumor cell challenge. Analysis of downstream targets of both pathways indicated a Stat5-dependent inflammatory-like induction of *E-selectin* and *Icam-1* expression which was CCR2-dependent [86].

Mice treated with AG490 (JAK2 inhibitor) or SB202190 (p38 Inhibitor) during the first three days upon MC-38GFP injection showed a significantly reduced metastasis. These observations indicate that targeting pathways downstream of the CCR2 receptor might have a potential therapeutically application in CCL2 expressing cancers.

Based on the presented data, we propose the following model describing the involvement of CCR2 in metastasis (Figure 53).

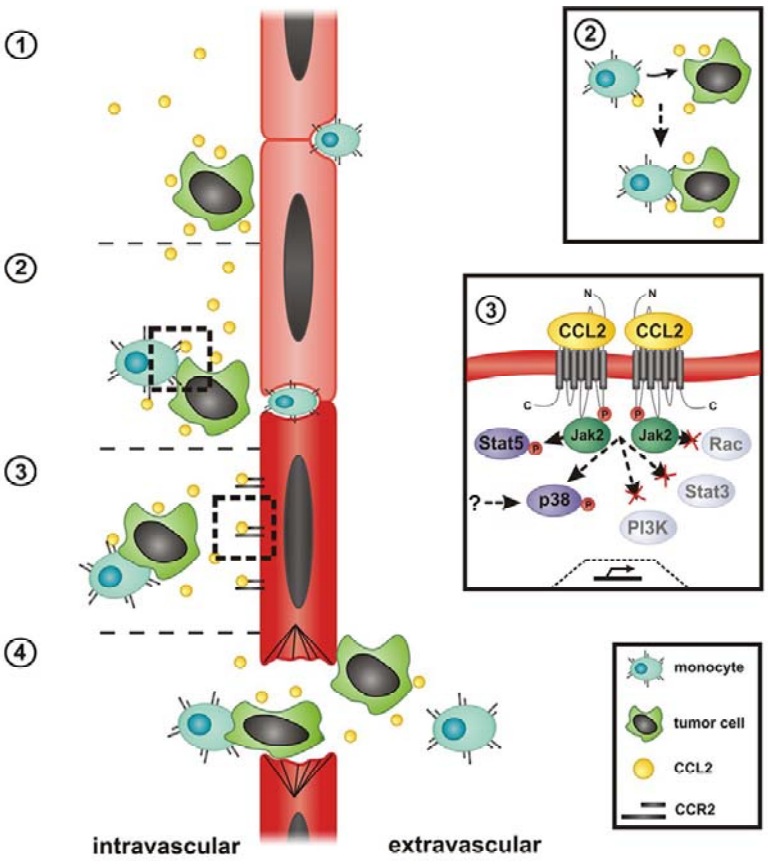

Figure 53: CCL2-CCR2 mediated tumor cell extravasation. This schematic model depicts the four steps how tumor cells may extravasate in a CCR2-dependent manner: Tumor cells attract Ly6C^{hi} monocytes by secreting CCL2 (step 1) and then closely interact with the monocytes (step 2). Binding of CCL2 to CCR2 on endothelial cells activates the endothelium and triggers JAK2-Stat5 and p38MAPK signaling downstream of CCR2 (step 3). These signaling pathways lead to an induction of permeability of the endothelial barrier and tumor cells can extravasate presumably via local opening of tight or adherent junctions (step 4).

Upon vascular arrest, CCL2 expressing tumor cells induce a local chemokine gradient that mediates the recruitment of CCR2-expressing inflammatory monocytes and interaction of monocytes and tumor cells. At the same time or subsequently, direct activation of the

endothelium is triggered by tumor cells through CCR2. This is required for efficient tumor cell extravasation, which is depends on activation of the JAK2-Stat5 or p38MAPK pathway. Induction of one of these signaling pathways leads to local opening of tight or adhesive junctions and extravasation of tumor cells facilitated by inflammatory monocytes.

Elevated CCL2 levels have been previously linked to malignancy and increased metastasis in a number of cancers [6, 8, 9, 57, 88]. The analysis of primary colon tumors (UICC stages I to IV) confirmed the link between CCL2 upregulation in stage IV colon carcinoma and metastatic capacity. Chemokines and chemokine receptors are more and more evaluated as potential targets for therapy in various diseases including metastasis [50, 106, 107]. Further studies will be required to understand the temporal and spatial hierarchy of chemokine-mediated crosstalk between monocytes, endothelial cells and metastasizing tumor cells. Certainly, the CCL2-CCR2 axis is just one possible chemokine-chemokine receptor axis that tumor cells utilize. Nevertheless, further studies will be required to identify which tumor use chemokine-chemokine receptor interactions for efficient tumor cell extravasation and metastasis. Our data describe that efficient inhibition of CCR2 or its downstream targets (JAK2/Stat5/p38MAPK) represents a novel, potential therapeutical strategy for preventing CCL2-mediated metastasis.

6 LYMPHOTOXIN'S ROLE IN INFLAMMATION-INDUCED CARCINOGENESIS

Parts of the 'Introduction', 'Material and Methods', 'Results' and 'Discussion' section are reproduced or adapted from the following publications:

"Lymphotoxin's Link to Carcinogenesis: Friend or Foe? From Lymphoid Neogenesis to Hepatocellular Carcinoma and Prostate Cancer"

Monika Julia Wolf, Gitta Maria Seleznik, and Mathias Heikenwalder

Institute of Neuropathology, Department of Pathology, University Hospital Zurich, Switzerland

Published in Adv Exp Med Biol (2011) 691:231-49

"The unexpected role of lymphotoxin β receptor signaling in carcinogenesis: from lymphoid tissue formation to liver and prostate cancer development"

MJ Wolf[1], GM Seleznik[1], N Zeller[1] and M Heikenwalder[1,2]

[1] Department of Pathology, Institute of Neuropathology, University Hospital Zurich, Switzerland

[2] Institute of Virology, Technische Universität München/Helmholtz Zentrum München, Munich, Germany

Published in Oncogene (2010) 29(36):5006–5018

"A lymphotoxin-driven pathway to hepatocellular carcinoma"

J Haybaeck,[1,16] N Zeller,[1,15,16] MJ Wolf,[1] A Weber,[2] U Wagner,[3] MO Kurrer,[4] J Bremer,[1] G Iezzi,[5] R Graf,[6] PA Clavien,[6] R Thimme,[7] H Blum,[7] SA Nedospasov,[8,9] K Zatloukal,[10] M Ramzan,[11] S Ciesek,[12] T Pietschmann,[12] PN Marche,[11] M Karin,[13] M Kopf,[5] JL Browning,[14] A Aguzzi,[1] and M Heikenwalder[1]

[1] Department of Pathology, Institutes of Neuropathology and [2] Clinical Pathology, University Hospital Zurich

[3] Functional Genomics Center Zurich, University Zurich, Switzerland

[4] Department of Pathology, Cantonal Hospital Aarau, Switzerland

[5] Institute of Integrative Biology, Molecular Biomedicine, Swiss Federal Institute of Technology (ETH) Zurich

[6] Swiss HPB (Hepato-Pancreatico-Biliary) Center, Department of Surgery, University Hospital Zurich, Switzerland

[7] Department of Internal Medicine, University of Freiburg, Germany

[8] Engelhardt Institute of Molecular Biology, Moscow, Russia

[9] German Rheumatism Research Center (DRFZ), Berlin, Germany

[10] Institute of Pathology, Medical University of Graz, Austria

[11] INSERM and Université Joseph Fourier-Grenoble, Unité 823, Institut Albert Bonniot, Grenoble, France

[12] Division of Experimental Virology, TWINCORE, Centre for Experimental and Clinical Infection Research, Medical School Hannover (MHH) and the Helmholtz Centre for Infection Research (HZI), Hannover, Germany

[13] University of California, San Diego and University of California, Los Angeles, USA

[14] Department of Immunobiology, Biogen Idec, Cambridge, MA, USA

[15] Present address: Department of Neuropathology, University of Freiburg, Germany

[16] These authors contributed equally to this work

Published in Cancer Cell (2009) 16(4):295-308

6.1 Introduction

6.1.1. Inflammation-induced carcinogenesis

In the last decade, several experimental and epidemiological studies have reported a tight link between chronic inflammation, tissue damage and the risk of developing cancer [108]. However, only recently, the inflammatory microenvironment was indeed added as the seventh hallmark of cancer [108], being now generally accepted to be on eye level with self-sufficiency in growth signals, insensitivity to anti-growth signals, tissue invasion and metastasis, limitless replicative potential, sustained angiogenesis, and evasion from apoptosis, as defined by Hanahan and Weinberg in 2000 [109] and summarized in Figure 54.

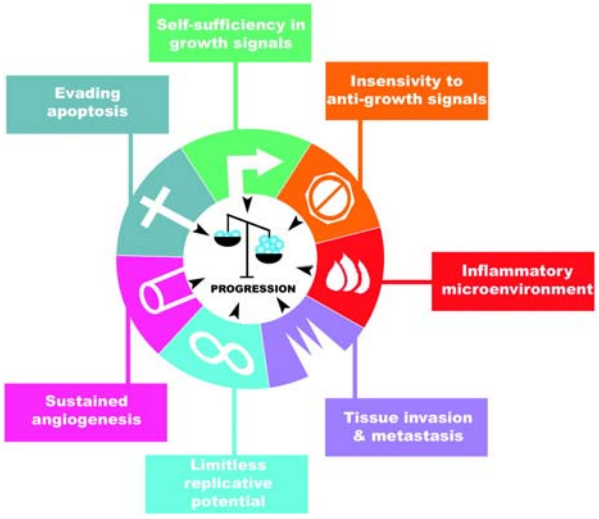

Figure 54: The seven hallmarks of cancer [108]. Hanahan and Weinberg summarized that most if not all types of cancer show six biologically common features acquired during the development of tumors. They described that evasion from cell death, insensitivity to growth suppressing signals from the surrounding tissue, self-sufficiency in proliferative signaling, constant formation of new vessels, limitless replicative potential and the capacity to invade adjacent tissue and to form metastases [109]. Due to increasing knowledge that inflammation can be pro-tumorigenic by increasing e.g. genomic instability, the inflammatory microenvironment is now also recognized as a hallmark of cancer [108].

This was ultimately the result of more than 100 years of research – indeed – the concept of a potential link between cancer and inflammation is dating back to the second half of the nineteenth century when Rudolph Virchow and others made the observations that tumors often arise at sites of chronic inflammation, scars and wound healing [110].

In the last few years, it became more and more obvious that chronic inflammation cannot only induce tissue damage and compensatory proliferation which can drive cancer development. It can also provide a microenvironment consisting of various mediators such as cytokines, chemokines, and prostaglandins possessing tumor-promoting effects by enhancing cell proliferation, cell survival, angiogenesis, and tumor cell migration [111]. At the same time, the inflammatory microenvironment can as well execute immune-suppressive effects on e.g. cytotoxic T-cells or NKT-cells and thereby weaken the anti-tumor immune response [112, 113].

In line, it was shown that tumors can contain immune cells, secreting various cytokines, e.g., TNFα, IFNγ, IL1β, IL6, IL8, reactive oxygen species (ROS), growth factors such as hepatocyte growth factor (HGF) and transforming growth factor β (TGFβ), as well as matrix-degrading

enzymes which unexpectedly can promote DNA damage, cell proliferation leading to pre-neoplastic lesions or cancer [114-116].

Due to their cellular and molecular composition, tumors are considered as "wounds that do not heal" and the tumor stroma was found to be similar to the tissue of healing skin wounds [117]. Indeed, several studies revealed similarities between wound healing and tumorigenesis as both processes aim at the clearance of dead cells and restoration of tissue integrity [118]. Even more interestingly, in both processes inflammatory responses are found, however in tumorigenesis, the inflammatory response seems to have lost its self-limiting control [119].

Several types of cancer were shown to be preceded by chronic inflammation, which is often due to chronic infections; estimations assume about 15% of human cancers being associated with inflammation [120]. Chronic hepatitis, most often caused by hepatitis B or C virus (HBV, HCV), was shown to lead to the development of hepatocellular carcinoma (HCC) [121-123], intestinal inflammation, e.g. in patients suffering from ulcerative colitis or Crohn's disease, have an increased risk of developing colorectal carcinoma [124, 125], increasing with the duration and the severity of the inflammatory disorder [125]. Gastritis, which is mainly caused by *Helicobacter pylori*, is a risk factor for the development of gastric cancer and mucosa-associated lymphoid tissue (MALT) lymphoma [126, 127]. Furthermore, chronic inflammation due to infection with parasites (e.g. Schistosoma) can facilitate the development of bladder cancer [128].

Early this year, Hanahan and Weinberg modified their description of the hallmarks of cancer by adding some key features that are common to many types of cancer. They note that there are emerging hallmarks such as deregulation of cellular energetics and avoidance of immune destruction. Furthermore, so-called enabling characteristics such as genome instability and mutation as well as tumor promoting inflammation were shown to support development and growth of tumors [4].

6.1.2. Lymphotoxin and its link to inflammation

Lymphotoxin (LT) was described and denoted as a "cytotoxic factor" in the late 1960s by Nancy Ruddel and colleagues. Isolated lymph node cells from rats showed cytotoxic effects on syngeneic or allogeneic fibroblasts in the presence of specific antigens [129, 130].

Besides, *in vitro* stimulation of murine lymphocytes led to secretion of these earlier described cytotoxic factors into the culture medium, capable of killing various cell types (e.g., *L* cells, fibroblasts) [131, 132]. LT was later isolated from stimulated lymphocytes and characterized in various species including mouse, guinea pig, and human [133, 134] and defined as a "lymphokine" being a non-antibody mediator of cellular immunity generated by lymphocyte activation [135]. In 1984, human LT was the first cytokine to be purified from a b-lymphoblastoid cell line [136] and thereafter its amino-acid sequence and structure were determined [137, 138].

The amino-acid sequence determination revealed a close relationship of LT to TNFα, first described in 1975 as a substance causing efficient necrosis in various tumor types *in vivo* by cytotoxic activity [139]. As a consequence LT was renamed into TNFβ [136, 137, 140]. It became evident that these two cytokines are prototypic members of a gene superfamily, later defined as the TNF superfamily (TNFSF) [141]. These molecules subsequently caught attention of several research groups using these cytotoxic, tumor necrotizing capabilities for their therapeutic potential in the treatment of human cancer.

Later a third ligand – homologous to TNFβ – was identified within the major histocompatibility complex locus and named LTβ (TNFSF3) [142-145], as a result TNFβ was termed backed to LTα or TNFSF1B. At present, 19 different ligands belong to the TNFSF, including, for example, TRAIL, RANKL, BAFF, CD40 [146], mediating their cellular response through 29 receptors, which contain an extracellular cysteine-rich domain [146] and in some cases (for example, TNFR1, TNFR2, TRAIL R1, TRAIL R2, Fas) a death domain.

Interestingly, besides their biochemical similarities LTα, LTβ, and TNFα (TNFSF1A) are found in close proximity on genomic level within the major histocompatibility complex region (mouse, chromosome 17 [147, 148]; man, short arm of chromosome 6 [149, 150].

Under physiological conditions, LTα and LTβ are expressed by activated T-, B-, natural killer (NK) and lymphoid tissue inducer cells [146]. LTα expression is inducible in B-cells, whereas LTβ *mRNA* is constitutively produced [144, 151]. Like most of the TNFSF ligands, LTβ is a type II transmembrane protein (intracellular N-terminus), while LTα is soluble, but can be recruited to the cell membrane to form membrane-anchored heterotrimeric complexes with membrane-bound LTβ ($LT\alpha_1\beta_2$ and $LT\alpha_2\beta_1$) [144, 152]. Recently it was described that LTαβ heterotrimers can also be cleaved from the cell surface by matrix metalloproteases eliciting responses on distal cells [153]. Similar to TNFα, LTα can be secreted as a soluble $LT\alpha_3$ homotrimer and bind to and signal via the TNF receptors TNFR1 (p55) or TNFR2 (p75) and herpes virus entry mediator (HVEM). $LT\alpha_1\beta_2$ exclusively and $LT\alpha_2\beta_1$ mainly trigger LTβR [154], which is predominantly found on stromal and parenchymal cells but apparently also on myeloid cells [155]. LTβR signaling might enable the communication between lymphocytes and stromal cells, thereby influencing various biological processes such as lipid metabolism, proliferation, etc [154, 156-158].

In addition $LT\alpha_2\beta_1$ was reported to bind TNFR1 and TNFR2, but this is a diminutive LT form expressed by T-cells (<2%) with a yet undefined biological role [154]. LIGHT (TNFSF14) is an alternative ligand for the LTβR but also interacts with HVEM [159]. Figure 55 summarizes the above mentioned TNF and LT/LIGHT pathway.

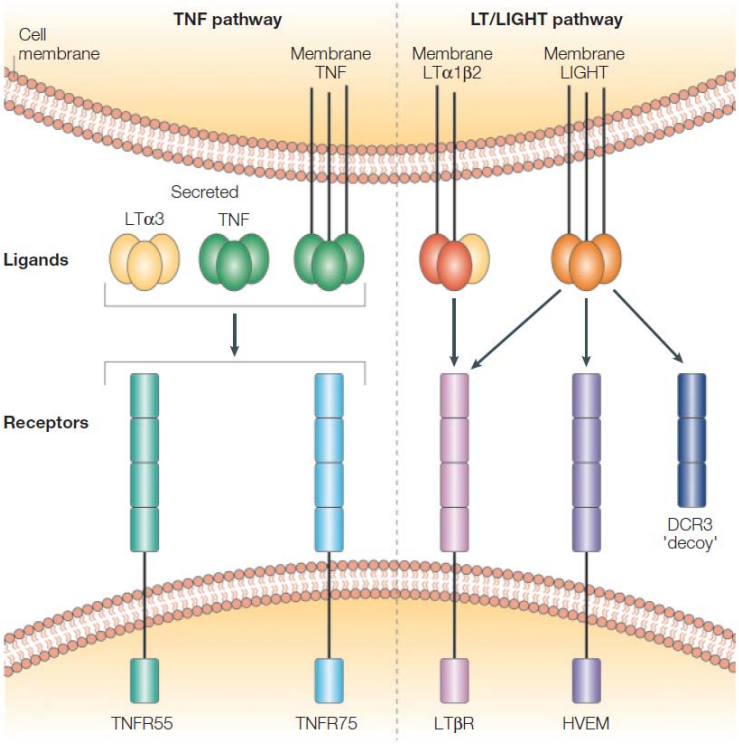

Figure 55: Ligands and receptors of the TNF/LT system [156]

The TNF pathway is characterized by the expression of two receptors – TNFR1 (p55) and TNFR2 (p75). These receptors become activated by binding either $LT\alpha_3$, $TNF\alpha$ (being both secreted molecules) or membrane bound $TNF\alpha$ (left). The LT/LIGHT pathway involves two receptors, namely $LT\beta R$ and HVEM, which can both bind LIGHT. Furthermore, $LT\alpha_1\beta_2$ and $LT\alpha_2\beta_1$ serve also as ligands for $LT\beta R$.

6.1.3. Pathways incorporating lymphotoxin signaling

The pro-inflammatory signals from $LT\alpha$, $LT\beta$, $LT\beta R$, or other TNFSF members can be integrated by the transcription factor nuclear factor κB ($NF\kappa B$) [160]. Signaling via $NF\kappa B$ is usually triggered in response to microbial and viral infections as well as pro-inflammatory cytokines and can activate the canonical (classical) or non-canonical (alternative) pathway [154]. The $NF\kappa B$ pathway is thought to be a major regulator of innate and adaptive immune responses, inflammation and homeostasis, cell survival or apoptosis, cellular stress responses, development and maintenance of lymphoid organs [160, 161]. Figure 56 summarizes and explains the most important events downstream of TNFR or $LT\beta R$ which lead to activation of the canonical or non-canonical $NF\kappa B$ pathway. Activation of the canonical $NF\kappa B$ pathway mainly occurs in response to inflammatory cytokines such as TNF, and IL1, engagement of the T-cell receptor and in response to bacterial infection (e.g. LPS). Interestingly, $LT\beta R$ activation (through LIGHT or $LT\alpha\beta$ heterotrimers) can also activate the canonical $NF\kappa B$ [162-164].

This leads to activation of the $I\kappa B\alpha$ kinase complex ($IKK\alpha$, β, γ) complex and degradation of $I\kappa B$ inhibitors enabling the translocation of transcription factors RelA, cRel, and p50 [161]. The non-canonical pathway is independent of $IKK\beta$ but depends on the $NF\kappa B$-inducing kinase (NIK) and $IKK\alpha$ [165].

Phosphorylation of IKKα by NIK results in the phosphorylation and processing of p100 leading to nuclear translocation of RelB/p52 dimers. Both pathways lead to the transcription of target genes being involved in the mediation of various biological functions [161].

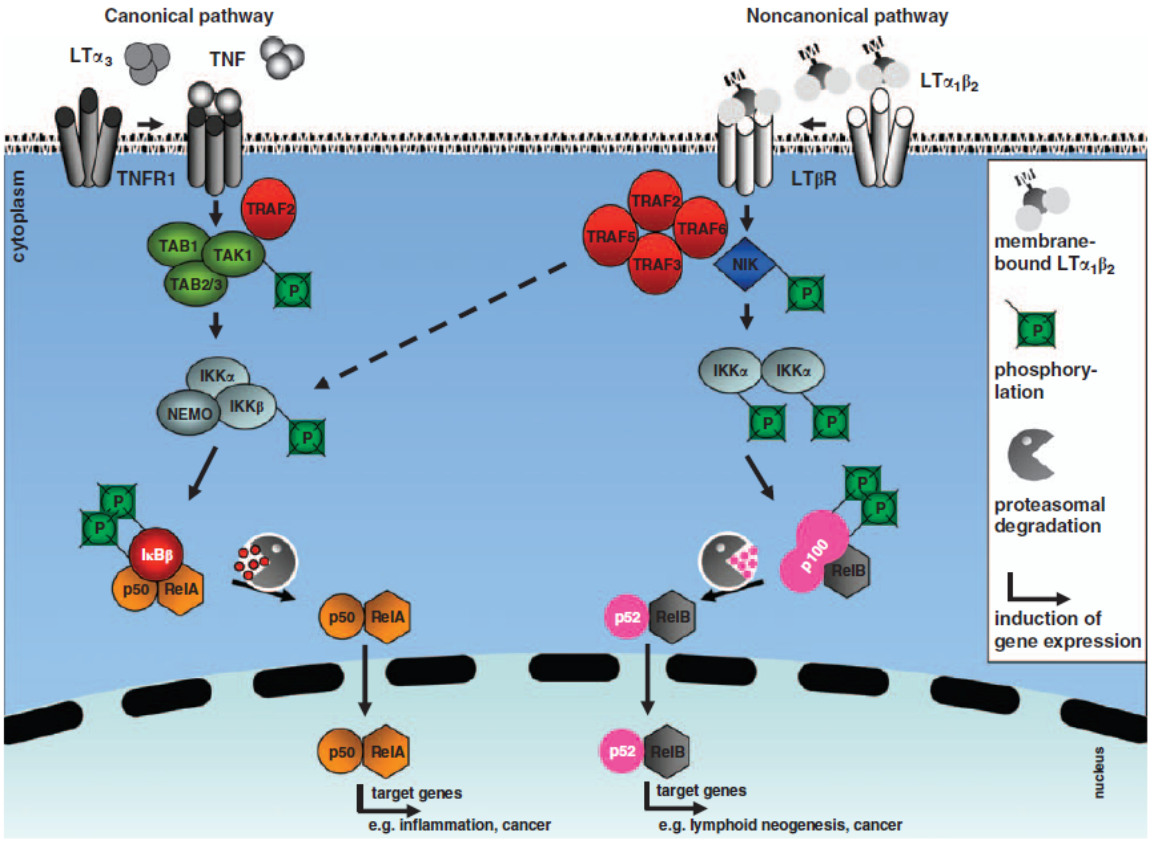

Figure 56: TNFR and LTβR signaling pathways lead to the activation of NFκB through different pathways. (Left): The canonical NFκB pathway is induced by a large number of agonists, representatively, TNF and LTα3 are shown. Stimulation of TNFR leads to the activation of the TAK1 complex through TRAF proteins. This leads to the activation of the IKK complex by phosphorylation of NEMO/IKKγ and IKKβ, which results in the phosphorylation of IκBα, its subsequent ubiquitylation and proteasomal degradation. Finally, the heterodimeric p50/RelA complex translocates to the nucleus, where it binds to specific κB-sequences and induces the expression of target genes, including pro-inflammatory cytokines or genes involved in cell survival, cell proliferation and pro-carcinogenesis. (Right): The non-canonical pathway becomes activated by membrane-bound LTα1β2 heterotrimers, which results in the activation of NFκB-inducing kinase (NIK). This leads to the phosphorylation and activation of the homodimeric IKKα complex. As a consequence, the precursor p100 becomes phosphorylated and proteasomally processed to the p52 subunit establishing now the RelB/p52 heterodimeric complex that translocates to the nucleus and induces the expression of target genes. Besides, LTβR was shown to activate the canonical NFκB signaling pathway.

Despite the well-characterized involvement of NFκB signaling in immunity and inflammation [160], the role of this signaling in cancer development and progression is only bit by bit revealed and actually very controversial [166]. Only recently, two independent studies showed NFκB-dependent activation as a molecular link between inflammation and cancer. Using a colitis-associated cancer model, it was shown that although the absence of IKKβ in intestinal epithelial cells does

not decrease inflammation it leads to a dramatic decrease in tumor incidence without affecting tumor size [167, 168]. Moreover, NFκB signaling was shown to drive the development of HCC in mice lacking multidrug resistance gene 2 (*mdr2*$^{-/-}$ mice) [169]. In line, in another study constitutive NFκB activity was found in diffuse large B-cell lymphoma indicating a role for this signaling pathway as a primary pathogenic event in the development of lymphoma [170].

On the other hand, a controversial role of NFκB signaling was described in mice lacking IKKβ specifically in hepatocytes [171], which display an increased HCC formation after DEN application, suggesting a protective, anti-carcinogenic function of canonical NFκB signaling under the conditions of chemically-induced carcinogenesis. Interestingly, mice lacking IKKγ/NEMO specifically in hepatocytes develop steatohepatitis and HCC [172]. Therefore, the role of NFκB signaling in liver cancer development most likely depends on the mouse model and the type or degree of liver inflammation and injury [166].

6.1.4 Chronic inflammation and carcinogenesis in the liver

Within the human body the liver is the largest metabolic organ conducting several essential tasks to support metabolism and homeostasis to ensure the health of the individual. Key functions of the liver are to detoxify the body from endogenously produced or absorbed substances, production of complement components (involved in innate immune response), blood filtration as well as synthesis of amino acids and proteins (e.g. albumin). The most prominent cell type within the liver are hepatocytes, which are exposed to permanent cell stress and damaged cells have to be removed to maintain tissue homeostasis and physiological function. Liver homeostasis requires an efficiently regulated balance, thus it is not surprising that the liver has a remarkable capacity to regenerate. Complete regeneration of the liver is possible even if up to two-thirds of the hepatic mass is removed (e.g. partial hepatectomy) [173]. Constantly imbalanced liver homeostasis, which can be caused by various etiologies, including chronic alcohol consumption, chronic drug abuse, autoimmune disorders, toxins (e.g., aflatoxin), or infections with hepatotropic viruses (e.g. HBV or HCV), can lead to liver disease. Continuous destruction and regeneration of the liver parenchyma causes chronic hepatitis, liver fibrosis, and cirrhosis. HBV and HCV infections are by far the most common cause of chronic hepatitis in humans [174]. Chronic HBV and HCV infections are frequently associated with HCC [175], the most prevalent primary human liver cancer [176], and except for HBV infections, liver cirrhosis precedes HCC in most cases. The world-wide spread of HBV and HCV not only in developing but also in industrialized countries has led to approximately 500 million people persistently infected with HBV or HCV. This has resulted in a strong rise in HCC incidence [10]. HCC is one of the most lethal human cancers, being the third leading cause of cancer-related deaths worldwide [119, 177].

A causal relationship between chronic hepatitis, hepatocellular damage, fibrosis, and carcinogenesis is well established [176]. The exact mechanisms driving hepatitis-induced liver cancer remain elusive, however, compensatory proliferation preceded by hepatocyte cell death and inflammatory cell infiltration are thought to be critically involved [178]. Moreover, aberrant expression of cytotoxic cytokines is thought to play an important role in the progression from hepatitis to HCC [166, 168, 179, 180]. Pre-malignant hepatocytes can obtain a competitive advantage over normal liver cells by possessing proliferative and survival advantages that can drive preneoplastic lesions and hepatocarcinogenesis [181].

In recent studies a possible involvement of LTβR signaling in the host response to liver infection in the case of hepatitis B (HBV) and hepatitis C viruses (HCV) was investigated *in vivo* and *in vitro*. Increased LTβ expression was found in livers of HCV-infected patients especially not only in liver progenitor (oval) cells but also in small portal hepatocytes as well as immune cells [179]. Besides, LTα was shown to be up-regulated as a consequence of hepatitis B virus X protein expression in liver cell lines [180] and siRNA knockdown of various components of the LTβR signaling pathway (e.g., LTβ; RelA) was shown to interfere with HCV replication *in vitro* [182]. Indeed, several reports suggest an interaction of the HCV core protein with the LTβR, leading to the modulation of the LTβR signaling pathway [183-185]. Results from these studies suggest that HCV core protein is very likely to be a modulator of the host's immune system by enabling HCV to evade mechanisms of host defense [183]. Moreover, cytolytic effects triggered by LTβR signaling are aggravated by binding of HCV core protein to LTβR [185], however the exact mechanisms of this interaction remain elusive.

LT can directly act on hepatocytes, which physiologically express high levels of LTβR but little LT [186]. LT and LIGHT signaling from T-cells to hepatocytes controls lipoprotein homeostasis [157]. In addition, LTβR signaling was shown to be important for liver regeneration through T-cell derived LT expression [158] and regulates hepatic stellate cell function and wound healing [187]. Thus, hepatic LTβR signaling controls liver homeostasis in both health and disease. Moreover, it has recently been demonstrated that pharmacological inhibition of LTβR signaling reduces virus-, bacteria- and concavalin A-induced liver injury [188-190].

Promotion of HCC formation by chronic inflammatory stimuli has been recapitulated in various animal models. Chronic inflammation, NFκB activation and signaling by members of the TNFSF have been shown to contribute to hepatocellular carcinoma (HCC) progression. Ablation of MDR2 induces spontaneous cholestatic hepatitis, elevated hepatocyte proliferation and subsequently HCC [169]. In this study, it was shown that NFκB signaling promotes HCC development in *mdr2*$^{-/-}$ mice and that anti-TNFα treatment was protective.

Liver-specific expression of the hepatitis B surface antigen (HBsAg) in mice demonstrates that chronic immune-mediated liver cell injury is critical for HCC formation [191].

Triggering TNFR1 or LTβR induces the classical and alternative NFκB signaling pathways, which are linked to inflammation-induced carcinogenesis [168]. However, the precise role of these pathways in HCC pathogenesis is controversial [166]. In a model of chemically-induced carcinogenesis, the anticipated pro-tumorigenic role of canonical NFκB signaling in hepatocytes was confounded by the finding that mice lacking IKKβ only in hepatocytes ($Ikk\beta^{\Delta hep}$) exhibited a profound increase in hepatocarcinogenesis after diethlynitrosamine (DEN) application [171, 192], suggesting a protective function of IKKβ in HCC development. This was associated with augmented hepatocyte death, indicating that compensatory proliferation might be a crucial step in HCC development. Further, the authors describe that the absence of IKKβ in both hepatocytes and BM-derived Kupffer cells (macrophages in the liver) decreased compensatory proliferation and carcinogenesis. This suggests that canonical NFκB activation in Kupffer cells is essential for the promotion of compensatory hepatocyte proliferation resulting in DEN-induced HCC.

Only recently, late events of tumor progression and malignant conversion in the DEN model were studied by using a transplant system which allows initiated mouse hepatocytes to form HCC [193]. In this study deletion of IKKβ long after tumor initiation accelerated HCC development in a cell-autonomous manner. Furthermore, the absence of IKKβ in hepatocytes was associated with STAT3 activation. Hepatocyte-specific ablation of STAT3 blocked HCC development, suggesting an interface between NFκB and STAT3 signaling in the context of DEN-mediated HCC development.

Other members of the IKK complex were also shown to be crucially involved in the protection or promotion of HCC. Ablation of NEMO/IKKγ in hepatocytes results in the development of steatohepatitis and HCC [172]. In this model, spontaneous HCC development is preceded by steatohepatitis, increased hepatocyte apoptosis and compensatory liver regeneration. These findings suggest that NFκB has an active role in protecting the liver from cancer and emphasizes the role of IKKγ as a tumor suppressor [172]. Moreover, in this context, it was described that the MAP3-kinase TGFβ-activated kinase 1 (TAK1) suppresses a NEMO-dependent but NFκB-independent pathway to liver cancer [194]. Consequently, the role of NFκB signaling in hepatocarcinogenesis might depend on the mouse model and the type or degree of liver inflammation and injury [166].

Future experiments will aim at developing new mouse models but also at investigating the already generated models of HCC. A major aim will be to analyze what pathological features those models contain and what subtypes or types of HCC they resemble when compared to human HCC. It remains to be determined, which of these already generated models are of importance for understanding hepatocarcinogenesis (especially in the human situation) and can potentially lead to new and effective treatments against HCC and which mouse models do only reflect minor sub-forms of HCC and do not have any impact for the clinics [10].

6.2 Scientific aims

Lymphotoxin was shown to be important for liver homeostasis and regeneration. Involvement of LTβR signaling in HCV replication and increased hepatic LT expression related to HBV and HCV infections suggested a link between virus-induced hepatitis and LT signaling.

The goal of this project was to assess LT's role in various cases of human chronic hepatitis and HCC and to characterize a mouse model over-expressing LTα and LTβ in a hepatocyte-specific manner under the albumin promoter.

I aimed to identify the expression profile of LT in various forms of hepatitis and HCC, which cells express LT in hepatitis and HCC and whether HCV replication can be influenced by altered LT signaling.

Since mice over-expressing LTαβ on hepatocytes develop chronic hepatitis and HCC at a late time point, I further characterized this mouse model on RNA and protein level.

6.3 Material and methods

6.3.1 Mice

Mice were housed under specific-pathogen-free conditions and performed animal experiments in accordance with the Swiss Animal Protection Law and conform to the regulations of the Veterinary Office (Canton Zurich). Mouse experiments were performed under licenses 198/2007, 83/2007, and 30/2005 according to the regulations of the Veterinary Office of the Canton Zurich. *Tg*1223, *tg*1222, *Tnfr1*$^{-/-}$, *Tnfr2*$^{-/-}$, *Rag1*$^{-/-}$, *Ltβr*$^{-/-}$, *Ikkα*$^{AA/AA}$, and *Ikkβ*$^{\Delta hep}$ mice were generated as previously published [171, 195-199].

6.3.2 Genotyping

PCR specific for *tg*1222 and *tg*1223 mice: For transgenic LTα the following primers were used: Forward primer: (*Prp* 5'): 5'-CTG AGT ATA TTT CAG AAC TG-3'. Reverse primer: (LTα rev): 5'-CAG AGA AAA CCA CCT GGG AG-3'. For transgenic LTβ the following primers were used: Forward primer (Prp 5'): 5'-CTG AGT ATA TTT CAG AAC TG-3'. Reverse primer: (LTβ rev): 5'- GAG TCT CTG AGA GGC TAG AG-3'. The following PCR conditions were established on a Gene Amp® PCR System 9700 PCR machine (Applied Biosystems): 95°C 60 sec denaturation; 55°C 50 sec annealing; 72°C 50 sec elongation; 35 cycles.

6.3.3 Human liver tissue

Human liver biopsy specimens were obtained from University Hospitals Zurich, Freiburg, Grenoble, Heidelberg, and Graz. Biopsy specimens were registered in the respective biobanks and kept anonymous. The research project was authorized by the ethical committees of the ''Gesundheitsdirektion Kanton Zürich'' (Ref. Nr. StV 26-2005), Freiburg (Nr. 299/2001), Heidelberg (Prof. Bannasch), Graz (Ref. Nr. 1.0 24/11/2008), and Grenoble (Ref. Nr. 03/APTF/1). The study protocol was in accordance with the ethical guidelines of the Helsinki declaration. Patients were enrolled after giving their written informed consent. HBV- or HCV-infected patients with chronic hepatitis were not treated with ribavirin or other immuno-modulatory drugs at the time point of needle biopsy.

6.3.4 RNA isolation and quantitative PCR

RNA isolation: Total RNA from human and mouse liver samples was isolated using RNeasy Mini kit (Qiagen). The quantity and quality of the RNA was determined spectroscopically using a nanodrop (Thermo Scientific). For microarray analysis, RNA quality was tested using a bioanalyzer (Agilent). Purified RNA was reversely transcribed into cDNA using Quantitect Reverse Transcription Kit (Qiagen) according to the manufacturer's protocol.

Real-time PCR: For *mRNA* expression analysis real-time PCR was performed using Fast Start SYBR Green Master Rox (Roche) or specific TaqMan probes (Applied Biosystems, AB). Primers were custom made by Microsynth or purchased from AB or on a LightCycler® 480 Probes Master (Roche Diagnostics). Real-time PCR was performed on an ABI PRISM 7700 Sequence Detection System or on a 7900 HT Fast Real-Time PCR System (AB). Data were generated and analyzed using SDS 2.3 and RQ manager 1.2 software.

For human *LT*β and *LT*α Taqman Gene Expression assays from AB were purchased. Hu-*LT*β: Hs00242739_m1 (FAM-labelled); probe sequence: 5'-GCC CAC CTC ATA GGC GCT CCG CTG A-3'. Hu-*LT*α: Hs00236874_m1 (FAM labeled); probe sequence 5'-ACC TCA TTG GAG ACC CCA GCA AGC A-3'. TaqMan analysis for human 18S rRNA was performed with a TaqMan® ribosomal RNA control reagent (VICTM Probe; AB; Part. No. 4308329). *mRNA* expression levels were normalized to the housekeeping gene GAPDH (mouse) or 18S rRNA and HPRT (human). Further primers used are listed in the following table. Efficiency of DNase digest was controlled by PCR of $DNase^{+}RT^{-}$ treated liver RNA samples.

6.3.5 Histology and immunohistochemistry

Paraffin sections (2µm) and frozen sections (5 or 10µm) of livers were stained with haematoxylin/eosin or various primary and secondary antibodies. Paraformaldehyde (4%) fixed and paraffin embedded liver tissue was incubated in Ventana buffer and staining was performed on a NEXES immunohistochemistry robot (Ventana instruments, Switzerland) using an IVIEW DAB Detection Kit (Ventana). Antibodies against $B220^{+}$ B-cells (Pharmingen; 1:400), F4/80 (Serotec, 1:50) for macrophages, $CD4^{+}$ (YTS 191; 1:200) and $CD8^{+}$ T-cells (YTS 169; 1:50), CD3+ T-cells (clone SP7, Neomarkers; 1:300) were kindly provided by R. Zinkernagel [68]. Anti-murine GP73 (both Santa Cruz Biotechnology, Inc.) and anti-murine Glutamine Synthetase (Abcam, Code ab16802; 1:500) were used as tumor markers. Liver microarchitecture was evaluated by Collagen IV (IVIEW DAB Kit; 1:50), oval cell proliferation by A6 staining (1:50), kindly provided by Dr. Valentina Factor; both on a Ventana stainer from Roche. Ki67 (NeoMarkers Code RM-9106-S; 1:200) stained proliferating hepatocytes and lymphocytes. Image acquisition was either performed on an Axiophot-microscope (Zeiss), or an Olympus SZX12, equipped with a JVC digital camera (KY-F70; 3CCD) or on an Olympus BX61TRF fluorescent microscope equipped with an F-View camera and analyzed with the Analysis software.

6.3.6 Extraction of human liver cells and freezing

For the isolation and analysis of liver cells we included six patients with histologically proven HCC who had undergone curative hepatectomy and proven persistent HCV infection in the University Hospital, Grenoble.

Exclusion criteria included co-infection with human immunodeficiency virus, hepatitis B or hepatitis delta virus other causes of liver disease, alcohol consumption higher than 30g/day, inflammatory syndrome, previous antiviral treatment and previous liver transplantation. Liver and tumor tissues derived from curative hepatectomy were washed twice in a complete medium, containing RPMI 1640 supplemented by 10% Fetal Calf Serum (Gibco), and continuous shaking for 2 min. Tissues were cut into pieces with in Petri dishes containing 10ml complete medium and 100µl DNase (3mg/ml) (Boehringer Mannheim). 10% collagenase D (10mg/ml) (Roche Diagnostic Germany) was added and incubated for 20 to 30 min at 37°C. Cell suspensions were then filtered (100µm mesh) and 10% of fetal calf serum (FCS) was added in the final volume and then centrifuged at 15000 rpm twice to remove debris. The cells were then counted with a hemocytometer and stored in 10% DMSO in liquid nitrogen or on -80°C.
Cell sorting of human liver cells requires large numbers of cells and thus was conducted only on pieces of liver tissues derived from surgical resections. Liver specimens from healthy and untreated donors are extremely rare and reserved, in case they are accessible, to liver transplantation. It was therefore not possible to obtain larger pieces of healthy livers, since ethical concerns exclusively allow preservation of healthy donor livers for transplantations in a medically precisely indicated setting. Therefore, for healthy livers only *mRNA* could be isolated via liver needle biopsies. The amount of this material sufficed for various analyses but was not sufficient for cell sorting.

6.3.7 Separation of $CD45^+$ and $CD45^-$ cells by microbeads

Frozen cell suspensions were thawed and viability was checked by Acridine/propidium iodide with the help of fluorescent microscope and the percentage of living cells was quantified. Leukocytes numbers were then counted with a hemocytometer. Cell sorting was performed as previously described [200] with the following modifications: Cells were incubated with a biotinylated antihuman CD45 antibody (BD Pharmingen) (1µl of anti CD45 for 1×10^6 of target cells) for 20 min on ice and in dark followed by a washing step with 10 volumes of PBS to remove unbound antibody. Then the cells were incubated with streptavidin-coupled microbeads (Invitrogen, Norway) in PBS with 0.1% BSA and 2mM EDTA, pH 7.4 for 30 min at 2-8°C with gentle tilting and rotation according to the manufacturer instructions (50µl of microbeads for 2.5×106 target cells). Cells were then separated into two fractions with a magnetic column i.e. one with cells bound to microbeads (leukocytes) and the second fraction consisting of unbound cells (hepatocytes, tumor cells and others). After performing additional washing steps to remove trapped liver or tumor cells, cells were eluted from the column. Both cell fractions were then used for RNA extraction.

6.3.8 Cell culture with HCV replicon cells

EN5-3^{+} [201] cells were cultured in DMEM containing 10% FCS and G418 (Sigma). Cells were transfected with 10µM siRNA against LTβR (Santa Cruz) or LTβ (Sigma) using Oligofectamine (Invitrogen) according to the manufacturer's protocol. For experiments triggering LTβR signaling, EN5-3^{+} cells were split and plated in 6 wells plates and left over night. LTβR peptide (Santa Cruz) or IFNα (R&D Systems) was added at various concentrations. 72 hrs after transfection or addition of the peptide, cells were lysed and RNA was isolated using RNeasy Mini Kit (Qiagen). Real-time PCR analysis for LTβ, LTβR and HCV was carried out as described in section 6.3.4

6.3.9. Infectious HCV experiments

For cytokine/chemokine expression Huh7.5 [202] was challenged with HCVcc [203]. After 48 and 72 hrs, cells were lysed, RNA was isolated and real time PCR analysis was carried out. For HCV replication experiments, Huh7.5 and Huh7-Lunet [204] cells were transfected with Con1 luciferase construct as described previously [205]. Luciferase counts were measured after 72 hrs [205]. BS1 antibody (Biogen Idec) or LTβR peptide (Santa Cruz) were added at various concentrations 4 hrs post-transfection.

6.3.10 Western Blot analysis

Liver homogenates (10%) were prepared in RIPA buffer (50mM Tris; 1%NP40; 0.25% Deoxycholic acid sodium salt; 150mM NaCl; 1mM EGTA) containing 1mM Na_3VO_4 and a protease inhibitor cocktail (Complete Mini Tablets; Roche) and quantified with a BCA protein assay kit (Pierce) according to the manufacturer's manual. 60µg protein were denatured in Laemmli buffer containing 5% β-mercaptoethanol and separated by gel electrophoresis on a 12% Bis-Tris gel (Invitrogen) with a 1x NuPAGE MES-SDS running buffer (Invitrogen) and blotted by wet blotting onto a nitrocellulose membrane (Protran BA 85 pore size 0.45µm; Whatman). After blotting the membrane was blocked in Roti-Block (Carl Roth) for 2 hrs at RT. Primary antibody GP73 (sc-48011; Santa Cruz; 1:500 dilution) was incubated at 4°C over night under shaking conditions. Incubation with the secondary antibody (HRP-donkey anti goat IgG H+L; 705.035-147 Lot72963; 1:15000; Jackson) was performed under shaking conditions for 1 hr. Primary antibody AFP (#2137; Cell Signaling; 1:500 dilution) was incubated at 4°C over night under shaking conditions.

Detection was achieved with SuperSignal West, Chemiluminescent Substrate (Pierce). For signal detection a VersaDoc, standard exposure 15-30 sec was used. To assure equal loading, the membranes were re-probed with anti-β-actin antibody (Sigma) and detected as described above.

6.3.11 ELISA

CXCL10 protein levels from liver homogenates or sera were measured using a Quantikine-Elisa-Kit from R&D Systems. The procedures closely followed the manufacturer's instructions. The detection limit was 16pg/ml. The homogenization buffer was tested as a negative control.

6.3.12 Cytokine assay for TNFα

Livers were homogenized with a Dispomix (Medic tools) in 10 vol of Tris-HCl buffer (50mM, pH 7.4) with NaCl (0.6M), Triton X-100 (0.2%) and bovine serum albumin (0.5%) containing freshly dissolved protease inhibitors: benzamidine (1mM), phenylmethyl-sulfonyl fluoride (0.1mM) and Complete Mini Tablets (protease inhibitor cocktail Tablets; Roche). The supernatants were aliquoted and frozen at -80°C until the cytokine assays were performed. Profiling mouse kit for TNFα was purchased from R&D Systems. The procedures closely followed the manufacturer's instructions. The analysis was conducted using a conventional flow cytometer (LSRII from Becton Dickinson). The detection limit for TNFα was 0.4pg/ml.

6.3.13 Multiplex-bead assay

Cytokine protein levels from liver homogenates or sera were measured using a multiplexed particle-based flow cytometric cytokine assay [206]. Bioplex mouse cytokine kits were purchased from BioRad. The procedures closely followed the manufacturer's instructions. The analysis was conducted using a conventional flow cytometer (FC500 MPL, BeckmanCoulter). Detection limits were as follows: CCL2 (12pg/ml), CXCL1 (1pg/ml), IL1β (0.3pg/ml), IL6 (0.3pg/ml), IFNγ (2.8pg/ml). The homogenization buffer was tested as a negative control.

6.3.14 TNFα and 3C8 treatment

Twelve to fourteen-week-old male mice (C57BL/6 and knock-out mice) were intravenously injected with either PBS, murine recombinant TNFα (50 mg/kg bodyweight; R&D Systems), agonistic LTβR antibody (50 mg/mouse; clone 3C8; eBioscience), or rat IgG (50 mg/mouse; eBioscience) and sacrificed for analysis 45 min after injection. All substances were injected at a total volume of 100 ml dissolved in PBS.

6.3.15 Measurement of aminotransferases

The analysis for AST and ALT was performed with mouse serum on a Roche Modular System (Roche Diagnostics) with a commercially available automated colorimetric system at the Institute of Clinical Chemistry at the University Hospital Zurich using a Hitachi P-Modul (Roche).

6.3.16 Analysis of different HCV genotypes

Different HCV genotypes were analyzed as recently published [207].

6.3.17 *mRNA* microarray experiment of liver samples

Gene expression microarray experiment and data analysis: An Agilent one-color microarray-based gene expression analysis (Mouse DNA Microarray 4x 44K) was performed on 3 and 9 month-old *tg*1223 (n=4) and *Ikkβ*$^{\Delta hep}$ (n=4) livers in comparison to age matched C57BL/6 livers (n=3). For HCC arising in 12 or 18 month-old *tg*1223 (n=3) or *tg*1223/*tnfr1*$^{-/-}$ (n=4) liver tissue was compared to non-affected *tg*1223 (n=3), non-affected *tg*1223/*tnfr1*$^{-/-}$ (n=4) liver regions as well as age matched C57BL/6 livers. In addition to biological replicates technical replicates were investigated.

RNA was extracted from liver tissue using the RNeasy Mini kit (Qiagen). RNA quality was tested on a Bioanalyzer (Agilent), only samples with RNA integrity index (RIN) of at least 7.45 were used for further analysis. For microarray, 600ng of RNA were used and prepared according to the manufacturer's protocol. For further analysis only those samples with a yield of at least 2 μg were accepted. Dye incorporation rate – calculated as 1000x (pmol/μl divided by ng/μl) – was between 9.0 and 14.3pmol/ng.

Gene expression was quantified using Agilent Feature Extraction Software Version 9.5.3.1. Expression values were imported into GeneSpring 7.3 (Agilent Technologies, USA) and following Agilent's recommendation, all values less than 5.0 were set to a value of 5.0. For each sample all values were normalized to the respective 50th percentile. In case of the characterization of the *tg*1223 and *Ikk*β$^{\Delta hep}$ liver samples at 3 and 9 months of age, hierarchical clustering and principal component analysis of the normalized values indicated a slight confounding effect based on different dates for the hybridization of the different samples. In order to compensate this effect, for each gene on each array, the expression values were normalized to the median of the values obtained from the C57BL/6 control samples on the respective day, giving rise to ratio values. Those genes were filtered out that did not have at least 75% present flags in at least one of the C57BL/6, *tg*1223 or *Ikk*β$^{\Delta hep}$ conditions at 3 or 9 months. Assuming normal distribution of the data, statistically significant, differentially expressed genes in *tg*1223 or *Ikk*β$^{\Delta hep}$ livers were selected using a one-sample t-test that assessed whether the respective ratios did significantly differ from 1. The false discovery rate was controlled at a level of 0.05 using the method of Benjamini and Hochberg.

Gene Ontology microarray data analysis: Lists of significantly differentially expressed genes were investigated in respect to enrichment of Gene Ontology categories using the Gene Ontology Browser as implemented in GeneSpring 7.3. A Fisher's exact test was used to show

whether more genes belonging to a Gene Ontology category are found in the list under investigation than in a randomized gene list of the same size.

Accession numbers: Gene expression microarray data are deposited in the ArrayExpress database under accession number E-MEXP-1998.

6.3.18 Counting of proliferating hepatocytes

The total number of $Ki67^+$ hepatocytes was counted (number of $Ki67^+$ hepatocytes / visual field of 2 mm^2). For each mouse/ genotype (n=8) 10 visual fields were counted. Statistics was performed (*tg*1223 versus C57BL/6 mice).

6.3.19 Statistical analysis

Human specimens and various mouse groups were compared using a one-way ANOVA with post-hoc Bonferroni test and a Fisher's exact test with Bonferroni correction and a chi-square test with exact *P*-values to evaluate statistical significance.

Analyses were evaluated by using the program SPSS 13.0 (SPSS Inc., Chicago, IL). Student's t-test was used to evaluate the statistical significance of hepatic cytokine and transaminase levels.

6.4 Results

6.4.1 Up-regulation of *LTα*, *LTβ*, and *LTβR* in HBV- or HCV-infected human livers and in HCC

The role of LT signaling in the pathogenesis of virus-induced hepatitis and HCC formation has remained elusive. Together with Johannes Haybäck, I analyzed transcriptional levels of various members of the TNFSF (*LTα*, *LTβ*, *LIGHT*, *TNFα*, *LTβR*, and *TNFR1*) in biopsies of human HBV- or HCV-induced chronic hepatitis and HCC or in non-viral HCC and compared them to healthy liver specimens (Figure 57).

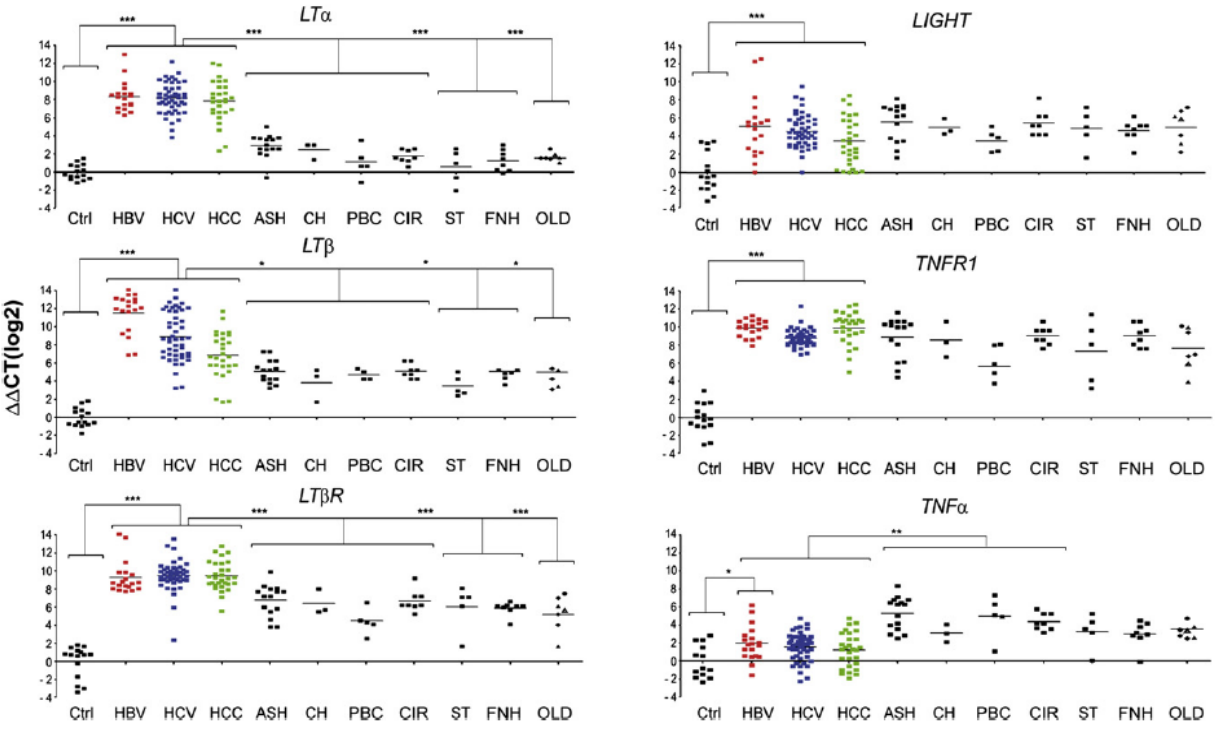

Figure 57: Analysis of hepatic *LTα*, *LTβ*, *LTβR*, *LIGHT*, *TNFR1*, and *TNFα* transcription by real-time PCR. Healthy individuals (Ctrl; n=15), patients chronically infected with HBV (n=19) or HCV (n=49), affected by HCC (n=30), or suffering from various non-virus related liver disorders were investigated. Non-virus related liver diseases with hepatitis include alcoholic steatohepatitis (ASH; n=13), cholestasis (CH; n=3), primary biliary cirrhosis/ autoimmune cholangitis (PBC; n=5), end-stage liver cirrhosis due to alcoholic liver disease (CIR; n=8), a1-antitrypsin deficiency (a1AT; n=1), and focal liver fibrosis (FLF; n=2). Non-virus related liver diseases without hepatitis include steatosis (ST; n=5), hemochromatosis/siderosis (HE/SID; n=3), and Wilson's disease (WD; n=1). Focal nodular hyperplasia (FNH; n=8) was investigated as a benign primary liver tumor. Diseases such as a1AT (black circles), FLF (black triangles), HE/SID (black diamonds), and WD (white diamonds) are listed under ''other liver diseases'' (OLD). Horizontal bars represent the average *mRNA* expression level. The y axis describes the ΔΔCT values on a log2 scale. Asterisks indicate statistical significance: * p≤0.05; ** p<0.001; *** p<0.0001

LTα, *LTβ*, and *LTβR mRNA* expression was dramatically increased, on average, ~2^7 to 2^{10} fold in HBV- or HCV-induced hepatitis and HCC (p<0.001); *LIGHT* transcripts were less, but still

significantly, elevated (on average, ~2^3 to 2^5 fold; p<0.001). Likewise, *TNFR1 mRNA* expression was significantly increased in HBV- or HCV-induced hepatitis and HCC (on average, ~2^7 to 2^9 fold; p<0.0001). In contrast, *TNFα* was only slightly up-regulated in HBV-induced hepatitis (p=0.04) but not in HCV-induced hepatitis (p=0.3) and HCC (p=0.4).

To determine whether up-regulation of LT and its receptors was specific for HBV- and HCV-induced liver diseases, Johannes Haybäck and I examined transcript levels in biopsies from non-viral liver diseases. These included liver disorders with hepatitis (alcoholic steatohepatitis [ASH], cholestasis [CH], primary biliary cirrhosis/autoimmune cholangitis [PBC], and end-stage liver cirrhosis due to alcoholic liver disease [CIR]) and liver diseases without inflammation (steatosis [ST] and focal nodular hyperplasia [FNH]). Additionally, other liver diseases (OLD), such as hemochromatosis/siderosis, Wilson's disease, focal liver fibrosis, a1-antitrypsin deficiency (Figure 57), and non-viral HCC (NVH; Figure 58) were investigated.

Levels of *LTα*, *LTβ*, and *LTβR mRNA* were significantly lower in all non-viral liver diseases analyzed except NVH, compared with virus-induced chronic hepatitis and HCC (*LTα*, p<0.0001; *LTβ*, p=0.05; *LTβR*, p<0.0001).

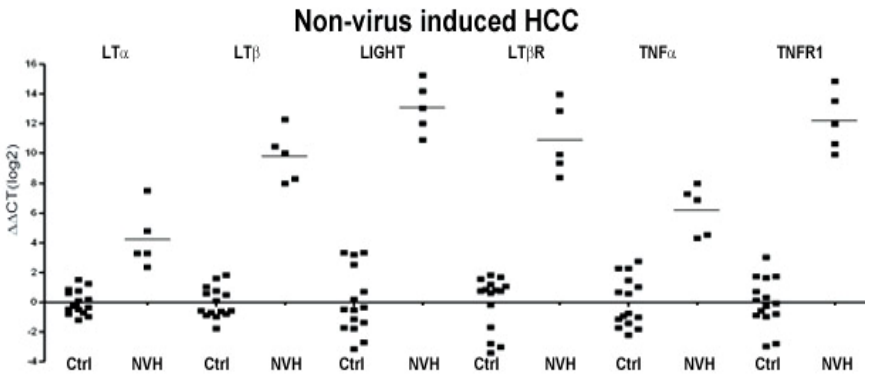

Figure 58: *mRNA* expression levels of various members of the TNFSF in non-virus related HCC. Real-time PCR analysis for *LTα*, *LTβ*, *LIGHT*, *LTβR*, *TNFα* and *TNFR1* transcripts in non-virus related HCC (NVH). Each symbol represents one individual patient. Horizontal bars represent the average *LTα* or *LTβ mRNA* expression level. The y-axis describes the ΔΔCT values on a log2 scale. Ctrl: healthy control liver tissue. NVH: HCC without HBV or HCV infection.

This was irrespective of non-viral liver diseases being associated with inflammation. *LIGHT* and *TNFR1 mRNA* expression in non-viral liver diseases including NVH was similar to HBV- or HCV-induced chronic hepatitis and HCC. In contrast, *TNFα mRNA* expression was significantly higher in non-viral liver diseases with inflammation and NVH, compared with healthy livers (p<0.0001), HBV- or HCV-induced hepatitis and HCC (p<0.0001).

In most cases, HCV genotype, degree of inflammation (Knodell score), fibrosis (Metavir score), and liver enzyme levels (ALT; AST) were assessed.

No significant correlation between patient age (p=0.05) or gender (p=0.05) and the expression levels of *LTα*, *LTβ* and *LTβR mRNA* was found (Figure 59).

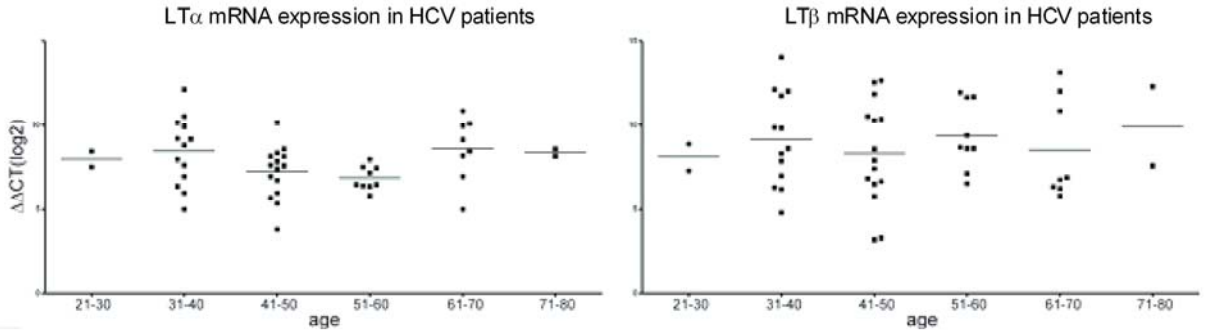

Figure 59: Correlation analysis of *LTα* and *LTβ* expression in HCV-infected livers with patient age. *LTα* (left) or *LTβ* (right) *mRNA* expression levels for individual patients are presented as a ΔΔCT values on a log2 scale (y-axis) with horizontal bars representing the average. Patients were ranging from the 3rd to the 8th decade (x-axis).

Furthermore, levels of *LTα* and *LTβ mRNA* did not correlate with the degree of liver inflammation (p=0.5) as assessed with Knodell score for HCV-infected patients or fibrosis (p=0.5) (classified with Metavir score). Also HCV genotype or type of virus infection (HBV, HCV, HBV/HCV co-infection in the case of some HCC did not show any correlation with *LTα* and *LTβ* expression levels (p=0.5) (Figure 60).

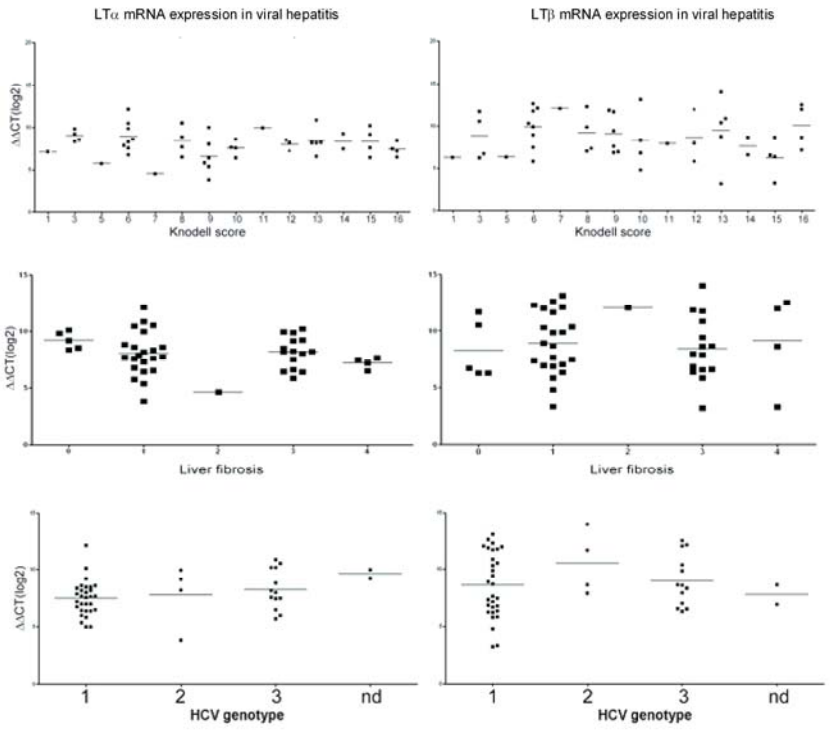

Figure 60: Correlation analysis of *LTα* and *LTβ mRNA* expression with inflammation, fibrosis score and HCV genotype in HCV infected patients. *LTα* (left) and *LTβ* (right) *mRNA* expression levels did not correlate with Knodell score (for inflammation; ranging from 0-16; upper row), with fibrosis score (Metavir; ranging from 0-4; middle row) and HCV genotype (lower row) in HCV-infected livers. Each symbol represents one individual patient. Horizontal bars represent the average *LTα* or *LTβ mRNA* expression level. The y-axis describes the ΔΔCT values on a log2 scale.

6.4.2 Increased chemokine expression in HBV- or HCV-induced hepatitis and HCC

To confirm that pro-inflammatory signaling cascades are activated during HBV- or HCV-induced hepatitis and HCC formation, chemokine *mRNA* levels were measured (Figure 61).

CCL2, *CCL3*, *CCL5*, and *CXCL10 mRNA* expression was significantly higher in human HBV-induced ($p<0.0001$) or HCV induced ($p<0.0001$) hepatitis and HCC ($p<0.0001$) than in healthy controls. *CXCL1 mRNA* expression was significantly increased in HBV-induced hepatitis ($p<0.0001$) and HCC ($p=0.02$), but not in HCV-induced hepatitis ($p=0.07$).

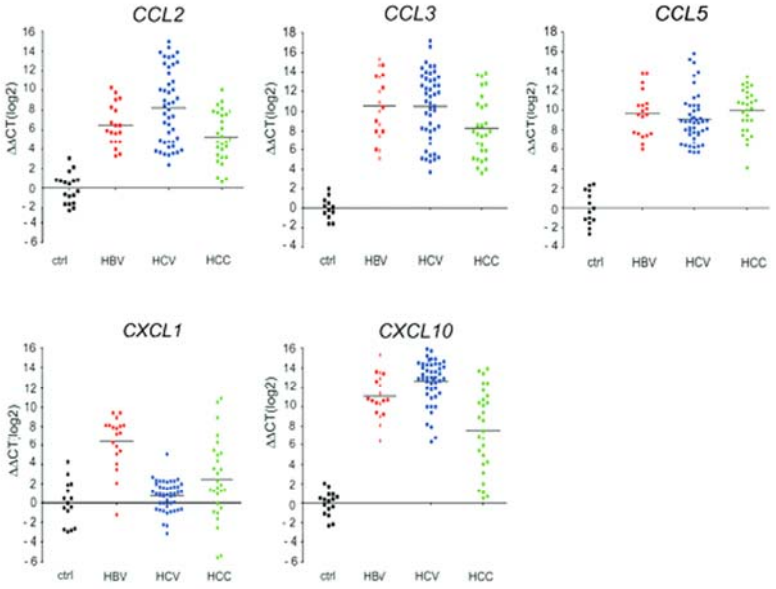

Figure 61: Analysis of *CCL2*, *CCL3*, *CCL5*, *CXCL1* and *CXCL10 mRNA* expression by real-time PCR in human liver biopsies. Healthy controls (n=15), patients chronically infected with HBV (n=19) or HCV (n=49) and patients suffering from HCC (n=30) were analyzed. Horizontal bars represent the average *mRNA* expression level. The y-axis describes the ΔΔCT values on a log2 scale.

6.4.3 Up-regulation of *LTα*, *LTβ* and *LIGHT* in human hepatocytes upon *in vitro* HCV infection

Next, I investigated whether *LTα*, *LTβ*, *LIGHT* and *LTβR* transcripts can be up-regulated in hepatocytes as a consequence of viral infection. Together with Prof. Dr. Thomas Pietschmann and Dr. Sandra Ciesek at the Twincore Center, Hannover, the human hepatocyte cell line Huh-7.5 [202] was challenged with infectious, cell culture derived HCV (HCVcc) [203], and expression of selected cytokines and chemokines was measured (Figure 62).

At 48-72 hrs post infection, I found that transcripts of *LTα* ($p=0.05$), *LTβ* ($p=0.05$), *LIGHT* ($p=0.05$), *LTβR* ($p=0.05$), and chemokines (*CCL2*, *CCL3*, *CXCL1*, and *CXCL10*) were increased (2- to 32-fold) in HCVcc-infected, compared with non-infected Huh7.5 cells.

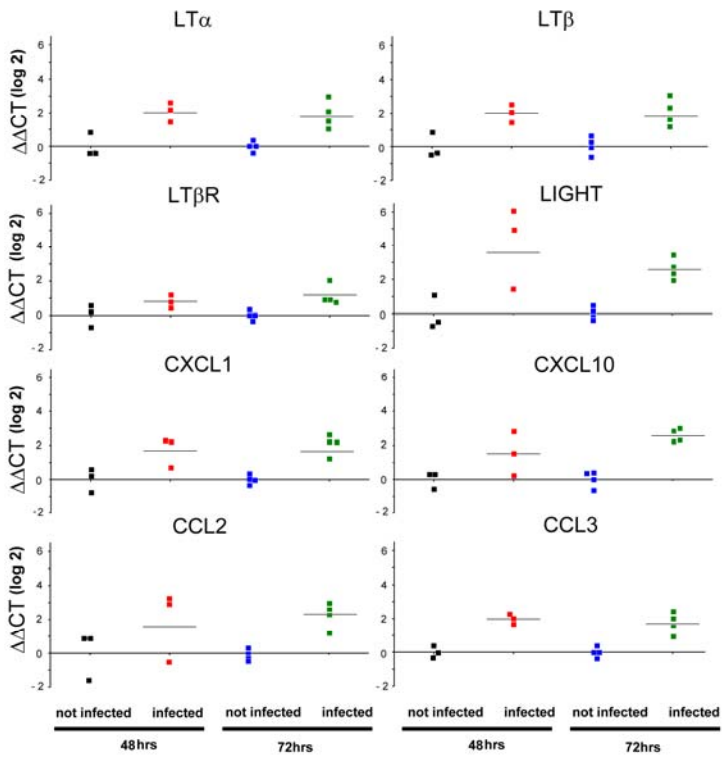

Figure 62: HCVcc infection of human hepatocytes *in vitro* up-regulates several chemokines and cytokines. Real-time PCR analysis for the *mRNA* expression of *LTα*, *LTβ*, *LIGHT*, *LTβR*, *CXCL1*, *CXCL10*, *CCL2* and *CCL3* in a human hepatocyte cell line upon challenge with infectious HCVcc at 48 and 72 hrs post infection compared to non-infected Huh7.5 cells. Horizontal bars represent the average *mRNA* expression levels. The y-axis describes the ΔΔCT values on a log2 scale.

6.4.4 Identification of liver cells expressing *LTβR* and its ligands in HBV or HCV infections

Having observed with the previously described infection experiment that stromal cells, in this case a human hepatocytic cell line, are capable of producing *LTα* and *LTβ*, I planned to identify the cellular source of *LTα*, *LTβ*, *LTβR*, and *LIGHT* expression in human HCV-infected livers. Therefore, with the help of Dr. Patrice Marche from the University Hospital Grenoble, lymphocytic cells were collected from fresh, curative resections derived from patients with HCV-induced hepatitis and HCC with HCV etiology (further denoted as HCV/HCC).

The following representative images should first give an overview of the obtained material from the curative hepatectomy (Figure 63).

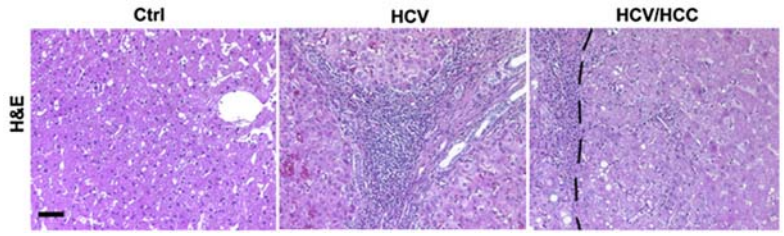

Figure 63: H&E staining of paraffin sections of HCV-infected livers, HCC with HCV etiology and healthy controls. HCV-infected livers (HCV) and tumors (HCV/HCC) display leukocyte infiltration. The tumor border is indicated by a dashed line (scale bar, 100μm).

Compared to healthy control tissue, samples from HBV- or HCV-infected patients as well as HCC-derived samples display increased infiltration of the liver with immune cells ($CD20^+$ B-cells and $CD3^+$ T-cells; Figure 64).

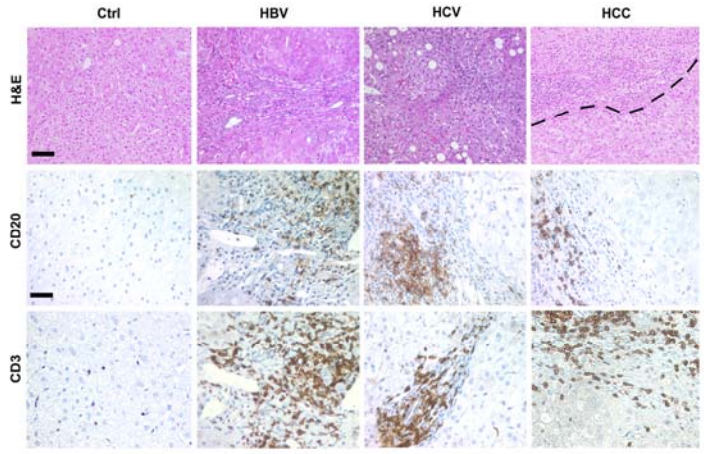

Figure 64: Immunohistological analysis of human healthy controls, HBV- and HCV-infected livers or HCC. H&E staining and staining for CD20 (B-cells) and CD3 (T-cells) was performed. H&E staining indicates morphological features of inflamed and fibrotic liver tissues (HBV- and HCV-infected livers). HCC display transformed hepatocytes. The HCC border zone is indicated by a dashed line (upper row, right column). Inflammatory infiltrates were detected in HBV- or HCV-infected livers as well as at the border zones of HCC (scale bar: 100µm).

To determine the cell types responsible for *LT* and *LTβR* up-regulation, liver cells were sorted according to their CD45 surface expression, resulting in CD45-enriched (T-, B- and NK-cells; monocytes, macrophages, Kupffer cells; dendritic and cells) or CD45-depleted (hepatocytes, oval cells and bile duct epithelial and endothelial cells) fractions. Purity of these fractions was assessed by real-time PCR for lymphocyte (CD3, CD20, and CD45) or hepatocyte (cytokeratin 18) markers (Figure 65).

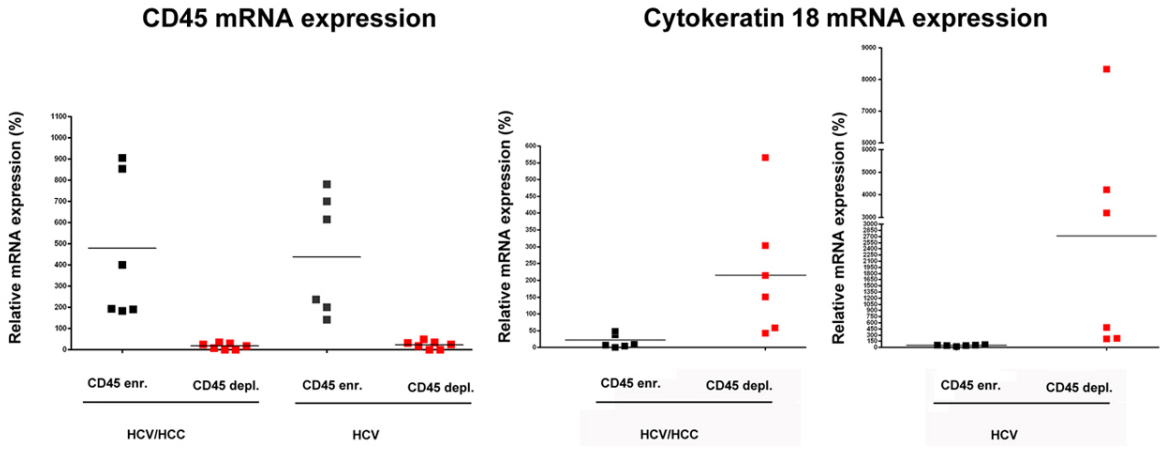

Figure 65: Real-time PCR analysis for CD45 and Cytokeratin 18 expression on CD45-sorted liver cells. To quantify the purification efficiency of CD45-enrichment or CD45-depletion, cells were prepared from HCV-infected, inflamed livers (HCV) or from HCC with HCV etiology (HCV/HCC). Horizontal bars represent the average *mRNA* expression level. The y-axis describes the relative expression in percentage normalized to healthy controls.

CD45-depleted fractions displayed only a minor contamination with CD45 *mRNA* (~1%–10%), and CD45-enriched fractions showed only a minor amount of cytokeratin 18 *mRNA* transcripts (~2%–20%). Unsorted liver cells of healthy individuals were included as controls. Because of ethical consideration, not enough human healthy liver tissue was available in order to perform cell sorting.

Within HCV-induced HCC, CD45-enriched and -depleted liver cells expressed similar *LTα* and *LTβ mRNA* levels (*LTα*, p=0.8; *LTβ*, p=0.1) that were significantly higher than in controls (p<0.0001) (Figure 66).

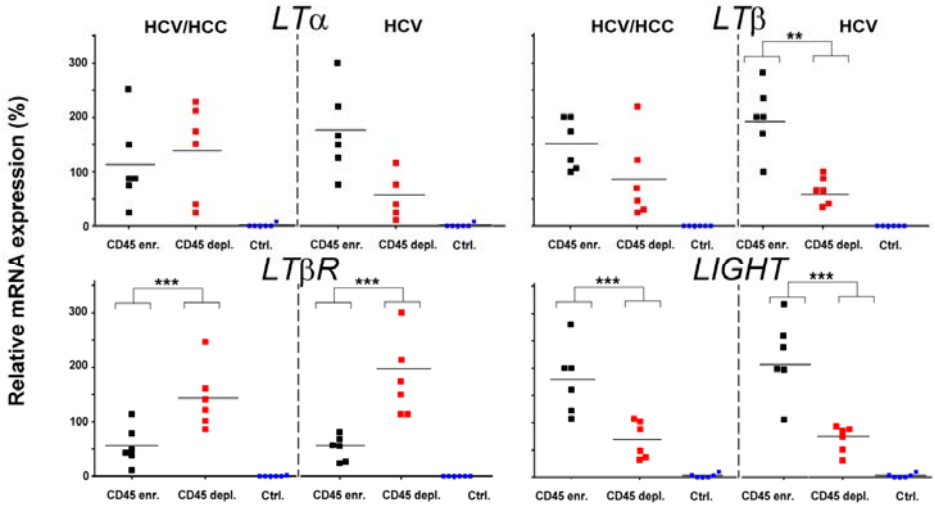

Figure 66: Identification of cell types expressing members of LT signaling pathway. Real-time PCR analysis of sorted, CD45-enriched or CD45-depleted liver cells. For control, whole liver cell populations derived from healthy or diseased livers (HCV infected/HCC) were used. *mRNA* expression levels are normalized to unsorted, total cell populations of the respective liver disease and calculated as 100%. The average expression level is indicated as percentage of control (unsorted cells of the respective disease) and demarcated by horizontal bars. Asterisks indicate statistical significance (Student's t test): *p< 0.05; **p < 0.001; ***p < 0.0001.

LTβR transcript levels were significantly higher in CD45-depleted cells, compared with CD45-enriched cells (p=0.006) or controls (p<0.0001). In contrast, *LIGHT mRNA* expression was significantly increased in CD45-enriched cells when compared to CD45-depleted cells (p=0.008) or controls (p=0.0007).

Within HCV-induced hepatitis, CD45-enriched cells exhibited a trend toward increased *LTα mRNA* levels (p=0.089) and a significant increase in both *LTβ* and *LIGHT* transcripts, compared with CD45-depleted cells (*LTβ*, p=0.006; *LIGHT*, p=0.01), or controls. Similar to HCV-induced HCC, *LTβR mRNA* expression was significantly higher in CD45-depleted cells than in CD45-enriched cells (p=0.002) or controls (p<0.0001).

Thus, both CD45-enriched and CD45-depleted cell fractions express *LTα*, *LTβ*, and *LIGHT* in HCV-induced hepatitis and HCC. Our analysis revealed that most likely the hematopoietic non-

parenchymal cells express more LT when compared to the parenchymal compartment. Immunohistochemical and immune-fluorescent analysis for LTβ confirmed these data as $CD3^+$ and $CD20^+$ lymphocytes as well as hepatocytes in HBV- or HCV-induced hepatitis and HCC - but not in healthy liver specimens - express LTβ protein (Figure 67).

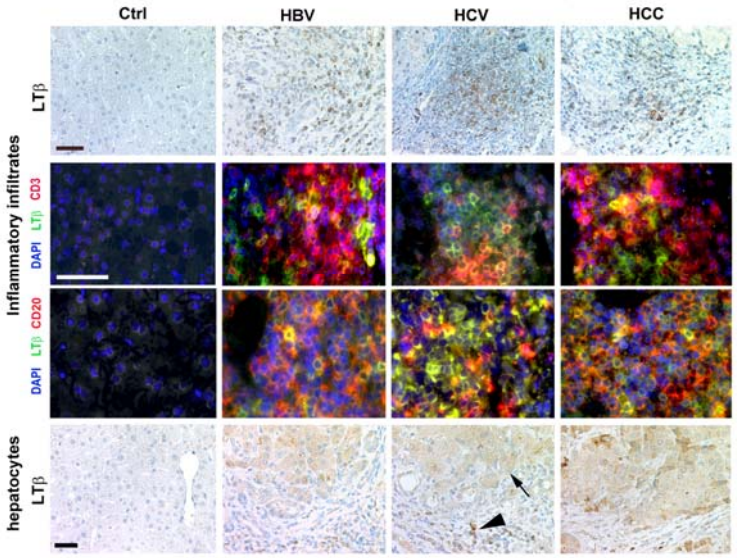

Figure 67: LTβ is expressed by B-cells, T-cells and hepatocytes.
Immunohistochemical (upper and lower panels) and immunofluorescent analysis (middle panels) for LTβ expression in healthy, HBV- or HCV-infected and HCC-affected livers (scale bar, 50μm). Arrowhead depicts $LT\beta^+$ leukocytes and arrows depict $LT\beta^+$ hepatocytes.

6.4.5 LTβR signaling directly influences HCV replication

Having observed that in situations of chronic infection with HCV, not only lymphocytes express LT, but also hepatocytes up-regulate LT expression levels, I next wanted to address the question, whether LT signaling has a direct influence on HCV replication. These experiments were performed using a liver cell line (Huh7) that is stably transfected with a subgenomic HCV replicon [201]. The HCV construct contains only non-structural parts of HCV genotype 1b, which are non-infectious, and replication can be tested by quantitative PCR for HCV. Figure 68 shows the organization of the subgenomic HCV replicon.

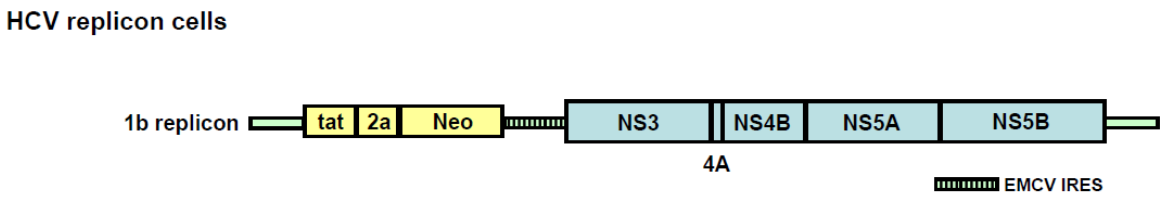

Figure 68: HCV subgenomic construct used for studying LTβR signaling and HCV replication. The HCV genotype 1b construct contains the non-structural proteins of HCV (NS3, NS4A, NS4B, NS5A and NS5B), and a tat-2A-neo cassette, containing a neomycin resistance (Neo), FMDV2A proteinase (foot-and-mouth disease virus polypeptid possessing autocatalytic activity resulting in the release of Neo) and HIV tat protein (transcriptional transactivator).

In a first set of experiments, I tested whether silencing of LTβ or LTβR would inhibit HCV replication. For LTβ, I could reproduce the findings from Ng et al, who showed that HCV replication is decreased, when LTβ is transiently silenced using siRNA. When LTβR is knocked-down in the replicon cells, HCV replication could be also decreased, meaning that LT signaling most likely influences the extent of HCV replication in an infected cell in a dose-dependent manner (Figure 69).

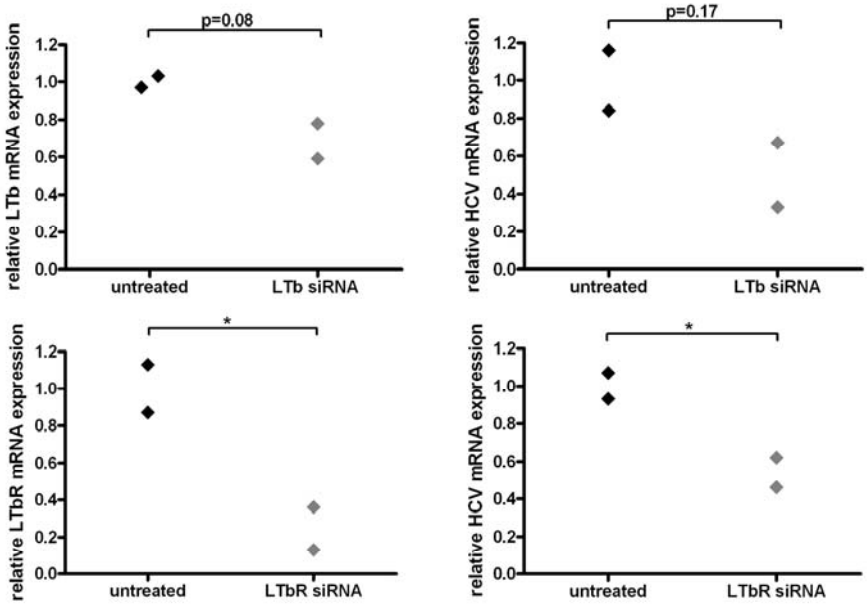

Figure 69: HCV replication is suppressed when LTβ or LTβR expression levels are decreased. Replicon cells were transfected with siRNA for LTβ (upper row) or LTβR (lower row) and expression levels of *HCV mRNA* were assessed by real time PCR after 72 hrs. Statistical significance: * = p<0.05.

For comparison, I investigated how strong the inhibitory effects of blocking LTβR signaling on HCV replication are, cells were treated with IFNα, which leads to an efficient inhibition of HCV replication (Figure 70).

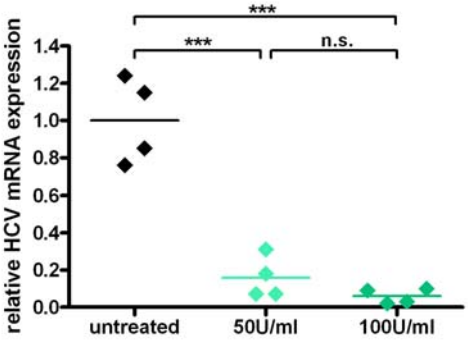

Figure 70: HCV replication is suppressed after IFNα treatment. HCV replicon cells were treated with IFNα (50 U/ml and 100 U/ml) for 72 hrs and expression levels of *HCV mRNA* were assessed by real time PCR after 72 hrs. Statistical significance: *** = p<0.001; n.s. = not significant

As a next step, I tested whether increased LT signaling would also lead to increased HCV replication. Therefore, I used a small 20 amino-acid peptide, which binds between aa25 and aa75 to LTβR, a region which is thought to lead to oligomerization of LTβR. Interestingly,

addition of this peptide to the medium led to a strong increase in HCV replication over time (Figure 71).

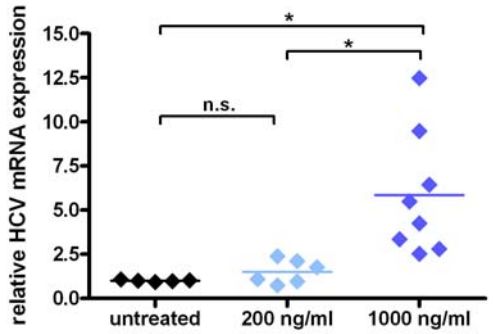

Figure 71: Agonistic stimulation of LTβR leads to an increase in HCV replication. HCV replicon cells were treated with a peptide binding to LTβR (200ng/ml and 1000ng/ml) for 72 hrs and expression levels of *HCV mRNA* were assessed by real time PCR after 72 hrs. Statistical significance: * = $p<0.05$; n.s. = not significant.

Having observed that HCV replication can be influenced by modulating LTβR signaling in a non-infectious setting, I next studied whether these findings could be reproduced using fully infectious HCV. Again, these studies were performed in collaboration with Prof. Dr. Thomas Pietschmann and Dr. Sandra Ciesek from the Twincore Center, Hannover.

In a first experiment, we used the LTβR peptide and assessed the replication of HCV-Con1, a full length genotype 1b replicon in Huh7.5 cells, a clone of the human hepatoma cell line Huh7. Assessing HCV replication after 72 hrs showed that also in this infectious setting an approximately 5-fold increase in HCV replication was found (Figure 72).

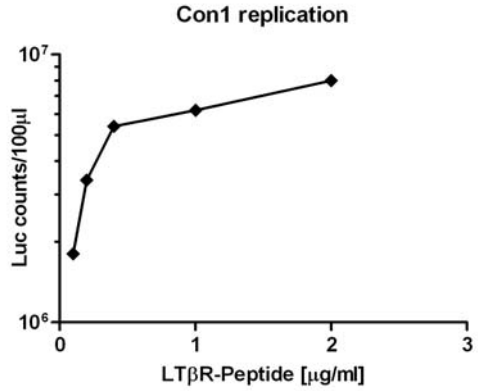

Figure 72: HCV genotype 1b replication can be increased by agonistic stimulation of LTβR signaling. Huh7.5 cells were electroporated with HCV-Con1 and treated with various concentrations of LTβR peptide (0.1-2µg/ml). HCV replication was assessed by measuring luciferase counts after 72 hrs.

These findings could be reproduced in an experiment using HCV-Con1 infection in Huh7.5 and in Lunet cells – which is another clone of Huh7 being highly susceptible to HCV infections. In both cell lines, triggering of LTβR signaling using the peptide binding to LTβR increased HCV replication approximately 3 fold – however it seemed like the effect was slightly more pronounced in Lunet cells (Figure 73; left panel). Therefore we used this cell line to test whether triggering of LTβR signaling with another substance would also lead to an increase in HCV replication. For this experiment, BS1, a tetravalent, bispecific anti-human LTβR antibody was

used. Also with this antibody, an approximately 3 fold increase in HCV replication was observed (Figure 73; right panel).

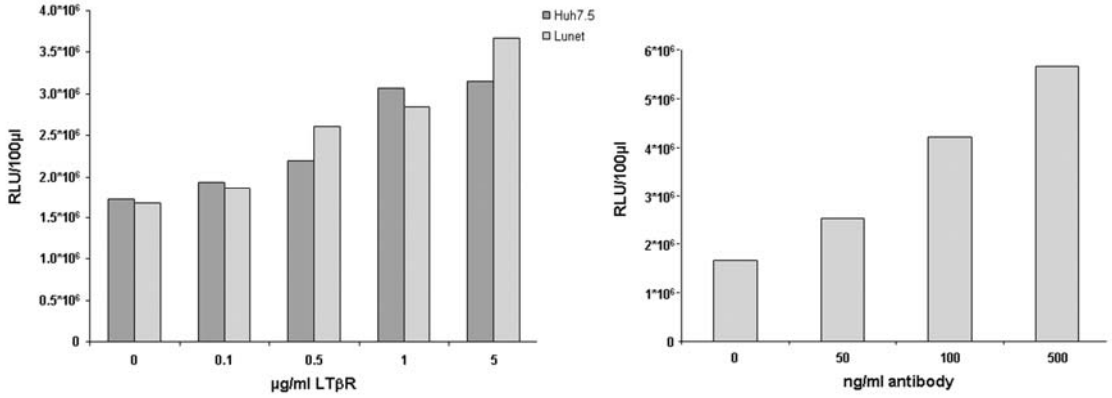

Figure 73: HCV-Con1 replication can be increased by agonistic stimulation of LTβR signalling in various cell lines. Huh7.5 and Lunet cells were electroporated with HCV-Con1 and treated with various concentrations of LTβR peptide (0.1-2µg/ml). HCV replication was assessed by measuring luciferase counts after 72 hrs (left). Using Lunet cells and BS1 (an anti-LTβR antibody) led to similar results.

6.4.6 Hepatocyte-specific LTα and LTβ over-expression induces chronic hepatitis

To determine whether sustained hepatic LTβR signaling is causally linked to chronic hepatitis and liver cancer, Johannes Haybäck and I analyzed two transgenic mouse lines that expressed LTα and β under the Albumin promoter in a liver specific manner at low (*tg*1222) or high (*tg*1223) level [208] (Figure 74).

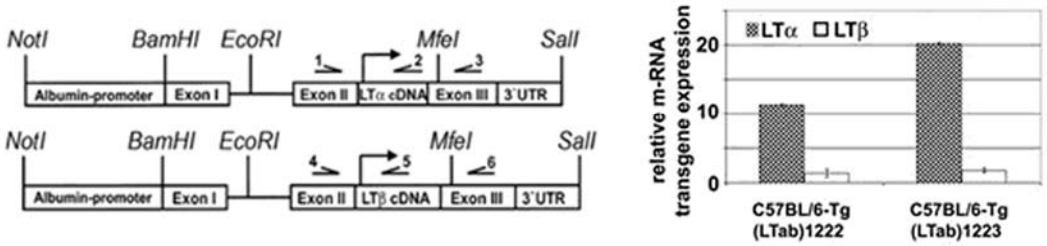

Figure 74: Liver specific over-expression of lymphotoxin. Scheme of constructs used for the over-expression of LTα or LTβ (inserted into a "half genomic" Prnp minigene); arrows indicate the primers used for RT-PCR analysis (left).Transgene-specific real-time RT-PCR analysis identifying *tg*1222 as low expressor and *tg*1223 as high expressor line (right) [208].

We analyzed this mouse model at various time points (3, 6, 9, 12 and 18 months) for macroscopical, microscopical and molecular alterations within the liver.

At three months of age, no histological changes were visible in livers of *tg*1222 and *tg*1223 mice compared to those of control littermates. No increase in the numbers of infiltrating B-cells, T-

cells or macrophages was found in both transgenic lines at three months of age (Figure 75), indicating that no signs of liver inflammation were found at that early time point.

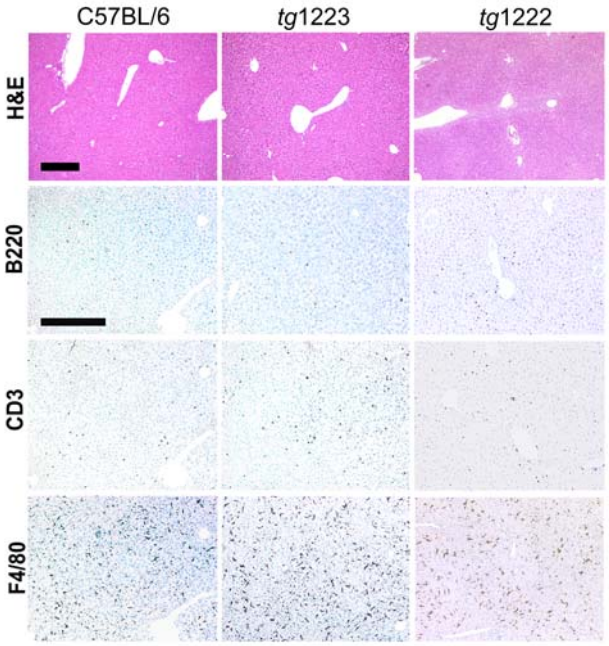

Figure 75: Immunohistological analysis of paraffin-sections derived from 3 month-old C57BL/6 and transgenic livers. C57BL/6, *tg*1222 and *tg*1223 livers lacked detectable inflammatory infiltrates as highlighted by H&E (scale bar: 200μm), by staining for B-cells (B220), T-cells (CD3), macrophages, Kupffer cells (F4/80) (scale bar: 100μm).

However, the hepatic transcriptome was already considerably altered in *tg*1223 and to a lesser degree in *tg*1222 mice. Genes with the most dramatic expression changes were first identified by DNA microarray analysis in an unbiased manner and I then subsequently tested the 30 most up- and down-regulated candidates by real-time PCR (Figure 76), confirming the previously gained data from microarray analysis.

As expected, *Lt*α and *Lt*β transcripts were increased in *tg*1222 and *tg*1223 livers. Additionally, *mRNA* expression of chemokines (*Ccl2*, *Ccl7*, *Cxcl1*, and *Cxcl10*), genes involved in early growth response (e.g., *Egr1* and *Egr2*), cholesterol metabolism (e.g., *Ch25h*), and immediate early response (e.g., *c-Fos*, *Jun-b*, and *Socs3*) were significantly ($p<0.0001$) elevated. Besides, other genes described in the context of carcinogenesis in the liver (e.g., *Gaddg45*) or cancer in general (e.g., *E-selectin* and *P-selectin*) were found to be up-regulated.

In contrast, genes involved in cell cycle control, histone modifications, and cell metabolism were significantly down-regulated ($p<0.0001$). The most down-regulated gene we could find was the *g0/g1* switch gene, which – if normally expressed – should prevent the exit of hepatocytes from G0 into G1 phase of the cell cycle and thereby inhibit mitosis.

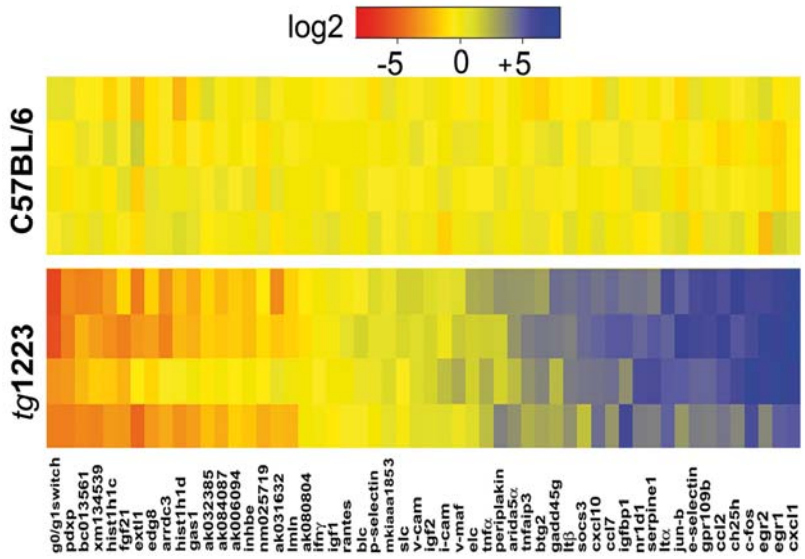

Figure 76: Real-time PCR analysis for *mRNA* expression in liver of candidate genes at the age of 3 months. Data are presented in a log2 scale (blue, up-regulated; red, down-regulated). Rows indicate individual mice; columns represent particular genes. Each data point reflects the median expression of a particular gene resulting from three to four technical replicates, normalized to the mean expression value of the respective gene in C57BL/6 livers.

At the age of 4 months, a slight increase in intrahepatic CD11b$^+$, CD68$^+$, and MHCII$^+$ cells was detected in *tg*1223 mice, compared with age-matched C57BL/6 mice (Figure 77 left).

At this time point, no significant increase in IL1β, IFNγ, IL6, and TNFα protein levels was found in the livers or serum of transgenic mice when compared to wild-type littermates (data not shown). At 4-6 months, transgenic livers started to develop strong portal and lobular (*tg*1223) or weak portal (*tg*1222) inflammation consisting of CD3$^+$ T-cells, B220$^+$ B-cells, and F4/80$^+$ macrophages (Figure 77, right).

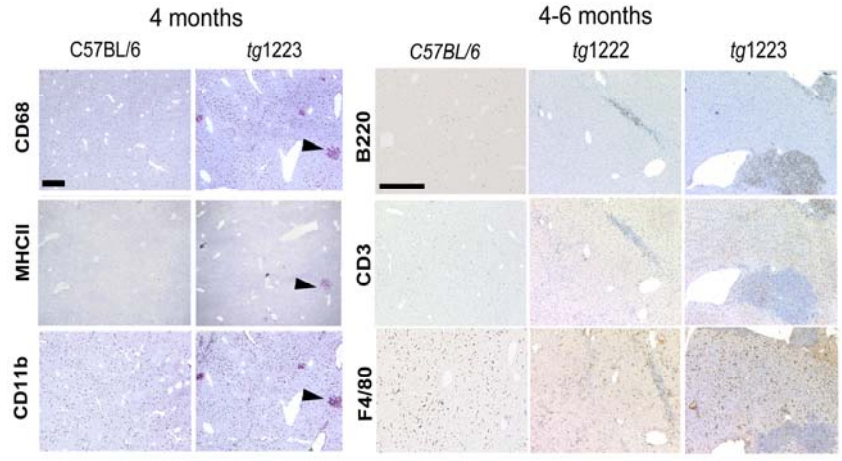

Figure 77: Immunohistological analysis for myeloid cells at the age of 4-6 months in *tg*1223 and C57BL/6 livers. A slight increase in the number of CD11b$^+$, CD68$^+$ and MHCII$^+$ cells was detected on cryosections of *tg*1223 livers at 4 months of age when compared to age matched C57BL/6 livers (left panel). Already at this time-point, small aggregates mainly consisting of myeloid cells (arrow heads) could be detected. At the age of 4-6 months, B220$^+$, CD3$^+$ or F4/80$^+$ cells accumulated at portal sites of *tg*1223 livers (right panel). In *tg*1222 livers, only small portal inflammatory infiltrates could be observed (scale bar: 200µm).

At 9 months of age, *tg*1223 livers exhibited strong portal and lobular lymphocytic infiltrates (Figure 78). A pronounced influx of F4/80$^+$ macrophages and proliferation of A6$^+$ oval cells was observed by immunohistochemical analysis. Chronic inflammation coincided with increased

proliferating Ki67$^+$ hepatocytes (*tg*1223, 17 ± 5 Ki67$^+$cells/mm^2 liver section; C57BL/6, 0.5 ± 0.3 Ki67$^+$cells/mm^2 liver section; p=0.003), which was not significant in age-matched *tg*1222 livers (p = 0.08; data not shown). Chronic hepatitis was observed in 100% of the *tg*1223 mice at 9 months of age (n=65) whereas none of the C57BL/6 control mice showed signs of inflammation within their liver (n=40).

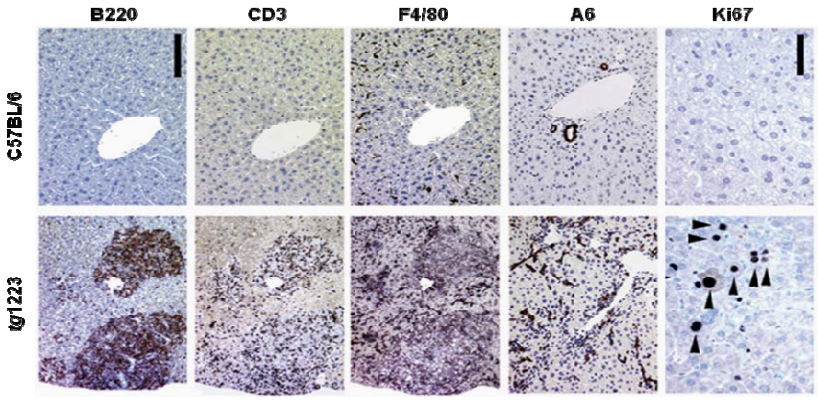

Figure 78: Lymphocytic infiltrates are found in 9-month old *tg*1223 mice. Immunohistochemical analysis of representative paraffin sections from livers of 9-month-old C57BL/6 and *tg*1223 mice. B220$^+$ B-cells, CD3$^+$ T-cells, F4/80$^+$ macrophages (Kupffer cells) and A6$^+$ oval cells (scale bar, 150μm). Proliferating Ki67$^+$ hepatocytes (arrowheads) and inflammatory cells are indicated (scale bar, 50μm).

At this stage, hepatitis was accompanied by increased protein levels of IL1β (p<0.05), IFNγ (p<0.05), and IL6 (p<0.05), and, to a lesser degree, TNFα in *tg*1223 livers. In *tg*1222 livers, we observed only a slight elevation of these cytokines, compared with C57BL/6 (Figure 79).

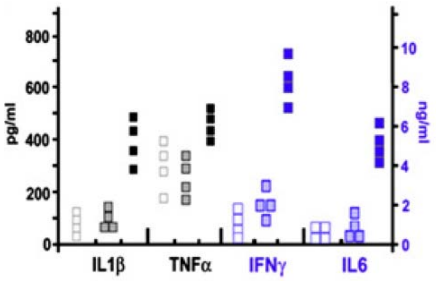

Figure 79: Increased chemokine and cytokine expression in 9-month-old *tg*1223 mice. ELISA for IL1β, TNFα, IFNγ, and IL6 in liver homogenates from 9-month-old C57BL/6 (hollow symbols), *tg*1223 (filled symbols), or *tg*1222 (dotted symbols) mice (left).

6.4.7 LTα and LTβ over-expression induces hepatotoxicity

To determine whether chronic hepatitis leads to hepatocyte damage and cell death in *tg*1222 or *tg*1223 mice, Johannes Haybäck and I analyzed serum transaminase levels (alanine transaminase ALT and aspartate transaminase AST). From the age of 19 weeks on, serum ALT and AST levels were significantly elevated (p=0.05) in *tg*1223, but not in *tg*1222 mice (Figure 80), and apoptotic hepatocytes were frequently detected in *tg*1223 mice (tg1223, 40.3 ± 11.4 TUNEL$^+$ cells/mm^2 liver section; C57BL/6, 3.9 ± 6.2 TUNEL$^+$ cells/mm^2 liver section;

p=0.0005), but rarely in *tg*1222 and virtually absent in C57BL/6 mouse livers from the age of 6 months on (Figure 80).

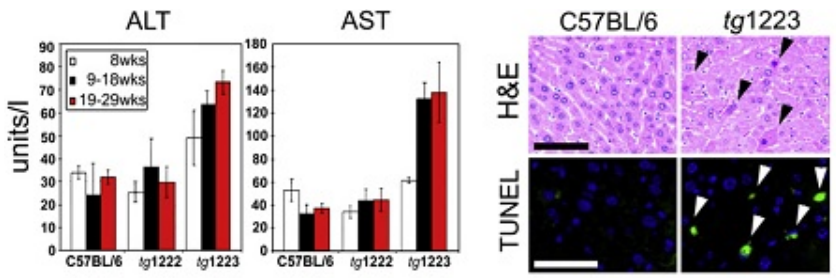

Figure 80: Chronic liver injury in *tg*1223 mice. Analysis of transaminase levels (ALT and AST) in sera of transgenic and control mice. Standard deviation is indicated by error bars (left panel). Increased hepatocyte cell death in tg1223 livers shown by H&E staining and TUNEL/DAPI assay. Black arrowheads indicate apoptotic hepatocytes. TUNEL, green TUNEL+ hepatocyte nuclei indicate apoptosis (white arrowheads; scale bars, 50 μm; right panel).

Hepatitis persisted in both transgenic lines for ≥18 months. Phenotypes were much milder in *tg*1222 mice, implying that the LT expression level determined the severity of inflammation and liver injury. Therefore, *tg*1223 mice were selected for additional experiments and further key results were obtained from this mouse line.

Microarray and real-time PCR analyses that I performed together with Johannes Haybäck revealed elevated *mRNA* expression of genes involved in embryogenesis (e.g., Dmrta1), liver inflammation (e.g., *Pbfe1*), carcinogenesis (e.g. *Phlda3* and *Thrsp* [209]), glucose homeostasis and insulin sensitivity (e.g. *Fgf21*), and reduced *mRNA* expression of genes responsible for cell-cycle control (*Gadd45g*) and protease inhibition (*SerpinA9*) in 9-month-old *tg*1223 livers compared with C57BL/6 livers (Figure 81).

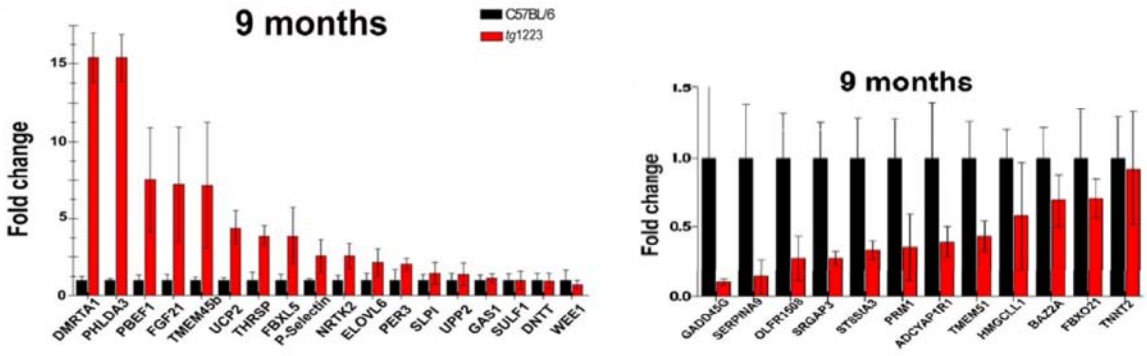

Figure 81: Analysis of *mRNA* expression in 9 month-old *tg*1223 compared to age-matched C57BL/6 livers. Based on a non-supervised DNA-microarray analysis, the expression of candidate genes was assessed by real-time PCR. Differences are reported as fold change. Standard deviation (+/- SD) is indicated by error bars. Strong up-regulation of various genes involved in inflammatory processes and carcinogenesis (e.g. *Spl1, Dmrta1, Phlda3*), cell adhesion and metastasis (e.g. *P-Selectin*), fibrogenesis (e.g. *Fgf21*), or carcinogenesis (*Nrtk2, Tmem45b*) were detected (left). Genes responsible for cell cycle control (e.g. *Gadd45g*) were significantly down-regulated in *tg*1223 livers compared to C57BL/6 livers (right).

Several genes strongly up- or down-regulated in 3-month-old *tg*1223 livers (Figure 76) returned to normal levels at 9 months of age. However, as expected, expression of *Lt*α and *Lt*β *mRNA*s remained at high levels at that time-point.

On the other hand, genes involved in cell division, liver inflammation, lipid metabolism, wound healing, and tumorigenesis were significantly up-regulated ($p<0.001$), whereas genes involved in growth arrest and apoptosis were significantly down-regulated ($p<0.001$) in 9-month-old compared with 3-month-old *tg*1223 livers (Figure 82).

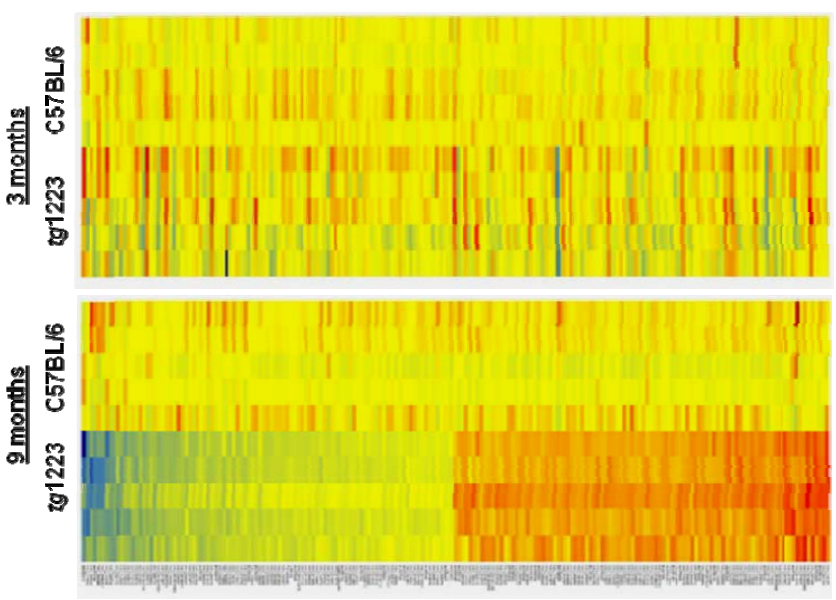

Figure 82: Real-time PCR analysis of C57BL/6 and *tg*1223 livers at 3 and 9 months of age. Indicated are the 100 highest up- and down-regulated genes in 9 month-old *tg*1223 livers, when compared to 9 and 3 month-old C57BL/6 as well as 3-month-old *tg*1223 livers. Rows represent particular genes, columns indicate individual mice;. Data are presented in a log2 scale (blue: up-regulated; red: down-regulated).

6.4.8 LTα and LTβ over-expression induces HCC development

At 12 months of age, about 20% (6/34) of *tg*1223 mice developed macroscopically visible nodules (Figure 83). Tumor frequency increased in *tg*1223 mice with age, reaching ~35% (18/51) by 18 months, whereas C57BL/6 mice did not develop any tumors (0/35; $p<0.0001$).

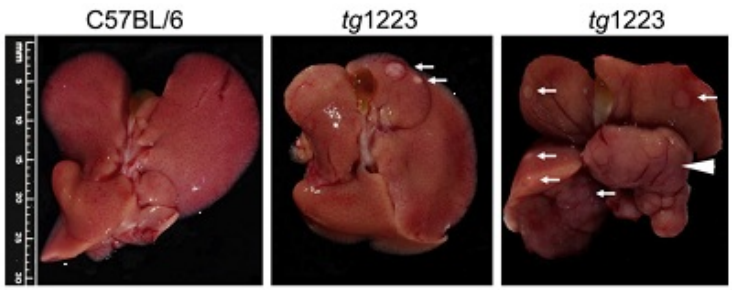

Figure 83: Over-expression of LTαβ in the liver leads to HCC development. Macroscopy of C57BL/6 (left panel) and *tg*1223 livers at the age of 12 (middle panel) and 18 months (right panel). White arrows indicate tumor nodules. White arrowhead indicates a liver lobe completely affected by HCC. Scale bar size is indicated.

The following scheme summarizes tumor development observed in *tg*1223 mice at 12 and 18 months of age (Figure 84).

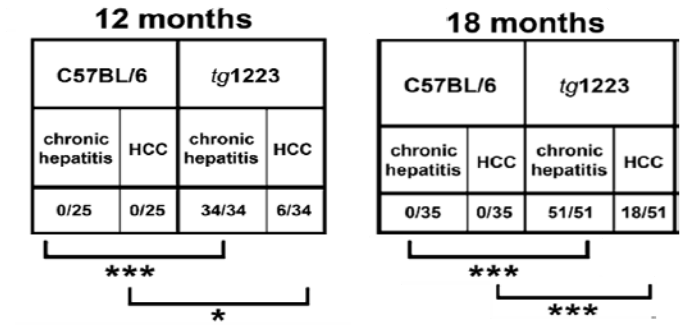

Figure 84: Chronic hepatitis and HCC incidence in *tg*1223 mice. Chronic hepatitis and HCC incidence in 12-month-old *tg*1223 and C57BL/6 mice (left) and in 18-month-old *tg*1223 and C57BL/6 mice (right).

With the help of Prof. Dr. Achim Weber - liver pathologist at the Department of Pathology, University Hospital Zurich - tumor nodules were classified histologically as HCC, including broadening of liver cell cords, loss of collagen IV networks, and increased proliferative activity. In contrast, age-matched C57BL/6 livers lacked HCC (0/20; p=0.05; Figure 85).

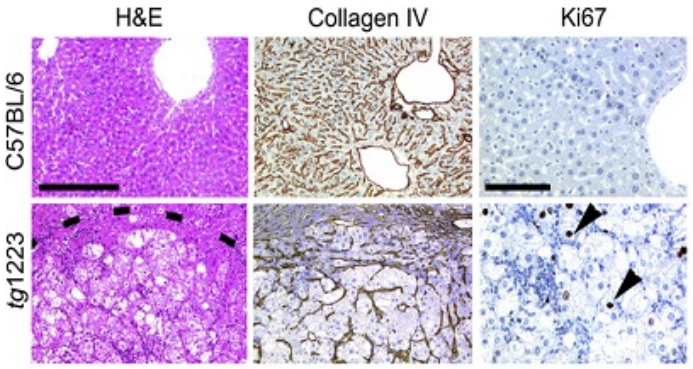

Figure 85: Histological analysis of livers from *tg*1223 and C57BL/6 mice. Dashed line depicts the HCC border. Collagen IV staining shows the broadening of the liver cell cords and loss of collagen IV networks indicative of HCC in *tg*1223 mice (scale bar, 200μm). High numbers of Ki67+ proliferating hepatocytes (arrows) are only found in *tg*1223 HCC (right column; scale bar, 100μm).

Tumors varied in size (1-25mm) and histology. Interestingly males and females were affected with similar frequencies (males: females=13:11; p=0.3). $A6^+$ oval cells [210] were focally (8/24) or diffusely (2/24) distributed within some *tg*1223 HCC. The remaining HCC from *tg*1223 mice (14/24) lacked $A6^+$ cells but were surrounded by them at the border zone of HCC (Figure 86).

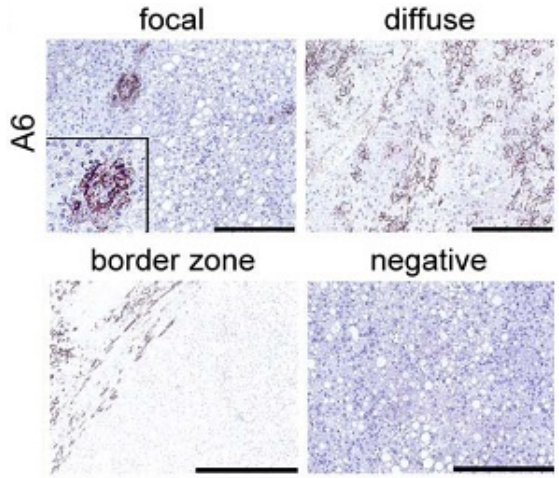

Figure 86: Immunohistochemical analysis of $A6^+$ cells in HCC in 12 or 18 month-old *tg*1223 livers. Approximately 45% of *tg*1223 HCC were composed of $A6^+$ cells (presumably oval cells), which were either focally or diffusely distributed. Other *tg*1223 HCC lacked $A6^+$ cells within the tumor (very right panel) but were surrounded by these cells at the border zone of the tumor (second right panel). The tumor border is marked by dashed line (scale bar: 200μm; insert: higher magnification).

6.4.9 Expression of tumor markers in HCC from *tg*1223 mice

I then evaluated expression of human liver tumor markers golgi protein 73 (GP73), glutamine synthetase (GS), and α-fetoprotein (AFP) in *tg*1223 livers on protein levels [211-213]. GP73, GS, and AFP expression was elevated in most *tg*1223 HCC, as detected by immunohistochemistry and immuno-blot analysis, compared with C57BL/6 livers or unaffected liver regions adjacent to HCC (Figure 87).

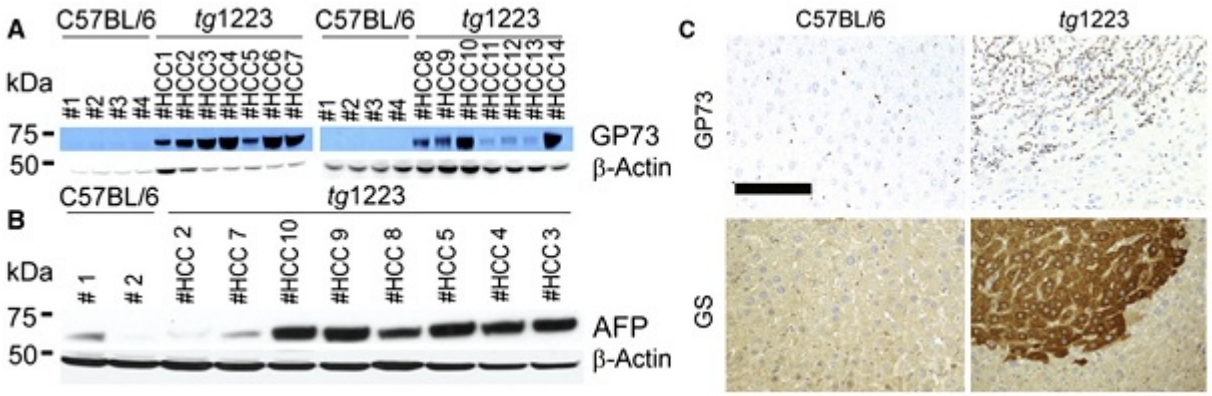

Figure 87: Expression of tumor markers in HCC from *tg*1223 mice. (A) Immuno-blot analysis of C57BL/6 and *tg*1223 HCC homogenates for GP73. Strong to moderate signal intensities were detected in all *tg*1223 HCC, but not in C57BL/6 livers. (B) Immuno-blot analysis of C57BL/6 and *tg*1223 HCC homogenates for AFP. β-actin served as a loading control (kDa, kilo Dalton). (C) Immunohistochemistry for GP73 and GS in a representative *tg*1223 HCC and age-matched C57BL/6 control (scale bar, 100μm).

6.4.10 Mechanisms driving LTαβ-induced chronic hepatitis and liver cancer

To identify other receptors and molecular mediators potentially involved in LT-induced chronic hepatitis and HCC development, *tg*1223 were intercrossed with *Tnfr1*$^{-/-}$ and *Ikkβ*$^{\Delta hep}$ mice. The requirement of lymphocytes in chronic hepatitis and HCC formation was investigated by intercrossing with *Rag1*$^{-/-}$ mice, which lack mature lymphocytes.

The absence of IKKβ, TNFR1 or lymphocytes per se did not appear to influence transgenic Ltα and Ltβ *mRNA* expression. Initially, at 3 months of age, *tg*1223/*Ikkβ*$^{\Delta hep}$, *tg*1223/*Tnfr1*$^{-/-}$ and *tg*1223/*Rag1*$^{-/-}$ mice lacked histological evidence of hepatitis similar to *tg*1223 mice (data not shown). The aberrant hepatic gene expression pattern described for 3-month-old *tg*1223 mice developed only partially in *tg*1223/*Ikkβ*$^{\Delta hep}$ and *tg*1223/*Rag1*$^{-/-}$ mice, whereas *tg*1223/*Tnfr1*$^{-/-}$ livers displayed an expression profile similar to that of *tg*1223 mice (Figure 76 & Figure 88).

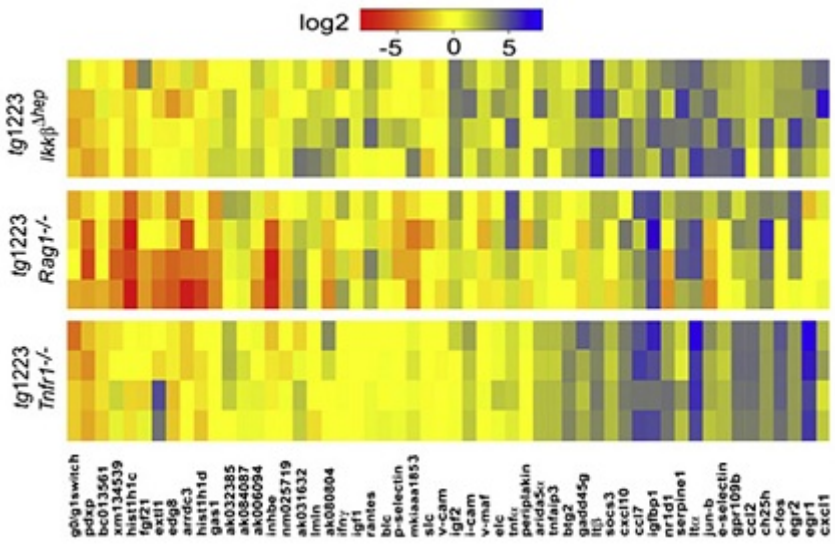

Figure 88: Real-time PCR *mRNA* expression analysis in livers of *tg*1223/*Ikkβ*$^{\Delta hep}$ *tg*1223/T*nfr1*$^{-/-}$ and *tg*1223/*Rag1*$^{-/-}$ mice. Data (blue: up-regulated; red: down-regulated) are presented on a log2 scale. Columns represent particular genes, rows indicate individual mice. Each data point shows the median expression of a particular gene resulting from three to four technical replicates, normalized to the mean expression value of the respective gene in C57BL/6 livers.

At 9 months of age, *tg*1223/*Rag1*$^{-/-}$ (n=26) and *tg*1223/*Ikkβ*$^{\Delta hep}$ (n=18) livers lacked hepatitis, hepatocyte or oval-cell proliferation, while *tg*1223/*Tnfr1*$^{-/-}$ (n=8) livers were indistinguishable from those of *tg*1223 mice (Figure 89, left).

At the age of 18 months, *tg*1223/*Rag1*$^{-/-}$ (n=26) and *tg*1223/*Ikkβ*$^{\Delta hep}$ (n=25) mice were devoid of hepatitis and HCC ($p<0.0001$) (Figure 89, right), suggesting that both lymphocytes and hepatocyte-specific IKKβ expression are required for LT-induced chronic hepatitis and HCC development.

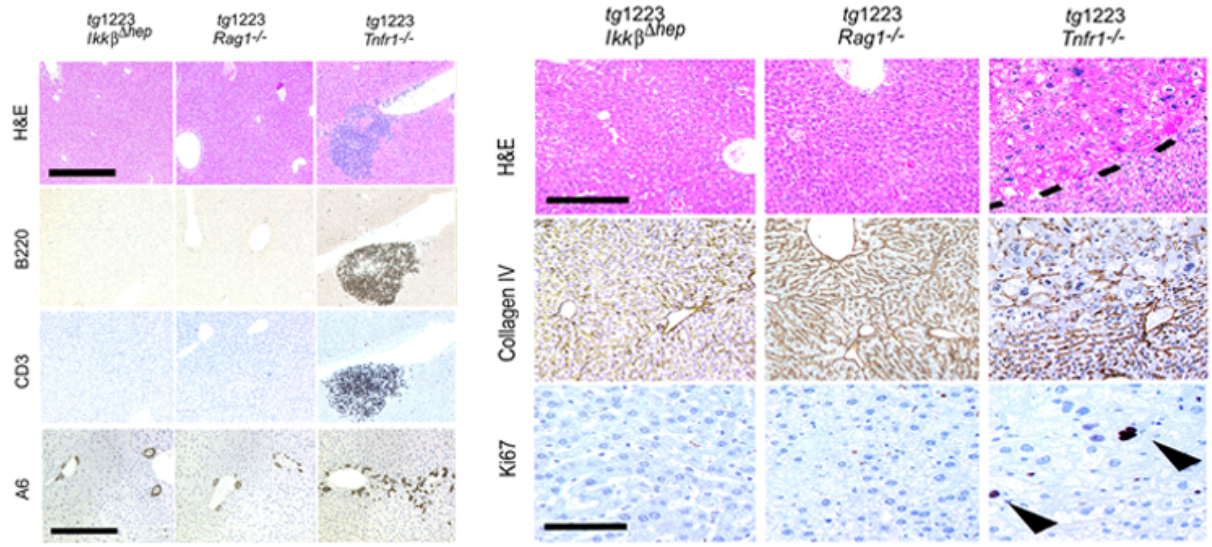

Figure 89: Histological and immunohistochemical analysis of livers of *tg*1223/*Ikkβ*$^{\Delta hep}$, *tg*1223/*Rag1*$^{-/-}$ and *tg*1223/*Tnfr1*$^{-/-}$ mice at 9 months age (left) and 18 months (right). A6 staining for oval cells, CD3 for T cells, B220 for B-cells (scale bar, 500μm; left panel). Dashed line depicts the HCC border (upper row; scale bar, 200μm). Collagen IV staining highlights the broadening of liver cell cords and loss of collagen IV networks in *tg*1223/Tnfr1$^{-/-}$ HCC. Ki67^{+}-proliferating hepatocytes are indicated by arrowheads (lower row; scale bar, 50μm; right).

Notably, *tg*1223/*Tnfr1*$^{-/-}$ mice displayed HCC (4/12) with an incidence similar to that among *tg*1223 mice indicating that TNFR1 signaling is not essential for LT-induced HCC formation in *tg*1223 mice.

6.4.11 Hepatocytes are the major responsive liver cells to agonistic LTβR antibody treatment

To investigate whether hepatocytes represent the major LT responsive liver cells and to investigate LTβR signaling in *Tnfr1*$^{-/-}$ and *Ikkβ*$^{\Delta hep}$ livers, TNFα (positive control), agonistic LTβR antibody (3C8), and appropriate negative controls (PBS or rat IgG) were administered intravenously to C57BL/6 and various knockout mice. Nuclear p65 (RelA) translocation in hepatocytes and non-parenchymal cells (NPC, e.g. Kupffer cells and lymphocytes), alterations in the hepatic transcriptome, and protein expression of selected chemokines were examined.

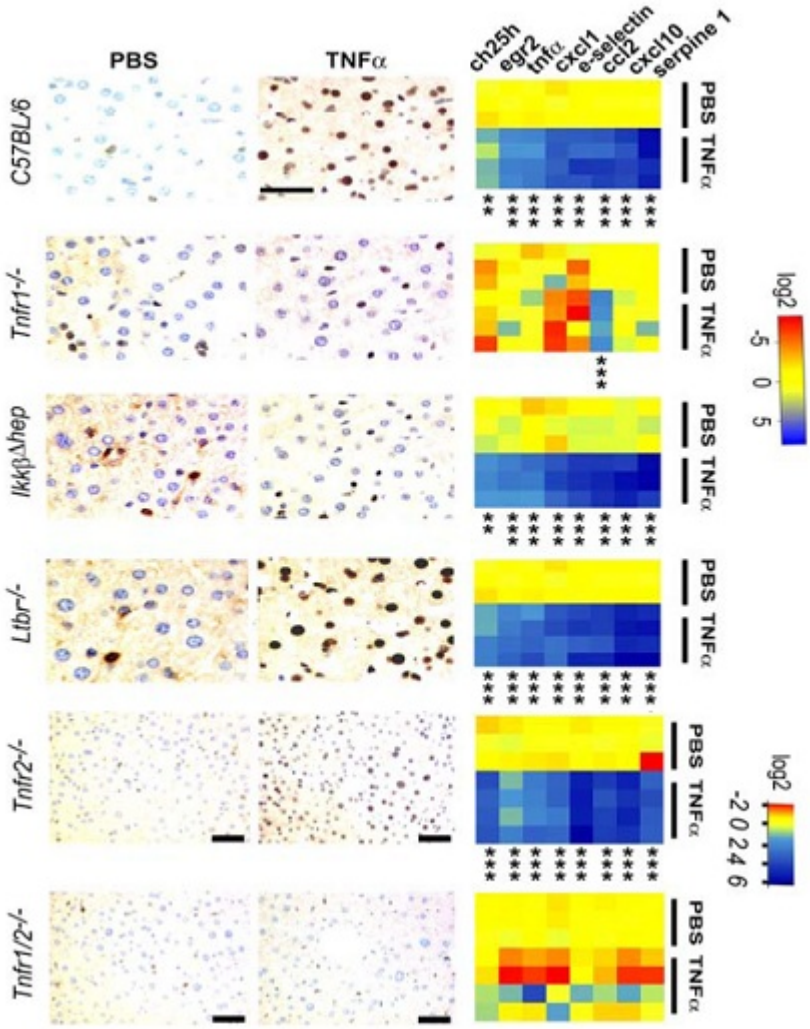

Figure 90: Hepatocytes respond to TNFα injection.
Immunohistochemical analysis of nuclear translocation of p65 (RelA) and real-time PCR for *mRNA* expression of selected NFκB target genes in livers of C57BL/6 and various knockout mice treated with TNFα. Real-time PCR data are presented on a log2 scale (blue, up-regulated; red, down-regulated). Rows indicate individual mice; columns represent particular genes. Each data point reflects the median expression value of a particular gene resulting from 3-4 technical replicates 45min after TNFα administration, normalized to the mean expression value of the respective gene in C57BL/6 livers. Statistical significance was evaluated by t-test: *p≤0.05; **p<0.001; ***p<0.0001 (scale bar, 50μm).

As expected, intravenous administration of TNFα but not PBS treatment caused a strong response in the livers of C57BL/6 and *Ltβr*$^{-/-}$ mice with nuclear translocation of p65 in hepatocytes and NPCs. Moreover, transcription levels of selected NFκB target genes were elevated in these mice similar to livers from 3 month-old *tg*1223 mice. In *Ikkβ*$^{\Delta hep}$ mice, TNFα administration did not induce p65 translocation in hepatocytes but did in NPC. However this induction sufficed to an up-regulation of the examined NFκB target genes (Figure 90).
Tnfr1$^{-/-}$ mice served as a negative control with hardly any change in the transcription profile. No increase in p65 translocation was found in livers of *Tnfr1*$^{-/-}$ mice compared to the PBS-treated control group. Acute administration of TNFα in *Tnfr2*$^{-/-}$ livers caused nuclear p65 translocation in hepatocytes and NPC, as well as elevated expression of selected NFκB target genes. In contrast, administration of TNFα in *Tnfr1/2*$^{-/-}$ mice failed to induce nuclear p65 translocation in hepatocytes and NPC, as well as up-regulation of selected NFκB target genes except *Ccl2*.

Administration of 3C8 induced nuclear p65 translocation, primarily in hepatocytes and some NPC of C57BL/6 livers (Figure 91), as well as transcriptional changes and up-regulation of selected chemokines reminiscent of those observed in 3-month-old *tg1*223 livers.

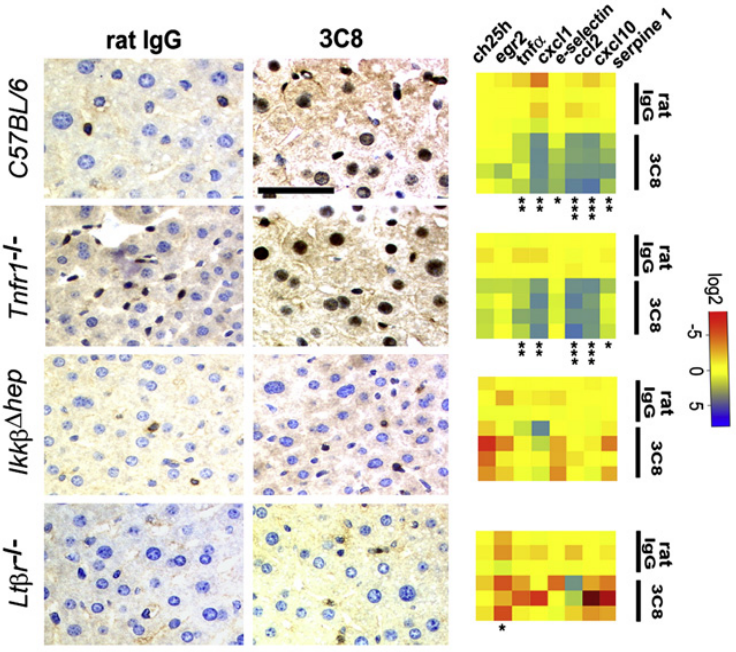

Figure 91: Hepatocytes can integrate LTβR signaling. Immunohistochemical analysis of nuclear p65 translocation and real-time PCR for *mRNA* expression of selected NFκB target genes in livers of C57BL/6 and various knockout mice treated with 3C8. Data are presented on a log2 scale (blue: up-regulated; red: down-regulated). Columns represent particular genes, rows indicate individual mice. Each data point reflects the median expression value of a particular gene resulting from three to four technical replicates, normalized to the mean expression value of the respective gene in C57BL/6 livers. Statistical significance was evaluated by t test: *p≤0.05; **p<0.001; ***p<0.0001; (scale bar, 50μm).

Similar results were obtained after 3C8 treatment of *Tnfr1*$^{-/-}$ mice, in contrast to *Ikkβ*$^{\Delta hep}$ livers, which were devoid of nuclear p65 translocation in hepatocytes and NPC. Furthermore, up-regulation of selected NFκB target genes could not be detected. Control *Ltβr*$^{-/-}$ mice treated with

3C8 lacked nuclear p65 translocation in hepatocytes or NPC, as well as up-regulation of selected NFκB target genes.

To examine whether lack of functional IKKα on hepatocytes and NPC would suppress LTβR-induced up-regulation of selected NFκB responsive genes, I also investigated livers of mice expressing a non-phosphorylatable $IKK\alpha^{AA}$ knock-in allele that we had received from the group of Prof. Dr. Michael Karin ($Ikk\alpha^{AA/AA}$ [196]). Upon 3C8 treatment $Ikk\alpha^{AA/AA}$ mice up-regulated selected NFκB responsive genes (Figure 92).

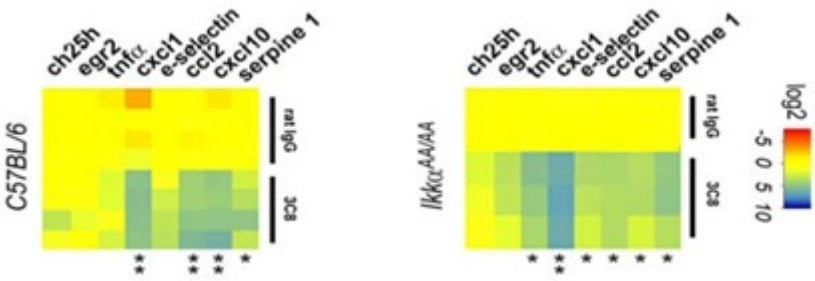

Figure 92: Real-time PCR for *mRNA* expression of selected NFκB target genes in livers of C57BL/6 and $Ikk\alpha^{AA/AA}$ mice treated with 3C8. Data are presented on a log2 scale (blue: up-regulated; red: down-regulated). Rows indicate individual mice; columns represent particular genes. Each data point reflects the median expression value of a particular gene resulting from 3-4 technical replicates, normalized to the mean expression value of the respective gene in C57BL/6 livers. Statistical significance was evaluated by t test: *p≤0.05; **p<0.001; ***p<0.0001.

The degree of *mRNA* up-regulation in liver was similar to that in 3C8-treated C57BL/6 mice. In contrast, control treated (rat IgG) $Ikk\alpha^{AA/AA}$ mice lacked up-regulation of selected NFκB responsive genes. This finding suggests that 3C8-mediated hepatic LTβR signaling is mainly integrated by hepatocytes involving canonical NFκB pathway.

6.4.12 Inhibition of LTβR signaling reduces chronic hepatitis and carcinogenesis

Together with Johannes Haybäck, I further investigated and analyzed the involvement of LTβR signaling in the transition of chronic hepatitis to HCC by long-term LTβR-Ig administration in *tg*1223 mice. Nine-month-old *tg*1223 mice with chronic hepatitis (n=31) or age-matched C57BL/6 mice (n=23) were treated with LTβR-Ig for 2 months, remained untreated for another 4 weeks, and were then sacrificed.

LTβR-Ig treatment significantly reduced chronic hepatitis incidence in *tg*1223 mice, compared with that in untreated *tg*1223 mice (treated: 4/31; untreated: 34/34; p<0.0001). Furthermore, LTβR-Ig treatment suppressed chronic hepatitis-driven HCC formation (treated: 0/31; untreated: 6/34; p<0.05) (Figure 93). LTβR-Ig treatment did not lead to overt histopathological alterations in C57BL/6 livers or overt changes in lymphocyte (B- and T-cells) or macrophage populations within spleens of C57BL/6 or *tg*1223 mice (data not shown).

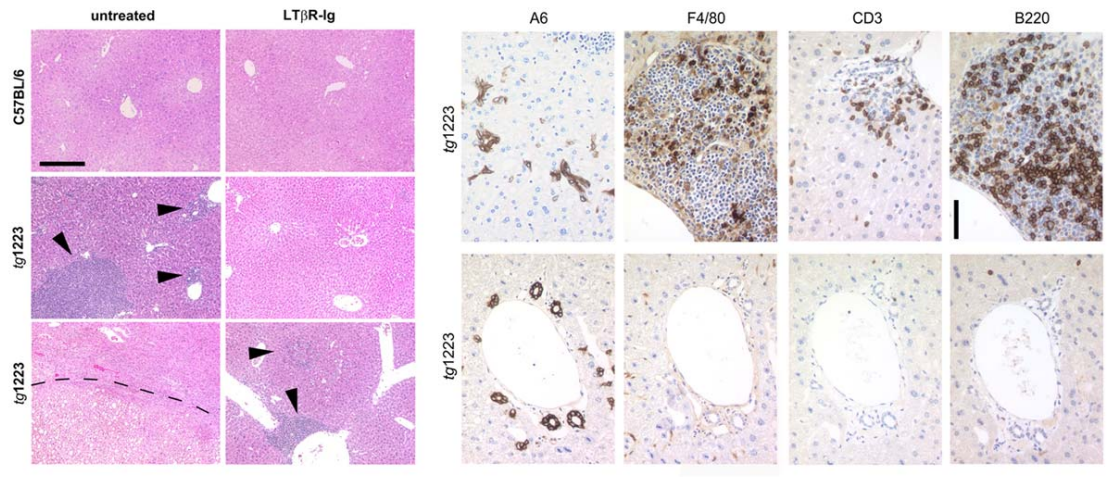

Figure 93: Histological analysis (left panel) and immunohistochemical analysis (right panel) of livers derived from 12 months-old LTβR-Ig treated mice. Left: Representative sections show no hepatitis or HCC in untreated or LTβR-Ig-treated C57BL/6 livers (upper row). Untreated *tg*1223 livers display hepatitis in 34/34 (middle panel, left column) and HCC in 6/34 cases (lower panel, left column). LTβR-Ig treatment reduces the incidence of hepatitis (4/31 mice) (middle and lower panel, right column) and prevents HCC formation in LTβR-Ig treated *tg*1223 mice. Arrowheads indicate inflammatory foci. Tumor border is indicted by a dashed line (scale bar, 200μm). Right: Immunohistological analysis of livers derived from LTβR-Ig-treated mice. Liver sections were stained with antibodies detecting T- (CD3), and B-cells (B220), macrophages and Kupffer cells (F4/80) as well as $A6^+$ oval cells. In the case of persistent inflammation in livers of LTβR-Ig treated mice we found B- (B220), T-cell (CD3) infiltrates, macrophages and Kupffer cells (F4/80), as well as oval cell proliferation (scale bar: 50μm).

Efficiency of LTβR-Ig treatment was ascertained by the loss of LTβR-dependent follicular dendritic cells (FDCs) as stained by MfgE8 within C57BL/6 and *tg*1223 spleens (Figure 94).

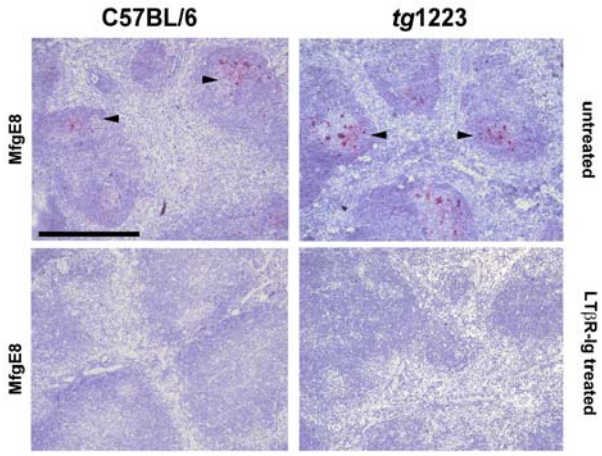

Figure 94: Successful application of LTβR-Ig leads to loss of FDCs. Immunohistological analysis for the presence of FDC networks in spleens of LTβR-Ig treated C57BL/6 or *tg*1223 mice. MFGE8 (FDC-M1) staining reveals a complete dedifferentiation of FDC networks in LTβR-Ig-treated C57BL/6 or *tg*1223 spleens. Arrowheads indicate FDC networks in spleens of untreated mice (scale bar: 200μm).

Thus, our results imply that long-term suppression of LTβR reduces chronic hepatitis incidence and can prevent the transition from chronic hepatitis to HCC in *tg*1223 mice. In the future, it will be investigated whether our results can be also translated to other models or even the human situation.

6.5 Discussion

6.5.1 Lymphotoxin in viral hepatitis and HCV replication

The first part of this study uncovered drastic and robust *mRNA* up-regulation of LTβR, LTα, and LTβ in biopsies from patients with HBV- or HCV-induced hepatitis and HCC. LT and LIGHT transcripts were mainly expressed by $CD3^+$ T-cells and $CD20^+$ B-cells; a significant proportion of LTα and LTβ expression was also attributable to hepatocytes. Notably, up-regulation of LTβR, LTα, and LTβ transcripts was also detected in non-virus related HCC, which could stem from activated, tumor-infiltrating lymphocytes and/or from neoplastic hepatocytes that have up-regulated LT, possibly in response to IL6. It was demonstrated that HCC-derived cell lines express IL6 [214] and that LT levels can be increased in response to IL6 and IL1β in hepatic and oval cell lines [215].

In a siRNA library screen, nine host genes related to LTβR and NFκB signaling were identified to influence HCV replication with the level of silencing of the host genes corresponding to the residual HCV replication activity [182]. Using similar HCV replicon cells containing a subgenomic construct derived from HCV genotype 1b, I could reproduce the findings for LTβ. However, I did not obtain the same efficient decrease in HCV replication, which could on the one hand be caused by less efficient silencing of LTβ, as in the study by Ng *et al.,* it was found that the decrease in HCV replication depends on the efficient silencing of at least one of the host genes identified. On the other hand, which appears to be more likely the reason, our HCV construct did not show additional mutations as in the case of the study by Ng *et al.,* which increases HCV replication, thus probably also leading to larger effects, when HCV replication is modified. Moreover, silencing of LTβR decreased HCV replication levels significantly – and it appears to be even more efficient than silencing its ligand. However, it remains to determine whether this also works with infectious HCV. The decrease in HCV replication is by far not as efficient as it is the case after treatment IFNα, however for patients that are not responding to IFNα and ribavirin therapy, who make up approximately 50% of all patients [216] [217], blocking of LTβR signaling might be beneficial for decreasing viral load and thereby potentially curing hepatitis.

Surprisingly, the opposed approach – triggering of LTβR signaling – increased HCV replication levels using replicon cells approximately 6 fold. More interestingly, also in an infectious setting, HCV replication levels were increased approximately 3 fold, which is a tremendous increase, as the replication capacity almost reached its limit in infectious cell culture systems. These results indicate that there is a strong link between LTβR signaling and HCV replication, making it more and more likely that interfering with LTβR signaling might be an effective therapeutic approach to decrease viral replication in HCV-infected patients. However, considering the studies, in which HCV core protein was shown to interact with the cytoplasmic tail of LTβR [183, 185], it is not

clear whether this interaction is sufficient to trigger signaling downstream of LTβR, which might enhance HCV's replicative potential. Therefore, it remains to be determined whether blocking of LTβR signaling with LTβR-Fc, a fusion protein of the LTβR and the Fcγ-portion of the constant IgG immunoglobulin molecule, binding efficiently to $LT\alpha_1\beta_2$ and LIGHT, would indeed prevent replication of HCV.

6.5.2 LTβR and NFκB signaling in viral hepatitis and HCC development

Recent publications have clearly indicated an important role of NFκB signaling in hepato-carcinogenesis. LT signaling induces both canonical and non-canonical NFκB pathways, whose role in controlling liver cancer formation remains controversial [166]. There is a big difference whether the role of NFκB signaling in liver cancer is investigated in the context of chronic hepatitis or DNA-damage induced by a chemical carcinogen. Our data indicate that in the context of chronic hepatitis NFκB signaling is a liver cancer promoting factor. In a mouse model with acute DEN exposure, depletion of functional NFκB signaling (*Ikkβ*$^{\Delta hep}$ mice) increased hepatocyte cell death, enhanced Kupffer cell activation, and elevated HCC incidence [171]. In contrast, NFκB signaling promotes HCC development in *mdr2*$^{-/-}$ mice [169], and hepatocyte-specific depletion of IKKβ prevents HCC formation in *tg*1223 mice. How can this contradictory role of IKKβ signaling in HCC formation be reconciled? On the one hand, IKKβ signaling might be required for hepatocytes to appropriately respond to and survive carcinogenic stimuli and acute liver injury (e.g. DEN exposure). On the other hand, IKKβ signaling might enable chemokine expression by hepatocytes, leading to hepatitis and HCC.

Consistent with this hypothesis, *tg*1223/*Rag1*$^{-/-}$ mice were devoid of chronic hepatitis, hepatocyte or oval-cell proliferation and failed to develop HCC.

But how can a contribution of immune cells to liver tumorigenesis be explained? One explanation might be that $CD4^+$ or $CD8^+$ T-cells expressing inflammatory cytokines (e.g. IL1β, TNFα, and IFNγ), as well as cytolytic proteins (e.g. Granzyme B), contribute to hepatocyte cell death, tissue remodeling, and transformation, finally resulting in HCC [191, 218]. Intrahepatic lymphocytes may also influence the production of inflammatory mediators, because 3-month-old *tg*1223/Rag1$^{-/-}$ livers displayed markedly reduced cytokine and chemokine levels. We propose that, rather than directly acting as a cell-autonomous oncogene on hepatocytes or $A6^+$ oval cells, hepatic LTαβ expression induces local up-regulation of chemokines (e.g., CCL2, CXCL10, CXCL1, and CCL7) by hepatocytes.

This potentially leads to the attraction of circulating inflammatory cells and a hyperproliferative, hepatotoxic environment stochastically leading to HCC formation. It is worth mentioning that

some chemokines which I have found to be strongly up-regulated in this study (e.g., CXCL10) have been reported to be mainly expressed by human hepatocytes in chronic hepatitis C [219].

Ablation of TNFR1 signaling did not prevent chronic hepatitis and HCC formation in *tg*1223 mice, although anti-TNFα antibody treatment prevents HCC development in *mdr2*$^{-/-}$ mice [169]. We investigated the mode of LT signaling in *Tnfr1*$^{-/-}$ livers upon 3C8 treatment. This treatment induced analogous hepatic changes seen in *tg*1223 mice at 3 months of age. Similar to our results with *tg*1223/*Tnfr1*$^{-/-}$ mice, this finding suggests that heterotrimeric LT causes p65 translocation in hepatocytes and induces a TNFR1-independent signaling cascade via LTβR, presumably contributing to chronic hepatitis and HCC. Most probably, HCC formation in *mdr2*$^{-/-}$ mice depends on pathways involving TNFR1 distinct from the LTβR-dependent pathways described in our study.

Intravenous administration of TNFα into *Ikkβ*$^{\Delta hep}$ mice did not cause p65 translocation in hepatocytes but up-regulated NFκB target genes, presumably through TNFα-activated NPC. In contrast, 3C8 treatment in *Ikkβ*$^{\Delta hep}$ mice had no effect. Therefore, hepatocytes but not NPC are likely to be the major liver cells integrating LT signaling. Interestingly, upon 3C8 treatment *Ikkα*$^{AA/AA}$ livers up-regulated selected NFκB target genes, similar to C57BL/6 mice. Therefore, the absence of IKKα in hepatocytes and NPC allows NFκB target gene expression upon 3C8 treatment, suggesting the involvement of the classical NFκB pathway in LTβR-induced hepatic signaling.

LTβR signaling was reported to induce oval-cell proliferation [220], which is thought to contribute to the development of liver tumors [221]. We observed proliferation of A6^{+} oval cells in chronically inflamed *tg*1223 livers at the age of 9 months and found A6^{+} cells within and at the border of *tg*1223 HCC. Whether those A6^{+} cells represent transformed oval cells contributing to liver carcinogenesis or whether A6 is up-regulated on aberrant hepatocytes within HCC remains to be determined.

Lack of lymphocytes or chronic hepatitis prevented oval-cell proliferation, although LTα and β transgene expression was unaltered. Therefore, it is conceivable that activated, infiltrating lymphocytes or Kupffer cells may contribute to oval cell proliferation by providing further LT or other cytokines in *tg*1223 livers.

On the basis of the presented data, Johannes Haybäck and I created a model that describes the sequence of events leading to chronic hepatitis and HCC in *tg*1223 mice can be proposed (Figure 95).

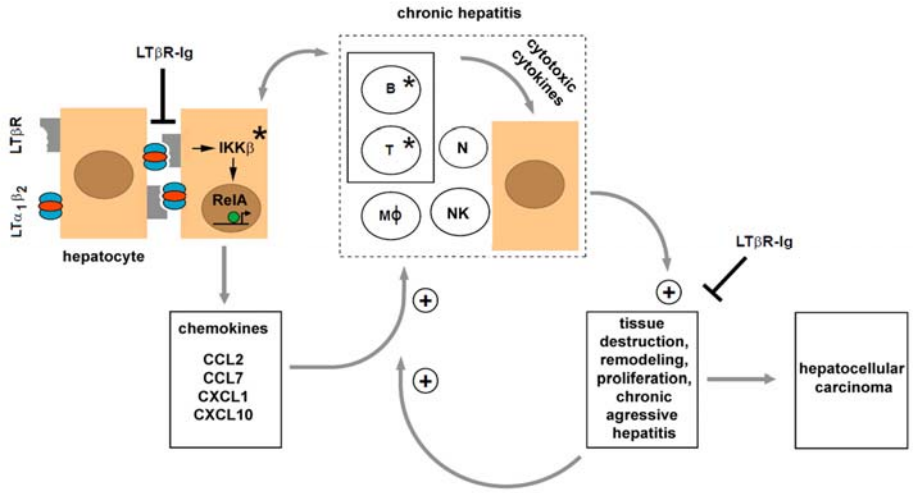

Figure 95: Scheme of chronic inflammation-induced liver carcinogenesis in *tg*1223 mice. Transgenic hepatocytes (brown) express LTαβ and induce chemokine production (e.g., CXCL1, CXCL10, CCL2, and CCL7) in the presence of IKKβ and intrahepatic lymphocytes. Chemo-attraction and activation of myeloid cells and lymphocytes expressing particular chemokine receptors (e.g., CXCR3, CXCR2, CCR2, and CCR1) cause hepatitis: CXCL10 attracts $CXCR3^+$ T- and NK-cells, CXCL1 $CXCR2^+$ T-cells, B-cells, neutrophils, and CCL2 $CCR2^+$ macrophages, and CCL7 attracts $CCR1^+$ monocytes. Activated, infiltrating immune cells secrete cytotoxic cytokines (e.g., IL6, IL1b, TNFα, IFNγ, and LTαβ) that cause tissue destruction, hepatocyte proliferation, cell death, and tissue remodeling. In such an environment, hepatocytes are susceptible to chromosomal aberrations leading to HCC. Tissue destruction and remodeling supports the infiltration of activated inflammatory cells (e.g., myeloid cells), leading to a feed-forward loop toward chronic aggressive hepatitis. Asterisks indicate that genetic depletion of those components (IKKβ; T and B cells) blocks chronic hepatitis development and HCC. Blocking LTβR signaling with LTβR-Ig in 9-month-old *tg*1223 mice reduces chronic hepatitis incidence and prevents HCC. (+) indicates the fortification of a described process. (⊥) indicates the suppression of a described process. The transcription factor RelA is schematically depicted as a green circle, inducing transcription of NFκB target genes (e.g., chemokines) (arrow). B, B cells; T, T cells; MØ, macrophages; N, neutrophils; NK, NK cells.

What are the potential clinical implications of our findings? It has recently been demonstrated that pharmacological inhibition of LTβR signaling reduces virus-, bacteria-, and concavalin A–induced liver injury [188-190], whereas triggering LTβR signaling on hepatocytes appears to be beneficial during liver regeneration [158]. Moreover, siRNA knock-down of various components of the LTβR signaling pathway (e.g., LTβ and RelA) were shown to interfere with HCV replication *in vitro* [182]. Therefore, inhibition of LTβR signaling might also impede the efficiency of HCV replication.

What are the possible side effects of blocking LTβR signaling? The reported effects include alterations in the micro-architecture of white pulp follicles and disappearance of FDC networks in non-human primates [222]. Despite the loss of FDCs and a reduced capacity to trap immune complexes, the primary antibody response to keyhole limpet-hemocyanin was not significantly altered [222].

Accordingly, together with Johannes Haybäck, I have investigated a possible beneficial effect of blocking LTβR signaling in *tg*1223 mice with chronic hepatitis. This partially reverted inflammation and prevented HCC formation, suggesting that LTβR-Ig treatment might be beneficial in liver pathologies with sustained LT signaling. Our results show that LT signaling is critically involved in hepatitis and subsequent HCC development and imply that blocking LTβR signaling might become a beneficial therapeutic approach in the context of HBV- or HCV-induced chronic hepatitis and other liver diseases displaying sustained hepatic LTβR signaling.

6.5.3 Interference with lymphotoxin signaling in other types of cancer

However, the concept that blocking LTβR signaling might interfere with cancer progression, as we could show with LTβR-Ig treatment in a mouse model of HCC is not entirely new.

Treatment with LTβR-Ig in a prostate cancer model (TRAMP; mice develop spontaneously prostate cancer with 100% penetrance and metastases) interrupted clonal T-cell deletion, reduced the size of the primary cancer, and completely prevented further metastasis - suggesting an important role of LT in controlling anti-tumor T-cell selection, showing the value of non-antigen based immune prevention for individuals with genetic predisposition to cancer [223].

Other studies have focused on the activation of LTβR signaling pathways in various cancer types. Bergsagel *et al*., have reported a constitutive activation of NFκB signaling in multiple myeloma as a result of mutations in the LTβR gene [224], emphasizing a critical role for the NFκB pathway in its pathogenesis. Furthermore, constitutive NFκB activity was detected in diffuse large B-cell lymphoma, indicating a role for this signaling pathway as a primary pathogenic event in lymphomagenesis [170].

In addition, LTβR-mediated signaling - most likely through the non-canonical NFκB pathway - is also involved in tumor angiogenesis. Activation of LTβR on fibrosarcoma cells by activated host lymphocytes is capable of initiating a novel, pro-angiogenic pathway leading to organized tumor tissue development. Conversely, in this model, inhibition of LTβR signaling prevented tumor angiogenesis and neovascularization, resulting in tumor growth arrest [225].

Data by Lukashev *et al*., clearly indicate that in a syngeneic colon tumor model, agonistic LTβR antibody treatment induces lymphocyte infiltration and tumor necrosis by enhancing tumor chemosensitivity [226]. One proposed mechanism might be the induction of pro-inflammatory chemokines functioning as chemo-attractants for T, NK, and dendritic cells, contributing to tumor destruction. However, extensive studies revealed that there are human cell lines resistant to agonistic LTβR treatment, indicating that treatment success may depend on the cancer cell type. Moreover, this treatment decreased tumor size and/or improved long-term animal survival in two out of six orthotopic xenografts derived from independent surgical colorectal carcinoma

samples. Therefore, it is questionable whether the results gained indeed point to the fact that in some cases or tumor entities activation of LTβR signaling might be anti-tumorigenic. Further studies are needed to reveal the details of this concept.

In addition to the previously described TRAMP model, subcutaneous allografts of mouse androgen-dependent AD-CaP cell line myc-CaP were used to facilitate better mechanistic analysis of CR-CaP development. To determine whether inflammation-responsive IKKβ participates in development of CR-CaP, IKKβ was knocked-out in prostate epithelial cells of TRAMP mice. This neither affected primary tumor growth nor CR-CaP emergence after castration [227]. In contrast, specific deletion of IKKβ in bone marrow-derived cells delayed development of CR-CaP emergence, although lacking effects on primary tumor development. These results suggested an involvement of immune cells promoting tumor emergence after castration. Indeed, after androgen ablation the regressing tumors were infiltrated with T- and B-cells, NK-cells and myeloid cell types.

Furthermore, inflammatory cytokines, for example, IL6, IL12, TNFα and LT, were up-regulated in the regressing myc-CaP allografts. Notably, LT ablation on B-cells, but not on T-cells delayed CRCaP growth. Accordingly, in addition to mediators released by dying CaP cells, critical participants in tumor emergence are tumor-infiltrating B-cells, producing LT that signals through LTβR on CaP cells to induce IKKα nuclear translocation and STAT3 activation.

Interventions preventing LT production or ablating LT signaling could delay regressing tumors in patients with androgen ablation therapy.

In a study on nasopharyngeal carcinoma (NPC), a distinct type of head and neck cancer, LTβR was shown to be frequently over-expressed in primary NPC tumors, concomitant with an amplification of chromosome 12p13.3 [228]. *In vitro* studies in nasopharyngeal epithelial cells revealed increased NFκB activity and cell proliferation due to LTβR over-expression. Addition of $LT\alpha_1\beta_2$ led to increased proliferation of nasopharyngeal epithelial cells and siRNA knockdown of LTβR expression inhibited growth of the NPC tumors with 12p13.3 amplification [228], further strengthening a tumor-promoting role of LTβR signaling in this type of carcinoma.

Interestingly, LTα signaling may also be involved in the maturation and recruitment of NK-cells and may have an important role in anti-tumor surveillance. It was shown that LTα deficiency leads to defects in NK maturation and recruitment and that formation of experimental pulmonary metastases upon injection of B16F10 melanoma cells was enhanced in $LT\alpha^{-/-}$ mice [229].

Therefore, LTα signaling may be involved in NK-cell maturation, recruitment and anti-tumor surveillance.

Figure 96 summarizes the previously discussed studies in which inhibition or activation of LTβR signaling had shown a beneficial effect on cancer progression.

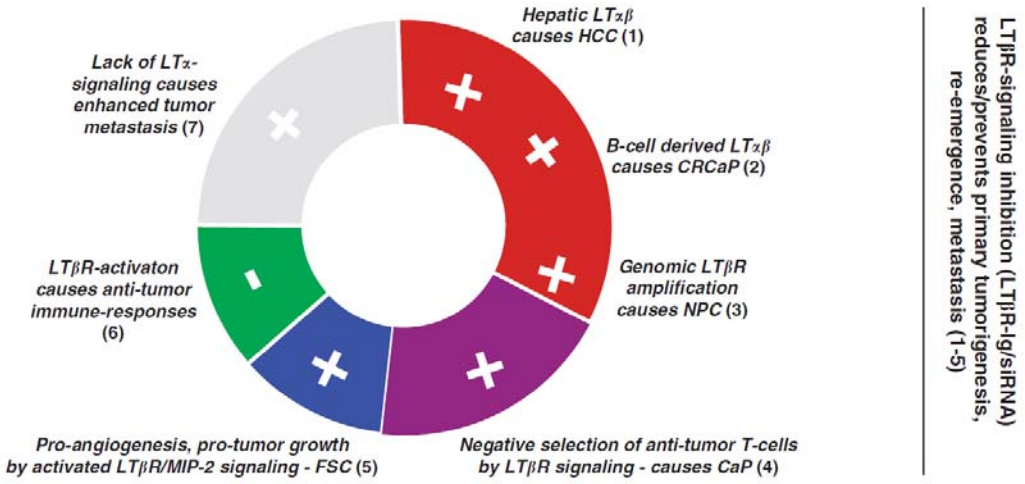

Figure 96: Scheme summarizing *in vivo* studies showing pro- and anti-tumorigenic effects of LTβR activation or inhibition. Experiments describing the pro- or anti-carcinogenic effects (depicted with + or -) of activated LTβR signaling *in vivo* [(1) [163]; (2) [227]; (3) [228]; (4) [223]; (5) [225]; (6) [226]; colored sectors]. The gray sector indicates that also lack of LTα signaling can influence anti-tumor surveillance causing significant enhancement of experimental pulmonary metastases upon injection of B16F10 melanoma (7) [229]). (Right column) Depicts various studies indicating that block of LTβR signaling might work as an anti-tumor strategy. CaP: prostate cancer; CRCaP: castration-resistant prostate cancer; FSC: fibrosarcoma; NPC: nasopharyngeal carcinoma.

The above-described results convincingly demonstrate a participation of LTβR signaling in carcinogenesis, however, involving various mechanisms and biological functions in the diverse *in vivo* paradigms tested. It will be an important future task to investigate and reveal in detail the mechanisms underlying the different effects of induced LTβR signaling in the various cancer models. What could be the reason(s) for the fact that increased LTβR signaling could in some instances generate a pro-carcinogenic environment [163] and in other paradigms lead to tumor reduction [226]? Apparently, this might have something to do with the tumor type investigated as well as the organ in which the tumor has developed. In this regard, it is also important to note that, e.g., transgenic mice expressing LT in other organs than liver have so far not been reported to display inflammation-induced carcinogenesis, although most of these models show strong signs of inflammation. It is very possible that tumorigenesis develops with low frequency at late stage of life in these animals (similar to *tg*1223 mice) and that this has escaped the attention of the experimentators. However, it is also possible that a highly regenerative, proliferative environment (e.g., like in liver) is needed to induce inflammation-induced carcinogenesis in the context of deregulated LTβR signaling.

However, LT's involvement is very unlikely to be universal to all cancer types or signaling pathways contributing to or enabling carcinogenesis: In an illuminating study, it was shown that neither lack of TNF nor LTα reduced tumor burden on a p53-deficient background, suggesting that in the context of p53-deficiency LTα signaling does not aggravate carcinogenesis [230].

Recent data of various laboratories indicate that there is still much more to be learned about the link between LT signaling and cancer, at the site of carcinogenesis as well as at the site where the host's adaptive immune response is triggered against cancer. Exciting times are ahead of us, verifying the utility of LTβR antagonists and agonists in the various different clinical settings and hopefully revealing the detailed mechanisms of LTβR signaling in the context of inflammation and cancer.

7 REFERENCES

1. WHO. Cancer Fact Sheet No 297. (2011).

2. Mehlen, P. & Puisieux, A. Metastasis: a question of life or death. *Nat Rev Cancer* **6**, 449-458 (2006).

3. Chambers, A.F., Groom, A.C. & MacDonald, I.C. Dissemination and growth of cancer cells in metastatic sites. *Nat Rev Cancer* **2**, 563-572 (2002).

4. Hanahan, D. & Weinberg, R.A. Hallmarks of cancer: the next generation. *Cell* **144**, 646-674 (2011).

5. Qian, B.Z.*, et al.* CCL2 recruits inflammatory monocytes to facilitate breast-tumour metastasis. *Nature* **475**, 222-225 (2011).

6. Soria, G.*, et al.* Inflammatory mediators in breast cancer: Coordinated expression of TNFalpha & IL-1beta with CCL2 & CCL5 and effects on epithelial-to-mesenchymal transition. *BMC Cancer* **11**, 130 (2011).

7. Yoshidome, H.*, et al.* Significance of monocyte chemoattractant protein-1 in angiogenesis and survival in colorectal liver metastases. *Int J Oncol* **34**, 923-930 (2009).

8. Zhang, J., Patel, L. & Pienta, K.J. CC chemokine ligand 2 (CCL2) promotes prostate cancer tumorigenesis and metastasis. *Cytokine Growth Factor Rev* **21**, 41-48 (2010).

9. Zijlmans, H.J.*, et al.* The absence of CCL2 expression in cervical carcinoma is associated with increased survival and loss of heterozygosity at 17q11.2. *J Pathol* **208**, 507-517 (2006).

10. Vucur, M.*, et al.* Mouse models of hepatocarcinogenesis: what can we learn for the prevention of human hepatocellular carcinoma? *Oncotarget* **1**, 373-378 (2010).

11. Yona, S. & Jung, S. Monocytes: subsets, origins, fates and functions. *Current opinion in hematology* **17**, 53-59 (2010).

12. Moser, B. & Loetscher, P. Lymphocyte traffic control by chemokines. *Nat Immunol* **2**, 123-128 (2001).

13. Yadav, A., Saini, V. & Arora, S. MCP-1: chemoattractant with a role beyond immunity: a review. *Clinica chimica acta; international journal of clinical chemistry* **411**, 1570-1579 (2010).

14. Gerard, C. & Rollins, B.J. Chemokines and disease. *Nat Immunol* **2**, 108-115 (2001).

15. Zlotnik, A., Yoshie, O. & Nomiyama, H. The chemokine and chemokine receptor superfamilies and their molecular evolution. *Genome biology* **7**, 243 (2006).

16. Cochran, B.H., Reffel, A.C. & Stiles, C.D. Molecular cloning of gene sequences regulated by platelet-derived growth factor. *Cell* **33**, 939-947 (1983).

17. Proost, P., Wuyts, A. & Van Damme, J. Human monocyte chemotactic proteins-2 and -3: structural and functional comparison with MCP-1. *J Leukoc Biol* **59**, 67-74 (1996).

18. Rodriguez-Frade, J.M.*, et al.* The chemokine monocyte chemoattractant protein-1 induces functional responses through dimerization of its receptor CCR2. *Proc Natl Acad Sci U S A* **96**, 3628-3633 (1999).

19. Mellado, M.*, et al.* The chemokine monocyte chemotactic protein 1 triggers Janus kinase 2 activation and tyrosine phosphorylation of the CCR2B receptor. *J Immunol* **161**, 805-813 (1998).

20. Shimizu, Y. & Hunt, S.W., 3rd. Regulating integrin-mediated adhesion: one more function for PI 3-kinase? *Immunology today* **17**, 565-573 (1996).

21. Knall, C., Worthen, G.S. & Johnson, G.L. Interleukin 8-stimulated phosphatidylinositol-3-kinase activity regulates the migration of human neutrophils independent of extracellular signal-regulated kinase and p38 mitogen-activated protein kinases. *Proc Natl Acad Sci U S A* **94**, 3052-3057 (1997).

22. Turner, L., Ward, S.G. & Westwick, J. RANTES-activated human T lymphocytes. A role for phosphoinositide 3-kinase. *J Immunol* **155**, 2437-2444 (1995).

23. Turner, S.J., Domin, J., Waterfield, M.D., Ward, S.G. & Westwick, J. The CC chemokine monocyte chemotactic peptide-1 activates both the class I p85/p110 phosphatidylinositol 3-kinase and the class II PI3K-C2alpha. *The Journal of biological chemistry* **273**, 25987-25995 (1998).

24. Yen, H., Zhang, Y., Penfold, S. & Rollins, B.J. MCP-1-mediated chemotaxis requires activation of non-overlapping signal transduction pathways. *J Leukoc Biol* **61**, 529-532 (1997).

25. Gerszten, R.E.*, et al.* MCP-1 and IL-8 trigger firm adhesion of monocytes to vascular endothelium under flow conditions. *Nature* **398**, 718-723 (1999).

26. Weber, K.S., von Hundelshausen, P., Clark-Lewis, I., Weber, P.C. & Weber, C. Differential immobilization and hierarchical involvement of chemokines in monocyte arrest and transmigration on inflamed endothelium in shear flow. *Eur J Immunol* **29**, 700-712 (1999).

27. Zhang, J., Patel, L. & Pienta, K.J. Targeting chemokine (C-C motif) ligand 2 (CCL2) as an example of translation of cancer molecular biology to the clinic. *Progress in molecular biology and translational science* **95**, 31-53 (2010).

28. Chetcuti, A.*, et al.* Identification of differentially expressed genes in organ-confined prostate cancer by gene expression array. *The Prostate* **47**, 132-140 (2001).

29. Lu, Y.*, et al.* Monocyte chemotactic protein-1 (MCP-1) acts as a paracrine and autocrine factor for prostate cancer growth and invasion. *The Prostate* **66**, 1311-1318 (2006).

30. Mazzucchelli, L.*, et al.* Monocyte chemoattractant protein-1 gene expression in prostatic hyperplasia and prostate adenocarcinoma. *Am J Pathol* **149**, 501-509 (1996).

31. Rhodes, D.R.*, et al.* ONCOMINE: a cancer microarray database and integrated data-mining platform. *Neoplasia* **6**, 1-6 (2004).

32. Saji, H.*, et al.* Significant correlation of monocyte chemoattractant protein-1 expression with neovascularization and progression of breast carcinoma. *Cancer* **92**, 1085-1091 (2001).

33. Ueno, T.*, et al.* Significance of macrophage chemoattractant protein-1 in macrophage recruitment, angiogenesis, and survival in human breast cancer. *Clin Cancer Res* **6**, 3282-3289 (2000).

34. Valkovic, T., Lucin, K., Krstulja, M., Dobi-Babic, R. & Jonjic, N. Expression of monocyte chemotactic protein-1 in human invasive ductal breast cancer. *Pathology, research and practice* **194**, 335-340 (1998).

35. Rodriguez-Frade, J.M., Mellado, M. & Martinez-A., C. CCR2. in *Cytokine Reference* (ed. J.J. Oppenheim & M. Feldmann) (Academic Press, 2000).

36. Boring, L.*, et al.* Impaired monocyte migration and reduced type 1 (Th1) cytokine responses in C-C chemokine receptor 2 knockout mice. *The Journal of clinical investigation* **100**, 2552-2561 (1997).

37. Kurihara, T., Warr, G., Loy, J. & Bravo, R. Defects in macrophage recruitment and host defense in mice lacking the CCR2 chemokine receptor. *The Journal of experimental medicine* **186**, 1757-1762 (1997).

38. Kuziel, W.A., *et al.* Severe reduction in leukocyte adhesion and monocyte extravasation in mice deficient in CC chemokine receptor 2. *Proc Natl Acad Sci U S A* **94**, 12053-12058 (1997).

39. Lu, B., *et al.* Abnormalities in monocyte recruitment and cytokine expression in monocyte chemoattractant protein 1-deficient mice. *The Journal of experimental medicine* **187**, 601-608 (1998).

40. Serbina, N.V. & Pamer, E.G. Monocyte emigration from bone marrow during bacterial infection requires signals mediated by chemokine receptor CCR2. *Nat Immunol* **7**, 311-317 (2006).

41. Weinberg, R.A. *The biology of cancer* (Garland Science, 2007).

42. Granot, Z., *et al.* Tumor entrained neutrophils inhibit seeding in the premetastatic lung. *Cancer Cell* **20**, 300-314 (2011).

43. Paget, S. The distribution of secondary growths in cancer of the breast. *Lancet* **1**, 571-573 (1889).

44. Gupta, G.P. & Massague, J. Cancer metastasis: building a framework. *Cell* **127**, 679-695 (2006).

45. Joyce, J.A. & Pollard, J.W. Microenvironmental regulation of metastasis. *Nat Rev Cancer* **9**, 239-252 (2009).

46. Francia, G., Cruz-Munoz, W., Man, S., Xu, P. & Kerbel, R.S. Mouse models of advanced spontaneous metastasis for experimental therapeutics. *Nat Rev Cancer* **11**, 135-141 (2011).

47. Tlsty, T.D. & Coussens, L.M. Tumor stroma and regulation of cancer development. *Annu Rev Pathol* **1**, 119-150 (2006).

48. Peinado, H., Lavotshkin, S. & Lyden, D. The secreted factors responsible for pre-metastatic niche formation: old sayings and new thoughts. *Semin Cancer Biol* **21**, 139-146 (2011).

49. Qian, B.Z. & Pollard, J.W. Macrophage diversity enhances tumor progression and metastasis. *Cell* **141**, 39-51 (2010).

50. O'Hayre, M., Salanga, C.L., Handel, T.M. & Allen, S.J. Chemokines and cancer: migration, intracellular signalling and intercellular communication in the microenvironment. *Biochem J* **409**, 635-649 (2008).

51. Kim, S., *et al.* Carcinoma-produced factors activate myeloid cells through TLR2 to stimulate metastasis. *Nature* **457**, 102-106 (2009).

52. Allavena, P., Germano, G., Marchesi, F. & Mantovani, A. Chemokines in cancer related inflammation. *Exp Cell Res* **317**, 664-673 (2011).

53. Struckmann, K., *et al.* pVHL co-ordinately regulates CXCR4/CXCL12 and MMP2/MMP9 expression in human clear-cell renal cell carcinoma. *J Pathol* **214**, 464-471 (2008).

54. Läubli, H. & Borsig, L. Selectins as mediators of lung metastasis. *Cancer Microenviron* **3**, 97-105 (2010).

55. Mishra, P., Banerjee, D. & Ben-Baruch, A. Chemokines at the crossroads of tumor-fibroblast interactions that promote malignancy. *J Leukoc Biol* **89**, 31-39 (2011).

56. Läubli, H., Spanaus, K.S. & Borsig, L. Selectin-mediated activation of endothelial cells induces expression of CCL5 and promotes metastasis through recruitment of monocytes. *Blood* **114**, 4583-4591 (2009).

57. Yoshidome, H., *et al.* Significance of monocyte chemoattractant protein-1 in angiogenesis and survival in colorectal liver metastases. *Int J Oncol* **34**, 923-930 (2009).

58. Mantovani, A. & Sica, A. Macrophages, innate immunity and cancer: balance, tolerance, and diversity. *Curr Opin Immunol* **22**, 231-237 (2010).

59. Loberg, R.D.*, et al.* Targeting CCL2 with systemic delivery of neutralizing antibodies induces prostate cancer tumor regression in vivo. *Cancer Res* **67**, 9417-9424 (2007).

60. Salcedo, R.*, et al.* Human endothelial cells express CCR2 and respond to MCP-1: direct role of MCP-1 in angiogenesis and tumor progression. *Blood* **96**, 34-40 (2000).

61. Loberg, R.D.*, et al.* CCL2 as an important mediator of prostate cancer growth in vivo through the regulation of macrophage infiltration. *Neoplasia* **9**, 556-562 (2007).

62. Mizutani, K.*, et al.* The chemokine CCL2 increases prostate tumor growth and bone metastasis through macrophage and osteoclast recruitment. *Neoplasia* **11**, 1235-1242 (2009).

63. Mildner, A.*, et al.* CCR2+Ly-6Chi monocytes are crucial for the effector phase of autoimmunity in the central nervous system. *Brain* **132**, 2487-2500 (2009).

64. Hohl, T.M.*, et al.* Inflammatory monocytes facilitate adaptive CD4 T cell responses during respiratory fungal infection. *Cell host & microbe* **6**, 470-481 (2009).

65. Borsig, L., Wong, R., Hynes, R.O., Varki, N.M. & Varki, A. Synergistic effects of L- and P-selectin in facilitating tumor metastasis can involve non-mucin ligands and implicate leukocytes as enhancers of metastasis. *Proc Natl Acad Sci U S A* **99**, 2193-2198 (2002).

66. Edovitsky, E., Elkin, M., Zcharia, E., Peretz, T. & Vlodavsky, I. Heparanase gene silencing, tumor invasiveness, angiogenesis, and metastasis. *Journal of the National Cancer Institute* **96**, 1219-1230 (2004).

67. Hostettler, N.*, et al.* P-selectin- and heparanase-dependent antimetastatic activity of non-anticoagulant heparins. *Faseb J* **21**, 3562-3572 (2007).

68. Odermatt, B., Eppler, M., Leist, T.P., Hengartner, H. & Zinkernagel, R.M. Virus-triggered acquired immunodeficiency by cytotoxic T-cell-dependent destruction of antigen-presenting cells and lymph follicle structure. *Proc Natl Acad Sci U S A* **88**, 8252-8256 (1991).

69. Raasch, J.*, et al.* IkappaB kinase 2 determines oligodendrocyte loss by non-cell-autonomous activation of NF-kappaB in the central nervous system. *Brain* **134**, 1184-1198 (2011).

70. Mack, M.*, et al.* Expression and characterization of the chemokine receptors CCR2 and CCR5 in mice. *J Immunol* **166**, 4697-4704 (2001).

71. Wang, L., Fuster, M., Sriramarao, P. & Esko, J.D. Endothelial heparan sulfate deficiency impairs L-selectin- and chemokine-mediated neutrophil trafficking during inflammatory responses. *Nat Immunol* **6**, 902-910 (2005).

72. Borsig, L.*, et al.* Heparin and cancer revisited: mechanistic connections involving platelets, P-selectin, carcinoma mucins, and tumor metastasis. *Proc Natl Acad Sci U S A* **98**, 3352-3357 (2001).

73. Reutershan, J.*, et al.* Critical role of endothelial CXCR2 in LPS-induced neutrophil migration into the lung. *The Journal of clinical investigation* **116**, 695-702 (2006).

74. Sykes, D.B. & Kamps, M.P. Estrogen-dependent E2a/Pbx1 myeloid cell lines exhibit conditional differentiation that can be arrested by other leukemic oncoproteins. *Blood* **98**, 2308-2318 (2001).

75. Hohenberger, W., Reingruber, B. & Merkel, S. Surgery for colon cancer. *Scand J Surg* **92**, 45-52 (2003).

76. Schmiegel, W.*, et al.* S3 guidelines for colorectal carcinoma: results of an evidence-based consensus conference on February 6/7, 2004 and June 8/9, 2007 (for the topics IV, VI and VII). *Z Gastroenterol* **48**, 65-136 (2010).

77. Hennig, G.*, et al.* Automated extraction of DNA and RNA from a single formalin-fixed paraffin-embedded tissue section for analysis of both single-nucleotide polymorphisms and mRNA expression. *Clin Chem* **56**, 1845-1853 (2010).

78. Serbina, N.V., Hohl, T.M., Cherny, M. & Pamer, E.G. Selective expansion of the monocytic lineage directed by bacterial infection. *J Immunol* **183**, 1900-1910 (2009).

79. Läubli, H., Stevenson, J.L., Varki, A., Varki, N.M. & Borsig, L. L-selectin facilitation of metastasis involves temporal induction of Fut7-dependent ligands at sites of tumor cell arrest. *Cancer Res* **66**, 1536-1542 (2006).

80. Andonegui, G.*, et al.* Mice that exclusively express TLR4 on endothelial cells can efficiently clear a lethal systemic Gram-negative bacterial infection. *The Journal of clinical investigation* **119**, 1921-1930 (2009).

81. Clausen, B.E., Burkhardt, C., Reith, W., Renkawitz, R. & Forster, I. Conditional gene targeting in macrophages and granulocytes using LysMcre mice. *Transgenic research* **8**, 265-277 (1999).

82. Goren, I.*, et al.* A transgenic mouse model of inducible macrophage depletion: effects of diphtheria toxin-driven lysozyme M-specific cell lineage ablation on wound inflammatory, angiogenic, and contractive processes. *Am J Pathol* **175**, 132-147 (2009).

83. Ishikawa, T.O., Oshima, M. & Herschman, H.R. Cox-2 deletion in myeloid and endothelial cells, but not in epithelial cells, exacerbates murine colitis. *Carcinogenesis* **32**, 417-426 (2011).

84. Agrawal, S., Gollapudi, S., Su, H. & Gupta, S. Leptin activates human B cells to secrete TNF-alpha, IL-6, and IL-10 via JAK2/STAT3 and p38MAPK/ERK1/2 signaling pathway. *Journal of clinical immunology* **31**, 472-478 (2011).

85. Feng, D., Nagy, J.A., Pyne, K., Dvorak, H.F. & Dvorak, A.M. Neutrophils emigrate from venules by a transendothelial cell pathway in response to FMLP. *The Journal of experimental medicine* **187**, 903-915 (1998).

86. Khatib, A.M.*, et al.* Characterization of the host proinflammatory response to tumor cells during the initial stages of liver metastasis. *Am J Pathol* **167**, 749-759 (2005).

87. Zhang, J., Lu, Y. & Pienta, K.J. Multiple roles of chemokine (C-C motif) ligand 2 in promoting prostate cancer growth. *Journal of the National Cancer Institute* **102**, 522-528 (2010).

88. Hu, H.*, et al.* Tumor cell-microenvironment interaction models coupled with clinical validation reveal CCL2 and SNCG as two predictors of colorectal cancer hepatic metastasis. *Clin Cancer Res* **15**, 5485-5493 (2009).

89. Staller, P.*, et al.* Chemokine receptor CXCR4 downregulated by von Hippel-Lindau tumour suppressor pVHL. *Nature* **425**, 307-311 (2003).

90. Ali, S. & Lazennec, G. Chemokines: novel targets for breast cancer metastasis. *Cancer Metastasis Rev* **26**, 401-420 (2007).

91. Lazennec, G. & Richmond, A. Chemokines and chemokine receptors: new insights into cancer-related inflammation. *Trends Mol Med* **16**, 133-144 (2010).

92. Raman, D., Baugher, P.J., Thu, Y.M. & Richmond, A. Role of chemokines in tumor growth. *Cancer letters* **256**, 137-165 (2007).

93. Vindrieux, D., Escobar, P. & Lazennec, G. Emerging roles of chemokines in prostate cancer. *Endocrine-related cancer* **16**, 663-673 (2009).

94. Ben-Baruch, A. Organ selectivity in metastasis: regulation by chemokines and their receptors. *Clin Exp Metastasis* **25**, 345-356 (2008).

95. Lu, Y.*, et al.* Activation of MCP-1/CCR2 axis promotes prostate cancer growth in bone. *Clin Exp Metastasis* **26**, 161-169 (2009).

96. Lu, X. & Kang, Y. Chemokine (C-C motif) ligand 2 engages CCR2+ stromal cells of monocytic origin to promote breast cancer metastasis to lung and bone. *The Journal of biological chemistry* **284**, 29087-29096 (2009).

97. Vande Broek, I.*, et al.* Chemokine receptor CCR2 is expressed by human multiple myeloma cells and mediates migration to bone marrow stromal cell-produced monocyte chemotactic proteins MCP-1, -2 and -3. *Br J Cancer* **88**, 855-862 (2003).

98. Huang, B.*, et al.* CCL2/CCR2 pathway mediates recruitment of myeloid suppressor cells to cancers. *Cancer letters* **252**, 86-92 (2007).

99. Sawanobori, Y.*, et al.* Chemokine-mediated rapid turnover of myeloid-derived suppressor cells in tumor-bearing mice. *Blood* **111**, 5457-5466 (2008).

100. Hiratsuka, S.*, et al.* Endothelial focal adhesion kinase mediates cancer cell homing to discrete regions of the lungs via E-selectin up-regulation. *Proc Natl Acad Sci U S A* **108**, 3725-3730 (2011).

101. Kowanetz, M.*, et al.* Granulocyte-colony stimulating factor promotes lung metastasis through mobilization of Ly6G+Ly6C+ granulocytes. *Proc Natl Acad Sci U S A* **107**, 21248-21255 (2010).

102. McIntyre, T.M., Prescott, S.M., Weyrich, A.S. & Zimmerman, G.A. Cell-cell interactions: leukocyte-endothelial interactions. *Current opinion in hematology* **10**, 150-158 (2003).

103. Muller, W.A. Leukocyte-endothelial-cell interactions in leukocyte transmigration and the inflammatory response. *Trends Immunol* **24**, 327-334 (2003).

104. Sanz-Moreno, V.*, et al.* ROCK and JAK1 Signaling Cooperate to Control Actomyosin Contractility in Tumor Cells and Stroma. *Cancer Cell* **20**, 229-245 (2011).

105. Tremblay, P.L., Auger, F.A. & Huot, J. Regulation of transendothelial migration of colon cancer cells by E-selectin-mediated activation of p38 and ERK MAP kinases. *Oncogene* **25**, 6563-6573 (2006).

106. Garin, A. & Proudfoot, A.E. Chemokines as targets for therapy. *Exp Cell Res* **317**, 602-612.

107. Balkwill, F. & Coussens, L.M. Cancer: an inflammatory link. *Nature* **431**, 405-406 (2004).

108. Colotta, F., Allavena, P., Sica, A., Garlanda, C. & Mantovani, A. Cancer-related inflammation, the seventh hallmark of cancer: links to genetic instability. *Carcinogenesis* **30**, 1073-1081 (2009).

109. Hanahan, D. & Weinberg, R.A. The hallmarks of cancer. *Cell* **100**, 57-70 (2000).

110. Balkwill, F. & Mantovani, A. Inflammation and cancer: back to Virchow? *Lancet* **357**, 539-545 (2001).

111. Mantovani, A. & Pierotti, M.A. Cancer and inflammation: a complex relationship. *Cancer letters* **267**, 180-181 (2008).

112. Willimsky, G. & Blankenstein, T. Sporadic immunogenic tumours avoid destruction by inducing T-cell tolerance. *Nature* **437**, 141-146 (2005).

113. Willimsky, G.*, et al.* Immunogenicity of premalignant lesions is the primary cause of general cytotoxic T lymphocyte unresponsiveness. *The Journal of experimental medicine* **205**, 1687-1700 (2008).

114. Coussens, L.M., Shapiro, S.D., Soloway, P.D. & Werb, Z. Models for gain-of-function and loss-of-function of MMPs. Transgenic and gene targeted mice. *Methods in molecular biology (Clifton, N.J* **151**, 149-179 (2001).

115. Coussens, L.M. & Werb, Z. Inflammatory cells and cancer: think different! *The Journal of experimental medicine* **193**, F23-26 (2001).

116. Sayi, A.*, et al.* The CD4+ T cell-mediated IFN-gamma response to Helicobacter infection is essential for clearance and determines gastric cancer risk. *J Immunol* **182**, 7085-7101 (2009).

117. Dvorak, H.F. Tumors: wounds that do not heal. Similarities between tumor stroma generation and wound healing. *N Engl J Med* **315**, 1650-1659 (1986).

118. Schafer, M. & Werner, S. Cancer as an overhealing wound: an old hypothesis revisited. *Nat Rev Mol Cell Biol* **9**, 628-638 (2008).

119. He, G. & Karin, M. NF-kappaB and STAT3 - key players in liver inflammation and cancer. *Cell Res* **21**, 159-168 (2011).

120. Coussens, L.M. & Werb, Z. Inflammation and cancer. *Nature* **420**, 860-867 (2002).

121. Llovet, J.M., Burroughs, A. & Bruix, J. Hepatocellular carcinoma. *Lancet* **362**, 1907-1917 (2003).

122. Weber, A., Boege, Y., Reisinger, F. & Heikenwalder, M. Chronic liver inflammation and hepatocellular carcinoma: persistence matters. *Swiss medical weekly* **141**, w13197 (2011).

123. Seeff, L.B. Introduction: The burden of hepatocellular carcinoma. *Gastroenterology* **127**, S1-4 (2004).

124. Itzkowitz, S.H. & Yio, X. Inflammation and cancer IV. Colorectal cancer in inflammatory bowel disease: the role of inflammation. *Am J Physiol Gastrointest Liver Physiol* **287**, G7-17 (2004).

125. Ullman, T.A. & Itzkowitz, S.H. Intestinal inflammation and cancer. *Gastroenterology* **140**, 1807-1816 (2011).

126. Cover, T.L. & Blaser, M.J. Helicobacter pylori in health and disease. *Gastroenterology* **136**, 1863-1873 (2009).

127. Ernst, P.B. & Gold, B.D. The disease spectrum of Helicobacter pylori: the immunopathogenesis of gastroduodenal ulcer and gastric cancer. *Annual review of microbiology* **54**, 615-640 (2000).

128. Mostafa, M.H., Sheweita, S.A. & O'Connor, P.J. Relationship between schistosomiasis and bladder cancer. *Clinical microbiology reviews* **12**, 97-111 (1999).

129. Ruddle, N.H. & Waksman, B.H. Cytotoxic effect of lymphocyte-antigen interaction in delayed hypersensitivity. *Science (New York, N.Y* **157**, 1060-1062 (1967).

130. Ruddle, N.H. & Waksman, B.H. Cytotoxicity mediated by soluble antigen and lymphocytes in delayed hypersensitivity. 3. Analysis of mechanism. *The Journal of experimental medicine* **128**, 1267-1279 (1968).

131. Granger, G.A., Shacks, S.J., Williams, T.W. & Kolb, W.P. Lymphocyte in vitro cytotoxicity: specific release of lymphotoxin-like materials from tuberculin-sensitive lymphoid cells. *Nature* **221**, 1155-1157 (1969).

132. Granger, G.A. & Williams, T.W. Lymphocyte cytotoxicity in vitro: activation and release of a cytotoxic factor. *Nature* **218**, 1253-1254 (1968).

133. Kolb, W.P. & Granger, G.A. Lymphocyte in vitro cytotoxicity: characterization of human lymphotoxin. *Proc Natl Acad Sci U S A* **61**, 1250-1255 (1968).

134. Williams, T.W. & Granger, G.A. Lymphocyte in vitro cytotoxicity: lymphotoxins of several mammalian species. *Nature* **219**, 1076-1077 (1968).

135. Granger, G.A. Lymphokines--the mediators of cellular immunity. *Series haematologica* **5**, 8-40 (1972).

136. Aggarwal, B.B., Moffat, B. & Harkins, R.N. Human lymphotoxin. Production by a lymphoblastoid cell line, purification, and initial characterization. *The Journal of biological chemistry* **259**, 686-691 (1984).

137. Aggarwal, B.B., Henzel, W.J., Moffat, B., Kohr, W.J. & Harkins, R.N. Primary structure of human lymphotoxin derived from 1788 lymphoblastoid cell line. *The Journal of biological chemistry* **260**, 2334-2344 (1985).

138. Nedwin, G.E.*, et al.* Structure and chromosomal localization of the human lymphotoxin gene. *J Cell Biochem* **29**, 171-181 (1985).

139. Carswell, E.A.*, et al.* An endotoxin-induced serum factor that causes necrosis of tumors. *Proc Natl Acad Sci U S A* **72**, 3666-3670 (1975).

140. Gray, P.W.*, et al.* Cloning and expression of cDNA for human lymphotoxin, a lymphokine with tumour necrosis activity. *Nature* **312**, 721-724 (1984).

141. Hehlgans, T. & Pfeffer, K. The intriguing biology of the tumour necrosis factor/tumour necrosis factor receptor superfamily: players, rules and the games. *Immunology* **115**, 1-20 (2005).

142. Hiserodt, J.C., Ware, C.F., Harris, P.C. & Granger, G.A. Identification of membrane-associated lymphotoxin (LT) on mitogen-activated human lymphocytes using heterologous anti-LT antisera in vitro. *Cell Immunol* **34**, 326-339 (1977).

143. Ware, C.F. & Granger, G.A. A physicochemical and immunologic comparison of the cell growth inhibitory activity of human lymphotoxins and interferons in vitro. *J Immunol* **122**, 1763-1770 (1979).

144. Browning, J.L.*, et al.* Lymphotoxin beta, a novel member of the TNF family that forms a heteromeric complex with lymphotoxin on the cell surface. *Cell* **72**, 847-856 (1993).

145. Pokholok, D.K.*, et al.* Cloning and expression analysis of the murine lymphotoxin beta gene. *Proc Natl Acad Sci U S A* **92**, 674-678 (1995).

146. Aggarwal, B.B., Kumar, A. & Bharti, A.C. Anticancer potential of curcumin: preclinical and clinical studies. *Anticancer research* **23**, 363-398 (2003).

147. Nedospasov, S.A.*, et al.* The genes for tumor necrosis factor (TNF-alpha) and lymphotoxin (TNF-beta) are tandemly arranged on chromosome 17 of the mouse. *Nucleic Acids Res* **14**, 7713-7725 (1986).

148. Nedospasov, S.A.*, et al.* Tandem arrangement of genes coding for tumor necrosis factor (TNF-alpha) and lymphotoxin (TNF-beta) in the human genome. *Cold Spring Harb Symp Quant Biol* **51 Pt 1**, 611-624 (1986).

149. Nedwin, G.E.*, et al.* Human lymphotoxin and tumor necrosis factor genes: structure, homology and chromosomal localization. *Nucleic Acids Res* **13**, 6361-6373 (1985).

150. Muller, U., Jongeneel, C.V., Nedospasov, S.A., Lindahl, K.F. & Steinmetz, M. Tumour necrosis factor and lymphotoxin genes map close to H-2D in the mouse major histocompatibility complex. *Nature* **325**, 265-267 (1987).

151. Worm, M. & Geha, R.S. CD40 ligation induces lymphotoxin alpha gene expression in human B cells. *Int Immunol* **6**, 1883-1890 (1994).

152. Browning, J.L.*, et al.* Characterization of surface lymphotoxin forms. Use of specific monoclonal antibodies and soluble receptors. *J Immunol* **154**, 33-46 (1995).

153. Young, J.*, et al.* Lymphotoxin-alphabeta heterotrimers are cleaved by metalloproteinases and contribute to synovitis in rheumatoid arthritis. *Cytokine* (2010).

154. Ware, C.F. Network communications: lymphotoxins, LIGHT, and TNF. *Annu Rev Immunol* **23**, 787-819 (2005).

155. Norris, P.S. & Ware, C.F. The LT beta R signaling pathway. *Adv Exp Med Biol* **597**, 160-172 (2007).

156. Gommerman, J.L. & Browning, J.L. Lymphotoxin/light, lymphoid microenvironments and autoimmune disease. *Nature reviews* **3**, 642-655 (2003).

157. Lo, J.C.*, et al.* Lymphotoxin beta receptor-dependent control of lipid homeostasis. *Science (New York, N.Y* **316**, 285-288 (2007).

158. Tumanov, A.V.*, et al.* T cell-derived lymphotoxin regulates liver regeneration. *Gastroenterology* **136**, 694-704 e694 (2009).

159. Schneider, K., Potter, K.G. & Ware, C.F. Lymphotoxin and LIGHT signaling pathways and target genes. *Immunol Rev* **202**, 49-66 (2004).

160. Vallabhapurapu, S. & Karin, M. Regulation and function of NF-kappaB transcription factors in the immune system. *Annu Rev Immunol* **27**, 693-733 (2009).

161. Karin, M. The IkappaB kinase - a bridge between inflammation and cancer. *Cell Res* **18**, 334-342 (2008).

162. Dejardin, E.*, et al.* The lymphotoxin-beta receptor induces different patterns of gene expression via two NF-kappaB pathways. *Immunity* **17**, 525-535 (2002).

163. Haybaeck, J.*, et al.* A lymphotoxin-driven pathway to hepatocellular carcinoma. *Cancer Cell* **16**, 295-308 (2009).

164. Muller, J.R. & Siebenlist, U. Lymphotoxin beta receptor induces sequential activation of distinct NF-kappa B factors via separate signaling pathways. *The Journal of biological chemistry* **278**, 12006-12012 (2003).

165. Senftleben, U.*, et al.* Activation by IKKalpha of a second, evolutionary conserved, NF-kappa B signaling pathway. *Science (New York, N.Y* **293**, 1495-1499 (2001).

166. Vainer, G.W., Pikarsky, E. & Ben-Neriah, Y. Contradictory functions of NF-kappaB in liver physiology and cancer. *Cancer letters* (2008).

167. Greten, F.R.*, et al.* IKKbeta links inflammation and tumorigenesis in a mouse model of colitis-associated cancer. *Cell* **118**, 285-296 (2004).

168. Greten, F.R. & Karin, M. The IKK/NF-kappaB activation pathway-a target for prevention and treatment of cancer. *Cancer letters* **206**, 193-199 (2004).

169. Pikarsky, E.*, et al.* NF-kappaB functions as a tumour promoter in inflammation-associated cancer. *Nature* **431**, 461-466 (2004).

170. Compagno, M.*, et al.* Mutations of multiple genes cause deregulation of NF-kappaB in diffuse large B-cell lymphoma. *Nature* **459**, 717-721 (2009).

171. Maeda, S., Kamata, H., Luo, J.L., Leffert, H. & Karin, M. IKKbeta couples hepatocyte death to cytokine-driven compensatory proliferation that promotes chemical hepatocarcinogenesis. *Cell* **121**, 977-990 (2005).

172. Luedde, T.*, et al.* Deletion of NEMO/IKKgamma in liver parenchymal cells causes steatohepatitis and hepatocellular carcinoma. *Cancer Cell* **11**, 119-132 (2007).

173. Fausto, N., Campbell, J.S. & Riehle, K.J. Liver regeneration. *Hepatology (Baltimore, Md* **43**, S45-53 (2006).

174. Malhi, H., Gores, G.J. & Lemasters, J.J. Apoptosis and necrosis in the liver: a tale of two deaths? *Hepatology (Baltimore, Md* **43**, S31-44 (2006).

175. Bosch, F.X., Ribes, J., Diaz, M. & Cleries, R. Primary liver cancer: worldwide incidence and trends. *Gastroenterology* **127**, S5-S16 (2004).

176. El-Serag, H.B. & Rudolph, K.L. Hepatocellular carcinoma: epidemiology and molecular carcinogenesis. *Gastroenterology* **132**, 2557-2576 (2007).

177. Parkin, D.M., Bray, F.I. & Devesa, S.S. Cancer burden in the year 2000. The global picture. *Eur J Cancer* **37 Suppl 8**, S4-66 (2001).

178. Block, T.M., Mehta, A.S., Fimmel, C.J. & Jordan, R. Molecular viral oncology of hepatocellular carcinoma. *Oncogene* **22**, 5093-5107 (2003).

179. Lowes, K.N., Croager, E.J., Abraham, L.J., Olynyk, J.K. & Yeoh, G.C. Upregulation of lymphotoxin beta expression in liver progenitor (oval) cells in chronic hepatitis C. *Gut* **52**, 1327-1332 (2003).

180. Lee, S.H., Park, S.G., Lim, S.O. & Jung, G. The hepatitis B virus X protein up-regulates lymphotoxin alpha expression in hepatocytes. *Biochimica et biophysica acta* **1741**, 75-84 (2005).

181. Schulte-Hermann, R., Bursch, W., Low-Baselli, A., Wagner, A. & Grasl-Kraupp, B. Apoptosis in the liver and its role in hepatocarcinogenesis. *Cell Biol Toxicol* **13**, 339-348 (1997).

182. Ng, T.I.*, et al.* Identification of host genes involved in hepatitis C virus replication by small interfering RNA technology. *Hepatology (Baltimore, Md* **45**, 1413-1421 (2007).

183. Matsumoto, M.*, et al.* Hepatitis C virus core protein interacts with the cytoplasmic tail of lymphotoxin-beta receptor. *J Virol* **71**, 1301-1309 (1997).

184. Zhu, N.*, et al.* Hepatitis C virus core protein binds to the cytoplasmic domain of tumor necrosis factor (TNF) receptor 1 and enhances TNF-induced apoptosis. *J Virol* **72**, 3691-3697 (1998).

185. Chen, C.M., You, L.R., Hwang, L.H. & Lee, Y.H. Direct interaction of hepatitis C virus core protein with the cellular lymphotoxin-beta receptor modulates the signal pathway of the lymphotoxin-beta receptor. *J Virol* **71**, 9417-9426 (1997).

186. Browning, J.L. & French, L.E. Visualization of lymphotoxin-beta and lymphotoxin-beta receptor expression in mouse embryos. *J Immunol* **168**, 5079-5087 (2002).

187. Ruddell, R.G.*, et al.* Lymphotoxin-beta receptor signaling regulates hepatic stellate cell function and wound healing in a murine model of chronic liver injury. *Hepatology (Baltimore, Md* **49**, 227-239 (2009).

188. An, M.M.*, et al.* Lymphtoxin beta receptor-Ig protects from T-cell-mediated liver injury in mice through blocking LIGHT/HVEM signaling. *Biological & pharmaceutical bulletin* **29**, 2025-2030 (2006).

189. Anand, S.*, et al.* Essential role of TNF family molecule LIGHT as a cytokine in the pathogenesis of hepatitis. *The Journal of clinical investigation* **116**, 1045-1051 (2006).

190. Puglielli, M.T.*, et al.* Reversal of virus-induced systemic shock and respiratory failure by blockade of the lymphotoxin pathway. *Nat Med* **5**, 1370-1374 (1999).

191. Nakamoto, Y., Guidotti, L.G., Kuhlen, C.V., Fowler, P. & Chisari, F.V. Immune pathogenesis of hepatocellular carcinoma. *The Journal of experimental medicine* **188**, 341-350 (1998).

192. Maeda, S. & Omata, M. Inflammation and cancer: role of nuclear factor-kappaB activation. *Cancer Sci* **99**, 836-842 (2008).

193. He, G., Yu, G., Temkin, V., Ogata, H., Kuntzen, C., Sakurai, T., Sieghart, W., Peck-Radosavljevic,M., Leffert, H. and Karin, M. . Hepatocyte IKKβ/NF-κB inhibits tumor promotion and progression by preventing oxidative stress driven STAT3 activation *Cancer Cell* (2010).

194. Bettermann, K.*, et al.* TAK1 suppresses a NEMO-dependent but NF-kappaB-independent pathway to liver cancer. *Cancer Cell* **17**, 481-496 (2010).

195. Bluethmann, H., Rothe, J., Schultze, N., Tkachuk, M. & Koebel, P. Establishment of the role of IL-6 and TNF receptor 1 using gene knockout mice. *J Leukoc Biol* **56**, 565-570 (1994).

196. Cao, Y.*, et al.* IKKalpha provides an essential link between RANK signaling and cyclin D1 expression during mammary gland development. *Cell* **107**, 763-775 (2001).

197. Futterer, A., Mink, K., Luz, A., Kosco-Vilbois, M.H. & Pfeffer, K. The lymphotoxin beta receptor controls organogenesis and affinity maturation in peripheral lymphoid tissues. *Immunity* **9**, 59-70 (1998).

198. Heikenwalder, M.*, et al.* Overexpression of lymphotoxin in T cells induces fulminant thymic involution. *Am J Pathol* **172**, 1555-1570 (2008).

199. Mombaerts, P.*, et al.* RAG-1-deficient mice have no mature B and T lymphocytes. *Cell* **68**, 869-877 (1992).

200. Vigan, I.*, et al.* T lymphocytes infiltrating the liver during chronic hepatitis C infection express a broad range of T-cell receptor beta chain diversity. *J Hepatol* **38**, 651-659 (2003).

201. Yi, M., Bodola, F. & Lemon, S.M. Subgenomic hepatitis C virus replicons inducing expression of a secreted enzymatic reporter protein. *Virology* **304**, 197-210 (2002).

202. Blight, K.J., McKeating, J.A. & Rice, C.M. Highly permissive cell lines for subgenomic and genomic hepatitis C virus RNA replication. *J Virol* **76**, 13001-13014 (2002).

203. Pietschmann, T.*, et al.* Construction and characterization of infectious intragenotypic and intergenotypic hepatitis C virus chimeras. *Proc Natl Acad Sci U S A* **103**, 7408-7413 (2006).

204. Friebe, P., Boudet, J., Simorre, J.P. & Bartenschlager, R. Kissing-loop interaction in the 3' end of the hepatitis C virus genome essential for RNA replication. *J Virol* **79**, 380-392 (2005).

205. Koutsoudakis, G.*, et al.* Characterization of the early steps of hepatitis C virus infection by using luciferase reporter viruses. *J Virol* **80**, 5308-5320 (2006).

206. Vignali, D.A. Multiplexed particle-based flow cytometric assays. *J Immunol Methods* **243**, 243-255 (2000).

207. Neumann-Haefelin, C.*, et al.* Dominant influence of an HLA-B27 restricted CD8+ T cell response in mediating HCV clearance and evolution. *Hepatology (Baltimore, Md* **43**, 563-572 (2006).

208. Heikenwalder, M.*, et al.* Chronic lymphocytic inflammation specifies the organ tropism of prions. *Science (New York, N.Y* **307**, 1107-1110 (2005).

209. Kawase, T.*, et al.* PH domain-only protein PHLDA3 is a p53-regulated repressor of Akt. *Cell* **136**, 535-550 (2009).

210. Engelhardt, N.V.*, et al.* Common antigens of mouse oval and biliary epithelial cells. Expression on newly formed hepatocytes. *Differentiation; research in biological diversity* **45**, 29-37 (1990).

211. Marrero, J.A. & Lok, A.S. Newer markers for hepatocellular carcinoma. *Gastroenterology* **127**, S113-119 (2004).

212. Sakamoto, M. Early HCC: diagnosis and molecular markers. *J Gastroenterol* **44 Suppl 19**, 108-111 (2009).

213. Bachert, C., Fimmel, C. & Linstedt, A.D. Endosomal trafficking and proprotein convertase cleavage of cis Golgi protein GP73 produces marker for hepatocellular carcinoma. *Traffic (Copenhagen, Denmark)* **8**, 1415-1423 (2007).

214. Baffet, G.*, et al.* Autocrine activity of interleukin 6 secreted by hepatocarcinoma cell lines. *Mol Biol Med* **8**, 141-156 (1991).

215. Subrata, L.S.*, et al.* Hepatic expression of the tumor necrosis factor family member lymphotoxin-beta is regulated by interleukin (IL)-6 and IL-1beta: transcriptional control mechanisms in oval cells and hepatoma cell lines. *Liver Int* **25**, 633-646 (2005).

216. Manns, M.P.*, et al.* Peginterferon alfa-2b plus ribavirin compared with interferon alfa-2b plus ribavirin for initial treatment of chronic hepatitis C: a randomised trial. *Lancet* **358**, 958-965 (2001).

217. Fried, M.W.*, et al.* Peginterferon alfa-2a plus ribavirin for chronic hepatitis C virus infection. *N Engl J Med* **347**, 975-982 (2002).

218. Budhu, A. & Wang, X.W. The role of cytokines in hepatocellular carcinoma. *J Leukoc Biol* **80**, 1197-1213 (2006).

219. Zeremski, M., Petrovic, L.M. & Talal, A.H. The role of chemokines as inflammatory mediators in chronic hepatitis C virus infection. *J Viral Hepat* **14**, 675-687 (2007).

220. Akhurst, B.*, et al.* Differential lymphotoxin-beta and interferon gamma signaling during mouse liver regeneration induced by chronic and acute injury. *Hepatology (Baltimore, Md* **41**, 327-335 (2005).

221. Lee, J.S.*, et al.* A novel prognostic subtype of human hepatocellular carcinoma derived from hepatic progenitor cells. *Nat Med* **12**, 410-416 (2006).

222. Gommerman, J.L.*, et al.* Manipulation of lymphoid microenvironments in nonhuman primates by an inhibitor of the lymphotoxin pathway. *The Journal of clinical investigation* **110**, 1359-1369 (2002).

223. Zhou, P.*, et al.* Targeting lymphotoxin-mediated negative selection to prevent prostate cancer in mice with genetic predisposition. *Proc Natl Acad Sci U S A* **106**, 17134-17139 (2009).

224. Keats, J.J.*, et al.* Promiscuous mutations activate the noncanonical NF-kappaB pathway in multiple myeloma. *Cancer Cell* **12**, 131-144 (2007).

225. Hehlgans, T.*, et al.* Lymphotoxin-beta receptor immune interaction promotes tumor growth by inducing angiogenesis. *Cancer Res* **62**, 4034-4040 (2002).

226. Lukashev, M.*, et al.* Targeting the lymphotoxin-beta receptor with agonist antibodies as a potential cancer therapy. *Cancer Res* **66**, 9617-9624 (2006).

227. Ammirante, M., Luo,J., Grivennikov, S., Nedospasov, S. and Karin M. . B cell-derived lymphotoxin promotes castration-resistant prostate cancer. . *Nature, in press.* (2010).

228. Or, Y.Y.*, et al.* Identification of a novel 12p13.3 amplicon in nasopharyngeal carcinoma. *J Pathol* **220**, 97-107 (2010).

229. Ito, D., Back, T.C., Shakhov, A.N., Wiltrout, R.H. & Nedospasov, S.A. Mice with a targeted mutation in lymphotoxin-alpha exhibit enhanced tumor growth and metastasis: impaired NK cell development and recruitment. *J Immunol* **163**, 2809-2815 (1999).

230. Kuprash, D.V.*, et al.* Ablation of TNF or lymphotoxin signaling and the frequency of spontaneous tumors in p53-deficient mice. *Cancer letters* (2008).

8 CURRICULUM VITAE AND PUBLICATIONS

Name: Monika Julia Wolf
Date and place of birth: 18th of June 1983 in Bayreuth, Germany
Nationality: German

University education:

Since 11/2007	PhD student at the Institute for Neuropathology, University of Zurich
10/2004 - 09/2007	Studies of Biotechnology at the Ecole Supérieure de Biotechnologie de Strasbourg (ESBS), France
10/2002 - 09/2004	Studies of Biochemistry at the MLU Halle-Wittenberg, Germany

Teaching experience:

2008 – 2010	assistant in the course “Medical Immunology”, BIO430 University of Zurich

History of research experience and further training:

01/2007 - 08/2007	Master thesis at the Center for Infectious Medicine, Karolinska Institute Stockholm, Sweden
06/2006 - 08/2006	Summer student at the Instituto de Tecnologia Química e Biológica, New University Lisbon, Portugal
07/2005 – 08/2005	Summer student at University of British Columbia, Vancouver, Canada, Department of Medical Genetics

---

10/2009	Course “FACS Calibur” organized by BD Biosciences, Heidelberg
06/2008	Course in “Scientific Writing” organized by the Cancer Network Zurich
05/2008	Introductory Course in Laboratory Animal Science (LTK Modul 1) organized by the “Institut für Labortierkunde”, University of Zurich

Grants:

2008	Fellowship for PhD students from Roche Research Foundation
2007	Scholarship of the Alsace Region (Bourse d’Alsace)

Publications:

MJ Wolf, GM Seleznik, M Heikenwalder:
Lymphotoxin's link to carcinogenesis: Friend or foe? From lymphoid neogenesis to hepatocellular carcinoma and prostate cancer, Adv Exp Med Biol 2011

R Peters*, MJ Wolf*, M van den Broek, M Nuvolone, S Dannenmann, B Stieger, R Rapold, D Konrad, A Rubin, JR Bertino, A Aguzzi, M Heikenwalder, AK Knuth:
Efficient generation of multipotent mesenchymal stem cells from umbilical cord blood in stroma-free liquid culture, Plos One 2010

MJ Wolf, GM Seleznik, N Zeller, M Heikenwalder:
The unexpected role of lymphotoxin beta receptor signaling in carcinogenesis: from lymphoid tissue formation to liver and prostate cancer development, Oncogene 2010

K Bettermann*, M Vucur*, J Haybaeck, C Koppe, J Janssen, F Heymann, A Weber, R Weiskirchen, C Liedtke, N Gassler, M Müller, R de Vos, MJ Wolf, Y Boege, GM Seleznik, N Zeller, D Erny, T Fuchs, S Zoller, S Cairo, MA Buendia, M Prinz, S Akira, F Tacke, M Heikenwalder, C Trautwein, T Luedde:
TAK1 suppresses a NEMO-dependent but NF-kappa B-independent pathway to liver cancer, Cancer Cell 2010

J Haybaeck*, N Zeller*, MJ Wolf, A Weber, U Wagner, MO Kurer, J Bremer, G Iezzi, R Graf, PA Clavien, R Thimme, H Blum, SA Nedospasov, K Zatloukal, M Ramzan, S Ciesek, T Pietschmann, PN Marche, M Karin, M Kopf, JL Browning, A Aguzzi and M Heikenwälder:
A lymphotoxin-driven pathway to hepatocellular carcinoma, Cancer Cell 2009

M Hultcrantz, MH Hühn, M Wolf, A Olsson, S Jacobson, BR Williams, O Korsgren, M Flodström-Tullberg:
Interferons induce an Antiviral State in Human Pancreatic Islet Cells; Virology 2007

* these authors contributed equally

9 ACKNOWLEDGEMENTS

For providing lots of help & support to make this work successful I am grateful to many people:
First of all, I would like to thank Mathias Heikenwälder for all his support and encouragement during the four years of my thesis, for giving me the opportunity to work on these very interesting projects, for intensive scientific discussions, for his never-ending enthusiasm, and for many suggestions & ideas, about which additional experiments could be done.
I would like to thank Adriano Aguzzi for the opportunity to do my PhD thesis in his institute, for discussions, suggestions and critical questions on my projects and most importantly for his constant push to perform thorough and well-controlled experiments.

I would like to thank everybody involved in the CCR2 project, especially Lubor Borsig and Alexandra Hoos. It was fun working with all of you. Many thanks for sharing and exchanging ideas, knowledge and experiments.
Furthermore, I would like to thank everybody involved in the lymphotoxin project, especially Johannes Haybaeck for sharing the *tg*1223 mice & Sandra Ciesek and Thomas Pietschmann for the HCV experiments.

Many thanks to all co-workers in the Heikenwälder group, in particular to Judith Bauer and Yannick Böge, for lots of help with the experiments and for seemingly endless FACS and mouse-work sessions. Thanks a lot to Gitta Seleznik and Lukas Frick for many discussions and suggestions. I would like to thank all the past and present members of the Institute for Neuropathology. It's definitely too many people to name them all here – nevertheless, I am very grateful for many discussions, suggestions and advice, sharing of ideas and reagents and helps in everydays lab work. Special thanks to Tracy O'Connor and Juliane Bremer.
Furthermore, I would like to thank Mirzet Delic, Birgit Riepl, Jay Tracy, Renaud Maire, Mareike Wagner, Rita Moos, Petra Schwarz, Dimitri Goriounov, Bei Li, Karina Arroyo, Ahmet Varol, Giuseppe Manco, Cristobal Tostado, Marianne König and Silvia Behnke for lots of help, technical support and suggestions with experiments.

Special thanks to Achim Weber and Michael Kurrer for the pathologists' view, for taking a look at thousands of slides & for many discussions and ideas.

For discussions and suggestions, I would like to thank the members of my PhD committee, Anne Müller and Christian Münz.

I would like to thank the Roche Research Foundation for funding parts of this thesis with a fellowship for PhD students.

Last but not least, I would like to thank my parents & friends for their support and fun times in and outside Zurich.